

UNIVERSITY *of*
TASMANIA

The Antarctic Lithosphere Revealed by Multivariate Analysis

by

Tobias S. L. Stål

BSc, MSc

A thesis submitted in fulfillment of the requirements for
the degree of Doctor of Philosophy

School of Natural Sciences - Earth Sciences

University of Tasmania

March 24, 2021

Declaration of Authorship

I, Tobias STÅL, declare that this thesis titled, “The Antarctic Lithosphere Revealed by Multivariate Analysis” and the work presented in it are my own.

Signed: _____

March 24, 2021

Date: _____

Declaration of Originality

This thesis contains no material which has been accepted for a degree or diploma by the University or any other institution, except by way of background information and duly acknowledged in the thesis, and to the best of my knowledge and belief no material previously published or written by another person except where due acknowledgement is made in the text of the thesis, nor does the thesis contain any material that infringes copyright.

Authority of Access

The non-published content of the thesis (see below) may be made available for loan and limited copying and communication in accordance with the Copyright Act 1968.

Statement Regarding Published Work Contained in Thesis

The publisher holds the copyright for that content, and access to the material should be sought from the respective journal.

Chapter 3a and 3b of this thesis is published under a Creative Commons Attribution (CC BY) licence. You are free to copy, communicate and adapt the work, so long as you attribute the authors. To view a copy of this licence, visit <http://creativecommons.org/licenses/>.

Chapter 4 and 5 of this thesis are published, and accepted, with AGU publications. The use of this material complies with AGU permissions policy, as specified here: <https://www.agu.org/Publish-with-AGU/Publish/Author-Resources/Policies/Permission-policy>

Statement of Co-Authorship

The following people and institutions contributed to the publication of work undertaken as part of this thesis:

- Candidate Tobias Stål,
School of Natural Sciences (Earth Sciences) and Institute for Marine and Antarctic Studies, University of Tasmania
- Author 1 Anya M. Reading (Primary supervisor),
School of Natural Sciences (Earth Sciences) and Institute for Marine and Antarctic Studies, University of Tasmania
- Author 2 Jacqueline A. Halpin (Co-supervisor),
Institute for Marine and Antarctic Studies, University of Tasmania
- Author 3 Steven J. Phipps,
Institute for Marine and Antarctic Studies, University of Tasmania
- Author 4 Joanne M. Whittaker (Co-supervisor),
Institute for Marine and Antarctic Studies, University of Tasmania

Author Details and Their Roles

- Paper 1 ‘A grid for multidimensional and multivariate spatial representation and data processing.’, located in Chapter 3a
- Paper 2 ‘The Antarctic crust and upper mantle: A flexible 3D model and software framework for interdisciplinary research.’, located in Chapter 3b
- Paper 3 ‘A multivariate approach for mapping lithospheric domain boundaries in East Antarctica.’, located in Chapter 4
- Paper 4 ‘Antarctic geothermal heat model Aq1.’, located in Chapter 5

The candidate was the primary author on each paper. Author 1 contributed to the formalisation, development, refinement, and presentation of each paper. Author 2 and 4 contributed to the formalisation, development, refinement, and presentation of paper 2, 3, 4. Author 3 contributed to the refinement and presentation of paper 2.

Signed: _____

IV

The candidate was the primary author on each paper. Author 1 contributed to the formalisation, development, refinement, and presentation of each paper. Author 2 and 4 contributed to the formalisation, development, refinement, and presentation of paper 2, 3, 4. Author 3 contributed to the refinement and presentation of paper 2.

Signed: _____

Date: 25 Nov 2020

Anya M. Reading, Supervisor,
School of Natural Sciences University of Tasmania

Signed: _____

Date: 26 Nov 2020

Sebastien Meffre, Head of Discipline, Earth Sciences
School of Natural Sciences, University of Tasmania

Abstract

The Antarctic continent, at 14 million km², is larger than Australia; yet, due to the ice cover and inaccessibility, its geology and lithospheric structure are to a large extent unknown. During recent decades, particularly since the International Polar Year of 2007-08, a growing number of studies have provided new and improved datasets of the continent's surface, cryosphere, crust and upper mantle. The new data enable new or refined questions to be addressed in the Antarctic Earth sciences. For instance, how does large-scale geophysics correlate with sparse geological observations and interpretations? What are the extents of tectonic domains and affiliations with former neighbours in Gondwana? What is the spatial distribution of geothermal heat flow in the deep interior?

Advancing our understanding of the Antarctic continent addresses fundamental knowledge gaps in plate tectonics, the dynamic foundation for our planet. Understanding the Antarctic lithosphere is also of urgent relevance due to ongoing anthropogenic climate change and the consequent need to better constrain interactions between the solid Earth and the cryosphere. Challenges to build on existing research include the lack of agreement between different studies, and uncertainties that are difficult to constrain. Methodologies previously employed are generally univariate, modelling the solid Earth structure or character from only one observable. However, the growing number of datasets affords an opportunity to combine constraints from multiple observables, embrace the uncertainties, and draw new, considered interpretations. In this thesis, studies that employ multivariate syntheses of recently compiled data are presented, with a focus on combining geophysics and geology.

A new 3D model and software framework for spatial multivariate and multidimensional computation is presented. This is enabled by a newly developed software package, *agrid*, which contains methods for data import, visualisation, and export of results in compatible formats. Using this toolbox, a grid model of continental Antarctica is created from geophysics and geology combined. A range of illustrative maps of lithospheric properties are generated to exemplify the functionality of the framework. This includes a new isostatic model from seismic tomography data and a new approach to calculate geothermal heat flow from energy balance based on geophysics and geology. The dynamic and flexible 3D model of the lithosphere is designed with research addressing solid Earth and cryosphere interaction and feedbacks in mind.

Multivariate methodology is used to investigate the presence of deep-seated lithospheric boundaries in East Antarctica. Three independent datasets are utilised: seismic shear wave speed at 150 km depth, free air gravity anomaly, and surface elevation. From each dataset, boundaries that indicate transitions in value, gradient, frequency, or pattern are suggested,

with rated uncertainty and resolution. A range of likelihood maps is generated; the most conservative maps show regions where we are confident that an upper mantle boundary exists, whereas the least conservative maps contain a greater number of less confidently suggested boundaries. When boundary likelihood is compared with observed crustal geology, we find a good match. The East Antarctic lithosphere is revealed to comprise multiple domains, and internal geological complexity. Domains in the subglacial interior, with no geological outcrop, are very likely.

The computational framework, *agrid*, is used to generate a geothermal heat flow map using over 15 datasets as input observables. A multivariate similarity method is applied, carefully modified for application to the datasets available for Antarctica. The new map, Aq1, is of higher resolution than previous heat flow maps of the continent, and robustly constrained with quantified uncertainty. The map confirms higher heat flow in West Antarctica, and lower heat flow in East Antarctica. The highest values are computed for the Thwaites Glacier region and the Siple Coast, locally over 150 mWm^{-2} . High heat flow, over 80 mWm^{-2} , is also likely in parts of Marie Byrd Land and Palmer Land, and elevated values, above 70 mWm^{-2} , occur for Queen Mary Land. Parts of the interior of Wilkes Land, Wilkes Sub-glacial Basin, and Coats Land, show very low values, under 40 mWm^{-2} .

The thesis concludes with a synthesis of common themes running through the core research chapters, including a discussion of the value of probabilistic geological mapping. Spatial uncertainty metrics are outlined in terms of the added insights they provide in the appraisal of newly generated models. In summary, multivariate maps and models of the 3D continent including a wide variety of data from geophysics and geology are produced using newly written computational tools. Our understanding of the Antarctic lithosphere is thus advanced in a quantitative and repeatable way, and the new solid Earth geoscience results may be readily accessed for ongoing cryosphere and other interdisciplinary research.

Acknowledgement of Country

I acknowledge the palawa people of lutruwita, the traditional owners of the land on which the university is located and where I lived and worked while I conducted the studies and research for my thesis. I pay my respects to ancestors and Elders, past, present and emerging, and also those who did not reach Elder status. Aboriginal palawa people have owned, managed, farmed and connected with their lands since the dawn of time. I acknowledge this unique cultural and spiritual relationships to the land, waters, and seas and their rich contribution to society. I am grateful for the opportunity to live on this beautiful island, and saddened by the injustices, violence, and disruption it witnessed, and of which the society is still shaped.

Acknowledgments

This project was supported by the Australian research Council's Special Research Initiative for Antarctic Gateway Partnership (Project ID SR140300001).

My deepest gratitude goes first and foremost to my supervisors. A few lines here can not enough express my gratitude. Not only did you provide the best imaginable guidance, I am also deeply impressed, and inspired, by your research achievements and your mentoring and teaching skills.

Anya, your patience is admirable. Thank you for everything. We built a firm reef.

Jacqui, thank you for your support and guidance. Your sense for details is almost scary.

Jo, you inspired me to believe in my research. Thank you for your encouragement, and disagreements.

I am also grateful to my mentor, Matt King. Short emails can mean a lot.

I had inspiring and encouraging discussions with Sue Cook, Matt Cracknell, Ben Galton Fenzi, Martin Gal, Shawn Hood, Jodi Fox, Alessandro Maritati, Peter Morse, Miranda Nieboer, Ross Turner and many others. Thank you for your support!

Reaching the terminal degree, I also wish to mention a few teachers and colleagues from my previous studies, at University of Copenhagen, University Center at Svalbard, and University of Gothenburg. Lennart Björklund, Fabio Cammarano, Riko Noormets and Mohammad Yousof; thank you for everything you taught me. Particularly, I would like to thank my previous supervisor, Lars Nielsen. One day, I would love to get back to the chalk, and write that paper!

Long time ago, Åke Ring[†] showed me moraines and eskers, pointed out gneiss and iron ore in the post-glacial landscape where I grew up. Leif Ekberg taught me about the units of physics, and Sten-Åke Fallquist showed me the symbols of mathematics. Thank you.

I also wish to acknowledge that I am indebted to Alexandra Elbakyan for facilitating a reliable library for my studies and research.

I thank my father for teaching me all the practical skills, welding, driving, shooting, that actually took me places. Now, I will finally try to get a real job!

Svenne and Friberg, if not for your example, I don't think I would have got this idea.

Alberte, thank you for embarking this journey with me. I know that it has been frustrating, and I have not always been there for you. Now, it is your turn.

Finally, Konrad, my beloved son. You did not exactly help me with this project, however, you made everything worth it.

Contents

1	Introduction	1
1.1	Antarctica - The Least-known Continent	1
1.2	Thesis Motivation	2
1.3	Thesis Aims	3
1.4	Thesis Structure	3
2	Background	7
2.1	Overview	7
2.2	Tectonic Evolution	7
2.2.1	Archean Cratonic Nuclei and Nuna	11
2.2.2	Rodinia	12
2.2.3	Gondwana	13
2.2.4	West Antarctica	14
2.2.5	Post Gondwana	18
2.3	Geophysical Methods	19
2.3.1	Gravimetry	20
2.3.2	Magnetometry	21
2.3.3	Seismology	22
2.4	Solid Earth and ice sheets	28
2.4.1	Isostasy	28
2.4.2	Subglacial Topography	29
2.4.3	Geothermal Heat Flow	29
2.5	Improving Knowledge	31
2.5.1	A Statistical Toolbox	32
2.5.2	Application to Antarctica	35
3	The Computational Model	36
3a	A Grid for Multidimensional and Multivariate Spatial Representation and Data Processing	37
3a.1	Introduction	37
3a.2	The Computational Framework	38
3a.3	Implementation and Architecture	39
3a.3.1	Example of Grid Generation and Data Import	40

3a.3.2 Example of Visualization and Data Export	42
3a.4 Quality Control	43
3b The Antarctic Crust and Upper Mantle: A Flexible 3D Model and Software Framework for Interdisciplinary Research	47
3b.1 Introduction	48
3b.1.1 Geology, Geochronology, and Geochemistry	48
3b.1.2 Geophysics	49
3b.1.3 Solid Earth-Cryosphere Interactions	50
3b.1.4 Motivation for the 3D Grid Model	52
3b.2 Data	52
3b.3 Methods and Results	53
3b.3.1 Populating the 3D Grid	53
3b.3.2 Computational Framework: Usage Examples	53
3b.4 Discussion	65
3b.4.1 Limitations	65
3b.4.2 Insight from Examples	65
3b.4.3 Use Cases for the 3D Model and Software Framework	66
3b.5 Conclusions	67
4 A Multivariate Approach for Mapping Lithospheric Domain Boundaries in East Antarctica	72
4.1 Introduction	73
4.2 Data	75
4.3 Methods	75
4.3.1 Picking Boundaries	75
4.3.2 Generating Individual Spatial Likelihood Maps	76
4.3.3 Combining Distributions	77
4.4 Results	77
4.5 Discussion	78
4.5.1 Limitations	78
4.5.2 Correlation with Geological Observations in East Antarctica	78
4.5.3 Comparison with the Continent of Australia	79
4.5.4 New Insights into the Lithosphere of Antarctica	79
4.6 Conclusions	80
4.7 Acknowledgments	81
5 Antarctic Geothermal Heat Model: Aq1	86
5.1 Introduction	87
5.2 Data	89
5.2.1 Heat Flow Data	89
5.2.2 Observables	92
5.2.3 Data Preparation	95
5.3 Methods	96
5.3.1 Degree of Similarity	96

5.3.2	Weighting	97
5.3.3	Similarity Process and Optimization	97
5.3.4	Corrections of Heat Flow Values	99
5.3.5	Generating maps of heat flow and model metrics	100
5.4	Results	101
5.5	Discussion	104
5.5.1	Limitations of the Similarity Approach	104
5.5.2	Methodology Appraisal	104
5.5.3	Discussion of Uncertainties	105
5.5.4	Interpretation	105
5.5.5	Future Directions	107
5.6	Conclusion	108
5.7	Acknowledgments	109
6	Synthesis	110
6.1	Integrated Approaches	110
6.1.1	Enabling Computational Environment	110
6.1.2	Reconciling Results	111
6.1.3	Using Uncertainty to Advantage	113
6.1.4	Robust Results from Well-Posed Constraints	115
6.1.5	Probabilistic Approaches for Antarctica	115
6.2	Progress in Parallel	116
6.3	Ongoing Work	117
6.3.1	A Probabilistic Approach to Basement Geology	117
6.3.2	Regional Studies	117
7	Conclusion	120
	References	122
A	Supplementary Material: Chapter 3	171
A.1	Geological samples	171
A.2	Moho and Curie Temperature depth	173
A.3	Ternary maps	174
A.4	Short User Guide to agrid	179
A.4.1	Installation	179
A.4.2	Further resources	181
A.4.3	Version compatibility.	181
B	Supplementary Material: Chapter 4	182
B.1	Data	182
B.2	Methods	182
B.3	Results and Discussion	183
B.4	Additional material	184

C Supplementary Material: Chapter 5	190
C.1 NGHF Database. Heat flow Records Used in this Study	192
C.2 Aq1.AB, Generated with Additional <i>B</i> -rated Records in NGHF	193
C.3 Histogram of Misfit, and Sensitivity Analysis of Observables	195
C.4 RMSE and MAe Misfit with Decreased Weighting of Observables	196
C.5 Examples of Datasets Used	197
C.6 Comparing Global and Antarctic Datasets	202
C.7 Applied Glacial Isostatic Correction	203
C.8 Distance to Grid Centers	205
C.9 Aq1 in Lower Resolution	206
C.10 Similarity detection and Ψ values illustrated	208
C.11 Monte Carlo simulation of Ψ values for each observable to optimize similarity range	209
C.12 Parameter maps of metrics for K and Ψ , comparing step function similarity detection with the Gaussian similarity detection used.	211
C.13 Heat Production Diverging over Distance	212
C.14 Aq1.nv, Without Distance-to-Volcanoes Observable, Aq1.ns, without Moho and LAB Observables with Differences from Aq1, and Aq1.h250m, with a Differently Selected Heat Flow Catalog	213
C.15 Maps of Heat Flow Model Generated with Various Parameter Values	216
C.16 Aq1.nc, without Applied Correction, and Difference from Aq1.	218
C.17 Metrics of Cross-Validated Heat Flow Values	219
C.18 Aq1.au A Test Case for Australia, including Metrics and Brief Discussion . . .	221
C.19 Comparison of Heat Flow Distributions in Different Studies	223
C.20 Threshold Maps	224
C.21 Heat Flow Measurements in Antarctica	225
C.22 Robustness Map	226
C.23 Model Download and File Formats	227
C.24 Code Download	228

List of Figures

1.1	Exposed geology	2
1.2	Map of Antarctica, highlighting key geographical and geological regions.	6
2.1	Map of Antarctica with labels.	9
2.2	Suggested tectonic affinities from Boger (2011)	10
2.3	Tectonic reconstructions of the Neoproterozoic from Meredith et al. (2017)	15
2.4	Gondwana forming orogens	16
2.5	West Antarctic tectonic setting (Jordan et al., 2020).	17
2.6	Concepts of the lithosphere (Artemieva, 2011)	20
2.7	Potential field data from global and Antarctic studies.	25
2.8	Moho and LAB depth from global and Antarctic studies.	26
2.9	Crustal segmentation, seismic wave speed and mapped uncertainties.	27
3a.1	The structure of agrid.	40
3a.2	Examples of visualisations done in agrid.	46
3b.1	Oblique view of data held in the 3D grid model.	54
3b.2	Examples of simple calculated outputs and visualisation in map view.	56
3b.3	New maps generated to show the methodology of using data held in the 3D grid model.	57
3b.4	New maps generated for Wilkes Basin.	60
3b.5	New maps generated by combining constraints from geophysical and geological data.	61
3b.6	Comparison of heat flow models enabled by the 3D model and framework.	63
3b.7	Illustration of framework capability to extract depth profiles for model comparison.	64
4.1	Previously suggested boundaries and datasets used.	74
4.2	Likelihood maps of domain boundaries for each geophysical dataset used and cross section of likelihood field.	76
4.3	Six combined likelihood maps.	82
4.4	Correlation with observed geology.	84
5.1	Heat flow map of Antarctica, Aq1.	90
5.2	Cross plots of reference observables	91
5.3	Method optimization and correction applied.	98

5.4	Uncertainty metrics for the Aq1 heat flow model.	102
5.5	Comparison of Aq1 with previous published models.	103
5.6	Locations mentioned in text, and an alternative visualization of Aq1.	106
6.1	<i>agrid</i> layers.	112
6.2	Boundary model of Australia.	113
6.3	Information entropy and robustness for Aq1.	114
6.4	Preliminary results of fuzzy sets.	118
6.5	Aurora Subglacial Basin.	119
7.1	Icebergs on Prydz Bay.	122
A.1	Number of samples per 100 × 100 km bin in the compilation of Gard et al. (2019).	172
A.2	Illustration of framework capability: CTD and Moho.	173
A.3	Ternary map components.	176
A.4	Ternary maps.	178
B.1	Combined likelihood maps of the Australian continent.	184
B.2	Australian likelihood distributions with overlay crustal models.	185
B.3	Sketch of major boundaries suggested in previous studies and compilations.	187
B.4	Datasets used for this study and picked boundaries.	188
B.5	Tectonic reconstruction Australia and Antarctica.	189
C.1	NGHF database. Heat flow records used in this study	192
C.2	Aq1.AB, as generated from NGHF records with <i>A</i> and <i>B</i> ratings	193
C.3	Histogram of misfit, and sensitivity analysis of observables	195
C.4	RMSe and MAe misfit with decreased weighting of observables	196
C.5	Moho depth	198
C.5	LAB depth	199
C.5	Curie temperature depth	200
C.5	Curvature of gravitational field	201
C.6	Comparing global and Antarctic datasets	202
C.7	Applied glacial isostatic correction	204
C.8	Distance to grid centers	206
C.9	Aq1 in lower resolution	207
C.10	Similarity detection and Ψ values illustrated	208
C.11	a	209
C.11	Monte Carlo simulation of Ψ values for each observable to optimize similarity range	210
C.12	Parameter maps of metrics for <i>K</i> and Ψ	211
C.13	Heat production diverging over distance	212
C.14	Aq1.nv, Aq1.ns, Aq1.h250m variants	215
C.15	Maps of heat flow model generated with various parameter values.	217
C.16	Aq1.nc, without applied correction	218
C.17	Metrics of ross-validated heat flow values	219

C.17 (b) Detailed view of KDE plot of cross-correlated uncertainty and heat flow. . .	220
C.18 Aq1.au A test case for Australia	221
C.19 Comparison of heat flow distributions	223
C.20 Threshold maps	224
C.21 Heat flow measurements in Antarctica	225
C.22 Robustness map	226

Listings

3a.1	Initiation of Grid object	40
3a.2	Visualisation from agrid.	42
A.1	Setting up a grid model.	179
A.2	ant.ds content.	180
A.3	Make synthetic data.	180
A.4	Import data.	180
A.5	Make map.	181

List of Tables

3b.1 Datasets used to populate the grid, in alphabetic order.	69
3b.2 Thermal properties assigned to crustal domains.	70
5.1 Heat flow records in NGHF. Number of records after cleaning of data.	92
5.2 Observables used in this study. The content is discussed in the text.	94
B.1 Description of some of the main lithospheric features in Australia.	183

In loving memory of my mother.

Chapter 1

Introduction

1.1 Antarctica - The Least-known Continent

Hidden under kilometers of ice, the geology of Antarctica is enigmatic in its tectonic history and dynamic subglacial landscapes. There is a growing awareness of the need to overcome this inaccessibility and to better understand the least-known continent. The Scientific Committee on Antarctic Research (SCAR) provides international coordination of Antarctic research. In the context of *The 1st SCAR Antarctic and Southern Ocean Science Horizon Scan*, Kennicutt et al. (2014) compiled a list of 80 priority scientific questions. These questions cover a broad range of research areas, and many are directly linked to the subglacial geology and lithospheric structure. For example (Kennicutt et al., 2014, enumerated in supplementary material):

- 27 How do the characteristics of the ice-sheet bed, such as geothermal heat flux and sediment distribution, affect ice flow and ice-sheet stability?
- 35 How does the bedrock geology under the Antarctic Ice Sheet inform our understanding of supercontinent assembly and break-up through Earth history?
- 36 Do variations in geothermal heat flux in Antarctica provide a diagnostic signature of sub-ice geology?
- 37 What is the crust and mantle structure of Antarctica and the Southern Ocean, and how do they affect surface motions due to glacial isostatic adjustment?
- 38 How does volcanism affect the evolution of the Antarctic lithosphere, ice-sheet dynamics, and global climate?
- 40 How do tectonics, dynamic topography, ice loading and isostatic adjustment affect the spatial pattern of sea-level change on all time scales?

Accelerated by international initiatives associated with the 4th International Polar Year (IPY 2007/08, Luedeke et al. (2010)), new datasets have been systematically acquired in coordinated campaigns. Particularly, the cover of geophysical data advancing seismic, magnetic and cryospheric studies has been substantially improved (e.g., Golynsky et al., 2013b; Kanao et al., 2007; Mougnot et al., 2017).

An Australian contribution to address scientific questions about Antarctica, including those noted above, has been realised through the Antarctic Gateway Partnership between the University of Tasmania, the Australian Antarctic Division, and CSIRO, funded by the Australian Research Council's Special Research Initiatives scheme (Coleman, 2017). The thesis presented herein is an outcome from this partnership.

1.2 Thesis Motivation

The overarching motivation of this thesis is to contribute to two research areas: to better understand the lithospheric structure of Antarctica to gain insight as to the geological evolution of the continent, and to support interdisciplinary work, particularly studies of solid Earth and cryosphere interaction.

Antarctica has long been pictured as the hub in the break-up of Gondwana (Boger, 2011; Du Toit, 1937). Coastal outcrops have been linked to adjoined continents, but the architecture of the interior is not well understood (Whitehouse et al., 2019). Maps of the tectonic domains and boundaries with improved constraints for a range of lithospheric properties are required. With only 0.17% of Antarctica's surface exposed (Fig. 1.1), we depend on geophysical data and extrapolations to map the interior. Along the coast, as well as the Transantarctic Mountains, and at scattered nunataks (Fig. 1.2), we have sparse geological observations, geochemical and geochronological results (Boger, 2011). However, the analysis and contextualization of such information needs careful consideration and should be approached with an interdisciplinary

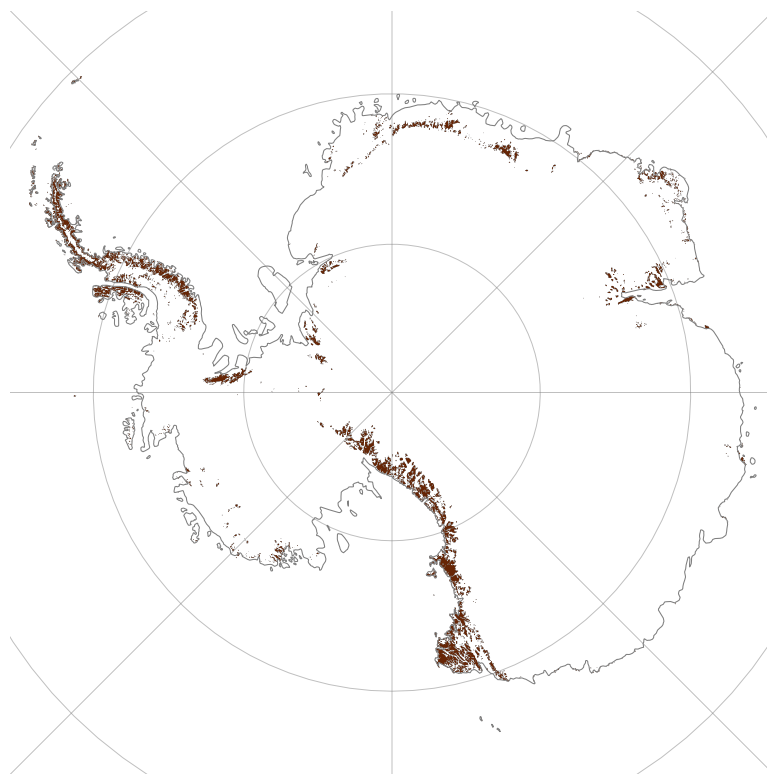


Figure 1.1: Only 0.17% of Antarctica is exposed outcrops, as highlighted by the orange regions on this map (modified from Burton-Johnson et al., 2016).

mindset.

Of highest importance, due to the immense volume of accumulated ice (Drewry et al., 1982), is the potential contribution of West and East Antarctica to global sea-level rise as a result of ongoing global heating (Rohling et al., 2019). Further, a recent study identified nine key areas where we are approaching an irreversible state, with severe impact for the world (Lenton et al., 2019). Such tipping points located in Antarctica are linked to properties of the upper mantle, the crust, and subglacial conditions. Understanding these areas from an Earth systems point of view is critical to unravel how tipping points may be reached and passed. The solid Earth plays a key role, via its interactions with ice sheets and glaciers due to isostatic adjustments, heat transfer, and erosion (Paxman et al., 2018; Whitehouse et al., 2019). Better understanding of the Antarctic lithosphere hence improves past and present ice-sheet models, as well as predictions of future ice mass changes. Physical properties, such as temperature, heat production, and viscosity, tens or hundreds of kilometers beneath the ice-covered Antarctic interior impact the livability of large areas of our planet and the future life for billions of people and ecosystems.

1.3 Thesis Aims

The research presented herein aims:

1. To enable multivariate models of the Antarctic lithosphere through a new computational framework and methodology. Particularly, this research addresses challenges in how to spatially combine low-resolution geophysical datasets with sparse geological observations. The framework shall facilitate probabilistic methods and improve the use of the uncertainties associated with the data.
2. To investigate the large-scale geology of Antarctica through probabilistic and multivariate methods. The research aims to develop existing methodology, introducing novel approaches to the identification of lithospheric boundaries and the nature of tectonic segmentation.
3. To reconcile the disparities in existing heat flow models through a multivariate and probabilistic approach. Heat flow is an important aspect of solid Earth and cryosphere interaction. This aim addresses the expressed need of ice sheet modellers for a robust estimate of the spatial distribution of geothermal heat flow into the base of the ice-sheets.

1.4 Thesis Structure

This thesis comprises four core chapters that have been published as papers in peer-reviewed journals. Each core chapter is structured and formatted for separate publication. References are merged and gathered at the end of the thesis. In the case of any minor differences between the published version and the text in this thesis, the published versions of the chapter take precedence. Such differences originates from final stage of proof editing in submitted papers. The core chapters are framed by this introduction, a literature review (Chapter 2), a synthesis of connecting concepts (Chapter 6.3.2), and final conclusions (Chapter 7).

The core research chapters stand alone as published in, or submitted to, their respective journals; therefore, background material is repeated as needed.

Chapter 2 - Background

In this chapter, I survey the existing literature that forms the background for the new studies in the core chapters. I provide an overview of the geological and geophysical research on Antarctica, including the interaction between the solid Earth and the cryosphere. A brief account is given of the statistical methods used in the following research.

Chapter 3 - The computational model

In this chapter, I present a new computational framework and a model of the Antarctic crust and upper mantle. The chapter is divided in two parts. I present *agrid*, a new software package, and second, a generated grid containing Antarctic solid Earth data and discussion about its potential use is presented.

Chapter 3a - A grid for multidimensional and multivariate spatial representation and data processing.

To perform complex computation involving multidimensional data and probabilistic approaches, a new spatial processing package is required. To meet this need, the package *agrid* is developed. The package is used to enable the research carried out in subsequent chapters. Here, I present the software structure and methods to import, process, and visualise data.

This chapter has previously been published: *Stål, T., and Reading, A. M. (2020). A grid for multidimensional and multivariate spatial representation and data processing. Journal of Open Research Software, 8(1), 1-10. <https://doi.org/10.5334/JORS.287>. Results have also been presented at ASOF, the Antarctica and Southern Ocean Forum - IEEE, 2018.*

Chapter 3b - The Antarctic crust and upper mantle: A 3D model and framework for interdisciplinary research.

By using *agrid*, a model of Antarctica is generated, containing published datasets of geophysics and geology. In this chapter, some of the functionality of the software package is exemplified and datasets are accessed to compute a new steady state heat flow model and maps of isostatic adjustment and segmentation. In the discussion, a probabilistic approach is suggested to account for the uncertainties in the Antarctic interior.

This chapter has previously been published: *Stål, T., Reading, A. M., Halpin, J. A., Phipps, S., and Whittaker, J. M. (2020). The Antarctic crust and upper mantle: a flexible 3D model and framework for interdisciplinary research. Frontiers in Earth Science doi: 10.3389/feart.2020.577502. Methods and preliminary results have also been presented at The International Union of Geodesy and Geophysics (IUGG) 27th General Assembly, 2019, and at the SCAR International Symposium on Antarctic Earth Sciences (ISAES), 2019.*

Chapter 4 - A multivariate approach for mapping lithospheric domain boundaries in East Antarctica.

In this chapter, I introduce a novel probabilistic method to combine multiple datasets with their uncertainty bounds, to map the likelihood of deep lithospheric boundaries. The resulting maps are compared with geological observations, where available, and are interpreted in terms of the geological complexity of the Antarctic interior.

This chapter has previously been published: *Stål, T., Reading, A. M., Halpin, J. A., and Whittaker, J. M. (2019). A Multivariate Approach for Mapping Lithospheric Domain Boundaries in East Antarctica. Geophysical Research Letters, 46(17-18), 10404-10416. <https://doi.org/10.1029/2019GL083453>*. Results have also been presented at the POLAR18 SCAR open science meeting, 2018.

Chapter 5 - Antarctic geothermal heat flow model Aq1.

A new geothermal heat flow map is produced to meet the need of the interdisciplinary community, working on modelling ice-sheet development and to advance our understanding of the Antarctic lithosphere. This study uses a large number of observables to link global heat flow data with Antarctica. In order to reach acceptable accuracy, existing similarity methodology that has been used elsewhere is refined to handle the large uncertainties and limited data in the sub-glacial interior of Antarctica. We utilize the software presented in Chapter 3a.

This chapter is accepted for publication (December, 2020): *Stål, T., Reading, A. M., Halpin, J. A., and Whittaker, J. M. (2020). Antarctic geothermal heat model: Aq1. Geochemistry, Geophysics, Geosystems*. Methods and preliminary results have also been presented at the SCAR Open Science Meeting, 2020.

Chapter 6 - Synthesis

In this chapter, I contextualize the contributions from this thesis. I also discuss emerging themes from the core research chapters and immediate future directions of research.

Methods and preliminary results have been presented at international (SCAR ISAES, Korea), and Australian (GSA SGTSG, Port Lincoln) meetings in 2019.

Chapter 7 - Conclusion

I conclude the thesis with a summary of the new tools, methods, and findings that have resulted during the course of the research described herein.

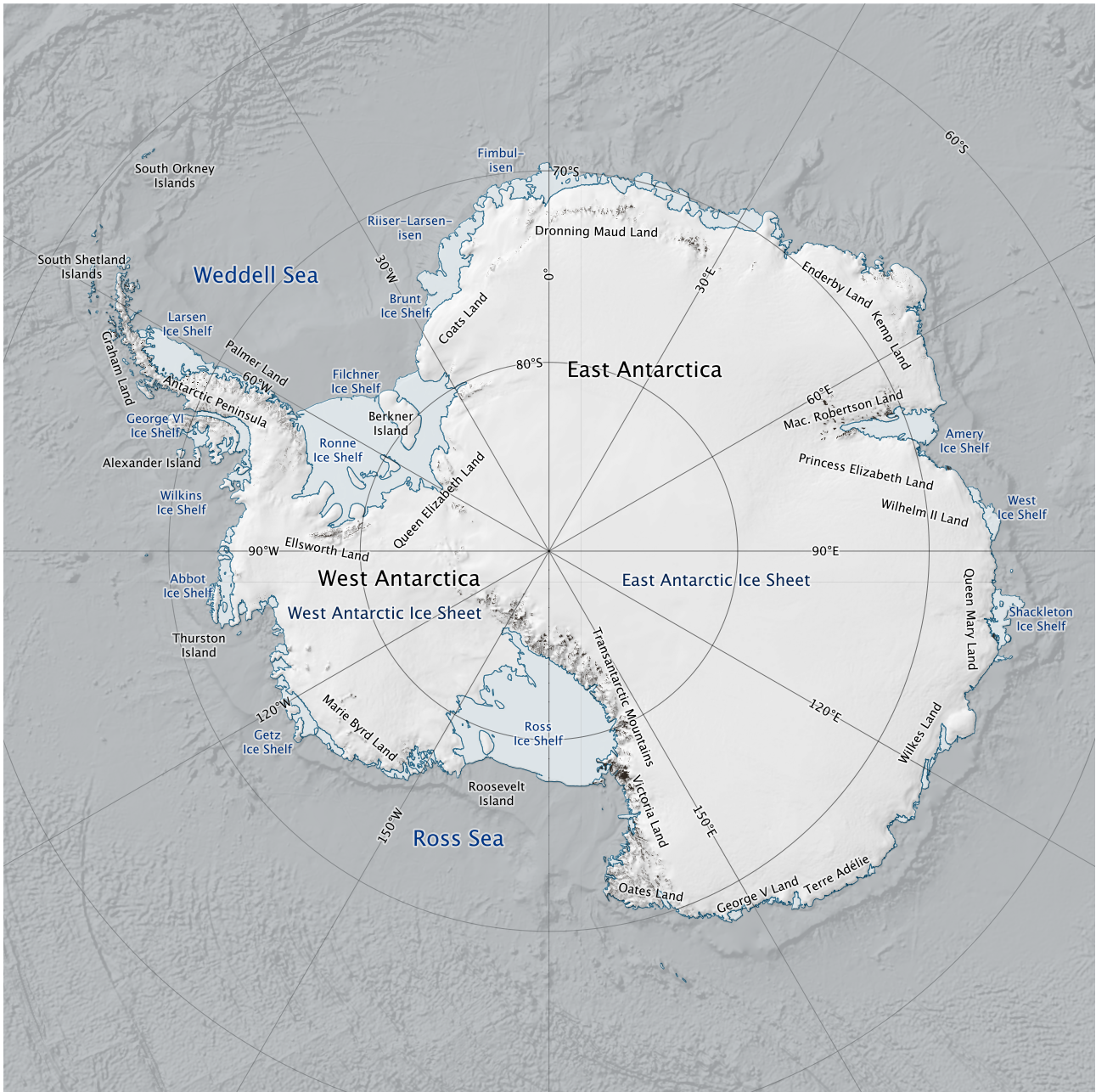


Figure 1.2: Map of Antarctica.

Chapter 2

Background

2.1 Overview

This chapter provides an overview of existing and ongoing research into the Antarctic lithosphere. The geologic background is presented as a summary of the current understanding of Antarctica's tectonic evolution. A survey of previous geophysical studies is then provided, together with research concerning the interactions between the ice sheets and the solid Earth, including geothermal heat flow. A critical appraisal follows, which gives the rationale for the focus on multivariate analysis and modelling in the research described in this thesis. Examples of such multivariate techniques are briefly summarised, followed by approaches to the constructive use of uncertainty metrics. Geochronological ages, and plate reconstruction timings in this chapter are stated in years, with a generally accepted tectonic narrative given in terms of the geological time scale. The review leads up to the state of understanding in 2018, with a few mentions of more recent studies. Locations mentioned in the text are indicated in Figures 1.2 and 2.1.

2.2 Tectonic Evolution

Early studies of the large-scale geology and tectonic structure of Antarctica provided impressive overarching insight, and many aspects remain unchallenged (e.g., Elliot, 1975; R. J. Adie, 1977; Ravich et al., 1965; Taylor, 1914). East and West Antarctica were identified as contrasting continental regions: East Antarctica being mostly Precambrian and including cratonic blocks, and West Antarctica being younger with some active tectonics. The exposed tectonic domains were mapped, named, and interpreted as pioneering studies spread more widely (Tingey et al., 1991). Fitzsimons (2003) pointed out the potential complexity of the East Antarctic interior by connecting Australian basement provinces to Antarctica and highlighting the uncertainties in the extrapolation of the mobile belts that run between the cratons. Boger (2011) presents an overview of the tectonic development of the whole continent, defining the extent of regions of Antarctica that have a tectonic affinity with surrounding Gondwana continents: African, Indian, and Australian affinities, West Antarctica, and a large block in the interior of no known affinity, the Crohn Craton (Fig. 2.2). Harley et al. (2013) discusses the geological segmentation

Figure 2.1: Place names within Antarctica, including localities discussed in this chapter. Shading is a smoothed version of BEDMAP2 subglacial topography from Fretwell et al. (2012). Smoothing is carried out using a Gaussian kernel with $\sigma = 10$ km. Geographic locations mentioned in text: AI = Alexander Island, AIS = Amery Ice Shelf, AP = Antarctic Peninsula, ASB = Aurora Subglacial Basin, BH = Bunger Hills, CL = Coats Land, DA = Dome Argus, DC = Dome Circle, DF = Dome Fuji, DML = Dronning Maud Land, ELL = Ellsworth Land, EnL = Enderby Land, GB = Gaussberg, GSM = Gamburtsev Subglacial Mountains, GVL = George V Land, HN = Haag Nunataks, KL = Kemp Land, KWL = Kaiser Wilhelm II Land, LD = Law Dome, LHB = Lützow-Holm Bay, LV = Lake Vostok, MBL = Marie Byrd Land, MF = Mirny Fault, MR = Miller Range, MRB = Mac. Robertson Land, OL = Oates Land, PCM = Prince Charles Mountains, PEL = Princess Elizabeth Land, PIG = Pine Island Glacier, PL = Palmer Land, QML = Queen Mary Land, SC = Siple Coast, SP = South Pole, SSB = Shmidt Subglacial Basin, SR = Shackleton Range, SRM = Sør Rondane Mountains, TA = Terre Adélie, TAM = Transantarctic Mountains, TG = Thwaites Glacier, TI = Thurston Island, VeH = Vestfold Hills, VoH = Vostok Highlands, VL = Victoria Land, VSB = Vincennes Subglacial Basin, WD = West Antarctic Ice Sheet (WAIS) divide, WL = Wilkes Land, WSB = Wilkes Subglacial Basin. Black pentagons indicate locations of year-round COMNAP listed stations. Labelling is shown for selected stations: 1 = Amundsen-Scott South Pole, 2 = Belgrano II, 3 = Bharati, 4 = Casey, 5 = Concordia, 6 = Davis, 7 = Dumont d’Urville, 8 = Great Wall, 9 = Halley VI, 10 = Jang Bogo, 11 = Mawson, 12 = McMurdo, 13 = Mirny, 14 = Neumayer III, 15 = Novolazarevskaya, 16 = Oasis, 17 = Orcadas, 18 = Palmer, 19 = Rothera, 20 = SANAE IV, 21 = Syowa, 22 = Troll, 23 = Vostok, Additional regions and locations are given in Figure 1.2.

of Antarctica in the present research context, noting the need to resolve questions relating to the early supercontinents, and highlighting the need for an interdisciplinary approach. Geophysical studies are acknowledged to provide the best constraints for the crustal architecture and derived properties in the Antarctic interior. A recent review by Jordan et al. (2020) summarized West Antarctic geology and tectonics and exemplifies how interdisciplinary perspectives can advance our understanding of solid Earth systems. Observations from sparse outcrops are contextualised and interpolated with geophysical datasets and provide insight to the tectonic processes that formed the region.

Antarctica may be described as the hub of Gondwana, as other continental blocks surrounded East Antarctica before the breakup (Du Toit, 1937; Harley et al., 2013; Torsvik et al., 2008). This concept is further accentuated by Antarctica’s relatively steady position near the geographical South Pole for the past 330 Ma while adjoining continents have been radiating northward (Torsvik et al., 2010; Williams et al., 2011). Antarctica is also relatively stable at present, with limited internal deformation and slow rotation (Amalvict et al., 2009). This low tectonic activity is reflected by observed low seismicity (Kanao, 2014; Reading, 2002). The few earthquakes that occur are mainly associated with the uplift of the Transantarctic Mountains and along the continental margin related to glacial isostatic adjustment (Reading, 2007). No earthquakes above M5 are reported on the Antarctic continent. Intraplate events up to M4 have been recorded in East Antarctica, with a similar density distribution to the Canadian shield (Lough et al., 2018). A number of stronger events have occurred closer to the surrounding spreading ridges and fault zones, such as the M8.1 earthquake in 1998 near Balleny Island (Kreemer et al., 2000; Tsuboi et al., 2000), and the 2004 M8 Macquarie Ridge Earthquake (Watson et al., 2010). The present movement of GPS sites located on the Antarctic conti-

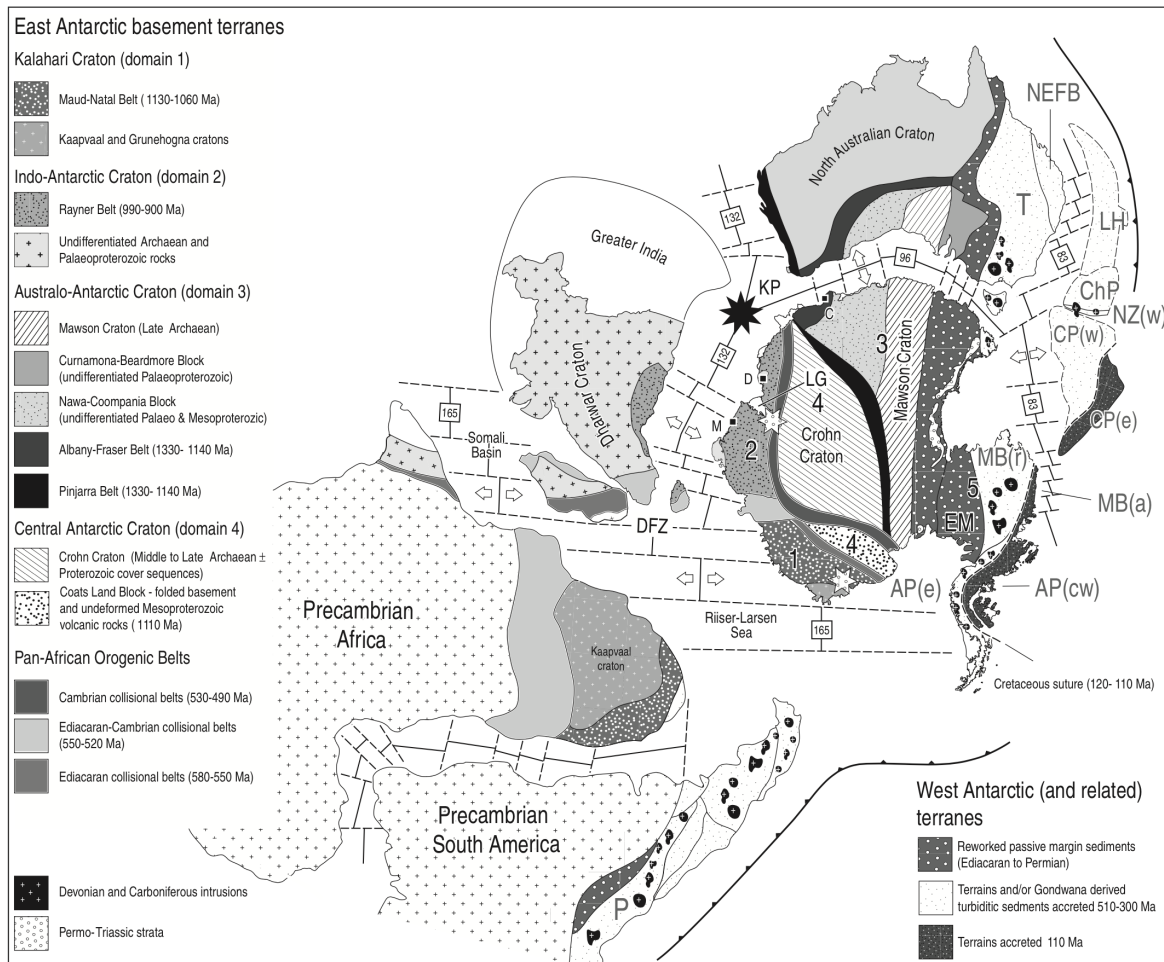


Figure 2.2: Suggested tectonic affinities for East Antarctic basement terranes from Boger (2011). 1: Rocks with African affinities. 2; rocks with Indian affinities. 3; rocks with Australian affinities. 4; A block with unknown affinity, 5: West Antarctica, accreted pre- and post-Gondwana sediments, arc, and para-autochthonous terranes. Zealandia (NZ) here is the continuation of West Antarctica. AP = Antarctic Peninsula, C = Casey Station, ChP = Challenger Plateau, CP(w) = Campbell Plateau, D = Davis Station, DFZ = Davey Fracture Zone, KP = Kerguelen Plateau, LG = Lambert Graben, LH = Lord Howe Rise, M = Mawson Station, MB = Marie Byrd Land, NEFB = New England Fold Belt, NZ = New Zealand, T = Tasmanides Outboard terranes.

mental plate is dominated by the tectonic plate motion, with a component of glacial isostatic adjustment (Cande et al., 2004; Martín-Español et al., 2016; Turner et al., 2020; Whitehouse, 2018).

The architecture of the Antarctic lithosphere is the result of continental building events related to the supercontinental cycle (e.g., Collins et al., 2005; Merdith et al., 2017; Nance et al., 2013; Nance et al., 2014). East Antarctica contains remnants of all known supercontinents with a geological history stretching over 3.6 Ga. A better understanding of Antarctica is of the highest priority to form robust reconstructions of early supercontinents, such as Nuna and Rodinia, and to improve the detailed fit of the continents forming Gondwana (Boger, 2011; Collins et al., 2005; Fitzsimons, 2000a; Harley et al., 2013; Zhao et al., 2004).

Ongoing initiatives aim to compile and facilitate analysis of large amounts of geological observations and samples for Antarctica. Gard et al. (2019) provided a database with geochemical and geochronological whole rock data. Cox et al. (2018) presented ongoing collaboration to compile geologic maps and standardise the legends. Such efforts can facilitate statistical analysis but also suffer from sample bias. Locations near stations are better studied, and more resistant outcrops remain when softer materials have been eroded.

2.2.1 Archean Cratonic Nuclei and Nuna

Each of the East Antarctic blocks defined by Boger (2011) contain Archean cratonic crust (Fig. 2.2) and could be regarded as the nucleus of the continent. However, by convention, this is usually accredited to the most ancient parts of Terre Adélie and George V Land, known as the Mawson Block (Boger, 2011; Payne et al., 2009). This domain was split between the Gawler Craton in Australia, and the Terre Adélie Craton in Antarctica at the break-up of Gondwana. The western part of Dronning Maud Land (Fig. 2.1) includes the Archean Grunehogna craton, composed of granitic gneisses and Mesoproterozoic sedimentary rocks. This block is related to the South African Kalahari-Kaapvaal Craton (Groenewald et al., 1995). Princess Elizabeth Land, Mac Robertson Land, Kemp Land, and Enderby Land have the greatest affinity with India; however, the timing of assembly for the various Indo-Antarctic domains has been debated (Boger, 2011; Harley et al., 2013; Mulder et al., 2019). Kemp Land contains the reworked Archean margin of the Napier Complex (Halpin et al., 2007a).

The geology between western Wilkes Land and eastern Princess Elizabeth Land is more difficult to correlate to present continents as the adjoined geology relates to part of Greater India that is now subducted beneath the Himalayan orogen. Microcontinents in the eastern Indian Ocean (Gardner et al., 2015; Halpin et al., 2017) and areas of extended continental crust adjacent to southwestern Australia (Halpin et al., 2008) and Wilkes Land (Halpin et al., 2020; Halpin et al., 2008) formed during the break-up of Gondwana and during subsequent continental drift between India and Australia. From geochemical and geochronological results from sediment cores, Daczko et al. (2018) suggested that the Gondwanan Australian-Greater India suture continues into Antarctica in the vicinity of the Mirny Fault. Pb isotope compositions in feldspar suggest that the coastal outcrops, Vestfold Hills and Napier Complex, show strong similarities with the Dharwar Craton in India (Flowerdew et al., 2013). However, samples from the Rauer Terrane and Ruker Complex, south of the Vestfold Hills and Napier Complex, respectively, show non-radiogenic compositions that do not resemble those found in any other

continent. Boger et al. (2004) and Flowerdew et al. (2013) postulates that they represent an Antarctic Craton that is unexposed in the interior beneath the East Antarctic Ice Sheet. Boger (2011) names this enigmatic domain 'The Crohn Craton' and argues that Prince Charles Mountains, the Ruker Complex, and perhaps the Rauer Terrane, are the northern flank of this craton. This craton would also reach the coast at Denman Glacier, wedged between blocks with Australian and Indian affinities. Other authors present evidence for a complex architecture in the Prince Charles Mountains, with multiple reworking events (Corvino et al., 2008; Phillips et al., 2009). Based on an extensive geochemical analysis, Mulder et al. (2019) suggest an Indo-Antarctic affinity for the Rauer and Ruker provinces. With this understanding, there is no need for another block (the Crohn Craton); rather, a major Gondwana plate boundary between Indo-Antarctic and Australo-Antarctic affinities.

For much of the Palaeoproterozoic, the ancient terranes of Antarctica and Australia probably formed an isolated block that amalgamated with Nuna in the earliest Mesoproterozoic, 2.5 to 1.6 Ga (Aitken et al., 2016; Betts et al., 2016; Harley et al., 2013; Maritati et al., 2019; Mulder et al., 2018; Tucker et al., 2017). The Nimrod-Kimban Orogeny was a collision between the Mawson block, the poorly constrained Beardmore micro continent, and the Curnamona and North Australian Cratons (Boger, 2011); however, the configuration of continental blocks is debated. The Terre Adélie Craton underwent metamorphic processes at 1.7–1.5 Ga (Ménot et al., 2007; Naumenko-Dèzes et al., 2020), and the extent of this orogen is not resolved. Some studies suggest that the belt continues uninterrupted across Antarctica, reaching the outcrops of the Miller Range, Shackleton Range (Fig. 2.1), and the Gawler Craton in Australia (Payne et al., 2009). The formation of the Miller Range is thus a key to informing the geometry and timing of the Nuna amalgamation. A link has been made between events that formed the Miller Range and processes on the active margin of Laurentia (Goodge et al., 2008). Mulder et al. (2018) suggests that the Miller Range is part of Laurentian crust, and its evolution at 1.7 Ga was unrelated to Australo-Antarctica.

2.2.2 Rodinia

East Antarctica's latitude is constrained by palaeomagnetic data dating to 1.1 Ga from Bunger Hills (Liu et al., 2018) and Dronning Maud Land (Jones et al., 2003). These findings suggest that Dronning Maud Land and Bunger Hills were not rigidly connected at the time of formation, and that the terranes have been rotated approximately 40° southward since the dykes were formed. In the middle to late Mesoproterozoic, extension and rifting took place along the proto-Darling Fault, west of the Mawson Block (Dentith et al., 1993). According to Boger (2011), at 1 Ga another block was added to East Antarctica, the aforementioned Crohn Craton. The formation of Rodinia is associated with the Grenville Orogeny. This global, long lasting mountain building event occurred over 250 million years (Fitzsimons, 2000b; Rivers, 1997), and impacted all present day continents (Fig. 2.3a). India, East Antarctica, and Australia were impacted by the events that built the Albany Fraser orogen, which extends along the southeastern edge of the present day Yilgarn Craton of west Australia and into coastal Wilkes Land as well as into the Eastern Ghats between Antarctica and greater India (Fig. 2.2). During the formation of Rodinia, the Grenville Orogeny formed terranes along the coast of what is now East Antarctica, such as the Grenville-aged Maud Province in Dronning Maud Land (Jacobs

et al., 1998). Island arcs were incorporated in to the orogen, including the Kottas Mountains (Groenewald et al., 1995; Jacobs et al., 2003, 1998). Dronning Maud Land changed from subduction-accretion, continental collision to post-collisional processes during and after the assembly of Gondwana, as suggested by U–Pb zircon geochronology and isotope geochemistry (Wang et al., 2020). From zircon analysis and geochemistry of detritus transported from the ice covered interior of Dronning Maud Land, Jacobs et al. (2015) proposed the existence of a large Tonian Oceanic Arc Super Terrane (TOAST). Its extent has also been constrained from airborne magnetic data (Ruppel et al., 2018).

The global reorganisation of tectonic plates from Rodinia to Gondwana was a dynamic period that again changed the configuration of the continents (Aitken et al., 2016; Collins et al., 2005). From 1 Ga to 420 Ma, East Antarctica was located at tropical and subtropical southerly latitude. From 400 Ma, it started drifting south (Torsvik et al., 2008; Torsvik et al., 2010). The Grenville-age orogenic belts have subsequently been reworked and overprinted (e.g., Fitzsimons, 2003; Jacobs et al., 1998).

2.2.3 Gondwana

The formation of Gondwana, as the most recent cycle in which the majority of continental material on Earth was joined, provides constraints with significant implications for the geology of the interior of East Antarctica (Fig. 2.3b). Although these are expected to be more robust than the evidence for the detailed configuration of earlier supercontinents, they are nevertheless subject to an ongoing debate. The absence of firm evidence for pre-Gondwana craton extent and terrane boundaries in Antarctica makes it difficult to draw cratonic boundaries, and date sutures (Boger, 2011; Fitzsimons, 2003; Meert, 2003; Mulder et al., 2019).

The extended Kaapvaal Craton, and the rest of what was to become West Gondwana, collided with Dronning Maud Land, Madagascar, and India, reworking previous terranes (Board et al., 2005; Fitzsimons, 2000a). At 550 Ma, Australia–Antarctica was one of the last continents to amalgamate. A central, however not well defined, concept in the formation of Gondwana is the Pan-African Orogeny (Figs. 2.4a–b), a series of spatially and temporally distinct Neoproterozoic to Cambrian events, that also affected Antarctica (600–450 Ma) (e.g. Yoshida et al., 2003).

One or two Gondwana-forming orogens are believed to intersect East Antarctica: The western East African Orogen (e.g., Jacobs et al., 1998), and the eastern Kuunga Orogen (e.g. Meert, 2003). The later is sometimes referred to as Pinjarra e.g. Fitzsimons, 2003, or Prydz-Denman, depending on how it is contextualised in relation to Africa, Australia, or regionally. Extrapolations of known structures from the rest of Gondwana provide a possibility to map the Antarctic interior, however, how they project inland is still controversial, as is their timing and how they interact (Boger, 2011; Grantham et al., 2013; Meert, 2003; Mulder et al., 2019). Rocks of similar metamorphic age from the Naturaliste Plateau, in the present-day Indian Ocean, have been dated to the later Indo-Australian Pinjarra Orogen at 515 Ma, and correlated to outcrops in the Denman Glacier region (Halpin et al., 2008). Fitzsimons (2003) provided suggestions of how the eastern orogen, here named Pinjarra, could intersect Antarctica inland from Prydz Bay; west, through Prince Charles Mountains, south-west towards Shackleton Range, or directly south, through Gamburtsev Subglacial Mountains.

Meert (2003) argued for a Kuunga belt across Africa, continuing between the suggested Crohn Block, Australia, and Greater India, welding Sri Lanka to Lützow Holm Bay (Boger et al., 2004; Yoshida et al., 1992). The Shackleton Range and Sør Rondane Mountains have also been associated with Pan-African events (Kleinschmidt et al., 2009; Will et al., 2010, 2009), and might form the junction where three generations of super-continent forming orogens meet. The relation with older tectonic events is, however, poorly constrained. How does the suggested trend of East African Orogen agree with the continuity of the older Nimrod–Kimban? Are the Archean Proterozoic domains, that are exposed at scattered outcrops around the East Antarctic Ice Sheet, connected in the formation of Rodina, or Gondwana? Or did they belong to the same cratonic shield, suggesting that the entire interior of East Antarctica remains unaffected by major tectonic events?

Regardless of the exact extent and internal correlation, the Pan-African orogeny is likely to be responsible for substantial East Antarctic crust formation. As a global reference, only 9% of continental crust was formed during the Archean, 56% formed during the Precambrian, and 35% formed during the Phanerozoic (Rudnick et al., 1995).

On the opposite side of Antarctica, along the Pacific margin of East Gondwana, the Ross–Delamerian Orogeny impacted East Antarctica, Zealandia, and eastern Australia during the Cambrian to Ordovician (e.g., Boger, 2011; Federico et al., 2009; Lindow et al., 2016; Wombacher et al., 2000). With this event, West and East Antarctica were joined, and the most recent, significant additions of Antarctic lithosphere were made to the Pacific side by terrane amalgamation and through crust generation (Jordan et al., 2020). Subduction ceased along Antarctic Peninsula at 20 Ma (Larter et al., 1991).

2.2.4 West Antarctica

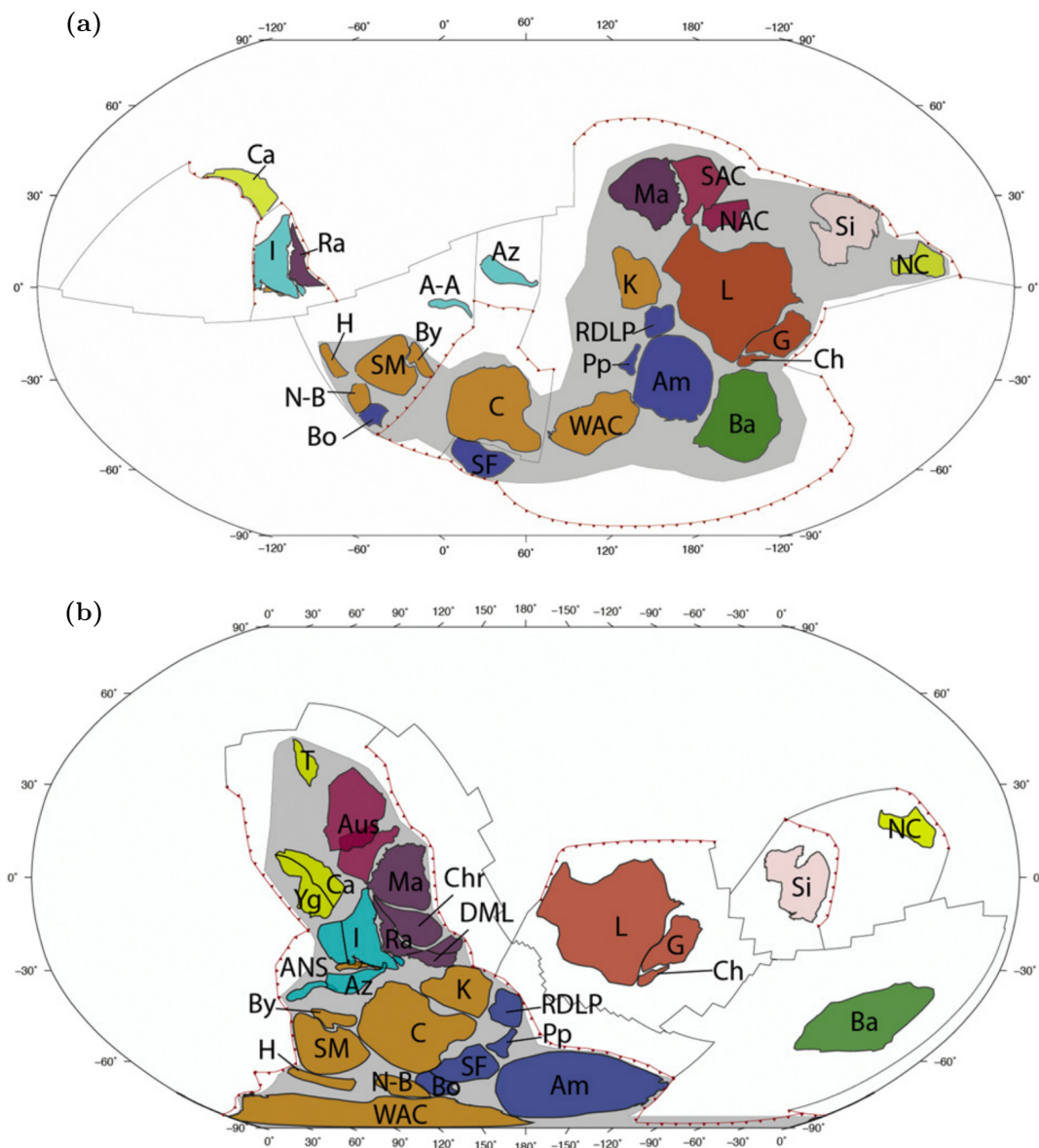


Figure 2.3: Tectonic reconstructions of the Neoproterozoic from Merdith et al. (2017). (a) 1000 Ma (b) 520 Ma; A-A, Afif-Abas Terrane; Am, Amazonia; Az, Azania; Ba, Baltica; Bo, Borborema; By, Bayuda; Ca, Cathaysia (South China); C, Congo; Ch, Chortis; Chr, Chron Craton; G, Greenland; H, Hoggar; I, India; K, Kalahari; L, Laurentia; Ma, Mawson; NAC, North Australian Craton; N-B, Nigeria-Benin; NC, North China; Pp, Paranapanema; Ra, Rayner (Antarctica); RDLP, Rio de la Plata; SAC, South Australian Craton; SF, São Francisco; Si, Siberia; SM, Sahara Metacraton; WAC, West African Craton. Cratonic crust is coloured by present-day geography: Antarctica, purple; North America, red; South America, dark blue; Baltica, green; Siberia, grey; India and the Middle East, light blue; China, yellow; Africa, orange; Australia, crimson.

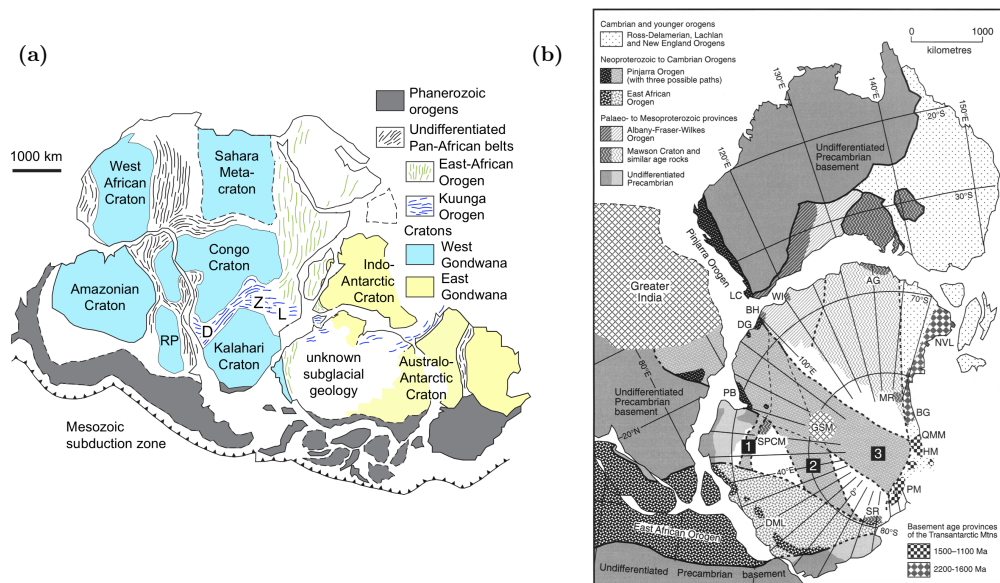


Figure 2.4: Overview of Gondwana forming orogens, showing East African Orogen and Kuunga Orogen, highlighting the uncertainties involved. (a) Modified from Fitzsimons (2016) The map also indicates the extent of later Phanerozoic orogens. D = Damara, Z = Zambezi, and L = Lurio belts. RP = Rio de la Plata Craton. (b) suggested potential pathways for the Pinjarra Orogen across the Antarctic interior from Fitzsimons (2003). AG, Terre Adélie-King George V Land; BG, Beardmore Glacier; BH, Bunger Hills; DG, Denman Glacier; DML, Dronning Maud Land; GSM, Gamburtsev Subglacial Mountains; HM, Horlick Mountains; LC, Leeuwin Complex; MR, Miller Range; NVL, northern Victoria Land; PB, Prydz Bay; PM, Pensacola Mountains; QMM, Queen Maud Mountains; SPCM, southern Prince Charles Mountains; SR, Shackleton Range; WI, Windmill Islands. Further details about the map are given in Fitzsimons (2003).

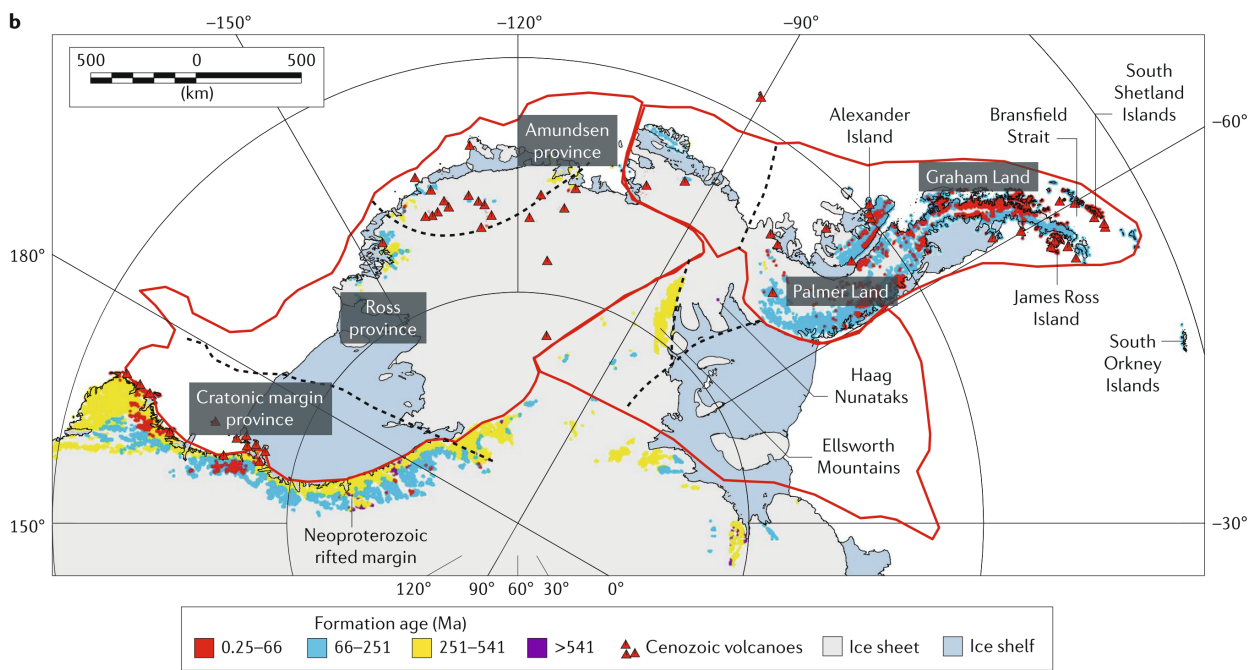


Figure 2.5: Structure of West Antarctica from Jordan et al. (2020). Red lines show the extent of pronounced domains.

West Antarctica's history is short and dynamic. The geology can be divided into three pronounced domains (Fig. 2.5): The oldest Weddell Sea region, the elevated Marie Byrd Land, together with low-lying the West Antarctic Rift System, and finally the Antarctic Peninsula (Jordan et al., 2020). In contrast to East Antarctica, the region is strongly influenced by volcanism, and the crust is thin (An et al., 2015a; Baranov et al., 2018; Chaput et al., 2014; Harley et al., 2013) (Fig. 2.8a). The only dated rocks of Precambrian age are from the Haag Nunataks in the southern Antarctic Peninsula (Wareham et al., 1998), which belong to the Weddell Sea Region. The central part of West Antarctica is believed to be shaped by a continental rift system (Huerta et al., 2007; Siddoway, 2008; Yakymchuk et al., 2015). Tectonic development along the Pacific margin dates back to the Ediacaran, when sediments from a passive margin started to be reworked in the Terra Australis orogen. Those reworked passive margin sediments now form the land between the Ross and Ronne Ice Shelves. The central part of West Antarctica consists of slope deposits and turbidites with volcanic intrusions. The Antarctic Peninsula was formed by an ocean-continent collision (Larter et al., 1991), associated with the formation of the South American Andes (e.g., Siddoway et al., 2004b). Accretion along the Pacific coast of the older parts of West Antarctica began in the Paleozoic (510–300 Ma). During the formation Pangea, further terranes were accreted up until 110 Ma to form today's Antarctic Peninsula. Volcanism occurs in the West Antarctic Rift System, a result of late Mesozoic and Cenozoic convergence and divergence between East and West Antarctica. Evidence for active Cenozoic extension comes from indirect data, such as marine magnetic surveying, plate reconstructions, and dynamic mantle models (e.g Cande et al., 2000; Huerta et al., 2007). 43 to 26 Ma was the main pulse of deformation when West Antarctica was extended by 180 km through crustal thinning. Studies report volcanism, high heat flow and basal melting of the West Antarctic ice sheet (e.g., Lough et al., 2013; Schroeder et al., 2014; Wyk de Vries et al., 2018).

Artemieva et al. (2020) provides an alternative interpretation of West Antarctica as a back-arc basin system, flanked by a volcanic arc. This suggestion puts West Antarctica in a similar setting as the present Japan Sea. The main justification for this alternative explanation is the low equivalent hypsometry of West Antarctica, down to -1.6 km (Fig. 2.1).

2.2.5 Post Gondwana

Jurassic pyroclastic rocks and tholeiitic basalts (Ferrar Group) are found in the Ross Sea sector of the Transantarctic Mountains (Elliot, 1992), and are interpreted to represent the onset of the rifting and break-up of Gondwana. The last separation of major continental blocks of East Antarctica was between Antarctica and Australia (Torsvik et al., 2008). A rapid seafloor spreading was established at 43 Ma (Whittaker et al., 2013b). Blocks of continental crust were detached to form microcontinents as the Batavia and Gulden Draak knolls. Extended continental crust, such as the Naturaliste Plateau and Bruce Rise, was formed on the continental shelves and slope (Gardner et al., 2015; Halpin et al., 2020; Halpin et al., 2008, e.g.). In the middle to late Eocene (30 Ma), Tasmania detached from Antarctica to open the first circum-antarctic oceanic gateway and initiated the oceanographic conditions we see today (Brown et al., 2006), with implications for Antarctic and global climate (e.g., Siebert et al., 2008). The details of the northward Australian drift from Antarctica and the geometry of the eastern

section of the Gondwana break-up have been debated. Particularly, the Kerguelen Plateau has been associated with deep mantle processes, continental fragments, or a combination of the two (Frey et al., 2000; Spain et al., 2020; Watson et al., 2016). Limited recent tectonism has taken place in East Antarctica, for example, the potassic volcanism at Gaussberg (Foley et al., 2004; Salvioli-Mariani et al., 2004; Sheraton et al., 1980a; Tingey et al., 1983). The volcano is located in a unique and poorly constrained geothermal setting, and the eruption history is largely unknown.

Using combined magnetic data and modern plate reconstruction tools, Whittaker et al. (2007) correlate the Australian path with the Hawaiian Emperor seamount chain and argue for a direction change at 53-50 Ma, related to the Pacific-Izanagi spreading ridge. With the addition of gravity data from Andersen et al. (2010) and Kuszniir (2008), Whittaker et al. (2013b) and Williams et al. (2011) present improved full-fit reconstructions of the Australian-Antarctic margins from 160 Ma with adjusted rotation angles. The correlation between Australia and Antarctica is further developed by Aitken et al. (2016, 2014), supporting the Williams et al. (2011) *Leeuwin model* and linking the Mertz Glacier Shear Zone with the Kalinjala Mylonite Zone (Fitzsimons, 2003; Williams et al., 2011) based on new subglacial topography, magnetic, and gravity data. Using this correlation, a tectonic map of Wilkes Land is generated by extrapolating Australian geology guided mainly by magnetic anomalies. A number of piercing points are defined and defended in further support the Leeuwin model (Williams et al., 2011); however, the geology of Southern Australia that was adjoined to Wilkes Land is covered under thick sediments. Maritati et al. (2019) uses data from remote outcrops in Wilkes Land to better constrain the covered basement at the conjugate margin, and hence show how observations from East Antarctica can help us to better understand the hidden geology of Australia.

2.3 Geophysical Methods to Constrain Lithospheric Properties

The theory of plate tectonics, on which the preceding section is based, depends on the idea of a rigid or elastic upper layer, the lithosphere, in contrast to the underlying plastic asthenosphere. The lithosphere consists of the crust and the upper part of the mantle, defined by chemical composition and density (Anderson, 1995; Artemieva, 2011; Barrell, 1914). Christensen (1988) defines the lithosphere based on its rheology and the lithosphere-asthenosphere boundary (LAB) as a transition into a zone that can respond as a weak material to stress and exhibits low seismic velocities. More generally, the concept of the lithosphere requires proper specification of the properties that have been considered in its definition, and recent literature provides a more general discussion of a number of approaches to define the lithosphere from mechanical, temperature, tectonic, or electrical properties (Artemieva, 2011; Rychert et al., 2009) (Fig. 2.6).

In the following section, geophysical investigations that yield information regarding the physical properties of the crust and deeper lithosphere are summarised. The focus is on studies that provide the most significant geophysical information on the lithosphere of Antarctica using gravimetry, magnetometry, and passive seismic methods.

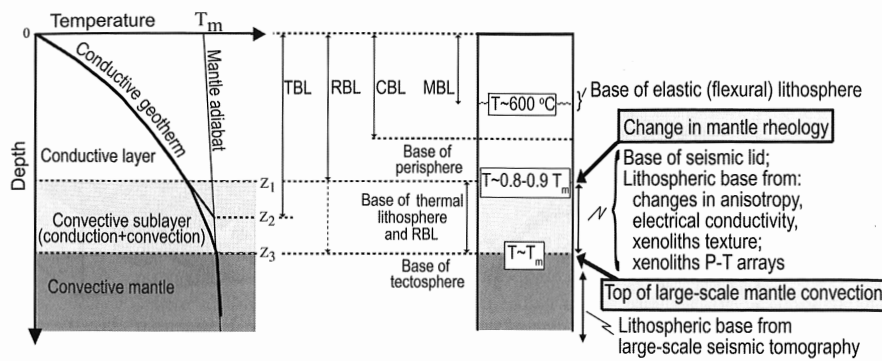


Figure 2.6: Alternate ways to define the lithosphere-asthenosphere boundary (LAB). This figure from Artemieva (2011) shows possible interpretations and uncertainties of the LAB depth and boundary layers. Z_1 is the depth where the lithosphere is stable and heat conducts to the surface. Z_2 is the depth to an extrapolated lithospheric geotherm, reaching the temperature of a convecting mantle (solidus). Z_3 is the actual depth to the mantle where heat is transported by convection. At this depth, the temperature difference between the continental lithosphere and oceanic lithosphere ceases.

2.3.1 Gravimetry

Gravimetry is the measurement of the gravitational attraction of Earth. By correcting for the influence of external celestial bodies and altitude, free-air gravity acceleration is calculated (Fig. 2.7b). This is the gravity force as it would be sensed at sea level (Kearey et al., 1991). Further, the horizontal force, that is the attraction to the terrain, is removed to produce a Bouguer anomaly model (e.g., Scheinert et al., 2016). This is the gravity as it would act on a flat surface in a perpendicular direction, and it represents varying density beneath the instrument. The method detects heterogeneities that might result from composition or temperature changes. A positive free-air anomaly combined with a weak Bouguer anomaly indicates a structure supported by the strength of the lithosphere, and a weak free-air anomaly with a strong negative Bouguer anomaly indicates that the structure is compensated with deep buoyant roots. When gravity measurements are acquired on 2D-lines or 3D surfaces, they can be filtered such that short wavelength anomalies represent shallow variations while long wavelengths represent deeper density anomalies.

Satellite surveys in Antarctica can essentially provide long-wavelength datasets of the same quality as for other continents. Gravity anomaly studies are important to infer low-resolution physical properties of the Antarctic interior. They are therefore most useful on a continental to regional scale (Tenzer et al., 2018). Airborne studies are still scarce in large parts of the interior of Antarctica, however needed to cover the polar satellite gap for some missions (Forsberg et al., 2017; Sneeuw et al., 1997). Global gravity datasets include EIGEN-6C2 (Förste et al., 2013) with Free-air and Bouguer anomalies calculated by the International Centre for Global Earth Models, GFZ-Potsdam (ICGEM) (Drewes et al., 2016), shown in Figure 2.7a. Additional insights come from other studies such as those examining the curvature of the gravity field that supports tectonic segmentation (e.g., Bouman et al., 2016). Two of the recent satellite missions, with particular importance for Antarctic research, are the Gravity Field and Steady-State Ocean Circulation Explorer (GOCE) and Gravity Recovery And Climate Experiment

(GRACE).

The GOCE project is an initiative of the European Space Agency (Visser, 1999). It produced a global gravity field model at a resolution of 100–200 km (Drinkwater et al., 2003; Förste et al., 2013). Models derived from GOCE provide high accuracy and resolution. GRACE data (Tapley et al., 2007) are a lower resolution of 400 km and are aimed at monitoring changes in the gravity field over time, for example, related to melting ice or isostatic adjustments (Peltier, 2004a). Combined models can take advantage of the high resolution in GOCE, and the long duration repeated measurements of GRACE data (Hirt et al., 2016; Pail et al., 2011). Early results for Antarctica from, for example, the ADGRAV compilation (Bell et al., 1999) have been refined with data from the GOCE and GRACE missions (e.g., Förste et al., 2013; Von Frese et al., 2013). Since the IPY 2007/08, a number of airborne surveys have also been initiated. Gravity data from those missions allowed Scheinert et al. (2016) to compile gravity maps containing free-air, and Bouguer anomalies using the elevation model BEDMAP2 (Fretwell et al., 2012). This Antarctic gravity anomaly grid covers 73% of the continent in 10×10 km resolution (Fig. 2.7b).

Chen et al. (2018a) uses ice thickness, bedrock topography and gravity data to estimate the elastic thickness of the Antarctic lithosphere. The elastic thickness is a parameter that combines thermal and rheological properties. The results converge with other metrics, and suggest a thin West Antarctic elastic thickness of $T_e = 5\text{--}20$ km. In East Antarctica, $T_e = 60\text{--}80$ km, with T_e up to 90 km in the Aurora Subglacial Basin.

2.3.2 Magnetometry

Magnetometry is used in various fields of geophysics, included as a guide for crustal segmentation (Aitken et al., 2014; Goodge et al., 2010; Ruppel et al., 2018) and to estimate the spreading rate and age of oceanic crust from alternating magnetic polarities, imprinted in the oceanic crust when formed in the mid-oceanic spreading zones (e.g., Heirtzler et al., 1968). Magnetic data vary over a large range, with magnetic anomalies showing the departure of the observed field from the expected global reference value (e.g., Thébault et al., 2010). This provides a detailed map of the crust, but interpretations can be ambiguous. Anomalies are typically related to magnetic minerals in given rock types, and crustal province boundaries are generally interpreted from a change in the character of such anomalies. Apparent boundaries and other artefacts can correspond to changes in resolution, especially when the resolution is low for the intended purpose.

Global maps of magnetic anomalies include EMAG2 (Maus et al., 2009) and precursors (Maus et al., 2002, 2007). For Antarctica, satellite, marine, and airborne data have been compiled into ADMAP (Frese et al., 2007; Golynsky et al., 2018, 2013a; Golynsky et al., 2013b). In large areas of East Antarctica, the map is only based on satellite data from the Magsat mission (e.g., Hulot et al., 2002). A recent compilation, ADMAP2 (Golynsky et al., 2018), contains additional aeromagnetic and marine magnetic data (Fig. 2.7d), consequently with variable resolution. There are, however, still large gaps over certain areas, particularly in East Antarctica.

Magnetometry has also been used to estimate the thickness of sedimentary basins, as they are non-magnetic whereas the underlying crystalline bedrock is more highly magnetised (e.g.,

Aitken et al., 2014). This property is of particular importance in Antarctica, where seismic data to constrain subglacial sedimentation is sparse. Magnetic data have also been used to estimate the thickness of the magnetic crust, defined as the depth to the Curie temperature isotherm. This property is used to derive heat flow from the resulting temperature gradient (e.g., Fox Maule et al., 2005; Martos et al., 2017).

2.3.3 Seismology

Seismic methods may be used to infer properties of buried structures and the deep Earth through the analysis of seismic waveforms and signal travel times (Aki et al., 2002). This is an extensive field of research, and the present section will restrict consideration to two of the most popular seismic techniques used to study lithospheric structure: receiver function analysis and seismic tomography.

Receiver function analysis

Receiver functions may be used to infer the nature and depth of discontinuities in the seismic structure near the receiver. Typically this approach is used to identify the Moho, thereby yielding crustal thickness, and the LAB, thereby yielding lithosphere thickness. The source of the seismic signal is generally a teleseismic event, such as an earthquake. Broadband, three-component stations enable the horizontal component (parallel the direction of wave travel) to be deconvolved from the vertical component, hence identifying waves generated by conversions across the discontinuity, and forming the receiver function (Ammon et al., 1990; Reading et al., 2012). In the following paragraph, indicative examples of results from receiver function studies are provided.

Reading (2006) generated broadband P-wave receiver functions from nine stations, mostly deployed on bedrock, near Lambert Glacier, which confirmed that the Lambert Glacier region encompasses major tectonic boundaries. Chaput et al. (2014) use P- and S-wave receiver functions from POLENET-ANET stations, combined with earlier work, to estimate crustal thickness in West Antarctica. The study finds Moho depths ranging from 20–40 km. The thinnest crust is beneath the Ross Shelf and eastern Ellsworth Land. Multiples from Moho P-to-S (Ps) conversions tend to mask conversions from the base of the lithosphere. Those P-wave receiver functions can be particularly difficult in Antarctica for stations deployed on ice sheets due to reverberations within the ice layer that may mask also P-to-S (Ps) conversions. However, S-wave receiver functions are less affected by ice multiples (Farra et al., 2000; Kumar et al., 2005), and are particularly suited for seismometers deployed in ice (Hansen et al., 2009, 2016). This application has been used in studies derived from major deployments such as TAMSEIS, a campaign targeting the Transantarctic mountains (Watson et al., 2006; Wiens, 2003), and GAMSEIS, similarly targeting the Gamburtsev Subglacial Mountains (An et al., 2016; Kanao et al., 2014). The crust in West Antarctica is thin, and the mantle is heterogeneous.

Lamarque et al. (2015) use receiver functions (and seismic anisotropy measurements) to investigate the terranes forming the Neoproterozoic-Palaeoproterozoic Terre Adélie Craton and the Mertz Shear Zone. The Moho depth they find is similar to that beneath the Australian Gawler Craton (40–44 km) west of Mertz Glacier, and this is in agreement with tectonic studies (e.g., Aitken et al., 2014; Williams et al., 2016). East of Mertz Glacier, the Moho is shallower

(28 km). Hansen et al. (2016) use S-wave receiver functions and Rayleigh wave phase velocities to map the crustal thickness beneath the Transantarctic Mountains in Victoria Land. The crustal thickness is estimated to within ± 4 km, with phase velocities constrained to within ± 0.1 km/s. The crust is 20 km thick near the Ross Sea, but it thickens to 46 km beneath the Transantarctic Mountains.

Baranov et al. (2013) present a Moho map on a $1^\circ \times 1^\circ$ grid from published seismic studies and geological observations, finding large differences when compared to the global CRUST 2.0 reference model (Laske et al., 2001), noted further below. The Gamburtsev Subglacial Mountains region is estimated to be 20 km thicker than the crust suggested by CRUST 2.0, whereas the Wilkes Sub-glacial Basin is 12 km thinner. Baranov et al. (2018) include updated datasets and compare seismic estimates of the Moho structure with gravity data. The study presents two alternative uni-variate models: a combined best estimate of Moho depth, and a refined estimate of sedimentary thickness.

Seismic tomography

Tomography studies form 2D sections or 3D volumes of the physical properties from observables (e.g. travel times of seismic waves) with crossing source-to-receiver paths (Stein et al., 2003). The global network of seismometers, earthquake catalogues with sources from across the planet, and ambient noise have facilitated S- and P-wave tomography of Earth's mantle (e.g., Becker et al., 2002; Bozdağ et al., 2016). Tomographic methods may also be applied to other types of seismic data, such as surface waves. The velocity of surface waves is dispersive in the Earth, which, in general, shows an increase in seismic velocity with depth. Lower frequencies propagate through oscillations of material at greater depths than higher frequencies and can therefore travel faster. The relative response at varying depths is described by sensitivity kernels. Surface waves are well-suited to study large-scale upper mantle structure. Their sensitivity to Earth structure is concentrated in the lithosphere, and they are very sensitive to seismic anisotropy (An et al., 2015a; Stein et al., 2003), which can yield additional insights.

Global models that begin to show heterogeneity within the lithosphere include CRUST 1.0/2.0 (e.g., Laske et al., 2013). These crustal models are generated from active seismic data, receiver functions, and gravity inversion, and are refined as new data become available. A continuation to the CRUST 1.0/2.0 project is the LITHO1.0, which integrates Moho and LAB datasets based on seismic and gravity data (Laske et al., 2001; Pasyanos et al., 2014). With an increasing number of broadband seismometers, Schaeffer et al. (2013) generated a global model of the lithosphere from both surface and body waves. Further lithospheric models are reviewed and compared for example by Steinberger et al. (2018).

A number of studies have mapped the crustal depth and lithospheric structure beneath Antarctica, limited by the sparse and unevenly distributed data (e.g., Morelli et al., 2004; Ritzwoller et al., 2001). Ritzwoller et al. (2001) present a $2^\circ \times 2^\circ$ model based on Monte Carlo inversion of Love and Rayleigh surface waves with a crustal thickness of up to 40 km under the Gamburtsev Subglacial Mountains and central East Antarctica. Such early studies reveal the general division of Antarctica into two domains, East and West, and suggest that the lithosphere beneath Dronning Maud Land is 220 km thick, increasing below Enderby Land and the Gamburtsev Subglacial Mountains, and reaching 250 km under Wilkes Land.

An et al. (2015a) use 122 broadband stations in a surface wave tomography study of the Antarctic continent and retrieve over 10,000 Rayleigh-wave fundamental mode dispersion curves from earthquakes, with some from ambient noise data as well. The study takes advantage of new data from IPY 2007/08 deployed seismographs. Their model is constructed with hexagonal cells, divided to 51 depth layers, with decreasing resolution with depth. Instead of using the established two-step process where dispersion is used to constrain the seismic velocity, An et al. (2015a)'s 3-D model is inverted from fundamental-mode Rayleigh group velocities in a single-step (Fig. 2.9b).

Body wave tomography has been used to study deeper mantle structures in global (e.g., Bozdağ et al., 2016) as well as regional Antarctic studies (e.g., Hansen et al., 2014). A regional study of the South Pole region (Shen et al., 2018b) reveals a thermally complex structure in the lower lithosphere suggesting lithospheric foundering that added constraints to understand the thermal state of the Transantarctic Mountains. In a somewhat later study by Shen et al. (2018a) create a seismic tomography model of the lithospheric structure for the larger part of Central and West Antarctica, and thereby refining earlier results. They describe a sharp contrast between the stable East Antarctica and the tectonically active West Antarctica, and slow seismic wavespeed beneath the Transantarctic Mountains. In some studies, receiver function and tomography methods have been combined, e.g. crustal thickness in tomographic models may be constrained or optimised by receiver functions (e.g., An et al., 2015a).

Seismic velocity, at a certain depth, may depend on composition, temperature, or a combination of both. Morelli et al. (2004) argue that although composition may have an impact on velocity, the more significant factor is temperature (see also Goes et al., 2000). Further, they define the seismic lithosphere from a 2% anomaly from the v_s model. The authors refrain from deriving heat flow estimates, as they argue that crustal heat production is unknown and could have a large impact on the total heat flow, depending on the geologic nature of the crust. Notably, this insight has not restricted later studies by other authors (An et al., 2015b; Fox Maule et al., 2005; Martos et al., 2017).

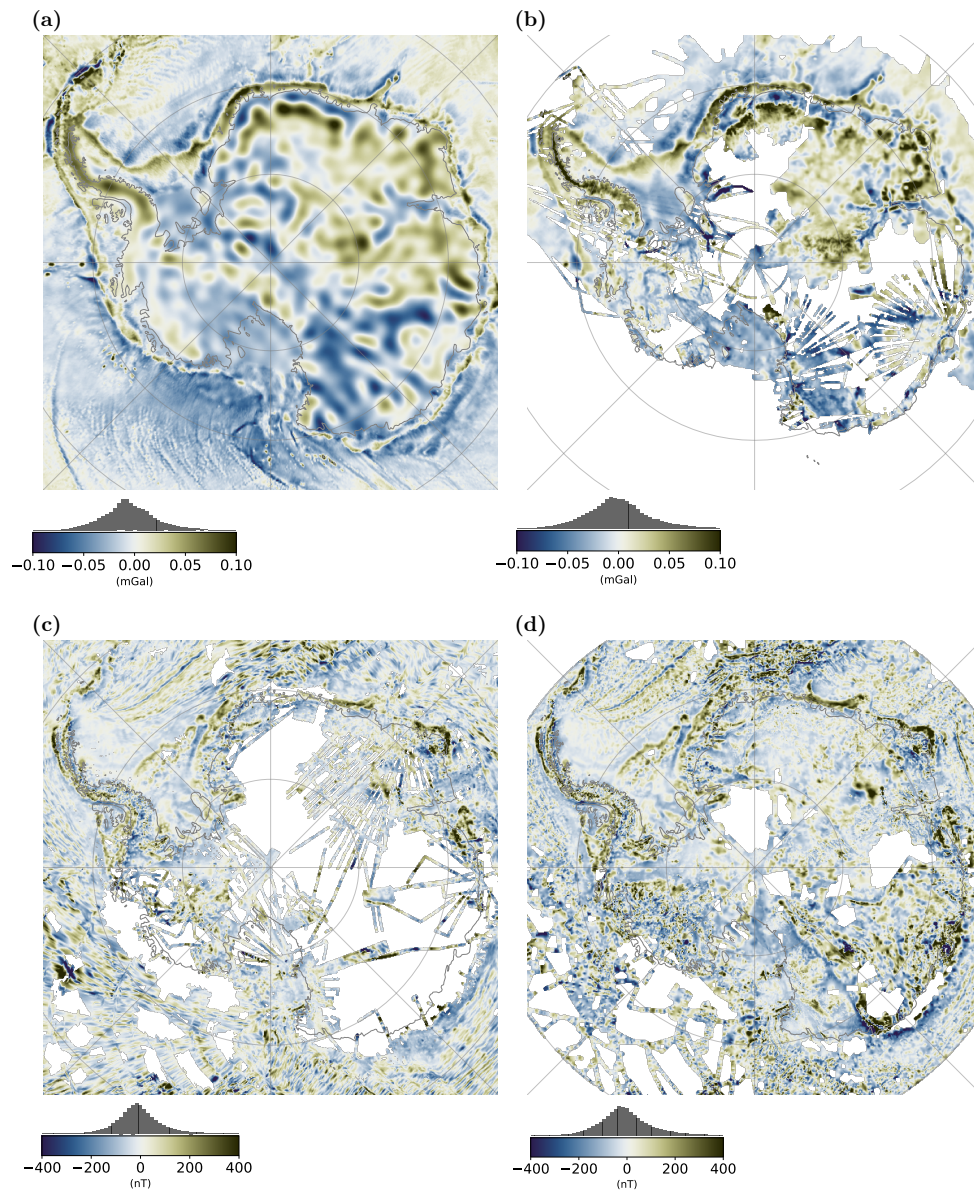


Figure 2.7: Potential field data from global and Antarctic studies. Free-air gravity anomalies from (a) the global compilation EIGEN-6C2 (Förste et al., 2013), and from (b) Scheinert et al. (2016). Magnetic anomalies from (c) Maus et al. (2009), and (d) Golynsky et al. (2018). Histograms on colour bars indicate the relative distribution of values included in the map.

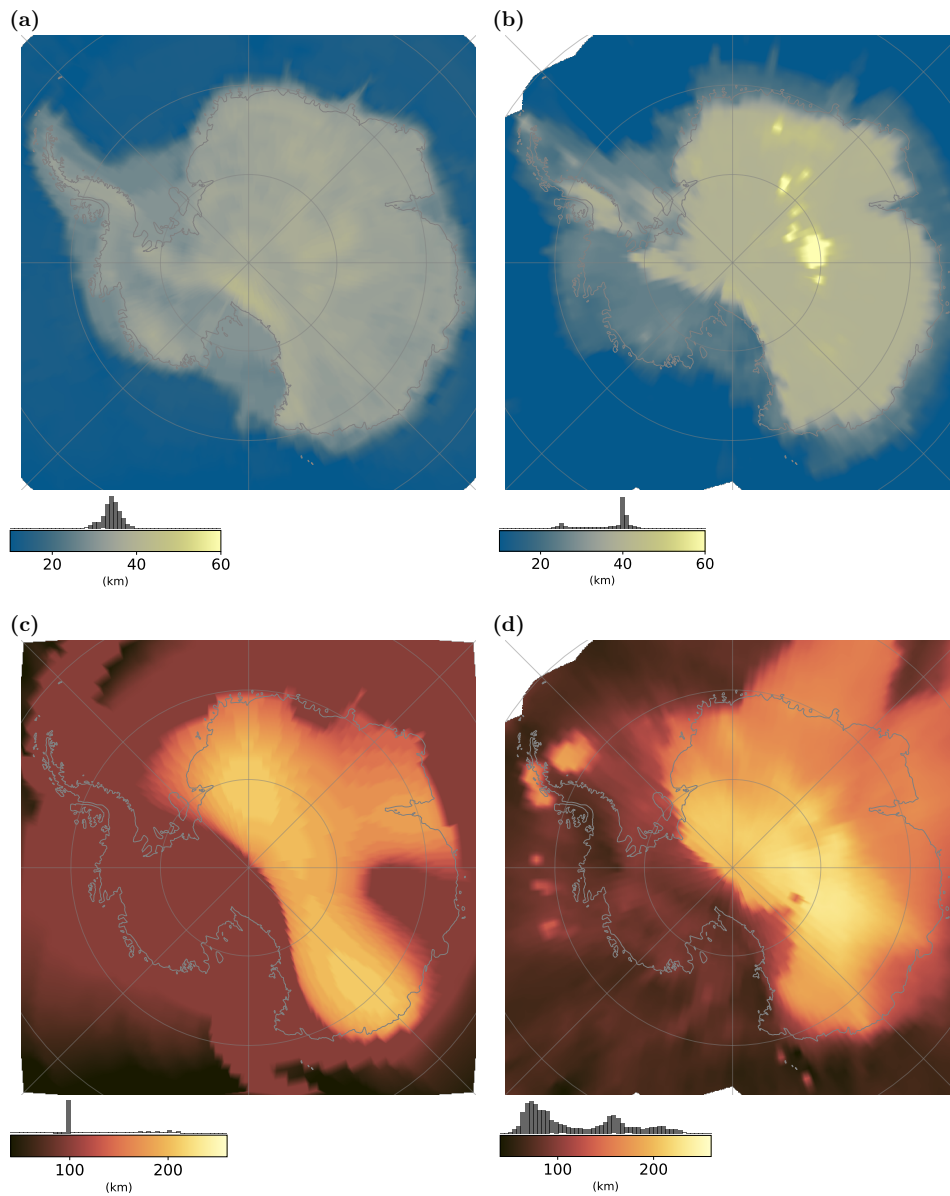


Figure 2.8: Moho (a and b) and LAB (c and d) depth from global and Antarctic studies. (a) CRUST 1.0 (Laske et al., 2013), (b) An et al. (2015a), (c) Conrad et al. (2006), (d) An et al. (2015b). Histograms on colour bars indicates the relative distribution of values included in the map.

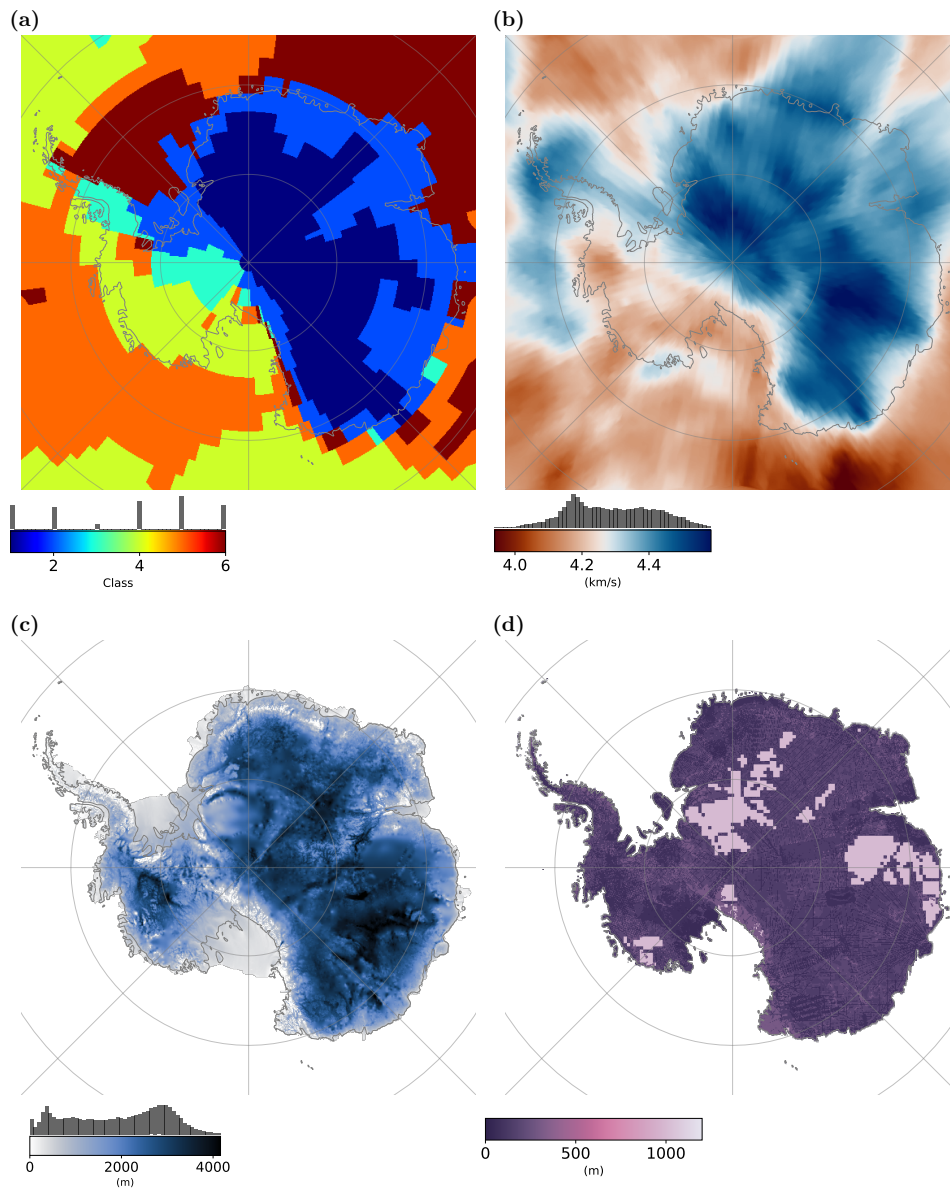


Figure 2.9: (a) Segmentation from a global seismic model (Schaeffer et al., 2015). 1 = Cratons, 2 = Precambrian Belts and Modified Cratons, 3 = Phanerozoic Continents, 4 = Ridges and Back arcs, 5 = Oceanic, 6 = Oldest Oceanic. (b) Seismic shear-wave speed at 150 km depth (An et al., 2015a), (c) Ice thickness, and (d) uncertainties associated with subglacial topography from BEDMAP2 (Fretwell et al., 2012).

2.4 Interactions Between the Ice Sheets and Solid Earth

Ice sheets in Antarctica have evolved over the last 50 Ma (Coxall et al., 2005; Gulick et al., 2017). Antarctica’s position near the pole, and the onset of the circumpolar current facilitated growth of glaciation around 34 Ma (e.g., Siegert et al., 2008). Notwithstanding recent research progress, the response of the Antarctic ice sheet to anthropogenic climate change is still poorly constrained (Noble et al., 2020). The present development and mass change of the Antarctic ice sheets is of great concern, as the decrease in ice volume will result in global sea level rise up to many metres, with grave implications for coastal regions (e.g., DeConto et al., 2016; Hanna et al., 2013). Three aspects of ice sheet and solid Earth interaction and feedbacks are considered most relevant (e.g., Whitehouse et al., 2019) and are reviewed in this section: isostasy, subglacial topography, and geothermal heat flow.

2.4.1 Isostasy

The weight of the ice sheet depresses the elevation of the crust and lithospheric mantle and deforms the plastic asthenosphere beneath. If the ice mass changes, the system responds to regain isostatic equilibrium, known as Glacial Isostatic Adjustment (GIA). The rate of uplift depends on the rate of mass reorganisation and the rheological properties of the mantle, which can have large spatial variations (Nield et al., 2018; Whitehouse et al., 2012). GPS measurements of crustal motion combined with satellite data, constrain the mass balance trends of the Antarctic ice sheets (e.g., Martín-Español et al., 2016). King et al. (2016) pointed out the difficulties of separating plate tectonic rotation from the horizontal component of glacial isostatic adjustment, as observed in GPS time series for Antarctica (Whitehouse, 2018). Turner et al. (2020) showed that separation is possible with spatial weighting. GPS receivers located at outcrops around the circumference of Antarctica and gravity inversion from satellite data enable modelling of the mechanisms for observed motion. However, due to the lack of outcrop and hence GPS measurements, related rheological parameters are still not known for the Antarctic interior, and uncertainties remain large also in coastal regions.

Mantle processes interact with exhumation and the aforementioned GIA response to form the dynamic topography of Antarctica. Some studies invoke mantle plumes as a mechanism, however, the concept is controversial (e.g., Foulger, 2005). Marie Byrd Land is an elevated region of West Antarctica, suggested to be underlain by a mantle plume (e.g., Sleep, 2006); however, an understanding of shallow tectonic processes is required to test this hypothesis (LeMasurier, 2006). The region is also associated with volcanism, and heat flow anomalies (Schroeder et al., 2014) and Cenozoic rifting in West Antarctica should arguably be incorporated in the isostatic models (Spiegel et al., 2016). The majority of other elevated areas in Antarctica, such as the Transantarctic Mountains and the Gamburtsev Subglacial Mountains, are also associated with ongoing debates as to their geodynamic origins.

The Transantarctic Mountains were not formed by ongoing tectonic plate collision in the manner of other major global mountain ranges. In agreement with Brink et al. (1997), Hansen et al. (2016) argue for a flexural East Antarctic margin. Baranov et al. (2013) speculate that the Transantarctic Mountains are either isostatically uncompensated or supported by an anomalously light mantle. Studies of the thermal structure, together with tectonic models are needed to resolve the mechanisms involved.

The Gamburtsev Subglacial Mountains are an enigmatic range under the ice in the interior of East Antarctica. The region is associated with a thick lithosphere, up to 250 km (An et al., 2016; Ferraccioli et al., 2011). Ferraccioli et al. (2011) suggest that their formation was caused by rift-flank uplift, root buoyancy and the isostatic response to erosion, however, that the topography is preserved by limited exhumation. The study uses radar, gravity, and magnetic data as well as receiver-function estimates to suggest a rift system that surrounds the range and thick roots within the range. The region is suggested to be of Rodinian (Ferraccioli et al., 2011), or Gondwanan origin (An et al., 2015a; Mulder et al., 2019), and reactivated in Permian and Cretaceous rifting that resulted in the rift-flank uplift. Crustal buoyancy of the range may have been further activated by the isostatic response to fluvial and glacial erosion. Paxman et al. (2016) suggest, however, that only a minor component of the uplift of the Gamburtsev Subglacial Mountains can be explained by valley incision.

Tectonic processes, such as the formation and rifting of continents, are important factors to understand the lateral variations of isostasy. Moreover, the interaction between dynamic ice sheets and subglacial topography is a two-way process (e.g., Whitehouse et al., 2019).

2.4.2 Subglacial Topography

The subglacial landscape is closely connected to ice-sheet development (e.g., Paxman et al., 2018). Subglacial topography data in Antarctica can only be acquired by ice-penetrating radar, seismic data, or through relatively long wavelength gravity inversion. The elevation model BEDMAP2 (Fretwell et al., 2012) is an updated version of BEDMAP (Lythe et al., 2001), whose results are based on 25 million ice thickness measurements from airborne and ground-based instruments. Such models provide an overview of the landscape; however, the uncertainties remain large. In some areas, the elevation uncertainty can be as much as 1000 m (Fig. 2.9c). Employed methods and data density might not capture the finer variations in roughness, that are difficult to interpolate from flight lines (Graham et al., 2017).

A number of studies have refined estimates of subglacial erosion and exhumation (Jamieson et al., 2010; Wilson et al., 2012). Paxman et al. (2019b) include a range of data sets to constrain the exhumation history of Antarctica. The study considers ice-sheet loading, erosion, and thermal subsidence and correlates the modelled exhumation with marine deposition data. However, recently interpreted marine data (Sauermilch et al., 2019) suggest that the volumes in previous studies might be underestimated. Regional studies estimate subglacial sediment from aeromagnetic data, for example (Aitken et al., 2014).

2.4.3 Geothermal Heat Flow

The geothermal heat flow in Antarctica represents '*the least known property of the least known continent*' (Hasterok et al., 2018b). Estimates of heat flow have the potential to provide insights into the tectonic architecture of the lithosphere (Artemieva, 2011; Beardsmore et al., 2001). Further, in Antarctica, the amount and distribution of heat have additional importance as it impacts the stability of the ice sheets as they respond to global change (Pattyn, 2010; Pittard et al., 2016; Ramirez et al., 2016). Geothermal heat impacts the ice rheology and can cause basal melting.

Estimates of heat flow values in global compilations are mostly inferred from in-situ measurements of the thermal gradient. Such measurements have been organised in growing spatial databases (e.g., Artemieva, 2006; Hasterok et al., 2008; Pollack, 1982; Stein, 1995). The modelled heat flow depends on assumptions of thermal conductivity, which can vary over a large range (McKenzie et al., 2005; Xu et al., 2004). Statistical efforts have linked measured heat flow to geological and geophysical properties to guide interpolation across areas with few direct measurements (Davies et al., 2010; Goutorbe et al., 2011).

2.4.3.1 Continental Scale Geophysics-Based Studies

Existing geothermal heat flow maps for Antarctica based on geophysical data utilise either analytical forward modelling from a geothermal gradient (An et al., 2015a; Fox Maule et al., 2005; Martos et al., 2017), or an empirical approach where geophysical data are matched with actual heat flow values elsewhere (Shapiro et al., 2004).

Fox Maule et al. (2005) use a satellite-derived magnetic equivalent dipole model to estimate geothermal heat flow and infer a range of 40–185 mW/m². The method was tested in Australia, where it could be compared with direct measurements, and gave a result with an error of up to 20%. Geothermal flux can vary locally, and the resolution of the satellite data are a few hundred kilometres. The combined uncertainties are 21–27 mW/m², according to the study. The study was further refined by Purucker (2013) to include additional magnetic data from the CHAMP satellite. Martos et al. (2017) also used magnetic data, and instead of modelling an equivalent magnetic field, they analysed the frequency distribution in mainly airborne magnetic surveyed data from an expanded ADMAP compilation (Golynsky et al., 2013b).

An et al. (2015b) estimated heat flow from wave speeds in a seismic tomography (An et al., 2015a). Similar to the magnetic models, this approach also depends in assumptions regarding heat production in the crust and variations on thermal conductivity. The methods used are valid in steady state condition up to 90 mWm⁻². Hence, the values inferred for interior West Antarctica are much lower than in studies constrained by magnetic data that relate to a shallower source for the thermal gradient. The An et al. (2015a) study finds values of up to 65 mWm⁻² in East Antarctica and higher values in West Antarctica, up to the model limit of 90 mWm⁻² in the Transantarctic Mountains.

2.4.3.2 The Crustal Component of Heat Flow

The geothermal heat flow under the Antarctic ice sheets originates only partly from the mantle with, most probably, a very significant proportion being generated within the crust from radiogenic decay. Crustal heat production accounts for 40% - 60% of the total heat flow (Artemieva et al., 2001; Beardsmore et al., 2001), and local shallow and transient heat sources might provide very large amounts of heat (e.g., Clow et al., 2014; Lough et al., 2013). Methods that estimate heat flow from seismic or magnetic measurements of the upper mantle or lower crust assume a chemically and thermally homogeneous crust and therefore neglect this important component (Burton-Johnson et al., 2017; Goodge, 2018; Jaupart et al., 2007). Heat is generated from the decay of specifically, Uranium, Thorium and Potassium (Beardsmore et al., 2001) Due to the incompatibility of those heat producing elements in the mantle, they have been fractionated into the crust, with regional and local geology resulting in their uneven dis-

tribution. Carson et al. (2014)'s study presents a notable illustrative example of the variation of geothermal heat flow along a coastal transect of exposed rocks. Geochemical data from rock samples from George V Land-Terre Adélie and eastern Prydz Bay illustrate that Antarctic crustal heat production is very heterogeneous. Median heat production values for these locations vary from $0.4\mu\text{W}/\text{m}^3$ to $12.9\mu\text{W}/\text{m}^3$ in 276 samples, with a highest measured value of $68.85\mu\text{W}/\text{m}^3$ (Carson et al., 2012).

2.4.3.3 Heat Flow and Subglacial Water

Siegert et al. (1996) compute heat flow at 77 sub-glacial lakes identified from airborne data. They estimated that the heat needed to produce sub-glacial melting is $79\text{--}104\text{ mW}/\text{m}^2$ for some locations. Fisher et al. (2015) present a direct measurement of heat flow in Lake Whillans, a subglacial lake in West Antarctica, with a value of $285 \pm 80\text{ mW}/\text{m}^2$, which is three times more than that estimated by Fox Maule et al. (2005). They also measure the heat flow through the ice and find a much lower value, $105 \pm 13\text{ mW}/\text{m}^2$. Fisher et al. (2015) propose that the heat trapped at the bottom of the glacier may be the cause of ice streams and subglacial lakes commonly found in the region west of Ross Ice Shelf and that the measured heat flow results in $7\text{--}1.5\text{ cm}/\text{yr}$ of basal melt. Approximately $175\text{ mW}/\text{m}^2$ is needed to melt ice; therefore measurements in ice only provide a minimum value (Begeman et al., 2017). The results are supported by Clow et al. (2014) who find heat a flow of $240\text{ mW}/\text{m}^2$ from thermal gradient measurements in the centre of the West Antarctic Ice Sheet. The high values are believed to at least have an extent of 30 km, as implied by a depression in the surface of the 3000 m thick ice sheet. Fisher et al. (2015) remark that heat flow can differ significantly from the relatively low values estimated from regional geophysical methods. The measured value is one of the highest values measured in the continental heat flux database, and such values are normally associated with volcanic and hydrothermal activity. Melting is also observed near the South Pole (Jordan et al., 2018), providing an example of high heat flow in East Antarctica. Regional models with limited resolution cannot capture local anomalies; nevertheless, it is important to understand the variation for ice-sheet models.

2.5 Improving Knowledge of the Lithosphere of Antarctica

Our present knowledge of the lithosphere of Antarctica, as reviewed in the previous sections of this chapter, is derived from diverse forms of data and interpretation. Geologic data provide detailed, although highly localised, information in regions with rock exposure, while geophysical data can provide extensive (although, as yet, not comprehensive) lower resolution constraints. There exists a tension between geology and geophysics that originates from the geological narrative, considering time as the main factor to understand observed features and geophysical data that provide a snapshot of the resulting Earth structures. Geophysical methods can provide an unbiased picture, however, the assumptions in the models and processing need to be understood, or accounted for. Together, these bodies of research suggest that the lithosphere beneath the East Antarctic interior is complex: cratonic blocks joined by wide accretionary belts arising from the formation of supercontinents (e.g., Boger, 2011; Fitzsimons, 2003; Harley et al., 2013). However, the location and extent of such domains are debated. Affiliation

with reconstructed conjugate margins is a useful concept; however, tectonic blocks should be expected to have a limited spatial extent, as seen in other continents (e.g., Begg et al., 2009; Shaw et al., 1996). We might expect the Antarctic interior to be as complex as any other continent.

With the dual motivation of gaining insight into the geological evolution of the continent, and to support interdisciplinary studies relating to solid Earth and cryosphere interaction, the following needs have emerged with regard to improving knowledge of the lithosphere of Antarctica.

Synthesise information from diverse data types. As data from Antarctica are, in general, extremely scarce, it should be possible to build more robust models of the hidden geology when multiple datasets from diverse sources are considered. Of particular importance is to include geological data as constraints in geophysical models, and equally, make use of geophysical constraints to interpret and extrapolate broad-scale geological studies.

Consider multiple interpretations. Given that the majority of studies on the Antarctic lithosphere are based on reconnaissance-level data, the resulting geological and other hypotheses are generally poorly constrained. This results in a risk of over-interpreting sparse and uncertain data. Furthermore, controversies arising from apparently conflicting research results stimulate scientific progress. Multiple interpretations, or lines of evidence, should therefore be carried forward in the analysis until a robust, preferred model emerges.

The two requisites noted above are both captured by many of the multivariate and probabilistic statistical methods available to scientific research. Such methods have perhaps been less-often used in geoscience than other research disciplines due to challenges associated with spatial data handling and sharing. The relatively new paradigm of making research results available as downloadable datasets (e.g., Wilkinson et al., 2016) and of community efforts to bring such datasets together in user-focused compilations (e.g., Roth et al., 2017) are important enabling developments.

The intention in developing statistical methods for Antarctic Earth Sciences research is that they coexist with conventional geological and deterministic geophysical studies. Univariate models do and will continue to, provide well-posed insights in many cases, and the research methods put forward in this thesis are intended to complement those approaches.

Datasets arising from the accelerated data collection during the IPY 2007/08 had recently been processed and made accessible. Therefore, it was extremely timely at the outset of the research described in this thesis to progress methods to make further and wider use of the diverse information that was newly available.

2.5.1 A Statistical Toolbox

A number of candidate statistical approaches are introduced below that allow for the combined analysis of multiple data types and the consideration of multiple constraints or interpretations.

2.5.1.1 Set Theory

Set theory is a body of mathematical logic to describe the relationship between collections of objects, and for constructing new objects from combinations (Berndt et al., 1980). Spatial objects, like polygons, are in essence a set of elements in a defined geographic region. A set theory approach, therefore, opens up a range of mathematical operations that can be applied to spatial data. Common vector methods in GIS software that derives from set theory include intersects of polygons, unions, and clip functions.

A geological domain represents an area with a defined history, that has an intuitive match to the concept of a set object as articulated above. Geological information is hence conventionally presented as choropleth maps with attributed labels and properties, i.e. not as continuous data. This representation is applied across the scales from local maps of stratigraphic units, to continental scale crustal domains. Domains constrained by the interpretation of geophysical data are also natural candidates for consideration as set-like objects. Set theory is therefore an attractive option in working with multiple geological or geophysical datasets in combination.

2.5.1.2 Similarity Methods

Similarity methods are used in a broad range of research applications to detect and quantify the similarity between given locations from one or multiple observables. The observables are often considered as systematically ordered lists of values, sometimes termed vectors. In concept, a large database of reference observables may be used to predict, or make a calculation relating to, a missing observable in the target location vector. Approaches include distance-based similarity, feature-based similarity, and probabilistic measures (Ashby et al., 2007).

Statistically based prediction is a well-posed option when a physics-based prediction is difficult due to a lack of knowledge of some elements of a structure or system process. In some cases, the statistics based prediction can inform an improved understanding of a structure or a process. Goutorbe et al. (2011) applied similarity detection to link heat flow measurements with similar tectonic settings. Various approaches have also been used for mineral resource assessments (e.g., Griffiths, 1983) or structural settings (Kaltwasser et al., 2005).

2.5.1.3 Uncertainty Metrics

Uncertainty is a key concept in the communication of research results and is particularly important when those results are to be carried forward across disciplines. An example of this relevant to this thesis are solid Earth results used as inputs or boundary conditions for modelling the response of ice sheets to changing climate.

A commonly used approach is to state the uncertainty as a constant range, such as a *two-sigma*, 95% confidence interval. In Earth Sciences research, it is advisable to present uncertainty measures as maps, to show their spatial variability. Uncertainty metrics are often not provided, or not quantified. When metrics are provided, they may account for numerical uncertainty, but the user should remain alert for systematic and subjective errors as well (Bond, 2015; Pérez-Díaz et al., 2020). A map of the standard deviation of the main output research result distribution is a reasonable first option, but does not capture the complexity of multi-modal distributions, for example. Further metrics may be readily calculated and may include information entropy in geological maps and models as a proxy for uncertainty (Kuhn et al.,

2016; Wellmann, 2013), particularly for multivariate and 3D modelling (Wellmann et al., 2012). Information entropy quantifies how much information a signal contains, for example, the degree of randomness in a distribution (Goodfellow et al., 2016; Kelbert et al., 2017; Shannon, 1948), and can therefore be a tool to determine if additional data improve a model, or add noise.

2.5.1.4 Fuzzy Logic

Fuzzy logic allows us to work with relationships based on the extent to which something could be true, rather than a simple 'true or false' formulation. An extension of set theory provides the possibility to describe membership as a function. These are referred to as fuzzy sets (Zadeh, 1965), and is related to fuzzy logic. The concept of a fuzzy set is a natural generalisation of ordinary, or crisply-defined, sets and has an intuitive potential application to the consideration of multiple possible classifications for a given spatial domain.

Applications of spatial fuzzy sets include geometrical shapes (e.g., Buckley et al., 1997) or spatial polygons (e.g., Chen et al., 2018b; Kharal et al., 2009). A few studies take advantage of fuzzy sets in a spatial application (e.g., Mironova, 2018), but the possibilities are yet to be explored in continental-scale models. Fuzzy sets, or fuzzy polygons, allow for the same location to belong partly to multiple domains or other classes. From the concept of fuzzy polygons, transition zones, or, fuzzy boundaries, can be extracted.

2.5.1.5 Bayesian Approaches

Degrees of belief may also be handled using the systematic mathematics of a Bayesian framework (Bayes, 1763). This approach is particularly strong with regard to finding a probability of some outcome that is conditional on a set of data that updates a prior belief. The concept has been known for a long time but due to the computational cost involved with integration of probability distributions, it is only in recent years that the method has been widely adopted in a quantified way (McGrayne, 2011). The Bayesian inference allows us to bring forward results from other disciplines, as geophysical data, to be strengthened by for example geological observations. However, the benefit of a Bayesian analysis can be cancelled if any data is regarded as 'ground truth'. The complete certainty in a prior belief excludes refined interpretation.

Applications for Bayesian methods include classification and regression (Denison et al., 2002). Classification could, for example, inform segmentation problems, in one or many dimensions (e.g., Fearnhead et al., 2006; Killick et al., 2012; Reading et al., 2010, 2013) and the approach has immense potential with regard to the requisites of improving knowledge in the Earth Sciences. Sampling the posterior distribution of probable models to find an appropriate solution has the added benefit of enabling uncertainty to be assessed, although this is beyond the scope of the current research.

2.5.1.6 Machine Learning

Machine learning allows a computer to make data-driven recognition of patterns and predictions without explicit knowledge of the underlying physical or other systems (Marsland, 2014). Machine learning has been used in a range of Earth Science applications over recent years (e.g., Cracknell, 2014; Kuhn et al., 2016; Rezvanbehbahani et al., 2017). Algorithms can be supervised, where a training set is provided on which to base the predictive output, or unsupervised,

where the algorithm itself identifies patterns in the data (e.g., Hood et al., 2018). Research insights frequently arise from the evaluation of the data-driven prediction, and techniques such as decision trees and random forests, currently provide the most tractable means of calculating metrics, such as information entropy (Cracknell et al., 2014; Kuhn et al., 2018). Machine learning techniques will certainly play a significant part in the future of Antarctic research as datasets continue to expand.

2.5.1.7 Well-posed presentation of results for interpretation

Research insights, especially in geophysics, are frequently drawn from coloured contour plots. It is very important that the colour scales are chosen with the understanding of how humans will perceive the features thus revealed (e.g., Morse et al., 2019). Smoothing and filtering is needed for overdetermined systems, and the amount to which this is carried out can be subjective (Foulger et al., 2013; Stein et al., 2003). Visualising uncertainty is also challenging, particularly for multidimensional data (e.g., Potter et al., 2013).

2.5.2 Application to Antarctica

In response to the opportunity following IPY 2007/08 which presented an increase in the amount and quality of Antarctic data, and noting the requisites for improving knowledge noted above, this thesis documents studies that take a largely statistical approach. The choice was made to utilise set theory and similarity approaches as strong, simple, multivariate methods to advance our understanding of the Antarctic lithosphere. Fuzzy sets are employed in an implicit way, and the research is informed by concepts from Bayesian and machine learning approaches. Attention is paid to uncertainty and well-posed presentation of coloured maps throughout. Questions regarding the extent of cratonic blocks and trends of mobile belts, are thus addressed with multiple datasets as constraints. New heat flow models are calculated from multiple datasets and are presented as an ongoing research product.

Chapter 3

The Computational Model

The following chapter is divided in two parts. First I briefly introduce the technical aspects of a new computational framework (Ch. 3a). Secondly, I use the framework to generate a model of the Antarctic lithosphere and discuss aspects of the datasets used (Ch. 3b).

Chapter 3a has been published as:

Stål, T., and Reading, A. M. (2020). A Grid for Multidimensional and Multivariate Spatial Representation and Data Processing. *Journal of Open Research Software*, 8(1), 1-10. <https://doi.org/10.5334/JORS.287>.

Chapter 3b has been published as:

Stål, T., Reading, A. M., Halpin, J. A., Steven J, P., and Whittaker, J. M. (2020). The Antarctic Crust and Upper Mantle: a Flexible 3D Model and Framework for Interdisciplinary Research. *Frontiers in Earth Science*. <https://www.frontiersin.org/articles/10.3389/feart.2020.577502/abstract>

The text is reproduced in its published form and therefore some material is repeated from the background chapter. In the case of any differences, the published versions of the chapter take precedence.

Chapter 3a

A Grid for Multidimensional and Multivariate Spatial Representation and Data Processing

Tobias Stål^{1,2} and Anya M. Reading^{1,2}

1. School of Natural Sciences (Earth Sciences), University of Tasmania
2. Institute for Marine and Antarctic Studies, University of Tasmania

Abstract

Researchers use 2D and 3D spatial models of multivariate data of differing resolutions and formats. It can be challenging to work with multiple datasets, and it is time consuming to set up a robust, performant grid to handle such spatial models. We share 'agrid', a Python module which provides a framework for containing multidimensional data and functionality to work with those data. The module provides methods for defining the grid, data import, visualisation, processing capability and export. To facilitate reproducibility, the grid can point to original data sources and provides support for structured metadata. The module is written in an intelligible high level programming language, and uses well documented libraries as numpy, xarray, dask and rasterio.

3a.1 Introduction

Spatial models are needed to enable numerical problems to be solved in a broad range of scientific applications. Representation of data and modelled properties can be discretised to a grid. Each cell in the grid can contain a value from measurements or a modelled value, at a position defined in space and time. Cells can also be assigned a value by interpolation of nearby data points or by assumptions. The location of each grid cell is specified along the dimensions by index number or coordinates from e.g. a geographic coordinate system. Grids that represent part of Earth must also be associated with a geodetic datum for reference to

the physical world. Cells in a regular grid represent the shape of parallelepipeds, and can be rectilinear or Cartesian. The latter is the special case where the cells are unit squares, or unit cubes. Some data, e.g. surface elevation, can be expressed in only two dimensions. Other parameters can vary in all spatial directions, and time, and need to be represented in a multidimensional grid. The cell size limits the resolution of the model, smaller cells can represent higher frequencies, but a denser and larger grid add exponentially to the computing cost (Thompson et al., 1998). To populate a grid model, data are generally imported from different sources and in various formats. Images and continuous data are often available as regular raster files, while some observations are provided as points in an irregular grid, or vector data as polygons and lines. Spatial data are published in different data, projections and coordinate systems. Given this variety of formats and reference conventions, it is inevitable that combining data from different sources often presents a challenge.

3a.2 The Computational Framework

We share *agrid*, a framework to produce a regular grid for multidimensional and multivariate spatial modelling, processing and analysis. The extended functionality of the grid addresses many of the challenges in working with spatial 2D and 3D data noted above. Following the principles of Wilson et al. (2014)(Wilson et al., 2014), the code is written in highest possible language level and made readable and intelligible. We use the general-purpose programming language Python 3. Python is equipped with libraries for fast array operations (Oliphant, 2007; Van Der Walt et al., 2011), basic statistics (McKinney, 2015), signal processing and other scientific tools (Jones et al., 2015), machine learning (Pedregosa et al., 2011), visualisation (Hunter, 2007; Ramachandran et al., 2011) and discipline specific libraries for e.g. seismology (Beyreuther et al., 2010; Megies et al., 2011), astronomy (Robitaille et al., 2013) and GIS (Gillies, 2013a,b; Jordahl, 2014). Python also provides interfaces for other languages as R, C and Fortran. All those tools and packages can be reached from the open structure of *agrid* (Fig. 3a.1).

A few related open-source projects provide useful code for the Earth Sciences community; *GemPy* (De La Varga et al., 2019) is a package that facilitates stochastic geomodeling and probabilistic programming. The package uses the linear algebra compiler *Theano* (Bergstra et al., 2010) for efficient computation. Another related project is *Verde* (Uieda, 2018) and the *Fatiando* tool box, which contains advanced methods for e.g. interpolation. There are also examples of successful projects that connect various data sources with users. *Quantarctica* (Roth et al., 2017) makes Antarctic datasets from various sources easily accessible in a Geographical Information System (GIS) application, *QGIS* (Qgis, 2015). However, even with some 3D functionality in recent upgrades, GIS is predominantly a 2D frame. Another related project is the multidimensional *DataCube* (Lewis et al., 2016, 2017). *DataCube* pre-processes and presents remote sensing geographical and geophysical attributes for researchers and the broader public. *DataCube* is mainly targeted for changes (e.g. in Landsat raster data) over time, but has a broad range of possible applications.

In comparison, *agrid* is relatively light, easy to modify, and the dependencies are kept to a minimum. Data held in the *agrid* environment are not regarded only as a set of values: each observation can include quantified uncertainty, probability or likelihood, and data can also be

associated with metadata for provenance. It is advantageous that cells of a grid model can be populated with such allied information, together with the dataset.

`agrid` was initially developed for studies of the Antarctic lithosphere (Stål et al., 2020c, 2019c), and pre-processing of geophysical data for visualisation purposes (Morse et al., 2019), but with updates as presented here, it can be used in any discipline, geographical region, projection, dimensionality and any resolution. This initial release of the code is presented with tutorial notebooks that demonstrate its usage. The examples given in this paper can be reproduced from the provided `SConstruct` script (Fomel et al., 2007; Fomel, 2013; Knight, 2010).

Subsequent versions of `agrid` will include additional functionality. We plan, e.g., additional methods for conversion and improved visualisation, support hexagonal 2D grids, curvilinear grid and increased polar and spherical functionality. We hope that colleagues will find this contribution useful, and hopefully encourage scientists to share code and publish reproducible studies.

3a.3 Implementation and Architecture

`agrid` is structured as a Python module that imports dependencies and defines an `agrid` class object, `Grid()`, when imported. When calling `Grid()`, an object is created that represents the spatial extent of the model space. The grid is initiated with projection, extent and resolution. When the instance of the `agrid` class object is created, an `xarray` dataset is defined with dimensions and populated with coordinates. Dimensions includes, but are not limited to, space (X, Y, Z), time (t) and frequency bands (e.g. RGB). Models might also include probability or likelihood. Extent is defined as `left`, `right`, `up` and `down`, and refers to the rectangular map view. Predefined coordinates are the default units for the projection, e.g. `x` and `y` in metres, and degrees in WGS 1984, EPSG:4326. At setup, there is an option of the grid can represent both the corners or the centre points of each cell. The default settings gives a coarse global grid of WGS84 (EPSG:4326), with a resolution of $1^\circ \approx 111.1$ km.

`agrid` facilitates access to array operations in the spatial domains, as projected grid cells. The data is stored as data arrays in an `xarray` dataset (Hoyer et al., 2016, 2017). `xarray` is built on `numpy` (Oliphant, 2007; Van Der Walt et al., 2011) and `pandas` (McKinney, 2015), and provides high level functions for labelled multidimensional datasets. `xarray` has a structure similar to `netCDF` file format (Rew et al., 1990) and `netCDF` is also used as the native format to store grids. By using `dask` arrays, only the data used is loaded into memory in chunks (Rocklin, 2015). `dask` also facilitates some parallel computing. Grid cells can be selected with the advanced indexing methods in `xarray` by geographical coordinates as well as index numbers in the grid.

Additional coordinates with different resolution can be created and added to the object at any point. Computations with data grids of different resolution are performed by generating vectors from chunks of the larger array so that the resulting grid sizes are identical. The vectors are unfolded back to the higher resolution grid after the computation. By using this approach, fast `numpy` operations can be applied on arrays of different shapes and size and there is no need to over-sample low resolution data.

In a research project, `agrid` can point directly to original data sources. This simplifies the

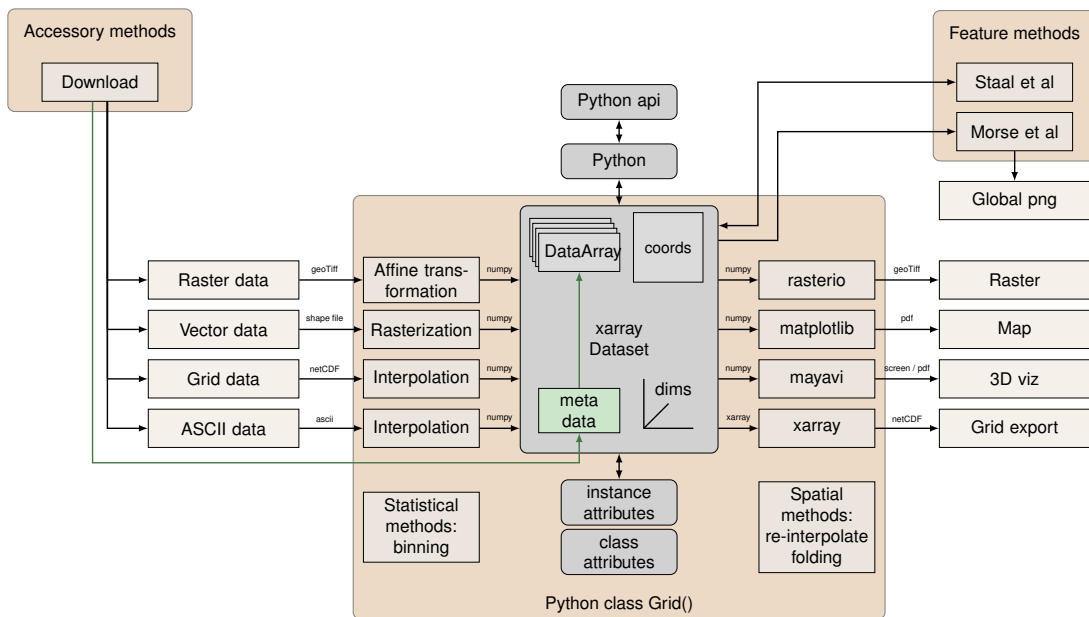


Figure 3a.1: Components of agrid: accessory methods, the class `Grid()` and example-specific code (feature methods). A class object (brown) contains functions for e.g. import and export. It also contains the xarray dataset (gray) and attributes. Various data formats (left) are converted to numpy arrays and incorporated as data arrays in an xarray dataset. Each data array can be associated to coordinates. The dataset also contains metadata (green). Data can be exported or visualized (right). Accessory methods include a download function to link the `Grid()` class directly to the data source if required, e.g. for dynamic updating. A few example-specific methods are also distributed together with the module (Morse et al., 2019; Stål, 2019b; Stål et al., 2019c).

workflow, as development can be done in low resolution or small extent, but larger grids can be used when required and data-sets can easily be swapped. Pre-processing and visualisation can be moved from third part software or stand-alone applications to a condensed workflow (Fig. 3a.1 and Listings 3a.1 and 3a.2). This provides overview and facilitates reproducibility and flexibility for the researcher (Hinsen, 2011).

3a.3.1 Example of Grid Generation and Data Import

Code in Listing 3a.1 generates a frame of Antarctica, using WGS 84 / Antarctic Polar Stereographic projection and a lateral cell size of $10 \text{ km} \times 10 \text{ km}$. The Extent is defined in the default unit of the projection. Coordinate reference system (CRS), is given as an integer and therefore interpreted as an EPSG code. For this example, the 2D grid is Cartesian and quadratic, but the depths slices are defined by the list `depths`. Due to the convention of indexing arrays as row - column and geographical coordinates as lat - lon, grid coordinates are also given as Y - X for consistency.

```

1 from agrid.grid import Grid
2 from agrid.acc import download
3 km = 1000
4

```

```

5 # Initiate a class object and set resolution and extent of model:
6 ant = Grid(res = [10*km, 10*km],
7           crs = 3031,
8           depths = [0*km, 10*km, 20*km, 50*km, 100*km],
9           left = -3100*km,
10          up = 3100*km,
11          right = 3100*km,
12          down = -3100*km)
13
14 # Download and import:
15 bedmap_url = 'https://link/to/bedmap2_tiff.zip'
16 bedmap_path = 'data/bedmap2'
17 download(bedmap_url, bedmap_path + '.zip')
18
19 GSFC_url = 'http://link/to//GSFC_DrainageSystems'
20 GSFC_files = 'data/GSFC_DrainageSystems'
21 for shape_ext in ['.shp', '.shx', '.prj', '.dbf', '.qix']:
22     download(GSFC_url + shape_ext, GSFC_files + shape_ext)
23
24 # Bulk import grid files from directory:
25 seis_url = 'http://link/to/AN1-S_depth_grd.tar.gz'
26 seis_path = 'data/an/'
27 download(seis_url, seis_path, bulk=True,
28          meta_dict = {'Model': 'AN1-S', 'DOI': '10.1002/2014JB011332'})
29
30 # Import raster files
31 for data_set, label in zip(['thickness', 'bed'], ['ICE', 'DEM']):
32     ant.ds[label] = (('Y', 'X'),
33                    ant.read_raster('%s/bedmap2_%s.tif' %(bedmap_path, data_set),
34                                   no_data = 32767.))
35
36 # Import polygons, here the attribute 'ID' is used to define segments.
37 ant.ds['DRAINAGE'] = (('Y', 'X'), ant.assign_shape(GSFC_file + '.shp', 'ID'))
38
39 # Import grid files to 3D data array.
40 # Keyword 'bulk' imports all files in directory
41 ant.ds['AN1-S'] = (('Y', 'X', 'Z'), ant.read_grid('../local/an/', bulk=True))

```

Listing 3a.1: Initiation of a grid object, defining extent and projection for Antarctica, in this example. The code downloads and assigns Bedmap(Fretwell et al., 2012), Antarctic drainage systems, GSFC (Zwally et al., 2012) and wave speed from 3D seismic tomography (An et al., 2015a) to the grid.

The instance of `Grid()` class contains a number of functions to import data of different types, visualisation and export (Fig. 3a.1). Raster data, e.g. GeoTiff, can be imported with a method using rasterio (Gillies, 2013b) and the underlying gdal (Warmerdam et al., 2018). Rasters are warped to fit the extent, resolution and projection of the grid. An imported raster is shown in Fig. 3a.2b. Vector data are imported with fiona (Gillies, 2014) and geopandas (Jordahl, 2014) with options for rasterization of attribute data and interpolation. Grids or data points can be read from a number of formats and interpolated. A rasterized polygon dataset is shown in Fig 3a.2a and is also used to crop and select data in Fig. 3a.2c-d.

3a.3.2 Example of Visualization and Data Export

The class also contains functions for visualisation using matplotlib (Hunter, 2007) and Cartopy (Met Office, 2016) (Fig. 3a.2a-c. Map views with e.g. coast lines and coordinates can be produced directly by agrid. Mayavi (Ramachandran et al., 2011) and the underlying VTK (Schroeder et al., 2005) are used for 3D visualisation (Fig. 3a.2 d. Data can be exported as netCDF, GeoTiff or ASCII formats. JSON format is used to import metadata and export model parameters.

```

1
2 # Select a few polygons:
3 ant.ds['SEL_ICE'] = ant.ds['ICE']*ant.ds['DRAINAGE'].isin(list(range(0, 53//2)))
4
5 # Make some 3D data, using e.g. Python or numpy functions
6 ant.ds['RANDOM'] = (('Y', 'X', 'Z'), np.random.rand(*ant.shape3))
7
8 # Make maps:
9 # Fig. 2a
10 ant.map_grid('DRAINAGE',
11             cmap='RdBu',
12             save_name='fig/drainage.pdf')
13
14 # Fig. 2b
15 ant.map_grid('SEL_ICE',
16             cmap='viridis',
17             save_name='fig/selected.pdf')
18
19 # Fig. 2c
20 ant.layer_cake('AN1-S',
21              cmap='BrBG_r',
22              save_name='fig/layers.pdf')
23
24 # Fig. 2d
25 ant.oblique_view('DEM',
26                 vmin=0, vmax=4200,
27                 cmap='bone',
28                 azimuth=180, roll=-90,
29                 save_name='fig/oblique_view.pdf')
30
31 # Analyse:
32 # Calculate the volume of the ice in selected segments.
33 volume = int(ant.ds['SEL_ICE'].sum()*np.prod(ant.res)/km**3)
34
35 # Export as geoTiff:
36 grid_to_raster('SEL_ICE', 'selected_ice.tif',

```

Listing 3a.2: Visualization, analyse and export. The code generates all figures in Fig.3a.2.

3a.4 Quality Control

The module is published with a number of tutorials to demonstrate the functionality with different data sources, scales and extent. Known limitations exist in the visualization methods for less common projections and some warnings are not handled smoothly. Error handling mainly relies on used dependencies with only limited functionality in agrid itself. Development errors have been ruled out by comparing results from other GIS applications. 2D data that have been imported, processed and exported, have been compared to similar processing in the GIS applications QGIS. Those test cases and additional test code are also available from the project's github repository (Stål, 2019a). The updated issue tracker is likewise available at github.

(2) Availability

Operating system

The code is developed and tested in Ubuntu 16.04, 18.04 and macOS High Sierra 10.13.6. It has also been tested on Windows 10.

Programming language

Python \geq 3.6 (tested on Python 3.6 and Python 3.7).

Additional system requirements

Very low requirements for basic use, but can be scaled up for larger grids. The use of disk arrays relax the need for large RAM.

Dependencies

The class depends on a number of Python packages that can all be installed by package managers, e.g. pip3 or conda: Minimum dependencies: cartopy geopandas matplotlib json numpy pyproj rasterio scipy xarray

Additional dependencies used and imported only by some methods: datetime fiona imageio mayavi requests shapely tarfile tqdm zipfile.

List of contributors

Tobias Stål, Anya M. Reading

Software location:

Name: agrid

Persistent identifier: <https://doi.org/10.5281/zenodo.2553965>

Licence: MIT License

Publisher: Tobias Stål

Version published: 0.4.0

Date published: March 24, 2021

Code repository

Name: GitHub

Persistent identifier: <https://github.com/TobbeTripitaka/agrid.git>

Licence: MIT License

Date published: March 24, 2021

Language

agrid was developed in English.

(3) Reuse potential

agrid is deliberately developed for reuse in a broad range of applications. The code is commented and explained to guide and advice modifications. The code could be useful for any spatial processing and analysis in areas such as solid Earth geophysics, geotechnical and environmental applications. For some uses, the complete package might be installed, but with the open architecture, copied snippets or methods can be included into other projects. The MIT license allows for a broad reuse. Functionality and issues may be discussed on the code repository. Python and the used libraries are also supported by large online communities.

Acknowledgements

We are grateful for discussions and test cases with Eleri Evans, Jacqueline Halpin, Shawn Hood, Peter E Morse and Joanne Whittaker. We also wish to thank two anonymous reviewers.

Funding statement

This research was supported under Australian Research Council's Special Research Initiative for Antarctic Gateway Partnership (Project ID SR140300001).

Competing interests

The authors have no competing interests to declare.

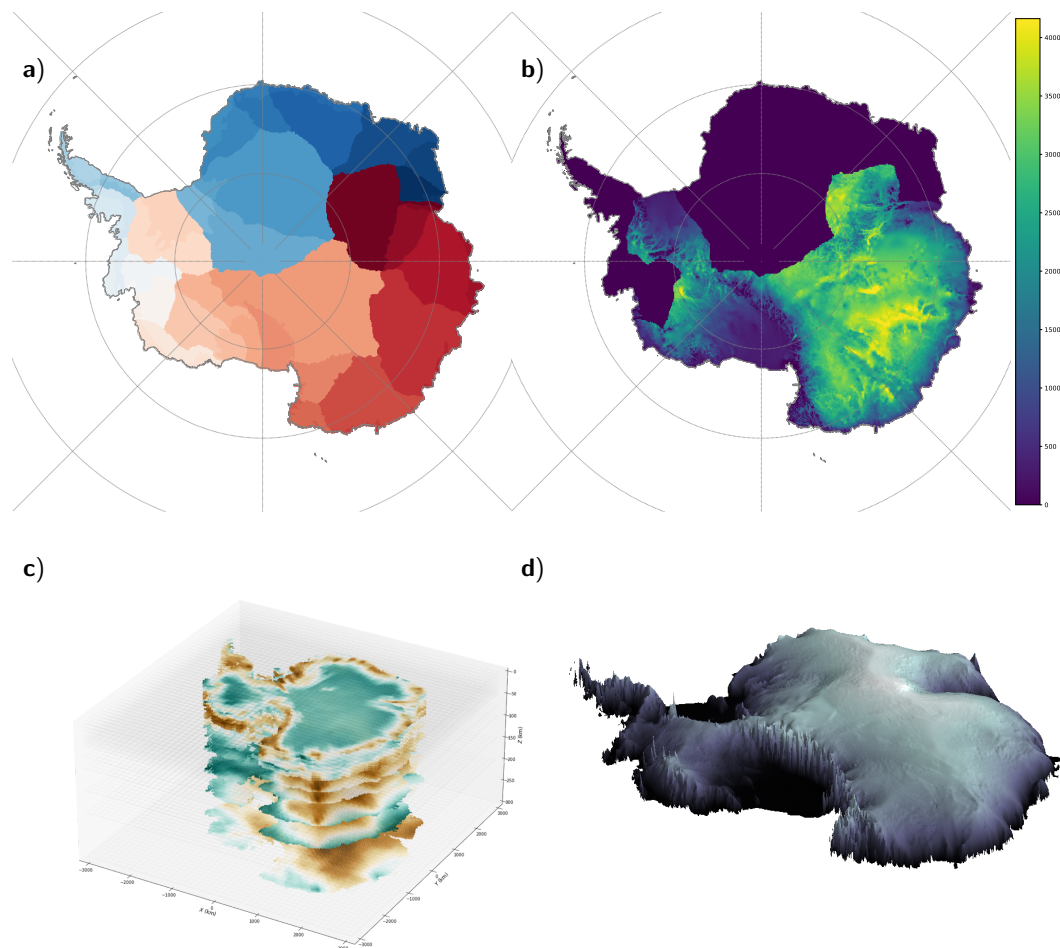


Figure 3a.2: Data input and visualisation examples generated by code Listings 3a.1 and 3a.2. (a) Vector polygon data (drainage systems (Zwally et al., 2012)). (b) Subset of raster data (ice thickness (Fretwell et al., 2012)) Polygon vector data (Zwally et al., 2012) is used to select a part of the continuous raster. (c) 3D layered plot of seismic data (An et al., 2015a). (d) Example of 3D rendering. Supplied tutorials and SCons script contain further details. The code may be used for any geographic area, at any scale.

Chapter 3b

The Antarctic Crust and Upper Mantle: A Flexible 3D Model and Software Framework for Interdisciplinary Research

Tobias Stål^{1,2}, Anya M. Reading^{1,2}, Jacqueline A. Halpin², Steven J. Phipps², and Joanne M. Whittaker²

1. School of Natural Sciences (Earth Sciences), University of Tasmania
2. Institute for Marine and Antarctic Studies, University of Tasmania

Abstract

Interdisciplinary research concerning solid Earth-cryosphere interaction, and feedbacks, requires a working model of the Antarctic crust and upper mantle. Active areas of interest include the effect of heterogeneous Earth structure on glacial isostatic adjustment, the distribution of geothermal heat, and the history of erosion and deposition. In response to this research need, we construct an adaptable and updatable 3D grid model in a software framework to contain and process solid Earth data. The computational framework, based on an open source software package *agrid*, allows different data sources to be combined and jointly analysed. The grid model is populated with crustal properties from geological observations and geochronology results, where such data exist, and published segmentation from geophysical data in the interior where direct observations are absent. The grid also contains 3D geophysical data such as wave speed and derived temperature from seismic tomographic models, and 2D datasets such as gravity anomalies, surface elevation, subglacial temperature and ice sheet boundaries. We demonstrate usage of the framework by computing new estimates of subglacial steady-state heat flow in a continental scale model for East Antarctica, and a regional scale model for the Wilkes Basin in Victoria Land. We hope that the 3D model and framework will be used widely across the solid Earth and cryosphere research communities.

3b.1 Introduction

Past, present, and future changes in the mass of the Antarctic ice sheets have a direct impact on global sea level (e.g., DeConto et al., 2016; Golledge et al., 2015; Golledge et al., 2019; King et al., 2012; Ritz et al., 2015; Shepherd et al., 2012). During the 21st century and beyond, the projected rise in sea level in response to anthropogenic climate change is expected to have enormous social and economic consequences (e.g., Kulp et al., 2019; Oppenheimer et al., 2019). Constraining the likely response of ice sheets to global climate change is therefore a high priority. The mechanisms controlling the extent and thickness of the cryosphere involve interaction with the atmosphere (e.g., DeConto et al., 2016; Frieler et al., 2015; Lenaerts et al., 2016), the ocean (e.g., DeConto et al., 2016; Dinniman et al., 2016; Rintoul et al., 2016), and the crust and mantle beneath, which is the focus of this contribution. Examples of solid Earth-cryosphere interaction include the impact of heterogeneous Earth structure on glacial isostatic adjustment (e.g., Whitehouse, 2018), the amount and distribution of geothermal heat (e.g., Pattyn, 2010), and the history of erosion and deposition over geological time (e.g., Paxman et al., 2018). The continental crust is a highly heterogeneous layer usually characterised by a combination of geological observations, geochronological results, tectonic plate reconstructions and geophysical surveys to obtain an overall picture of the composition, age, evolution and 3D architecture of its constituent units. A sharp change in seismic wave speed, the Mohorovičić discontinuity (Moho), defines the boundary between the crust, and the mantle beneath (An et al., 2015a; Christensen, 1988). The upper mantle provides a rigid and tectonically mobile component, which together with the crust forms the continental lithosphere. A deeper seismic discontinuity, the lithosphere-asthenosphere boundary (LAB) indicates the transition to ductile mantle as a result of increasing temperature and pressure with depth (Artemieva, 2011). Many aspects of the Earth’s crust and mantle have significant spatial variability that impact overlying ice sheets, hence, access to solid Earth research results has gained importance to the interdisciplinary research community (Whitehouse et al., 2019).

3b.1.1 Geology, Geochronology, and Geochemistry

Our understanding of the Antarctic crust is restricted by the ice cover that leaves only 0.18% of the rocks exposed (Burton-Johnson et al., 2016), with access further limited by logistical difficulties. Early field campaigns enabled geological investigations to map out crustal domains along the Antarctic coast and Transantarctic Mountains (Craddock, 1970; R. J. Adie, 1977; Ravich et al., 1965; Tingey et al., 1991). Those interpretations are, to a large extent, still valid, although more recent field geological studies have expanded the number of outcrops visited. Geochronology and geochemistry have added insight to refine our understanding by constraining event chronologies, derive likely tectonic environments, and, in conjunction with geophysics, also allows geological correlation (regional and local studies include e.g., clockwise around the Antarctic continent: Burton-Johnson et al., 2015; Corvino et al., 2008; Daczko et al., 2018; Di Vincenzo et al., 2007; Goodge et al., 1992; Halpin et al., 2012, 2005; Jacobs et al., 1998; Maritati et al., 2019; Marschall et al., 2010; Morrissey et al., 2017; Siddoway et al., 2004a; Tucker et al., 2017; Will et al., 2009; Williams et al., 2018; Yakymchuk et al., 2015).

Interpretations of Antarctic geology are often contextualised in a tectonic reconstruction framework (Du Toit, 1937; Matthews et al., 2016; Whittaker et al., 2013b; Williams et al.,

2019), and can hence be guided by data from continents that were adjoined in Gondwana, especially Australia, India and Africa (e.g., Aitken et al., 2014; Daczko et al., 2018; Fitzsimons, 2000a; Yoshida et al., 1992). Blocks of once continuous Archean cratons and orogenic belts are split between East Antarctica and Africa, India and Australia. West Antarctica mostly consists of younger Phanerozoic crust (Artemieva et al., 2020; Boger, 2011; Jordan et al., 2020; Siddoway, 2008). Archean and Paleoproterozoic crust is mainly cratonic, Proterozoic crust is formed by the reworked orogens of Nuna and Rodinia, and more recently, Phanerozoic crust has been added by Gondwanan and Cenozoic accretions and volcanism. Extensive reviews have drawn well founded interpretations for coastal regions (e.g., Boger, 2011; Harley et al., 2013; Jordan et al., 2020), but due to the lack of data, geological and tectonic maps of the ice covered interior rely significantly on extrapolation. An ongoing challenge is to access and incorporate the large amount of often inconsistent geological, geochronological and geochemical studies. Initiatives such as the GeoMAP project (Cox et al., 2018) and compilations of rock sample data (e.g., Gard et al., 2019) aim to facilitate geological studies of Antarctica, using the broad range of published data.

3b.1.2 Geophysics

Significant emphasis is placed on geophysical methods, particularly for East Antarctica, to infer geological information about ice-covered regions from remotely observed physical properties. Geophysical data are acquired from ground measurements, airborne instruments and satellites (Fowler, 1990).

Seismic measurements are sparse in Antarctica, and are often clustered according to the given regional study (e.g., Hansen et al., 2016, 2010; Heeszel et al., 2016; Reading, 2006; Shen et al., 2018a; Winberry et al., 2004). Data from Antarctic deployments and global databases are used to generate continental scale seismic models (An et al., 2015a; Lloyd et al., 2020). Airborne geophysics coverage is variable across the continent. Large international campaigns, such as ICECAP (e.g., Aitken et al., 2014; Graham et al., 2017; Roberts et al., 2011; Young et al., 2011), acquire data over multiple summer seasons enabling extensive spatial coverage. Multiple datasets, including high resolution magnetic and gravity anomalies, surface elevation and ice penetrating radar are usually acquired simultaneously (e.g., Aitken et al., 2014; Robert et al., 2017) and Antarctic research has been accelerated by carefully curated compilations of such data (Fretwell et al., 2012; Morlighem et al., 2019). Notable regional airborne campaigns include targets such as Gamburtsev Subglacial Mountains (Ferraccioli et al., 2011), the South Pole satellite polar gap (Forsberg et al., 2017; Sneeuw et al., 1997), Dronning Maud Land (Jacobs et al., 2015; Ruppel et al., 2018) and Transantarctic Mountains (Goodge et al., 2010). Magnetic data has been compiled as continental scale maps (ADMAP and ADMAP2, Frese et al., 2007; Golynsky et al., 2018, 2013a). Global satellite gravity surveys such as GOCE and GRACE are of particular importance in Antarctica due to the consistent cover of long-wavelengths anomalies (Förste et al., 2013; Pail et al., 2011; Visser, 1999). Continuous satellite measurements facilitate the identification of changes over time, such as mass loss (King et al., 2012; Velicogna, 2009), and changes in altimetry of the glacial surface from e.g. CryoSAT-2 altimetry (Slater et al., 2018).

Modelling studies that are particularly important in the Antarctic context include making

use of the curvature of gravity field (Ebbing et al., 2018), finding the elastic crustal thickness (Chen, 2019), comparison of models of e.g. Moho depth from various approaches (Baranov et al., 2018; Pappa et al., 2019a) and integrating density, compositional and thermal models (Haeger et al., 2019). Interpretation of magnetic anomalies combined with other datasets can support delineation of crustal domains (Aitken et al., 2014; Goodge et al., 2010; Paxman et al., 2019a; Ruppel et al., 2018) and used to infer depth to the Curie temperature isotherm (Fox Maule et al., 2005; Martos et al., 2017).

3b.1.3 Solid Earth-Cryosphere Interactions

Mapping tectonic domains from geological data provides a first order segmentation of the lithosphere for 3D glacial isostatic adjustment models (Kaufmann et al., 1999; Nield et al., 2018). Crustal heat production can to some extent be estimated from geochemistry (Hasterok et al., 2017) and geochronology (Jaupart et al., 2013). Likewise, mass transport by glacial exhumation and deposition is informed by geological and geochronological observations. From ground, airborne and satellite data, modelling exercises, and from comparisons with other continents, it is becoming increasingly apparent that we should expect large spatial variations in the subglacial physical properties of the crust and upper mantle in the Antarctic interior. This heterogeneity impacts solid Earth-cryosphere interaction on regional and local scales.

3b.1.3.1 Glacial Isostatic Adjustment

Glacial isostatic adjustment (GIA) is the response of the viscous mantle and rigid lithosphere to changes in ice load (e.g., Whitehouse, 2018). As ice sheets melt, mass is transferred from the continent to the ocean, and the continental crust rebounds in response to the resulting buoyancy force. Lateral variations in lithospheric thickness and the viscosity of the deforming Earth's mantle impact the rate and nature of this rebound e.g., Kaufmann et al., 1999; Nield et al., 2014, 2018. The crustal movement is measured by GPS time series (e.g., Martín-Español et al., 2016), and past uplift can be reconstructed from geomorphological observations by dating raised beaches, glacial erratics and sediments (MacKintosh et al., 2011; White et al., 2010). The observed elevation does not, in general, represent isostatic equilibrium as the Antarctic lithosphere is at present adjusting in response to changes in ice load and global sea level (Gunter et al., 2014; Peltier, 2004b; Whitehouse, 2018; Whitehouse et al., 2012).

3b.1.3.2 Subglacial Geothermal Heat

Geothermal heat flow, often termed 'heat flux' in ice sheet modelling studies, is a necessary boundary condition in many ice sheet models (e.g., Winkelmann et al., 2011). Heat at the base of slow flowing ice sheets can cause melting that impacts ice flow speed and can reduce the stability of the ice sheet. It can also impact the ice viscosity and hence affect internal deformation (e.g., Matsuoka et al., 2012; Pattyn et al., 2016; Petrunin et al., 2013). Heat is generated in the interior of the Earth and reaches the surface due to the temperature gradient. This is regulated by the thermal conductivity of the crust and mantle. Heat flow is known to be highly variable on continental, regional and local scales (Beardmore et al., 2001; Begeman et al., 2017; Cull, 1982; Jordan et al., 2018; McLaren et al., 2003; Pollett et al., 2019; Ramirez

et al., 2016). At plate margins and locations such as extensional basins, heat flow through convection or advection, by moving fluids and/or magma at depth, may be dominant.

Several different approaches are in current use to estimate the subglacial heat flow from modelled temperature gradients (Discussed by Burton-Johnson et al., 2020; Lösing et al., 2020). Magnetic derived heat flow maps are produced from either equivalent source magnetic dipole models (Fox Maule et al., 2005) or magnetic spectral analysis from high resolution airborne data (Martos et al., 2017). Both methods are used to estimate a depth to the Curie temperature isotherm. Another approach uses seismic wave speed as an indirect measure of temperature at depth. Temperature is the main controlling factor of lateral variations in seismic wave speed in the upper mantle (An et al., 2007; Cammarano et al., 2003; Goes et al., 2000; Shapiro et al., 2004). An et al. (2015a) presented a surface wave tomography model constrained by receiver functions. From the wave speed, upper mantle temperatures are inferred and thermal gradients to the surface estimated (An et al., 2015b). Both the magnetic and seismic approaches have limitations due to their underlying assumptions, accuracy and resolution. A significant challenge when estimating subglacial heat flow is the need to account for the unconstrained lateral variations in heat production and thermal conductivity in the crust. Heat production varies over a large range for different rock types (Carson et al., 2014; Hasterok et al., 2017; Jaupart et al., 2016), and including geological knowledge in regional studies is of great value (e.g., Burton-Johnson et al., 2017; Burton-Johnson et al., 2020; McLaren et al., 2003). Direct measurements of the subglacial heat flow are very sparse in Antarctica (e.g., Begeman et al., 2017; Fisher et al., 2015), and some studies derive subglacial conditions from measurements within the ice (discussed by e.g. Mony et al., 2020). Heat anomalies are also known from radar images of the ice sheet (e.g., Jordan et al., 2018; Schroeder et al., 2014), the presence of subglacial lakes (Pattyn et al., 2016) and by inversion of ice sheet models (Pattyn, 2010).

3b.1.3.3 Erosion and Deposition

The subglacial topography of Antarctica is the result of its tectonic evolution overprinted by cycles of erosion, exhumation and redeposition of sediment by rivers and glaciers. Topography can influence ice sheet dynamics through parameters such as direction of slope (e.g., Greenbaum et al., 2015), and fine-scale roughness (Goff et al., 2014; Graham et al., 2017). Subglacial topography is constrained by ice penetrating radar, gravity and seismic data. With data compilations such as Bedmap2 and BedMachine (Fretwell et al., 2012; Morlighem et al., 2019), a substantial part of the Antarctic subglacial landscape is revealed, but in many areas there are still large uncertainties (Fretwell et al., 2012; Graham et al., 2017). Glaciers are efficient in eroding and forming the landscape (Cowton et al., 2012; Koppes et al., 2009; Morlighem et al., 2019). Large amounts of sediment have been transported from Antarctica to the continental shelf and continental slopes (Sauermlch et al., 2019; Whittaker et al., 2013a), but in some areas the erosion has been very limited due to cold-based ice sheets that tend to preserve the existing topography (Jamieson et al., 2008; Paxman et al., 2018; Wilson et al., 2012).

Understanding of the subglacial landscape evolution by erosion and deposition calls for an interdisciplinary approach, whereby ice sheet development, geophysical data and geological data are combined to constrain Antarctica's past and present landscape, and isostasy (Jamieson et al., 2008; Jamieson et al., 2010; Mackintosh et al., 2014; Paxman et al., 2016; Paxman et al.,

2018, 2019a).

3b.1.4 Motivation for the 3D Grid Model

Reproducible models of the Antarctic crust and upper mantle are needed to progress interdisciplinary studies such as those relating to GIA, heat flow and topography. A better understanding of the solid Earth is achieved by combining multiple data sources (Begg et al., 2009; Pappa et al., 2019a; Stål et al., 2019c). Populating models with current data presents a challenge, especially given the present rate of new data releases that have the potential to improve existing results. Lateral variations of crustal properties are often absent from large scale geophysical studies. One successful attempt to facilitate data access is the Quantarctica project that links data to users via a GIS application (Roth et al., 2017). Quantarctica allows users to directly visualise and compare datasets of a different nature. However, GIS might not be the first choice for multidimensional data processing, and a scripted framework is desirable for geophysical modelling and analysis.

In this contribution we present a flexible 3D grid model of the Antarctic crust and upper mantle. We populate the grid with datasets that have been used in univariate studies to constrain lithospheric rheology, heat flow and erosion and uplift: e.g. seismic wave speed, thermal properties, subglacial topography, geology and crustal segmentation models (Table 3b.1). As a computational framework, we use *agrid*, an open software environment for storing, analysing and modelling multivariate and multidimensional data with functionality to visualize and export the results (Stål et al., 2020a). *agrid* depends on well documented Python packages such as *numpy* (Oliphant, 2006), *scipy* (Jones et al., 2015), *xarray* (Hoyer et al., 2017), *dask* (Rocklin, 2015) and *rasterio* (Gillies, 2013b). Computations using *numpy* are as fast and memory efficient as compiled code (Van Der Walt et al., 2011), and chunk parallelization is made possible using *dask* arrays.

The 3D grid model and computational framework are intended for a wide range of applications, and are designed to be updated as additional data become available. Thus, we make constraints and related uncertainty from geology, geochronology and geophysics available in a form that is usable by researchers in geoscience, glaciology and ice sheet modelling. Through this contribution, we aim to facilitate interdisciplinary studies on the interaction between the solid Earth and cryosphere of Antarctica.

3b.2 Data

Our model and framework includes numerous geological and geophysical datasets, together with the source reference, as listed in Table 3b.1. We limit the spatial extent of the grid to the present coastline and ice shelf grounding line (Mouginot et al., 2017). Some processing, such as resampling and interpolation, is applied when the data are imported. Data in global projections are first reprojected, then interpolated to avoid artifacts and distortion when interpolating across the South Pole and anti-meridian line. Some of the datasets included in this contribution certainly contain spatial distortion due to reprojection. This distortion typically has its origin when published are stored to a global grid. We do not aim to correct those artifacts in this contribution, as this would change the published datasets and require further discussion.

Instead, we include the datasets as they are published.

Uncertainty information relating to each parameter is included where available (E.g. Martos et al. (2017)). Those provided uncertainty values might not capture the total range of uncertainty that arise from necessary assumptions and resolution. Refined analysis of datasets and uncertainty can be achieved in the framework. However, this is beyond this contribution.

All data are also associated with provenance information and metadata that links the original source. Metadata are stored with the dataset in the grid. The *agrid* package (Stål et al., 2020a) contains methods to access the data directly from the original sources, open online repositories and through Quantarctica (Roth et al., 2017). Links to web addresses, current at the time of writing, are provided in the supporting material. In the case that a link becomes outdated, error handling is provided. There is no limitation to the number of datasets that can be included in a model. The datasets listed here are included to produce the test cases for appraisal of the framework.

3b.3 Methods and Results

In this section we outline the methods used to construct the 3D grid and illustrate the functionality of the computational framework through usage examples. All computations in this study are performed using the Python package *agrid* (Stål et al., 2020a). Use of *agrid* facilitates easy programming and compact scripts, with the underlying software being tailored to computations that use data, and metadata, held in the 3D grid. The figures in this study are generated using only a few lines of high level code, and functions provided with *agrid*. Where applicable, we utilize perceptually linear color representation (Crameri et al., 2019; Morse et al., 2019).

3b.3.1 Populating the 3D Grid

To populate the 3D model, the datasets listed in Table 3b.1 are imported. Datasets are re-sampled and interpolated to the defined extent, resolution, projection and cell sizes. Here we use bi-linear interpolation, but other refined techniques are available. Data imported from polygon vectors are rasterized and attributes saved to the grid using a map function. Observations at point locations, such as geochronological data (compiled by Gard et al., 2019), are binned to the containing grid cells. Datasets are projected to WGS 84 / Antarctic Polar Stereographic (EPSG:3031), with very limited distortion in continental Antarctica. The total grid extent is set to 6200×6200 km with a horizontal resolution of 20×20 km (fig. 3b.1, fig. 3b.2 and fig. 3b.3). The extent and resolution of the grid can easily be modified and multiple resolutions can be used simultaneously. Using the same code, but with smaller extent and higher resolution, the Wilkes Subglacial Basin is shown as a grid with 2×2 km cells (fig. 3b.4 and fig. 3b.5C-D). The choice of values for depth sections can also be easily modified and is illustrated in Figure 3b.1.

3b.3.2 Computational Framework: Usage Examples

The agility of our 3D framework allows the rapid generation of maps or other outputs. Such products may be used to support research discussion or as numerical inputs for other studies (e.g. boundary conditions for ice sheet models).

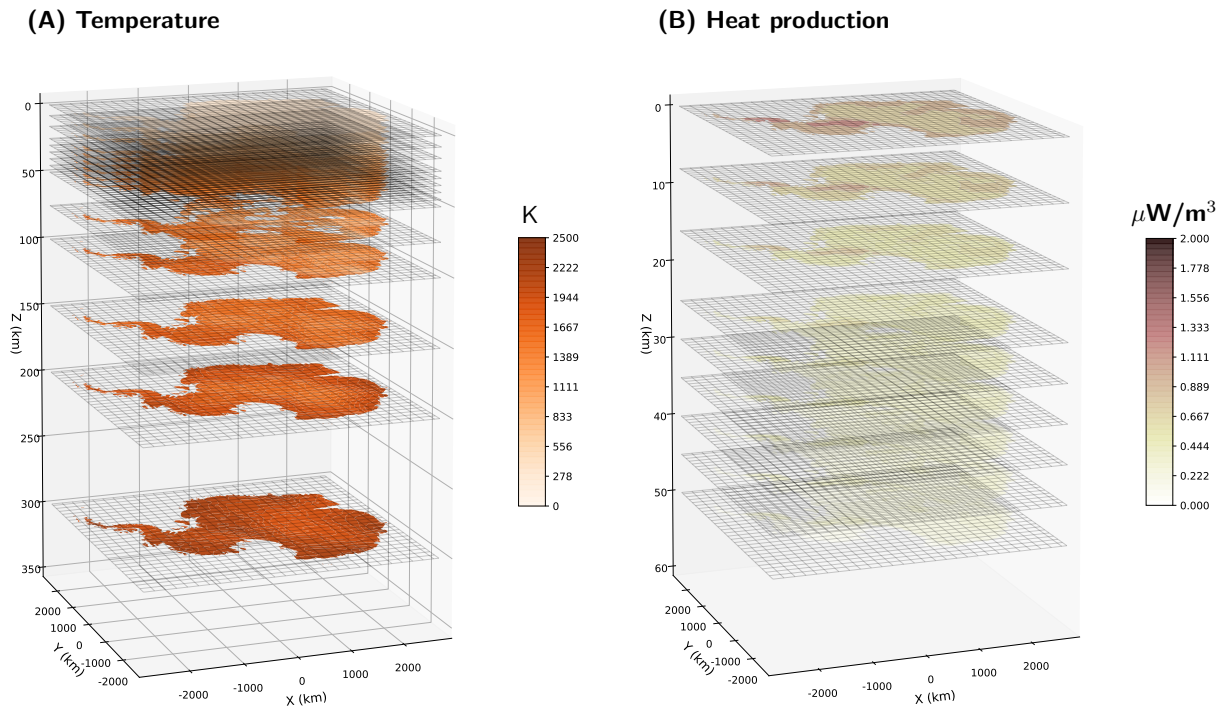


Figure 3b.1: Oblique view of data held in the 3D grid model and illustration of plotting functionality. The model space is delineated by the Antarctic coastline and ice shelf grounding line (Mouginot et al., 2017). Depth sections are set to; 0, 8, 16, 25, 30, 35, 40, 45, 50, 75, 100, 150, 200 and 300 km. **(A)** Temperature in the crust and upper mantle derived from shear wavespeed by merging models AN1-Tc and AN1-Ts (An et al., 2015b) interpolated to defined grid. **(B)** Heat production in the crust from a simplified exponential function of depth, average production from age (Jaupart et al., 2013), segmentation by Schaeffer et al. (2015) and crustal thickness from An et al. (2015a).

3b.3.2.1 Temperature in the Lithosphere and Heat Production in the Crust

Illustrating basic computation and oblique 3D visualisation using *agrid* and Antarctic datasets, Figure 3b.1A shows lithospheric temperatures combined from AN-Ts and AN1-Tc (An et al., 2015b), interpolated to fit the grid. Figure 3b.1B displays a first-order estimate of crustal heat production as a combination of crustal thickness (An et al., 2015a), segmentation (Schaeffer et al., 2015), heat production estimate from crustal age (Jaupart et al., 2016) and decreasing heat production as an exponential function of depth:

$$A = -A_0 \times e^{-z/d_{\text{Moho}}} \quad (3b.1)$$

where A is the value of heat production in W/m^{-3} , A_0 is the average heat production, given the age of the crust, at that location, and z/d_{Moho} is the fraction of depth to Moho, at the location.

3b.3.2.2 Calculated Outputs Based on Multiple Geophysical Datasets

Illustrating further examples of computation and visualisation in map view, Figure 3b.2 shows constraints from multiple heat flow models, and adjusted surface elevation based on multiple datasets. Minimum heat flow (fig. 3b.2A) and maximum heat flow (fig. 3b.2B) are the lowest and highest values at each grid cell in any of Fox Maule et al. (2005), An et al. (2015b) and Martos et al. (2017), including provided uncertainty. Figure 3b.2c shows the standard deviation as a measure of disagreement between the heat flow maps from aforementioned studies. Areas are readily seen where ice sheet modellers should be particularly careful when using the geothermal heat contribution as a boundary condition. The property maps shown in Figure 3b.2A-C could therefore be useful for sensitivity studies of the impact of geothermal heat on the ice sheet at a continental scale.

Isostatic models are used to understand how the Antarctic crust and upper mantle interact with the cryosphere (e.g., O'Donnell et al., 2014). Figure 3b.2d and 3b.4B show bedrock elevation for isostatically relaxed ice-free conditions. Such computations are easy to perform in our framework, for example, using the simplified formula:

$$\text{DEM}_{\text{iso}} = \text{DEM}_{\text{sg}} + \frac{(\text{DEM}_{\text{s}} - \text{DEM}_{\text{sg}}) \times \rho_{\text{ice}} \times D_{\text{LAB}}}{\rho_{\text{crust}} \times D_{\text{Moho}} + \rho_{\text{mantle}} \times (D_{\text{LAB}} - D_{\text{Moho}})} \quad (3b.2)$$

where DEM_{iso} is the adjusted elevation model, DEM_{sg} is the Bedmap2 subglacial elevation, DEM_{s} is the surface elevation (Fretwell et al., 2012), ρ_{ice} is the density of ice, assumed to be constant ($916.7\text{kg}/\text{m}^3$), and ρ_{crust} and ρ_{mantle} are applied from average crustal and lithospheric density in Afonso et al. (2019) reference model. We apply a 2D Gaussian kernel, with standard deviation of 60 km to include a simple constant model for the rigidity of the lithosphere. Figure 3b.2D shows the elevation if the present ice mass were to be removed and the lithosphere regained its isostatic buoyancy. For ice sheet reconstructions of the past, or predictions of the future, the isostatic response of the solid Earth must be considered, as the coastline and ice shelf grounding lines are not static. Using our 3D model and framework, research tasks, such as testing alternative reconstructed ice masses, and recalculating the isostatic correction, are as straightforward as importing the modelled map of ice thickness.

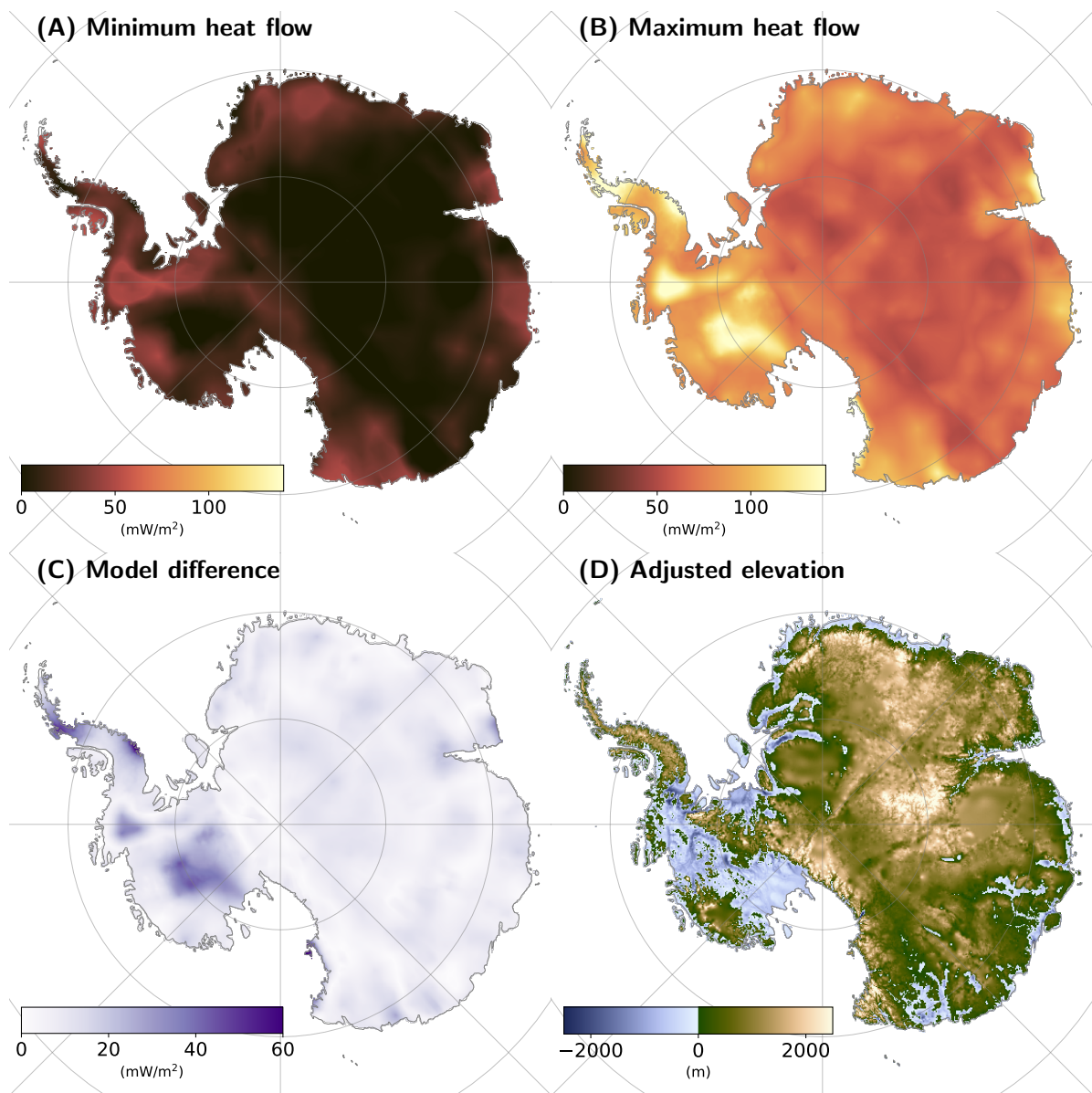


Figure 3b.2: Examples of simple calculated outputs and visualisation in map view. Colour representation is optimised for visibility. **(A)** Minimum subglacial heat flow from three studies (An et al., 2015b; Fox Maule et al., 2005; Martos et al., 2017) using provided uncertainty ranges. **(B)** Maximum heat flow from the same three studies using provided uncertainty ranges. **(C)** Disagreement as standard deviation of the spread of the three studies. **(D)** Surface elevation with adjusted isostasy for ice removed. Calculated from Fretwell et al. (2012) and assuming constant density of ice 916.7 kg/m^3 , the crustal and mantle densities from Afonso et al. (2019). Moho from (An et al., 2015a) and LAB from (An et al., 2015b). A simple smoothing represents the rigidity of the lithosphere, as described in text.

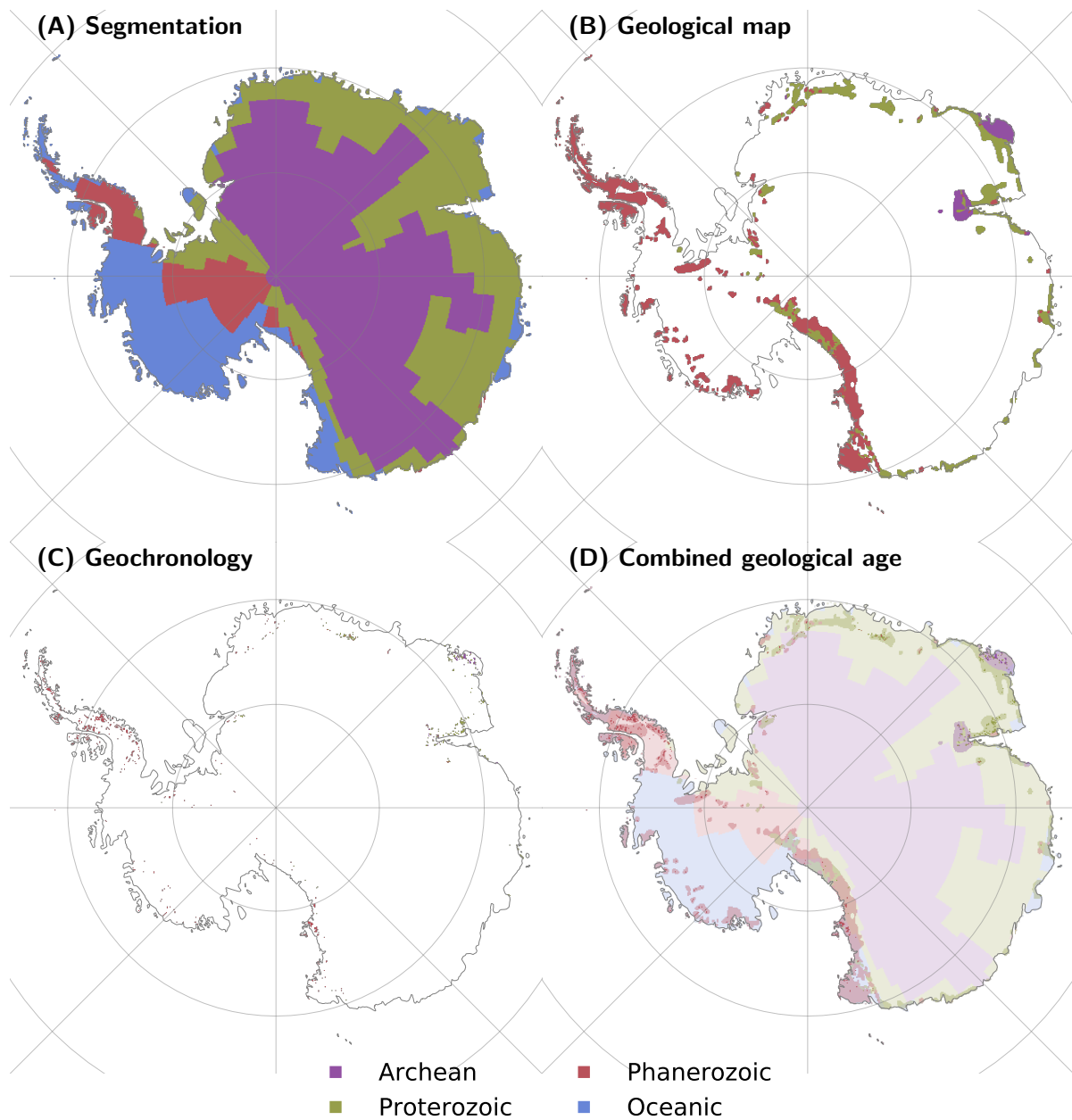


Figure 3b.3: New maps generated to show the methodology of using data held in the 3D grid model. **(A)** Segmentation from seismic tomography (Schaeffer et al., 2015). **(B)** Schematic geological age map (Tingey et al., 1991). **(C)** Actual geochronology compiled by (Gard et al., 2019). The dataset is clipped by mapped rock outcrops from Burton-Johnson et al. (2015) to mitigate errors. **(D)** Geological age estimated from a combination of the previous three datasets, with Gard et al. (2019) as preferred and indicated with shading in a strong tone, Tingey et al. (1991) as midtone, and Schaeffer et al. (2015) in faint tone. Continental crustal age, and geochronological data are divided into three classes (Janse, 1984) and as discussed in text: Archean (purple), Proterozoic (green) and Phanerozoic (brown). Suggested oceanic crust in Schaeffer et al. (2015) is shown in blue. White indicates no data (B-C).

3b.3.2.3 Mapping Crustal Age by Merging Geological and Geophysical Datasets

Mapping crustal age provides an illustration of merging geological and geophysical sources, addressing the challenge of combining categorical and numerical data types. We utilize geochronological measurements compiled by Gard et al. (2019). The number of samples (Supplementary material), mode, average value and standard deviation are calculated and binned to each cell. The legacy schematic geology map from Tingey et al. (1991) is used for reference and to guide moderate extrapolation of geology. Age estimates expressed in geological time are converted to age in years (Stål, 2019b). Where no geological observations or extrapolation are available, we use crustal segmentation informed by seismic tomography. Most global regionalization studies often exclude or oversimplify Antarctica due to the limited available data (e.g., Artemieva, 2006, 2009; Artemieva et al., 2001; Jordan, 1981). We implement one of the few continental scale segmentation models that covers Antarctica, the k-means clustering of surface-wave dispersion from Schaeffer et al. (2015), which makes use of methods by Lekić et al. (2010) and data first presented by Schaeffer et al. (2013). Examples of the standardised content reduced to three age classes and oceanic crust are shown on a continental (fig. 3b.3) and regional scale (fig. 3b.4C). The shading tone indicates the source, and hence, the robustness of the constraint. Direct observations (Gard et al., 2019) are strong in tone, schematic geological domains (Tingey et al., 1991) are shown in midtone and geophysical regionalisation (Schaeffer et al., 2015) is shaded in a faint tone. Combining data of different types is straightforward in concept, but challenging in practice, and the new framework shows that this can be achieved in a repeatable manner.

3b.3.2.4 Calculated Outputs at Higher Resolution

Illustrating the functionality of the 3D model and framework at a regional scale, Figure 3b.4 shows data held in the 3D grid and calculated outputs for the Wilkes Subglacial Basin. Figure 3b.4A is a representation of the Bedmap2 dataset (Fretwell et al., 2012). Figure 3b.4B shows the same simplified isostatic correction as Figure 3b.2D in higher resolution. Figure 3b.4C shows the combined model of crustal stabilisation age, using same methods as for Figure 3b.3D, again at higher resolution, for the Wilkes Basin.

3b.3.2.5 AqSS, a Steady-State Heat Flow Model

We further illustrate the functionality of the computational framework through generating a Steady-state heat flow model, AqSS, which combines geophysical and geological data. steady-state models can be reduced to two components that are identified as sources of geothermal heat: heat from the Earth's core and mantle, reaching the crust as heat flow through the Moho, q_m , and a commonly larger component, heat generated within the crust.

$$q_g = q_m + d_m \times A_c \quad (3b.3)$$

where q_g is the subglacial heat flow, q_m is the heat flow at the Moho, d_m is the crustal thickness (An et al., 2015a; Fretwell et al., 2012) and A_c is an average heat production within the crust.

From studies in different geological settings and methods, the mantle component has been constrained to $q_m = 14 \pm \sim 3 \text{mWm}^{-2}$ (Guillou et al., 1994; Jaupart et al., 2016; Roy et

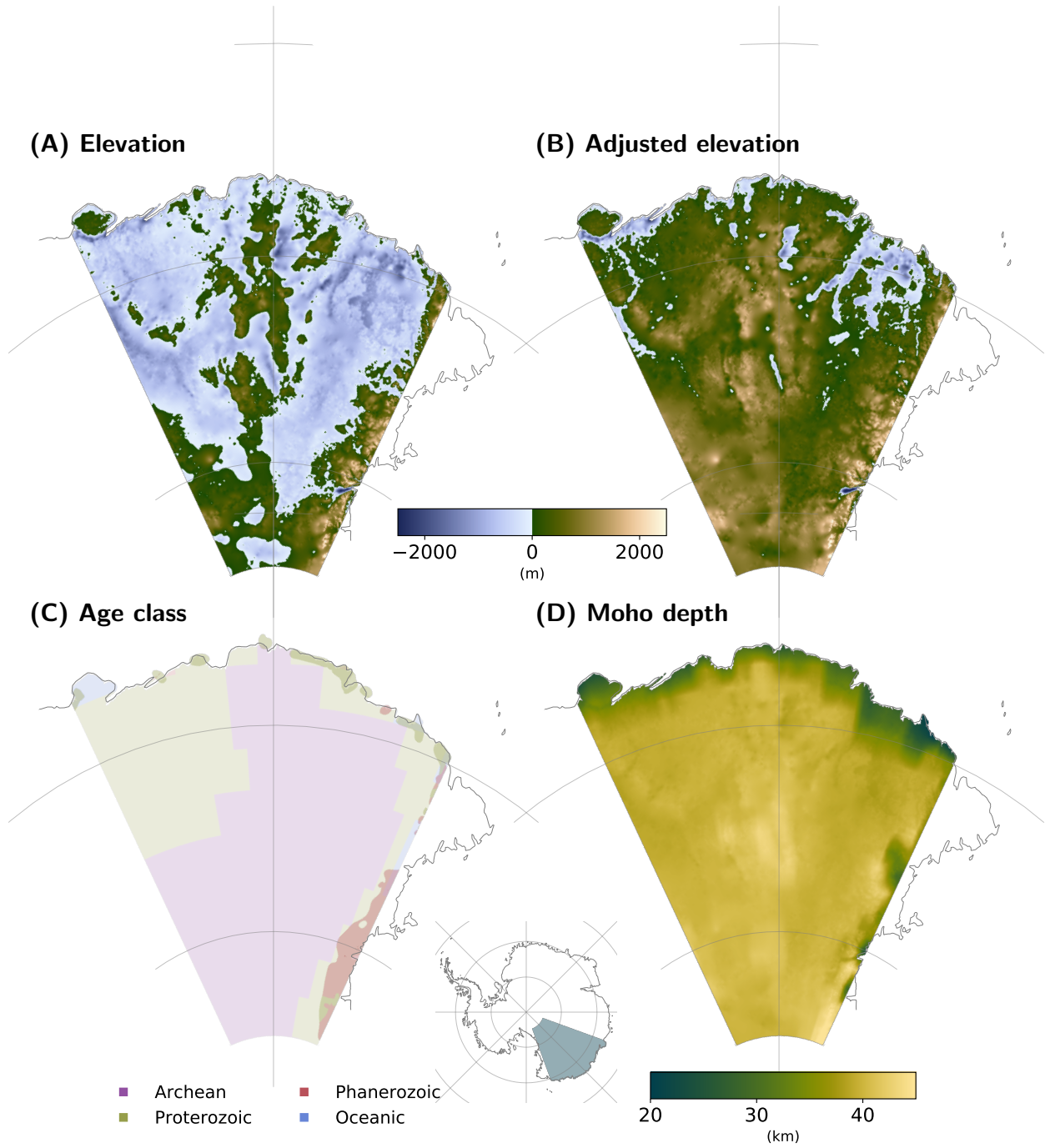


Figure 3b.4: (Caption next page.)

Figure 3b.4: New maps generated for Wilkes Basin showing data held in the 3D grid model and calculated outputs at higher resolution. **(A)** Present subglacial topography, Bedmap2 (Fretwell et al., 2012). **(B)** Subglacial topography, with ice removed and isostasy corrected using crustal thickness from An et al. (2015a) and lithospheric thickness from (An et al., 2015b). Crustal and upper mantle densities from (Afonso et al., 2019). Bedrock elevation and surface elevation from Bedmap2 (Fretwell et al., 2012). **(C)** Estimates of crustal age. Cells with geological observations in strong tone (Burton-Johnson et al., 2015; Gard et al., 2019), schematic geology (Tingey et al., 1991) in mid tone, and segmentation from Schaeffer et al. (2015) in light tone. Continental crustal age is classified into three classes, Archean (purple), Proterozoic (green), Phanerozoic (brown), together with oceanic crust (blue). Methods are discussed in the text. **(D)** Crustal thickness from An et al. (2015b).

al., 2003; Rudnick et al., 1999), which is within the uncertainty of most Antarctic heat flow estimates (e.g., Martos et al., 2017).

Uncertainty for AqSS is calculated from the uncertainty provided with each dataset, assuming they are independent.

$$\sigma_q = \sqrt{\sigma_{qm}^2 + \left(d_m \times A \sqrt{\frac{\sigma_{Ac}^2}{A} + \sigma_{d_m}^2}\right)^2} \quad (3b.4)$$

where σ_q is the absolute heat flow uncertainty, σ_{qm} is the absolute uncertainty of heat flow into the crust, 3 mWm^{-2} (reviewed by Jaupart et al., 2016). The relative uncertainty of crustal thickness (σ_{d_m}) is set to 15%, A is the absolute mean heat production and σ_{Ac} is half of the range of heat production as suggested by Jaupart et al. (2013) and listed in Table 3b.2.

By assuming steady-state conditions throughout East Antarctica and applying a constant contribution from the mantle (Mareschal et al., 2004), we avoid invoking any assumptions regarding temperatures in the lower crust or upper mantle. The larger part of the total heat flow is heterogeneous and originates from the crust (e.g., Burton-Johnson et al., 2017; Jaupart et al., 2016). To assign crustal heat production (A), we use the geological observations and crustal segmentation, as described in the previous section. We divide the crust into three classes according to stabilisation age: Archean-Paleoproterozoic, Meso-Neoproterozoic and Phanerozoic (Begg et al., 2009; Janse, 1984; Jaupart et al., 2013; Jaupart et al., 2016). For each class, an average heat production range is applied from Jaupart et al. (2013). Crustal thickness is constrained from seismology (An et al., 2015a) and shown in Figure 3b.4D. Details of the classification are given in Table 3b.2.

We use the segmentation in Figures 3b.3D and Figure 3b.4C to calculate new heat flow maps based on geophysical and geological input data using the methods described in the previous section. The resulting steady-state heat flow and associated uncertainties for the approach used, are shown in Figure 3b.5. This provides an illustration of the further ability to compute output based on data of different types. Figure 3b.5a shows our new mapped heat flow estimate, AqSS.ea, at continental scale. Figure 3b.5C shows a regional equivalent for the Wilkes Subglacial Basin, AqSS.wsb, as an illustration of working at higher resolution. Calculated uncertainties are shown in Figure 3b.5B, for East Antarctica, and Figure 3b.5D for Wilkes Subglacial Basin.

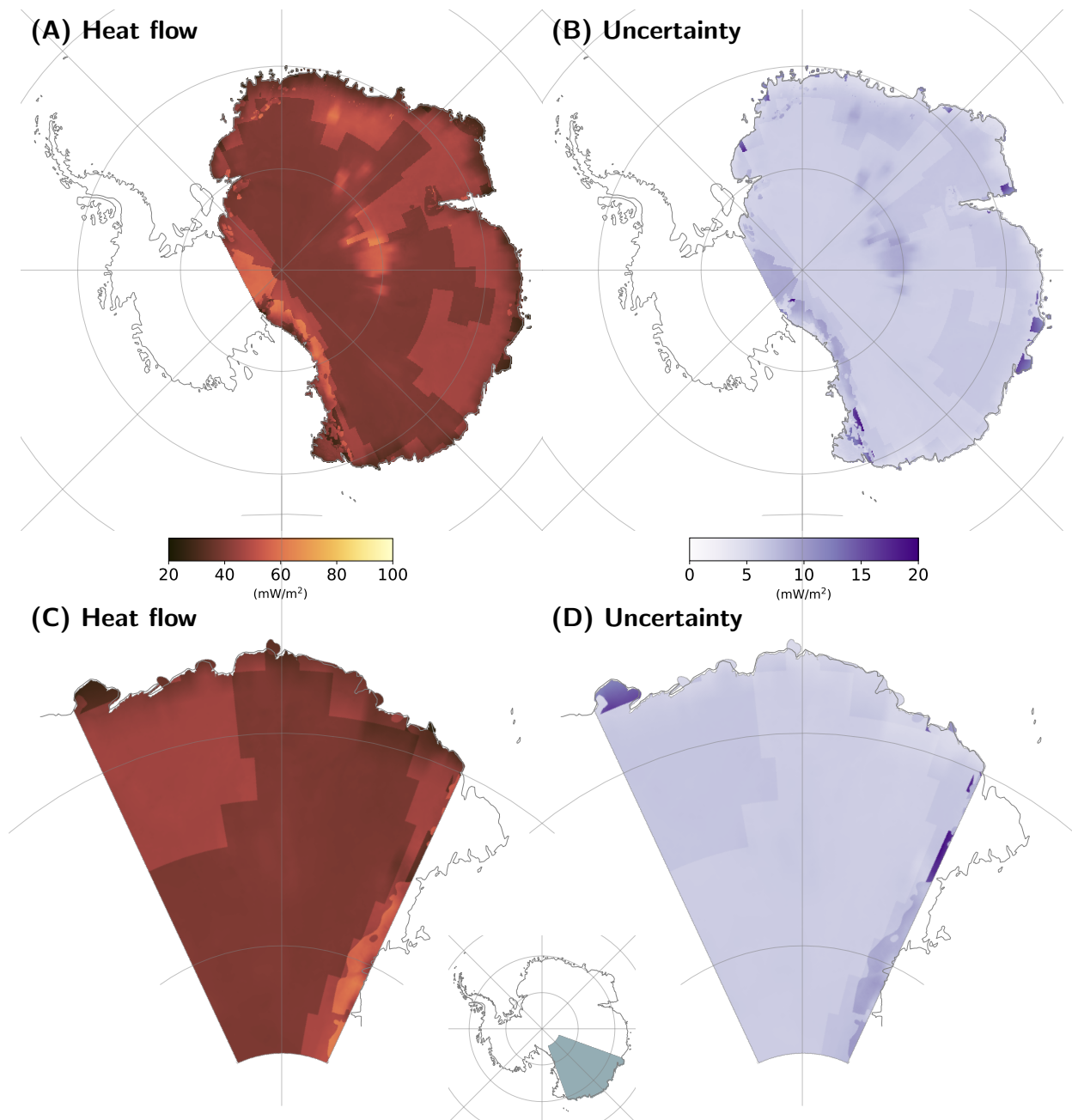
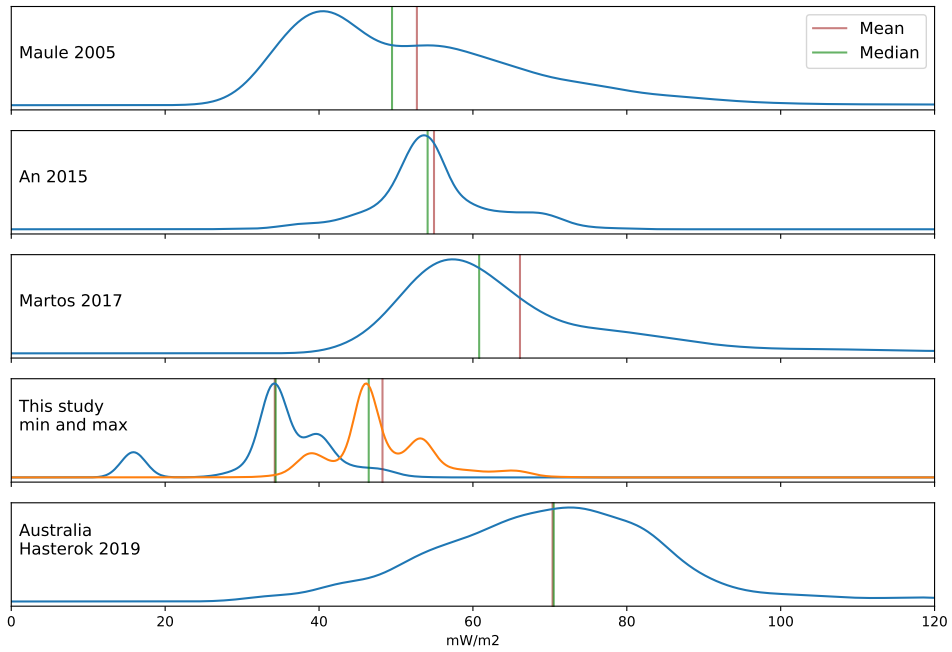


Figure 3b.5: New maps generated by combining constraints from geophysical and geological data held in the 3D grid model: a new steady-state heat flow model, as discussed in text. (A) Heat flow map of East Antarctica, AqSS.ea (B) Uncertainty, as defined by the datasets used, excluding lateral uncertainties. (C) Heat flow map of Wilkes Basin, AqSS.wsb, (D) Uncertainty.

(A) Distribution of heat flow values



(B) An 2015 - AqSS

(C) Martos 2017 - AqSS

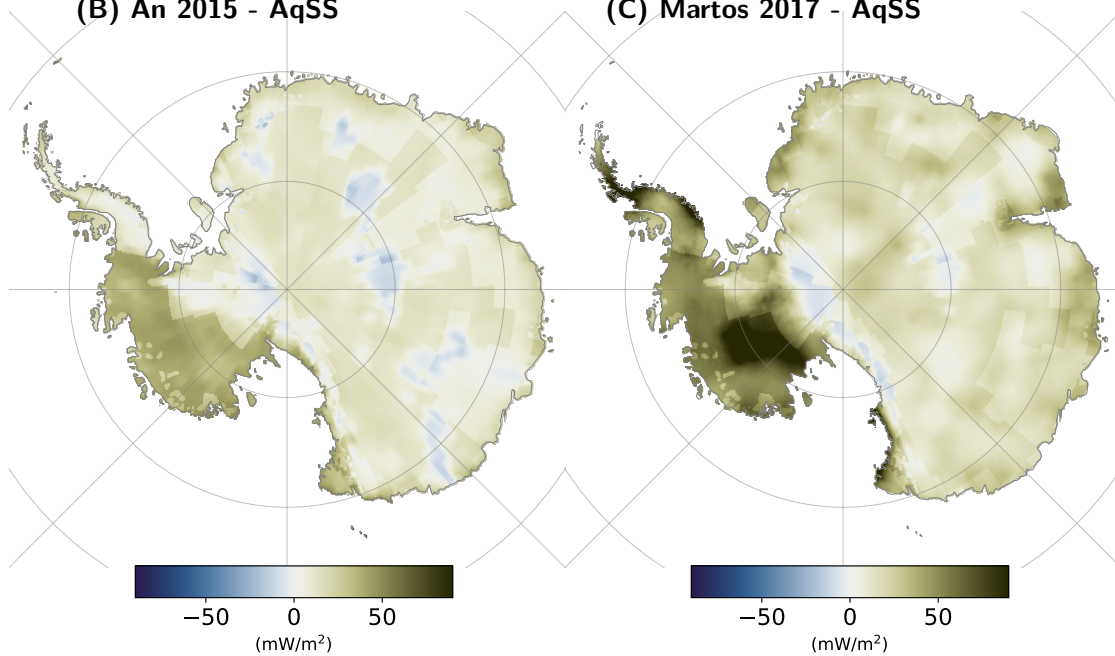


Figure 3b.6: (Caption next page.)

Figure 3b.6: Comparison of heat flow models enabled by the 3D model and framework. **(A)** Distribution of heat flow values. For East Antarctica, distributions from Fox Maule et al. (2005), An et al. (2015b), Martos et al. (2017), example heat flow values for AqSS (derived from values mapped in figures 5a and 5b) as minimum estimate (blue line) and maximum estimate (red line); for Australia, distribution of actual measurements in southern and western Australia compiled by Hasterok (2019). **(B)** Heat flow model from seismic data (An et al., 2015b) minus AqSS. **(C)** Heat flow model from magnetic data (Martos et al., 2017) minus AqSS. Subtracting AqSS, which is a steady-state heat flow model, from published maps of total heat flow indicates non-steady-state contributions to total heat flow.

3b.3.2.6 Appraisal of the Steady-State Heat Flow Model, AqSS, and Previous Models

Our final set of functionality examples illustrate using the framework to appraise alternate models for a given parameter. Figure 3b.6a compares AqSS, minimum and maximum values, with earlier published models and calculated heat flow from borehole measurements in western part of Australia (compiled by Hasterok, 2019). The Australian dataset includes transient and shallow processes, that are not captured in AqSS nor some of the other geophysically derived estimates.

Figures 3b.6B-C show examples of comparing two observation-derived datasets with a constructed reference model to inform the discussion of lithospheric properties. We show An et al. (2015b) and Martos et al. (2017) heat flow maps minus steady-state heat flow from AqSS. These two alternative results are effectively the additional heat flow likely generated from neotectonic and other non steady-state processes, such as recent rifting, volcanism and orogenesis.

3b.3.2.7 Variation of Thermal Gradients with Depth

Figure 3b.7 illustrates an example of extracting the variation of a property with depth. We show thermal gradients from locations in West and East Antarctica as a Gaussian kernel density estimate (KDE), including seismic-derived temperatures (An et al., 2015b) and magnetic-derived Curie temperature depth, including uncertainty bounds (Martos et al., 2017). The KDE is calculated over the depth dimension for East and West Antarctica separately. We also include uncertainties when defining the kernel size. In West Antarctica, the example is from Lake Whillans, the location of one of few direct measurements of heat flow in Antarctica (Fisher et al., 2015). In East Antarctica, the example is from Dome C. The location maps, showing West and East Antarctica, are obtained by importing a polygon vector to use as a factor (inset in Figs. 3b.7A-B).

The contours show the range of allowed values and how the two models, An et al. (2015b) and Martos et al. (2017), compare in depth section. The profile of temperature with depth varies over a large range for both example locations (Fig. 3b.7 red line), and when an average kernel is displayed (Fig. 3b.7 gray contours). This result, and the use of the 3D grid and framework in comparing models and sensitivity to different parameters, is further discussed below.

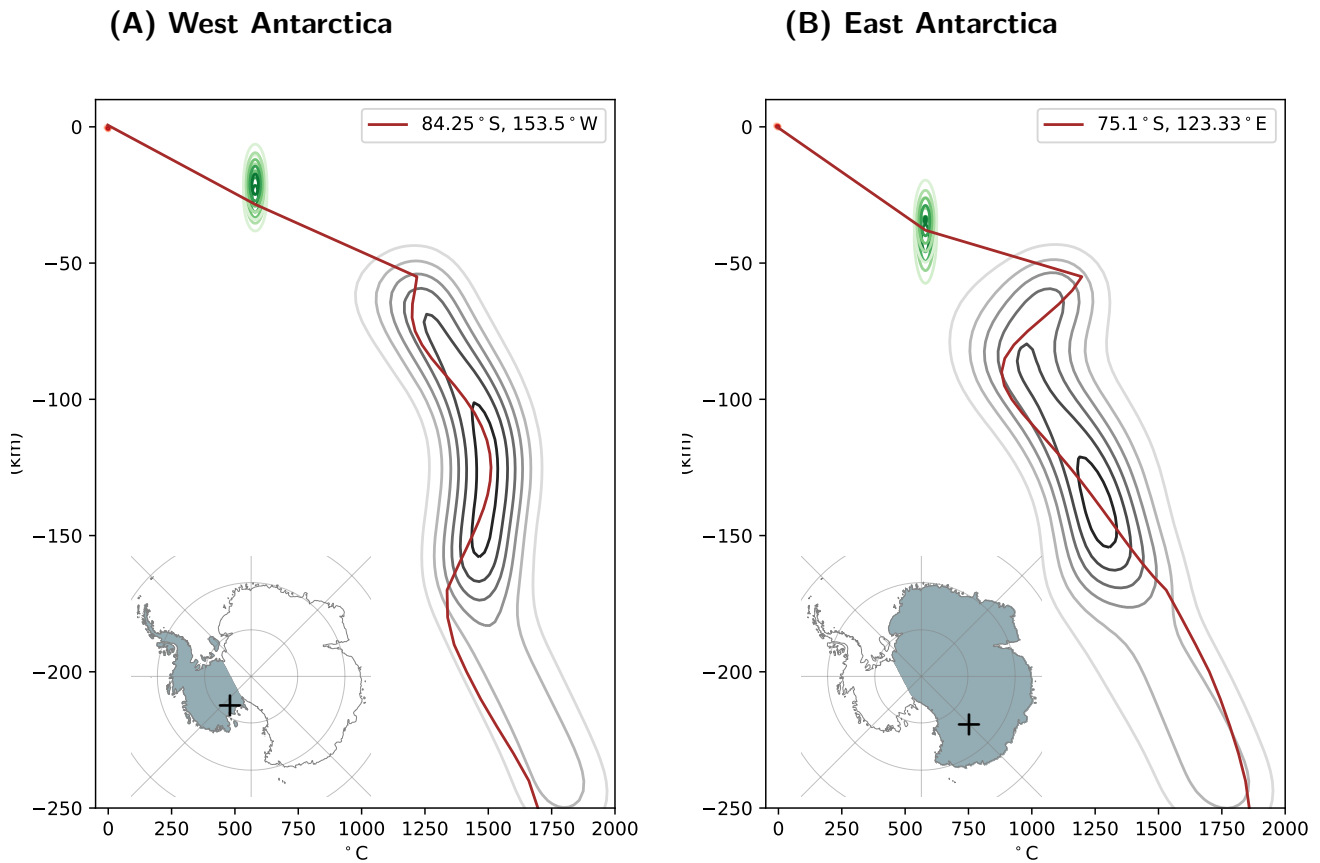


Figure 3b.7: Illustration of framework capability to extract depth profiles for model comparison. Thermal model of the lithosphere, populated with data from Antarctic heat flow models for West and East Antarctica reduced to kernel density estimations (KDE). Temperatures derived from seismic data, An et al., 2015b, in black contours showing highest concentration of thermal profiles. Depth to Curie temperature isotherm with uncertainty derived from magnetic data (Martos et al., 2017) in green contours. Surface and subglacial elevation from Fretwell et al., 2012 and subglacial temperature from Van Liefferinge et al. (2018) in red at the surface. KDE Gaussian kernel for mantle temperatures set to $100^{\circ}\text{C}/10\text{ km}$, for Curie temperature isotherm $25^{\circ}\text{C}/2\text{ km}$ and for surface $5^{\circ}\text{C}/0.1\text{ km}$. Plotted profiles in red show two examples locations of 1D temperature models using combined input. The subglacial heat flow is proportional to the gradient of temperature and the thermal conductivity in the upper crust. To facilitate KDE, only every fifth grid cell is computed. The figure is cropped at 250 km depth. Insets show sampled area.

3b.4 Discussion

We first outline the most significant limitations of the 3D model and framework, and then discuss aspects of our newly generated heat flow example, as an exemplar of how the research environment might be used.

3b.4.1 Limitations

There is a trade-off between resolution and computational expense for any numerical model. Moreover, numerical stability is, in general, required for grid-based calculations. The continental scale model in 20×20 km grid, is presented as an example that is too coarse to contain and represent detailed observed geology and finer crustal geophysics. In terms of continental scale heat, the segmentation used to estimate the likely crustal heat production is not sufficient for ice sheet models that depend on heat transfer on a fine scale (Van Liefferinge et al., 2018). The second provided example of the Wilkes Subglacial Basin in 2×2 km grid is more detailed in some areas, but includes interpolations from coarse data, and hence, the resolution appears finer than the data used. The open framework (Stål et al., 2020a) facilitates a transparent workflow where the impact of, for example, model resolution can be tested.

The model functionality allows for the inclusion of uncertainty values matching each dataset. Therefore, the impact of the noted limitations can be mitigated. The model can be realized with a desired extent, resolution and data content to suit the needed outcome and stage of research. In this contribution, we include the uncertainties provided with the datasets. Those metrics may not cover the true uncertainty of the datasets, when resolution and artifacts from the methodology are considered. The strength of the framework is that the impact of such concerns can be understood as data coverage improves.

3b.4.2 Insight from Examples

The heat flow estimate exemplifies how our multidimensional and multivariate grid may be used to combine input data of different types, and execute calculations across the grid. This provides, we hope, a constructive approach to reconcile the differences between published heat flow models for Antarctica (fig. 3b.2C).

The comparison of the results from magnetic and seismic studies provides new insight into deep Earth properties since both approaches estimate temperature gradients, but using different methods. The differences in Curie temperature depths from seismic (An et al., 2015b) and magnetic (Martos et al., 2017) studies are larger in East Antarctica than in West Antarctica (Supplementary material). These observations imply properties of the lithosphere such as fluid content and heterogeneous heat production that are not captured in the methods used. Compositional variations and presence of fluids impact the seismic wave speed and hence estimated temperatures (Goes et al., 2000; Haeger et al., 2019; Hirth et al., 1996). Magnetic models depend on a simplified crustal thermal and magnetic structure. As an example of a departure from the assumed case, shallow felsic intrusions can provide a large contribution to the surface heat flow, and this could be observed as a deeper Curie temperature isotherm because removal of radiogenic heat producing material facilitates cooling of the lower crust (Jaupart et al., 2016). Figure 3b.7 highlights the large range and uncertainties involved in

present heat flow estimates and also illustrates the much steeper thermal gradient in the crust compared to the upper mantle. We note that thermal conductivity generally decreases with temperature (McKenzie et al., 2005; Xu et al., 2004). However, geothermal heat is not lost rapidly through the crust, so crustal heat production must have a large influence on geothermal heat flow at the surface. New outputs such as Figure 3b.7 show how the limitations in available evidence give rise to temperature changes with depth in the upper mantle that are, taken together, implausible. For example, a temperature decrease with depth is highly unlikely in stable lithosphere. The valuable studies that we have compared note their underlying assumptions and logical simplifications. Our new model and framework allows the implications of such simplifications to be better understood.

We have introduced a new conceptual heat flow model, AqSS, where we base the calculations on the energy balance of the lithosphere, rather than estimated temperature gradients. Our method represents a new approach in the Antarctic context and uses a reduced number of assumptions. With negligible heat generated in the lithospheric mantle (An et al., 2015b; Jaupart et al., 2016; Martos et al., 2017), the Moho steady-state heat flux must be equal to the flux at the lithosphere-asthenosphere boundary. For old and stable crust, the mantle component of the heat can be reduced to a low and constant value in the range between 10–20 mWm^{-2} (Jaupart et al., 2016; Michaut et al., 2007; Roy et al., 2003), however, in more dynamic regions with thinner lithosphere, we need to include the non-steady-state contribution due to e.g. tectonism (estimated from a geothermal gradient, but understanding the thermal properties in the crust as discussed above). AqSS provides us with an initial model that maps stable regions of the Antarctic interior. We then estimate the amount of transient (non steady-state) heat by subtracting the steady-state model from comprehensive models. This difference highlights dynamic regions in West Antarctica (figs. 3b.6B-C). Including dynamic Earth processes ideally requires that not only crustal geology, but also hydrology, constraints from glaciology and the dynamic mantle are fully incorporated. Our framework, we hope, enables current and future progress towards that goal.

3b.4.3 Use Cases for the 3D Model and Software Framework

The main use cases for Antarctic research, with an emphasis on interdisciplinary studies of the interaction of the solid Earth and cryosphere, are listed below:

1. Computing results based on geophysical datasets. A broad range of datasets can be combined in the same frame and uncertainty bounds included, as illustrated in this contribution. The extensive toolboxes from e.g. the Python ecosystem are available for modelling and analysis. Import, export and visualisation functions simplify the workflow. Supplementary Material Figure S4 shows the potential for experimentation in data visualisation.
2. Combining geophysics and geological constraints, and making use of the merged result in ongoing calculations, as illustrated in this contribution. Constraints from glaciology could potentially be included in the same way, e.g. as a constraint on shallow processes to facilitate discussion of heat flow estimates for given regions.

3. Appraisal of models. Comparisons between datasets, or calculated differences, can provide insights that are beyond the potential of the individual contributing studies, again, as we have illustrated in this contribution.
4. Working with uncertainty and probabilistic methods. With the large uncertainties involved in Antarctic solid Earth research, probabilistic tools are essential to progress in the understanding of the Antarctic lithosphere. A productive way forward is to embrace the uncertainties and build probabilistic models (e.g., Stål et al., 2019c). The computational framework that is presented here is well-suited to this task and provides an environment where data and associated uncertainties, probabilities and likelihoods can be processed.
5. An enabling capability for the international research community. Building robust models of the Antarctic crust and upper mantle is a community effort, that will be refined incrementally with additional data. When a specific research product is desired, e.g. a reference heat flow map to include in ice sheet models, we can now draw constraints from multiple studies and/or easily test a range of alternative maps.

3b.5 Conclusions

We present a new 3D grid model and framework: a computing environment tailored to interdisciplinary research. The software framework is easy to use, allows geophysical and geological data to be combined, and provides a virtual laboratory to develop and test, for example, solid Earth models. The model points directly to published data sources and the data contained can easily be updated.

This contribution aims to facilitate progress in Antarctic research concerning solid Earth-cryosphere interaction. Physical property maps and grids, of utility to studies of glacial isostatic adjustment, geothermal heat and the shaping of topography can be performed; bridging between the solid Earth and cryosphere research communities. The usage examples that we provide include a conceptually new steady-state heat flow map based on the energy balance of the lithosphere for comparison with maps based on modelled thermal gradient.

Conflict of Interest Statement

The authors declare that the research was conducted in the absence of any commercial or financial relationships that could be construed as a potential conflict of interest.

Data Availability Statement

Code to generate the grid containing data listed in Table 3b.1 and interoperable formats of example outputs are archived at https://zenodo.org/record/3775167#.X0dVbEkRV_4, updated versions and additional information are available at https://github.com/TobbeTripitaka/ant_lithosphere). All data used are available from original authors or open repositories, linked in the provided Jupyter Notebook and Python script. All code is made available, and details are further presented in Stål et al. (2020a). The latest version of *agrid* can

be obtained from <https://github.com/TobbeTripitaka/agrid> and archived versions from <https://zenodo.org/record/3352603>.

Author Contributions

TS developed the software, built the 3D model, generated the examples and wrote the first draft text. AMR guided the overarching research direction and advised on the geophysics. JAH advised on the geology. SJP advised on the interdisciplinary context. JMW advised on the plate tectonics and basin geoscience. All authors contributed to revising the text.

Funding

This research was supported under Australian Research Council's Special Research Initiative for Antarctic Gateway Partnership (Project ID SR140300001) and the Centre for Southern Hemisphere Oceans Research, a joint research centre between QNLM and CSIRO.

Acknowledgments

This research is a contribution to the SCAR SERCE program.

Table 3b.1: Datasets used to populate the grid, in alphabetic order.

	Property	Source	Processing in this study
2D	Average crustal density	Afonso et al. (2019)	Resampling, interpolation
2D	Average lithospheric mantle density	Afonso et al. (2019)	Resampling, interpolation
3D	Seismic shear wave speed	An et al. (2015a)	Resampling, interpolation
2D	Moho depth	An et al. (2015a)	Resampling, interpolation
3D	Temperature	An et al. (2015b)	Resampling, interpolation
2D	Heat flow	An et al. (2015b)	Resampling, interpolation
3D	Mantle temperatures	An et al. (2015b)	Resampling, interpolation
3D	Crustal temperatures	An et al. (2015b)	Resampling, interpolation
2D	LAB depth	An et al. (2015b)	Resampling, interpolation
2D	Curie temperature depth	An et al. (2015b)	Resampling, interpolation
3D	Seismic shear wave speed	Becker et al. (2002) SMEAN2	Resampling, interpolation
3D	Seismic pressure wave speed	Becker et al. (2002) PMEAN	Resampling, interpolation
2D	Rock outcrops	Burton-Johnson et al. (2016)	Rasterized
2D	Segmentation from gravity curvature	Ebbing et al. (2018)	Resampling, interpolation
2D	Subglacial elevation	Fretwell et al. (2012)	Resampling, interpolation
2D	Surface elevation	Fretwell et al. (2012)	Resampling, interpolation
	Rock ages and heat production	Gard et al. (2019)	Remapped and classified ¹
2D	Magnetic compilation	Golynsky et al. (2018)	Resampling, interpolation
1D	P-velocity reference AK135	Kennett (2005)	Interpolation
1D	S-velocity reference AK135	Kennett (2005)	Interpolation
1D	Density reference AK135	Kennett (2005)	Interpolation
2D	Basal temperature	Van Lieferinge et al. (2013)	Resampling, interpolation
2D	Curie temperature depth	Martos et al. (2017)	Resampling, interpolation
2D	Heat flow	Martos et al. (2017)	Resampling, interpolation
2D	Heat flow uncertainty	Martos et al. (2017)	Resampling, interpolation
2D	Heat flow	Fox Maule et al. (2005)	Resampling, interpolation
2D	Grounding Line	Mouginot et al. (2017)	Rasterization and classification
2D	MEASURE Antarctic boundaries	Mouginot et al., 2017; Rignot et al., 2013	Rasterization and classification
2D	Segmentation	Schaeffer et al. (2015)	Resampling, interpolation
2D	Schematic geological map	Tingey et al. (1991)	Rasterized and classified ¹

¹. Converted records from geological periods to time (Stål, 2019b).

Table 3b.2: Thermal properties assigned to crustal domains.

ID ¹	Age group ²	Range of bulk heat production ³	Source	Schaeffer et al. (2015)
1 (archon)	Archean	[0.56, 0.73] μWm^{-3}	Jaupart et al. (2013) ⁴	C3
2 (proton)	Proterozoic	[0.73, 0.90] μWm^{-3}	Jaupart et al. (2013) ⁴	C2
3 (tecton)	Phanerozoic	[0.95, 1.21] μWm^{-3}	Jaupart et al. (2013) ⁴	C1
4	Oceanic crust	[0.50, 0.90] μWm^{-3}	Hasterok et al. (2017) and McKenzie et al. (2005) ⁵	O1, O2, O3

¹. Class used in this study, from Begg et al. (2009) and Janse (1984).

². Used to classify geological maps and data.

³. Bulk heat production for the continental crust age classes and oceanic crust.

⁴. And references therein.

⁵. Detailed analysis in Hasterok et al. (2017).

Introducing: "A Multivariate Approach for Mapping Lithospheric Domain Boundaries in East Antarctica"

Chapter 4 has been published as: Stål, T., Reading, A. M., Halpin, J. A., and Whittaker, J. M. (2019). A Multivariate Approach for Mapping Lithospheric Domain Boundaries in East Antarctica. *Geophysical Research Letters*, 46(17–18), 10404–10416. <https://doi.org/10.1029/2019GL083453>.

The text is reproduced in its published form and therefore some material is repeated from the background and other chapters. In the case of any differences, the published version of the chapter take precedence.

Chapter 4

A Multivariate Approach for Mapping Lithospheric Domain Boundaries in East Antarctica

Tobias Stål^{1,2}, Anya M. Reading^{1,2}, Jacqueline A. Halpin², and Joanne M. Whittaker²

1. School of Natural Sciences (Earth Sciences), University of Tasmania
2. Institute for Marine and Antarctic Studies, University of Tasmania

Abstract

Beneath the ice of East Antarctica lies a continent which is likely to be as geologically complex as its neighbors in Gondwana. An improved model of the heterogeneous lithosphere is required to progress research on Antarctica's tectonic evolution and support interdisciplinary studies of cryosphere and solid Earth interaction. We make use of multiple datasets, which were updated following the field campaigns and compilations of the International Polar Year of 2007/08. Seismic tomography results, gravity anomalies, and surface elevation are used in a novel method, which combines spatial multivariate data to map possible boundaries as projected likelihood functions. Six multivariate combinations are tested and compared with sparse geological observations in East Antarctica. The resulting lithospheric domain boundaries contribute to our understanding of the deep continental structure. New boundaries are suggested in the interior, and models agree with likely surface expressions of crustal tectonic boundaries exposed along the coast.

4.1 Introduction

Important aspects of Antarctica's continental structure are unknown. Better working models of the deep lithosphere are needed to progress investigations of the complex interaction between the solid Earth and the cryosphere. For example, glacial isostatic adjustment in response to changes in ice load depends on deep elastic and viscous properties (e.g. Kaufmann et al., 2005; Whitehouse, 2018; Whitehouse et al., 2006). Geothermal heat is identified as a spatially variable and poorly constrained parameter in ice sheet models (e.g. Burton-Johnson et al., 2017; Pollard et al., 2005). Deep boundaries subdivide the continental lithosphere into domains with similar physical properties. With a more detailed and robust map of lithospheric boundaries and domains, we can better infer the tectonic evolution of the continent and assign physical properties to provide a useful framework for interdisciplinary studies.

The main crustal domains in East Antarctica were identified along the perimeter and Transantarctic Mountains from geological observations by the 1980's, but no constraints were available for the subglacial interior (e.g. Craddock, 1972; Ravich et al., 1965; Tingey et al., 1991). Indirect observations of transported material from marine cores and moraines can suggest the large-scale hidden geology (Cook et al., 2017; Goodge, 2018; Tauxe et al., 2015), but the provenance of samples can be difficult to reconstruct. Some studies have projected coastal geology into the unexposed interior. Those predictions have been guided by extrapolation of known geology from adjacent Gondwanan neighbours or by using geophysical data (e.g. Aitken et al., 2014; Boger, 2011; Daczko et al., 2018; Ferraccioli et al., 2011; Fitzsimons, 2003; Jacobs et al., 2015; Veevers, 2012). Over the past decades, geophysical studies and plate reconstructions have advanced the understanding of Antarctica's continental structure, but there are still conflicting interpretations of the blocks and boundaries in the interior (Fig. 4.1 A).

We rely on geophysical data to map East Antarctica, and different datasets have particular strengths and limitations. Early seismic tomography studies revealed general heterogeneities within the lithosphere (Ritzwoller et al., 2001; Roult et al., 1994a,b). There were, however, few seismometers in Antarctica at this time and seismic tomography using local sources is precluded due to the inherent low seismicity (Reading, 2007). Global studies provide a reference, but are often of low resolution due to the limited data for Antarctica (Laske et al., 2013; Pasyanos et al., 2014; Ritzwoller et al., 2002; Schaeffer et al., 2015; Shapiro et al., 2002). Transects and regional studies have revealed the basement structure of the Transantarctic Mountains, Lambert Glacier region, Gamburtsev Subglacial Mountains and West Antarctica (e.g. Brenn et al., 2017; Chaput et al., 2014; Graw et al., 2017; Hansen et al., 2010; Heeszel et al., 2016; Reading, 2006; Shen et al., 2018b; Winberry et al., 2004). An et al. (2015a,b) presented an improved surface wave tomography model that is used to estimate crustal thickness, temperature, and lithospheric thickness. Teleseismic surface wave tomography captures the character of lithospheric blocks in the centers of domains but is less suited to the detection of their boundaries (An, 2012; Foulger et al., 2013). The edges of gravity anomalies are valuable in revealing boundaries between lithospheric domains (Block et al., 2009; Ferraccioli et al., 2011), but interpretation can be ambiguous and the resolution is often low. Gravity data can be obtained from ground measurements, airborne instruments, and by satellite. The GOCE and GRACE satellite missions have been important in Antarctica (Pail et al., 2010; Visser, 1999). Variations in bedrock topography can to some extent provide indication of much deeper struc-

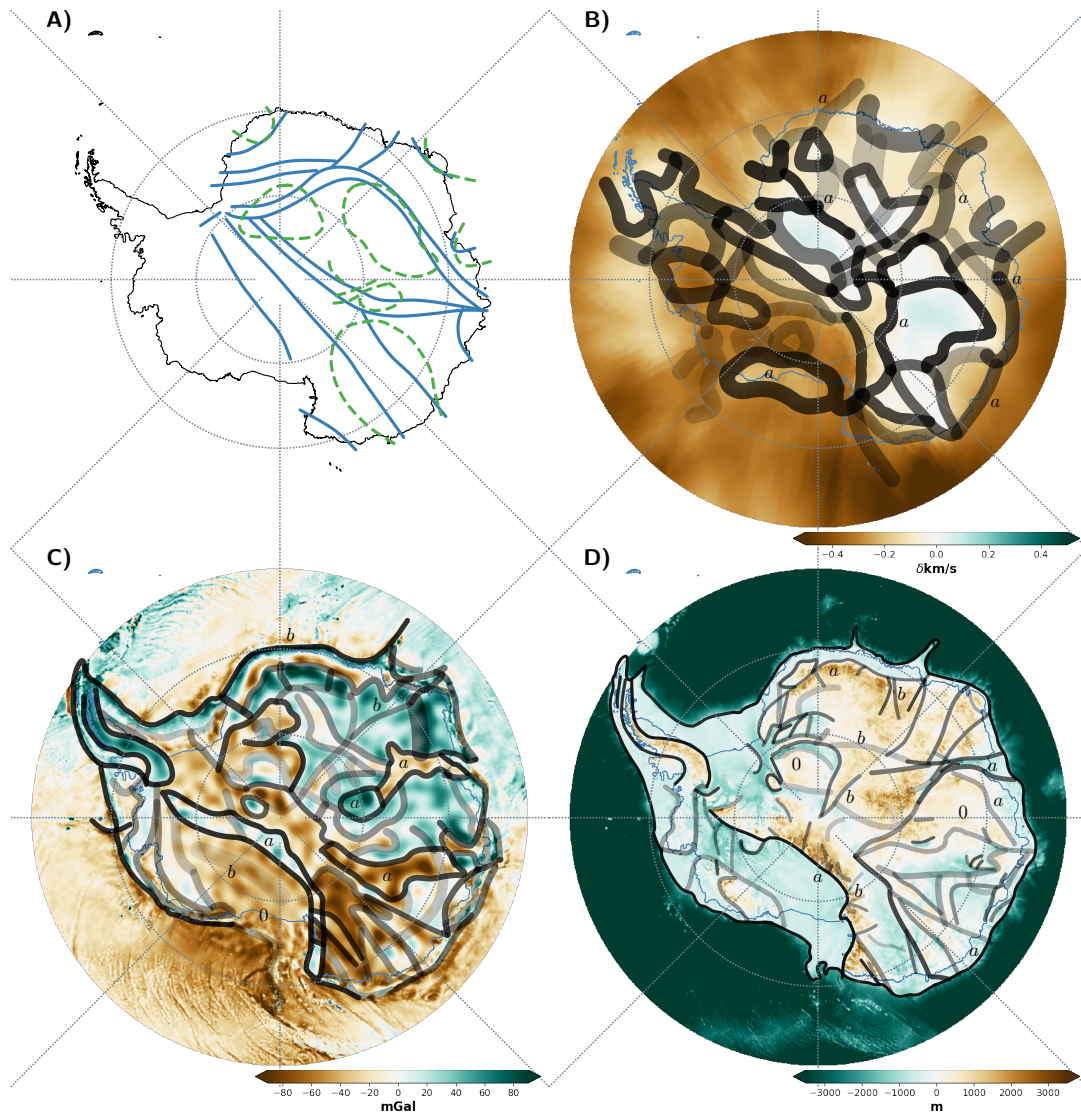


Figure 4.1: A) Sketches of major boundaries suggested in previous studies and compilations. Blue solid lines (Boger, 2011), the continent defined as an extrapolation from the Gondwanan and Rodinian neighbours, or lack of such candidates. Green dashed lines (e.g. Leitchenkov et al., 2016), Antarctica as an unknown entity with mainly inferred geophysical properties. B-D) Datasets used for this study and picked boundaries (black lines). Opacity illustrates the relative accuracy and line-widths indicate precision. B) Seismic shear wave speed at 150 km as perturbation from AK135 in absolute speed anomaly, modified from An et al. (2015a). C) Gravity anomaly map EIGEN-6C4, modified from Förste et al. (2013). D) Bed elevation model BEDMAP2 modified from Fretwell et al. (2012). Examples of detected boundaries are notated *a* for changes in value, *b* for changes in pattern. 0 indicates examples of artifacts that are not interpreted.

ture. In Antarctica, there are few direct observations. Instead, topography is inferred from for example airborne radar surveys (Fretwell et al., 2012). Finer scale features of topography may not be captured in interpolated elevation models (Graham et al., 2017).

Geological and geochronological information have sparse coverage in East Antarctica, but good resolution. Geophysical datasets might have good coverage, but often limited resolution.

Combined geological and geophysical studies to map and constrain the lithospheric structure has been conducted in Africa (e.g. Begg et al., 2009) and Australia (e.g. Kennett et al., 2018). The lithospheric domains in those continents suggest what we could expect to infer in Antarctica as data availability improves.

In this study, we introduce a novel method to identify domain boundaries in the lithosphere of Antarctica, with a focus on East Antarctica. In contrast to previous studies, which make interpretations based on a comparative analysis of univariate data, we use a multivariate interpretation of the relative probability of inferred boundaries. We map variations in geophysical observables that suggest deep boundaries or transitions. The new domain maps aim to progress the understanding of the large-scale tectonic structure of the interior of East Antarctica.

4.2 Data

To place constraints on domain boundaries within the lithosphere, we utilize three datasets: seismic shear wave speed (S), free air gravity anomaly (G), and subglacial elevation (E). The seismic dataset used is the 150 km depth slice in the lower lithosphere from An et al. (2015a). Gravity anomalies are taken from the Earth free air gravity model EIGEN-6C4 compilation. This dataset includes GRACE and GOCE data up to degree and order 2190 (Förste et al., 2013). In order to keep the datasets independent, we avoid the use of a Bouguer corrected gravity model, which incorporates the effects of topography. Subglacial elevation is taken from the digital elevation model BEDMAP2 (Fretwell et al., 2012). The datasets were prepared for analysis by reprojection, resampling, and clipping using for example the Python package rasterio (Gillies, 2013b). The seismic data are replotted using a diverging colour map (Fig. 4.1) as a perturbation from AK135 shear wave speed model at 150 km, 4.5060 km/s (Kennett, 2005). Gravity and elevation data are replotted as obtained from original data sources.

4.3 Methods

4.3.1 Picking Boundaries

For each dataset, boundaries are independently identified visually and manually picked as vector lines in a GIS software environment (Qgis, 2015). Effort is made by the analyst not to be biased by previous knowledge or other datasets. Rapid changes or obvious changes in trends are selected as boundaries (examples notated a in Fig. 4.1B-D). Changes in pattern, particularly for the gravity and elevation datasets, are also taken to indicate a domain boundary (examples notated b in Figs. 4.1B-D). The lines are not picked to be geological meaningful, they represent visual variations in the data. Known and obvious artifacts, such as flight lines, are avoided (examples notated 0 in Figs. 4.1B-D). Some boundaries fade out to become obscure and are only mapped as far as they are traceable. Boundary identification is carried out on a map screen display which uses an Antarctic Polar Stereographic projection and shows minimal scalar distortion in continental Antarctica.

Each picked line segment is associated with relative accuracy and precision ratings. The accuracy rating represents the certainty of the picked line representing a lithospheric boundary. The precision is the spatial uncertainty of the picking. Both ratings are given as a number

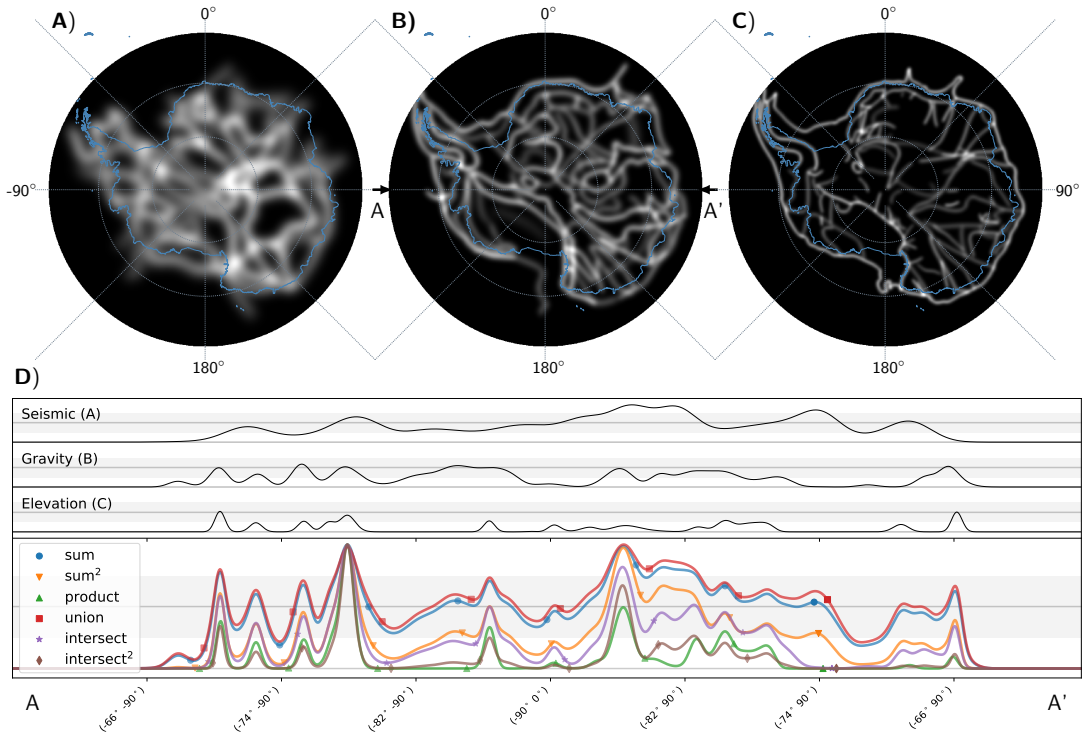


Figure 4.2: Likelihood maps of domain boundaries for each geophysical dataset used, here normalized to the maximum value within each dataset. Brighter shading indicates a higher likelihood of a domain boundary. A) Seismic derived boundary likelihood map. B) Free air gravity derived boundary likelihood map. C) Elevation derived boundary likelihood map. D) Cross-section (A-A'), showing convolved distributions for likelihood of boundary from each dataset and combined distributions, as described in text.

between 1 and 10 and later converted to likelihood value from 0 to 1, and standard deviation expressed as a distance.

4.3.2 Generating Individual Spatial Likelihood Maps

For each dataset, D , we calculate a likelihood map representing the picked boundaries as follows:

$$\mathcal{L}(x, y)_D = a_D \sum_{s(x, y) \in L'_D} a_s \times s(x, y) * \mathcal{N}_2(\mu(x, y), (\sigma_s + \sigma_D)^2). \quad (4.1)$$

where $\mathcal{L}(x, y)$ is the spatial likelihood function, projected to a (x, y) Polar Stereographic grid. $s(x, y)$ denotes the location of the line segments in the picked vector lines, L' . a_D is the weighting for the boundaries for each dataset and a_s is the accuracy rating for each picked line segment. $\mathcal{N}_2(\mu, \sigma^2)$ is a two-dimensional Gaussian kernel, with $\mu(x, y) = (0, 0)$ and $\sigma = \sigma_s + \sigma_D$, where σ_s is a user-defined precision rating for each line segment and σ_D is the standard deviation for the dataset used; a_s and σ_s are stored as attribute data in the vector file (L').

The width of the Gaussian kernel relating to the seismic data is indicated by the tomography methodology and data density (An, 2012; Ritsema et al., 2004). At 150 km depth, periods of over 100 s dominate and for most of continental Antarctica the resolution of features in the

tomogram is in the range 300–500 km (An et al., 2015a). The picked seismic boundaries are convolved with a Gaussian kernel with a standard deviation $\sigma_S = 200$ km (Fig. 4.2 A). The gravity field model EIGEN-6C4 has an estimated halfwidth resolution of $\Delta \approx 80$ km. The Antarctic interior has increased uncertainty due to the lack of ground-based observation data. The picked gravity boundaries are convolved with a standard deviation $\sigma_G = 100$ km (Fig. 4.2 B). The horizontal resolution of the digital elevation model (DEM) (Fretwell et al., 2012) is 1km, but the data in some areas are coarser due to the acquisition methods. For the picked topography boundaries, a Gaussian convolution with a standard deviation of $\sigma_E = 60$ km is applied to also account for sloping crustal structures (Fig. 4.2 C).

The relative amplitude of the Gaussian kernel for each of the three datasets is the product of the total weight for the dataset and the weights for the segments of the picked boundaries. We assign equal weight ($a_D = 0.33$) to each likelihood function.

4.3.3 Combining Distributions

We demonstrate six methods of combining individual likelihood maps (Fig. 4.2 D and Fig. 4.3). Sum (Fig. 4.3 A) is generated by adding the three map values for each grid cell. Product (Fig. 4.3 E) is generated by multiplying the three map values for each grid cell. Union (Fig. 4.3 B) and intersect (Fig. 4.3 D) are achieved from the inclusion-exclusion principle (Berndt et al., 1980). In our simple case with only three sets of independent distributions, we make the following calculation for union:

$$\mathcal{L}_S \cup \mathcal{L}_G \cup \mathcal{L}_E = \mathcal{L}_S + \mathcal{L}_G + \mathcal{L}_E - (\mathcal{L}_S \times \mathcal{L}_G + \mathcal{L}_S \times \mathcal{L}_E + \mathcal{L}_G \times \mathcal{L}_E) + \mathcal{L}_S \times \mathcal{L}_G \times \mathcal{L}_E. \quad (4.2)$$

and a similar calculation for intersect:

$$\mathcal{L}_S \cap \mathcal{L}_G \cap \mathcal{L}_E = \mathcal{L}_S \times \mathcal{L}_G + \mathcal{L}_S \times \mathcal{L}_E + \mathcal{L}_G \times \mathcal{L}_E - \mathcal{L}_S \times \mathcal{L}_G \times \mathcal{L}_E. \quad (4.3)$$

Squared sum (Fig. 4.3 C) and squared intersect (Fig. 4.3 F) emphasise the regions of highest likelihood of a boundary. We note that the combined likelihood is not a joint probability distribution as the projected axes represent spatial extent, not separate distributions. Figure 4.2 D shows transects across the probability fields along the 90°W and 90°E meridians through the South Pole. For clarity, each field is normalised according to its maximum value.

4.4 Results

Of the six resulting likelihood maps derived from the multivariate approach (Figure 4.3), sum (A) and union (B) are the method combinations that suggest the highest number of likely boundaries. An intermediate result is given by squared sum (C) and intersect (D). The most conservative results, suggesting fewest lithospheric boundaries, are product (E) and squared intersect (F). Conservative combinations indicate high likelihood for the existence of actual lithospheric boundaries with reduced false positive detection. The maps suggest high likelihood for lithospheric boundaries along the Transantarctic Mountains and subparallel to the coast in Dronning Maud Land (geographical locations are given in Fig. 4.4). The lithosphere appears

most heterogeneous, showing high likelihood of intersecting boundaries, in the region of Coats Land and Shackleton Range. In contrast, regions with lower likelihood of major lithospheric boundaries are suggested within Wilkes Land, Princess Elizabeth Land and around South Pole. In the discussion that follows, we use the intermediate results, intersect (D). However, the range of maps is also informative. An analysis of shallower neotectonic features in West Antarctica is beyond the scope of this contribution. With the datasets used in this study, we capture only the most deep-seated lithospheric boundaries in West Antarctica.

4.5 Discussion

4.5.1 Limitations

Our objective is to define domain boundaries in the deep lithosphere. Crustal domains might be different. We acknowledge that the different datasets used are sensitive to structure at differing depths and embedded in these data are also information on the upper crust and recent geomorphology. Hence, our method has an inherent assumption that all major lithospheric boundaries may be approximated as vertical. As more detailed 3D studies of the lithosphere are carried out in the future, we expect this assumption to be refined.

The total amplitude of the likelihood distributions is not meaningful in the scope of this study. The combined likelihood maps on which we base the following discussion have been presented with brighter shading indicating a higher likelihood over domain boundaries. The scaling of this brighter shading, each map being normalised individually, has been made to facilitate comparison between different geographic areas.

4.5.2 Correlation with Geological Observations in East Antarctica

The data used for this study are not targeted on shallow geology; however, our findings agree well with crustal boundaries identified from geological field observations, geochronology, and geochemistry (Fig. 4.4). Six major domain boundaries near exposed outcrops have been identified in East Antarctica (reviewed by e.g. Boger, 2011; Fitzsimons, 2000a; Harley et al., 2013). For example, the Shackleton Range is identified with high likelihood to include intersecting major boundaries (Fig. 4.4 A), which are indeed seen on the ground or identified subsequently from rock samples (Clarkson et al., 1995; Tessensohn et al., 1999; Will et al., 2010, 2009). The southern boundary of the Archean Grunehogna Craton in Dronning Maud Land (Fig. 4.4 B) is identified by our method and agrees well with geological studies (Bauer et al., 2003; Board et al., 2005; Jacobs et al., 1998; Jacobs et al., 2015; Jnr, 1995; Luttinen et al., 2000; Marschall et al., 2010). The Miller Range in the Transantarctic Mountains (Fig. 4.4 D) has a high likelihood of a lithospheric domain boundary running along its length. This agrees with geological and geochronological studies as well as magnetic data (Goodge et al., 2001, 2010, 1992). The Mertz Glacier region is also identified with a high likelihood of a major lithospheric boundary (Fig. 4.4 E) and matches well with ground observations and subsequent analysis (Di Vincenzo et al., 2007; Lamarque et al., 2016; Ménot et al., 2007, 2005; Peucat et al., 1999; Stüwe et al., 1989). The interpretation of the geology in Prydz Bay area (Fig. 4.4 F) is under debate (Boger et al., 2004, 2001; Corvino et al., 2008; Fitzsimons, 2000b; Kelsey et al.,

2008; Phillips et al., 2006; Phillips et al., 2009). Notwithstanding the challenges in interpreting the crustal structure, we identify the area with high likelihood for deep lithospheric boundaries. Enderby Land (Fig. 4.4 C) contains the Archean and Paleoproterozoic Napier Complex, and the Meso-Neoproterozoic Rayner Complex (Fitzsimons, 2000b; Halpin et al., 2007b; Kelly et al., 2002; Kelly et al., 2005; Morrissey et al., 2016; Phillips et al., 2009; Sheraton et al., 1987, 1980b). We detect the southern boundary of the Napier Complex with a lower likelihood than the exposed locations discussed previously. This complex reworking of MacRobertson Land and Kemp Land (Halpin et al., 2005; Halpin et al., 2007b; Morrissey et al., 2016) with lithospheric thinning could be the main reason why this particular boundary is less evident from the data sets used.

4.5.3 Comparison with the Continent of Australia

The approach is also tested for Australia, where the inland geology is better known (supporting information). The Australian example shows that craton boundaries are detected using the multivariate method, but superimposed orogens are more difficult to discern. False detection of major boundaries is unlikely when using a conservative product combination, where all individual likelihood maps must agree (Fig. 4.3 E). The Australian example also provides insight into relating surface geological boundaries to deep lithospheric boundaries. Major surface and deep boundaries appear to have a robust mutual association, lending weight to our inferences for East Antarctica. We note again that geological boundaries within such continental domains may not have a signature in the deep lithosphere, in particular for younger lithosphere such as eastern Australia and West Antarctica. Boundaries detected in the deep lithosphere associated with continental extension would not necessarily be seen in the surface geology. We show in the supporting information the extent to which boundaries may be traced between continents in the deep lithosphere.

4.5.4 New Insights into the Lithosphere of Antarctica

The new maps that we present enable insights regarding of the nature of the East Antarctic lithosphere to be drawn from geophysical datasets. By combining multiple datasets, in our case three datasets, we manage the possibility of including an arbitrary interpretation. The impact of false detections is mitigated by using accuracy and precision ratings in the calculations that result in the likelihood maps. Our maps show domain boundaries suggesting a complex interior. Coats Land and Dronning Maud Land appear to show lithospheric heterogeneity, while the interior of Wilkes Land is much less segmented, being divided by few boundaries. These suggestions are consistent with more detailed regional studies, where those exist (e.g. Aitken et al., 2014; Jacobs et al., 2015; Ruppel et al., 2018). A complex interior also agrees with recent geological studies that find large age variations in marine cores (Cook et al., 2017), glacial deposits in the Transantarctic Mountains (Goodge, 2018), and what might be expected from other Gondwana continents (e.g. Begg et al., 2009; Kennett et al., 2018; Korsch et al., 2016).

The structure of the lithosphere is the result of its tectonic evolution. With robust constraints for the interior boundaries, we can better infer the nature of the East Antarctic continental assembly. Our likelihood maps suggest that the interior has more domains than shown

in previous interpolations as in Fig. 4.1 (A). For example, it is unlikely that Terre Adélie, Miller Range and Shackleton Range belong to the same large uninterrupted domain. As a general comment, the extrapolation of major boundaries into the East Antarctic interior seems to be justified for a scale length of approximately 1000 km. In the interior, at greater than 1000 km inland, it is very likely that new domains and hence cross-cutting boundaries will be encountered. Possible plate tectonic implications of the newly identified domains are subject of ongoing work. Enigmatic interior domains, with no coastal expression, are highly likely.

Recent studies using different approaches than we present in the current paper also find interior domains or regions. Ebbing et al. (2018) infer a number of domains in the East Antarctic interior from the curvature index of gravity field with topographic and isostatic correction, and suggest the extent of cratonic lithosphere and orogens. Studies that includes both gravity and seismic data also find a heterogenous interior and provide strong arguments to suggest existence of domains (Baranov et al., 2013; Baranov et al., 2018; Pappa et al., 2019a). Our contribution complements these studies by providing a method for mapping the boundaries of such domains. The Australian example suggests these hidden domains will be varied, e.g. both cratonic and orogenic. Large-scale models of the Antarctic lithosphere (e.g. Haeger et al., 2019) can potentially be further developed from our mapped interior boundaries. Magnetic surveys and Curie depth variations are widely used to investigate the Antarctic crust (e.g. Ferraccioli et al., 2011; Ferraccioli et al., 2001; Goodge et al., 2010; Martos et al., 2017; Ruppel et al., 2018). While our contribution draws on constraints from the deeper lithosphere, we plan to incorporate magnetic data in future, regional scale, multivariate studies with a crustal and upper lithosphere focus.

We hope that our likelihood maps will find wide use in the Antarctic interdisciplinary research community. 3D glacial isostatic models of the viscosity variations in the lithosphere could incorporate segmentation. Improved knowledge of East Antarctic lithospheric boundaries thus supports future developments in this area. Understanding of the tectonic evolution and crustal segmentation is needed for mapping crustal heat production, as highlighted in a recent study from West Antarctica (Burton-Johnson et al., 2017). With our presented maps, geothermal heat properties from known geology or observations from neighbouring Gondwanan continents can be extrapolated into the hidden interior with better confidence for East Antarctica.

Our approach does not limit the number of datasets used, and with additional datasets, the likelihood maps will be further improved as additional data become available. The method can also be applicable on a regional scale, and regional datasets can also be incorporated in continental scale models. Multivariate mapping provides a quantitative, probabilistic, and therefore robust approach for the identification of lithospheric domain boundaries within the East Antarctic interior.

4.6 Conclusions

We introduce a novel method to combine likelihood maps from independent datasets to estimated locations of lithospheric boundaries in East Antarctica. We find good correlation between our findings and postulated crustal boundaries along the perimeter. The ice-covered interior is heterogeneous and is shown to likely comprise a larger number of distinct domains than suggested by previous work based on extrapolation of observations along the coast. The

largest lithospheric domains are likely located in Wilkes Land, Princess Elizabeth Land and around South Pole. Coats Land and Dronning Maud Land likely consist of smaller lithospheric domains. equations,

4.7 Acknowledgments

Likelihood maps in interoperable formats are archived in the digital data library PANGAEA (<https://doi.pangaea.de/10.1594/PANGAEA.901150>). Details are provided in the supporting material. We have made use of the following open access data sources: Seismic data are available from the author's web directories, An et al. (2015a). Gravity anomaly data raster (EIGEN-6C4) (Förste et al., 2013) and elevation model (BEDMAP2) are obtained as part of the Quantarctica3 GIS package (Roth et al., 2017). The full details of the methodology for reproduction of this research may be found in the provided SCons script (Knight, 2005). We thank the anonymous reviewers whose comments have greatly improved this manuscript. This research was supported under Australian Research Council's Special Research Initiative for Antarctic Gateway Partnership (Project ID SR140300001). The authors declare that they have no conflict of interest.

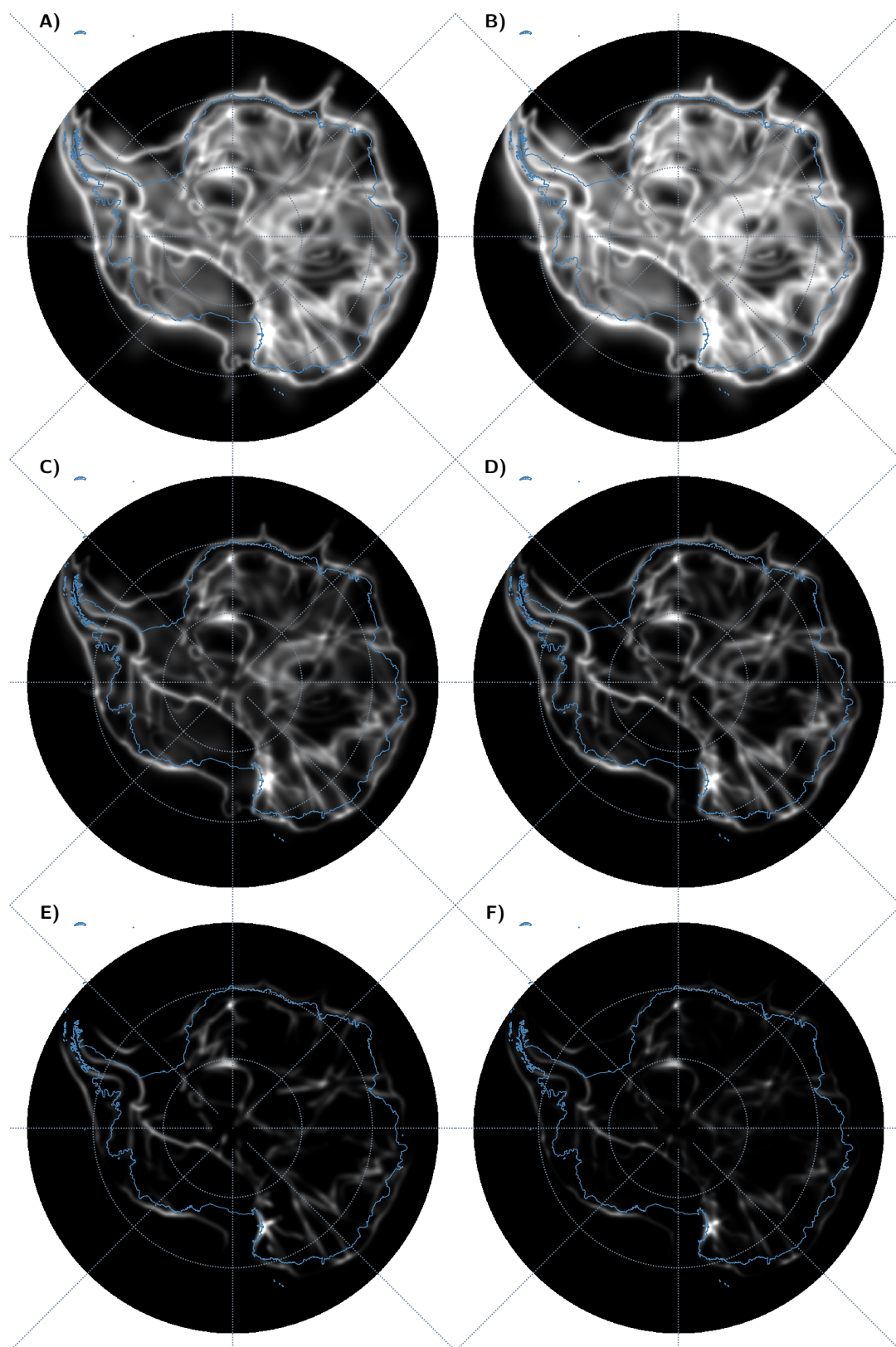


Figure 4.3: Combined likelihood maps, generated using six different methods. A) sum, B) union, C) squared sum, D) intersect, E) product, and F) squared intersect. Each map is normalised to the maximum value for each combination.

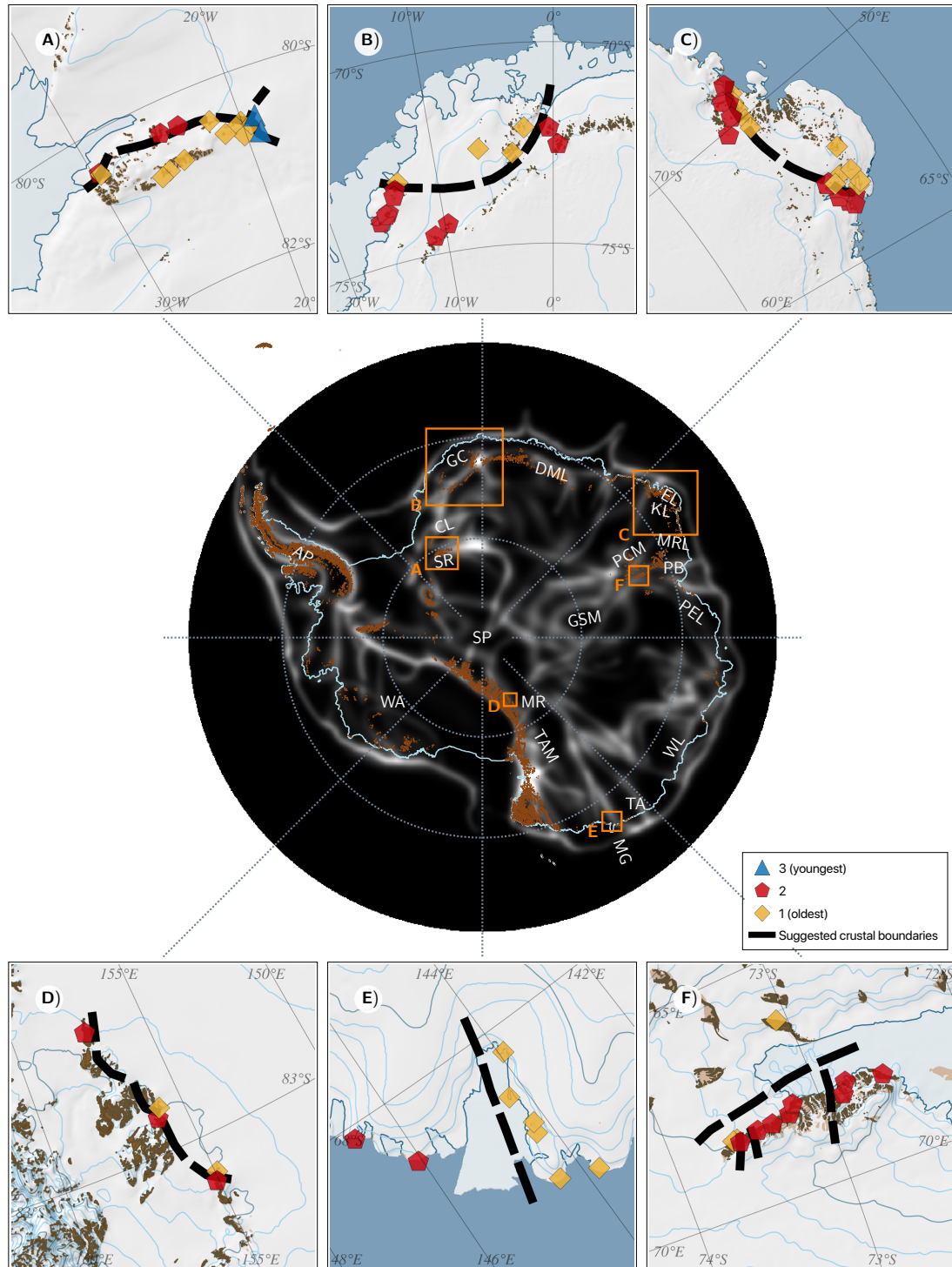


Figure 4.4: The intersect likelihood map (centre, enlarged from Fig. 4.3 D) related to major terrane boundaries exposed near outcrops in East Antarctica. A) Shackleton Range (e.g. Will et al., 2009). A major boundary separating rocks of Archean and younger ages which intersects a further boundary with even younger rocks, east of longitude 20°W. B) Dronning Maud Land (e.g. Marschall et al., 2010). A boundary between Maud Belt south of Grunehogna Craton. C) Enderby Land (e.g. Sheraton et al., 1987). The transitional boundary between the Archean and Paleoproterozoic Napier Complex and the reworked Rayner Complex. D) Miller Range (e.g. Goodge et al., 2001). The boundary between Archean and Paleoproterozoic Nimrod and younger Ross-Delamerian orogenic domains. E) Mertz Glacier region (e.g. Di Vincenzo et al., 2007). The Archean Terre Adélie Craton is exposed in the west, and Ross-Delamerian domain in the east. F) Prince Charles Mountains with the Mawson Escarpment (e.g. Boger et al., 2004; Corvino et al., 2008; Phillips et al., 2009). This region contains multiple major boundaries currently under debate. Symbols indicate relative ages of examples of geochronological samples from referenced literature. Yellow prisms denote oldest rocks, often Archean. Red pentagons denote younger orogenic rocks. Blue triangles are even younger age in the Shackleton Range. Black striped lines in insets are geological boundaries modified from original studies for guidance. Brown shade indicates the outline of rock outcrops (Burton-Johnson et al., 2016). AP = Antarctic Peninsula, CL = Coats Land, DML = Dronning Maud Land, EL = Enderby Land, GC = Grunehogna Craton, GSM = Gamburtsev Subglacial Mountains, KL = Kemp Land, MG = Mertz Glacier, MR = Miller Range, MRL = MacRobertson Land, PB = Prydz Bay, PCM = Prince Charles Mountains, PEL = Princess Elizabeth Land, SP=South Pole, SR = Shackleton Range, TA = Terre Adélie, TAM=Transantarctic Mountains, WA = West Antarctica, WL=Wilkes Land.

Introducing: "Antarctic Geothermal Heat Model: Aq1"

Chapter 5 has been published as: Stål, T., Reading, A. M., Halpin, J. A., and Whittaker, J. M. (2020). Antarctic Geothermal Heat Model: Aq1. *Geochemistry, Geophysics, Geosystems*. <https://doi.org/10.1029/2020GC009428>

The text is reproduced in its submitted form and therefore some material is repeated from the background and other chapters. In the case of any differences, the published version of the chapter take precedence.

Chapter 5

Antarctic Geothermal Heat Model: Aq1

Tobias Stål^{1,2}, Anya M. Reading^{1,2}, Jacqueline A. Halpin², and Joanne M. Whittaker²

1. School of Natural Sciences (Earth Sciences), University of Tasmania
2. Institute for Marine and Antarctic Studies, University of Tasmania

Abstract

We present a refined map of geothermal heat flow for Antarctica, Aq1, based on multiple observables. The map is generated using a similarity detection approach by attributing observables from geophysics and geology to a large number of high-quality heat flow values ($N = 5792$) from other continents. Observables from global, continental and regional datasets for Antarctica are used with a weighting function that allows the degree of similarity to increase with proximity and how similar the observables are. The similarity detection parameters are optimized through cross-correlation. For each grid cell in Antarctica, a weighted average heat flow value and uncertainty metrics are calculated.

The Aq1 model provides higher spatial resolution in comparison to previous results. High heat flow is shown in the Thwaites Glacier region, with local values over 150 mWm^{-2} . We also map elevated values over 80 mWm^{-2} in Palmer Land, Marie Byrd Land, Victoria Land and Queen Mary Land. Very low heat flow is shown in the interior of Wilkes Land and Coats Land, with values under 40 mWm^{-2} .

We anticipate that the new geothermal heat flow map, Aq1, and its uncertainty bounds will find extended use in providing boundary conditions for ice sheet modeling and understanding the interactions between the cryosphere and solid Earth. The computational framework and open architecture allow for the model to be reproduced, adapted and updated with additional data, or model subsets to be output at higher resolution for regional studies.

Plain Language Summary

We present a new map that shows how the heat from the deep Earth varies from place to place in Antarctica. The map shows where raised heat flow values beneath ice sheets need to be included to better predict how ice sheets will respond to the Earth's warming climate. Areas with volcanoes have high geothermal heat flow. Other medium-to-high heat flow locations are often hard to identify, especially as it is too difficult or expensive to measure the heat directly in the harsh and sensitive Antarctic environment. To overcome this challenge, we use a technique with computer-aided match between the best data we can compile for Antarctica and corresponding data and heat flow values from other continents.

5.1 Introduction

The distribution of continental heat flow is the result of Earth's dynamic processes through geological time: ongoing tectonic processes bring hot material to the surface, and enhance the local geothermal gradient; past tectonic processes distributed heat producing elements unevenly in the crust; exhumation and deposition controls the geothermal heat transfer on local, regional and continental scales. Subglacial geothermal heat in Antarctica has significance for studies of the tectonic history (Artemieva, 2011), and has also been identified as a boundary condition for ice sheet models (Matsuoka et al., 2012; Pattyn, 2010; Pattyn et al., 2016; Pittard et al., 2016; Van Liefferinge et al., 2018; Whitehouse et al., 2019; Winkelmann et al., 2011). Understanding the response of the Antarctic ice sheets to changing climate, and improving the prediction of related contributions to global sea level, is of highest importance (DeConto et al., 2016; Golledge et al., 2015). Due to limited geological data, and lack of values based on direct measurements, heat flow is difficult to constrain in the Antarctic interior, and existing maps have appreciable differences between them (discussed by e.g. Burton-Johnson et al., 2020; Stål et al., 2020c). The need for better estimates encourage us to develop methods to best constrain the spatial variation of heat flow using available data, while accepting that the uncertainties remain large. In this contribution, we present Aq1, a new approach to estimate Antarctic heat flow (Fig. 5.1).

The few direct heat flow estimates across Antarctica have been made using measurements from the base of the icesheet rather than in bedrock, as is typical on other continents. These subglacial measurements suggest high spatial variability and complex hydrological interaction between the cryosphere and solid Earth (Begeman et al., 2017; Fisher et al., 2015; Wright et al., 2012). Thermal gradients within the ice can provide insight for ice sheet models and models of subglacial hydrology (Price et al., 2002), but cannot be used to estimate the solid Earth contribution with any certainty, unless the exact conditions at the base are known, or assumed, and the borehole reaches sufficient depth (Mony et al., 2020; Tulaczyk et al., 2001). Constraints for subglacial heat flow can also be inferred from thermomechanical ice-flow models (e.g., MacGregor et al., 2016; Pattyn, 2010; Van Liefferinge et al., 2018), or mapping of subglacial lakes (e.g., Pattyn et al., 2016). Such models show the general trends in expected heat transfer, and also suggest large regional and local variability. Crustal geothermal heat flow is difficult to separate from the impact of basal friction of fast flowing glaciers (Larour et al., 2012; Pattyn, 2010), the energy needed for melting ice (Fudge et al., 2013), or advection by

ground water that occurs in sediment layers or other permeable rocks beneath (Siegert et al., 2016).

An alternative to calculating heat flow values from field measurements is to derive a temperature gradient using indirect methods applied to geophysical data, and calculate the resulting heat flow (An et al., 2015b; Fox Maule et al., 2005; Martos et al., 2017; Purucker, 2013). These methods are associated with large uncertainties regarding how well the temperature and depth are constrained (discussed by e.g. Burton-Johnson et al., 2020; Haeger et al., 2019; Lösing et al., 2020; Stål et al., 2020c). Studies that rely on the temperature in the lower crust or upper mantle also depend on assumptions regarding the 3D distribution of heat production and thermal conductivity in the crust, and shallow transient heat sources (e.g., Artemieva et al., 2001; Jaupart et al., 2016). Shapiro et al. (2004) used a global seismic model to match heat flow records in a global compilation (Pollack et al., 1993) to assign heat flow values in Antarctica. With this approach a realistic range of the crustal contribution is captured, noting that the result depends on how the low resolution seismic wave speed data of the lithosphere captures variations in the crust. Using recent seismic tomography models from Lloyd et al. (2020) and Shen et al. (2018a), and heat flow estimates in continental US, Shen et al. (2020) used similar approach to generate a heat flow map of higher resolution and defined uncertainty bounds. This body of work significantly progressed the understanding of particularly the thermal properties of West Antarctica, and accords to a great extent with the recently reviewed geological history (Jordan et al., 2020).

A large fraction of the heat flow originates from radioactive decay of elements within enriched material in the crust (e.g., Artemieva et al., 2001; Hasterok et al., 2011; Jaupart et al., 2013), and considering the crust can therefore substantially improve heat flow maps. Reviews suggest a general correlation between observed heat production and heat flow, but this relationship is not universal (e.g., Jaupart et al., 2016; Levy et al., 2010; McLaren et al., 2003). Studies of heat production in crustal rocks (e.g., Carson et al., 2014; Goodge, 2018) provide us with a first insight into the variability of heat production in Antarctica. Heat production in rocks has a weak correlation with thermal age and is informed by geochemical composition (e.g., Hasterok et al., 2018a, 2017; Jaupart et al., 2013), but such properties are to a large extent unknown in the subglacial interior. Burton-Johnson et al. (2017) provided a detailed study for the Antarctic Peninsula with heat production in the upper crust assigned from geological and geochemical observations, and limited extrapolation, to account for 6–70% of the total heat flow. However, such studies can not be performed on a continental scale as over 99.8% of Antarctica is unexposed (Burton-Johnson et al., 2016). A steady-state Antarctic geothermal heat flow model, AqSS (Stål et al., 2020c), uses a constant mantle heat flow component and introduces a first order approach for integrating heterogeneous heat production within segmented crust. Heat that is not generated by crustal heat production or heat flow across the Moho, must be associated to dynamic and transient heat transfer by ongoing tectonics or shallow processes. Significant differences between estimates from available Antarctic heat flow models and this steady-state model, AqSS, can therefore indicate regions with such conditions.

Heat flow studies for Antarctica’s neighbors prior to the breakup of Gondwana (e.g., McLaren et al., 2003; Pollett et al., 2019; Roy et al., 2003; Rudnick et al., 1999), and the continental shelf (e.g., Dziadek et al., 2017; Morin et al., 2010) suggest the nature of heterogeneity of heat flow to expect in Antarctica. However, extrapolations must be treated with

caution due to the high spatial variability of heat flow (e.g., Carson et al., 2014; Jaupart et al., 2013), and limited extent of shared coastal domains (e.g., Aitken et al., 2014; Maritati et al., 2019; Stål et al., 2019c; Tucker et al., 2017). Cenozoic processes of deposition and exhumation have a different history in domains that were recently separated at Gondwana breakup, as seen in the asymmetric distribution of terrigenous sedimentation in the marine environment between the Australian and the Antarctic margins (e.g., Sauermilch et al., 2019). Sedimentation, erosion and exhumation have large impact on heat flow (Beardsmore et al., 2001; England et al., 1980; Jessop et al., 1994), but are still poorly constrained in the Antarctic interior, and is the subject of ongoing work (e.g., Paxman et al., 2019b).

A much greater number of estimates of heat flow from *in situ* thermal gradient and conductivity measurements exist for continents other than Antarctica. Motivation for those measurements includes studies underpinning hydrocarbon reservoirs, geothermal energy, structural studies for potential mineral exploration, and understanding of Earth’s energy balance and age (Beardsmore et al., 2001). The research area has been facilitated by cumulative compilations (e.g., Hasterok, 2019; Lucazeau, 2019; Pollack et al., 1993). Measurements are, however, irregular in distribution, and are of variable quality. To improve interpolation, Goutorbe et al. (2011) developed a similarity method where heat flow is linked to geological and geophysical observables. A heat flow value for a given location is derived from measurements with a similar geological context. When a number of observables combined suggests a heat flow value within a given range, this is more robust than a heat flow value constrained by only one dataset. Lucazeau (2019) applied the method to a larger number of measurements from the New Global Heat Flow database (NGHF). In this study, using 14–19 sets of observables produces a misfit of less than 10 mWm^{-2} , and a larger number of datasets does not improve the estimates significantly yet risks the introduction of noise. Observables as crustal type, age, and sediment thickness provide robust constraints to link heat flow measurements to target locations. However, such datasets are not available for the subglacial interior of Antarctica and this method must therefore be adapted for application with a limited range of observables.

Our new model, Aq1, uses a modification of the similarity approach employed by Goutorbe et al. (2011) to infer Antarctic heat flow from global comparisons. We also provide uncertainty metrics to inform the interpretation of the resulting map and its further use. The Aq1 model is provided with a computational framework to facilitate generation of e.g. refined regional studies and include future datasets (discussed by Stål et al., 2020c).

5.2 Data

In the following section we describe the datasets used in the study, and any necessary initial data preparation.

5.2.1 Heat Flow Data

New Global Heat Flow is an extended compilation of earlier heat flow catalogs, associated with meta data attributes with links to original studies (Lucazeau, 2019). We exclude records in the case of missing coordinates, missing heat flow values, and a few high latitude measurements, where map distortion might impact some observables used (Fig. S1a). In order to remove

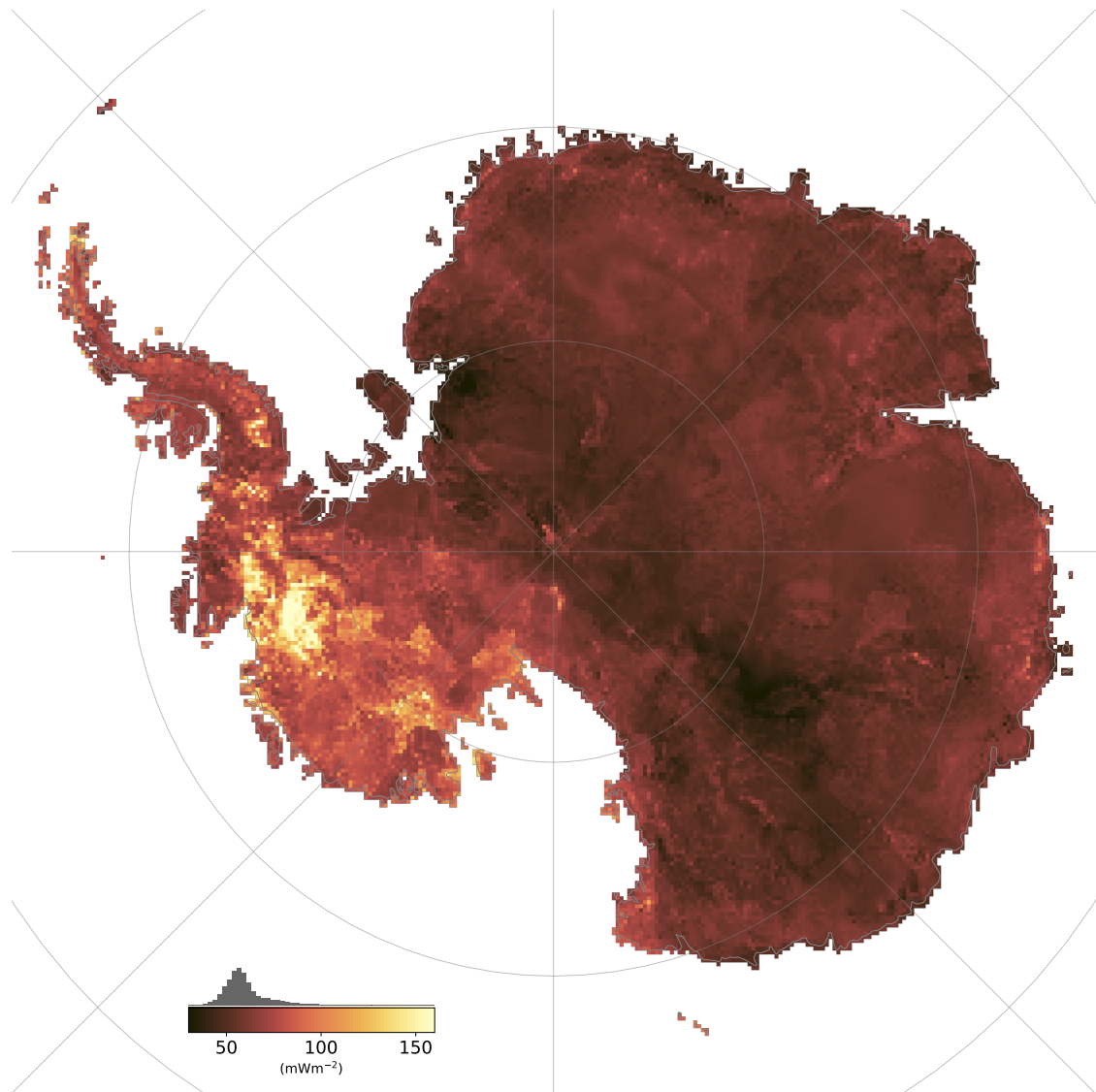


Figure 5.1: Heat flow map of Antarctica, Aq1.

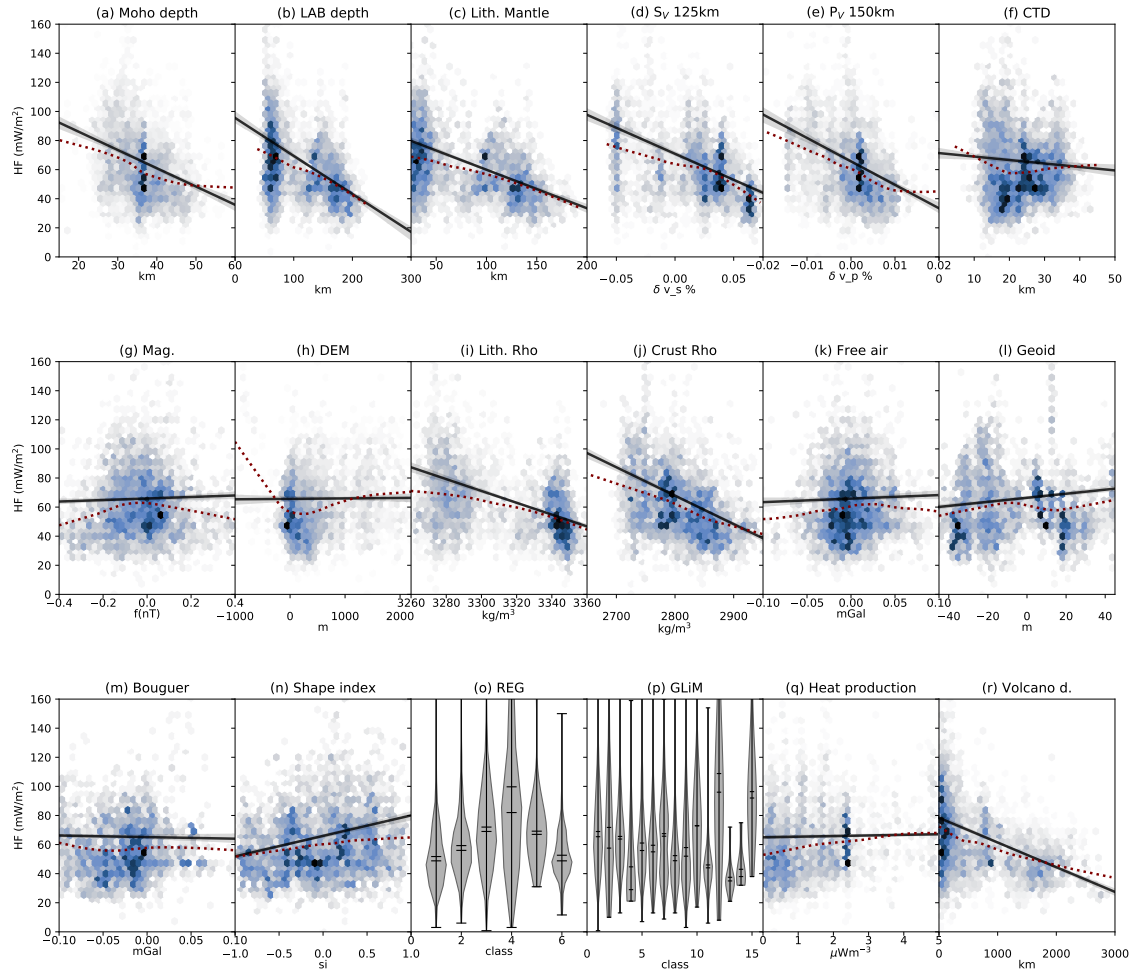


Figure 5.2: Cross plots of reference observables (O_R) and used heat flow records from NGHF (Lucazeau, 2019), as described in text. Observable value and heat flow value are binned to a hexagonal grid, where the color represent the relative frequency of heat flow values. Classes are shown as violin plots with the distribution of heat flow measurements for each class. Linear regression (black line) highlights any general relation between observable and heat flow. A non-parametric locally weighted scatterplot smoothing (LOWESS) is plotted as dotted red line (Cleveland, 1979; Waskom et al., 2020). (a) Moho depth (Szwilius et al., 2019), (b) Lithosphere thickness (Afonso et al., 2019), (c) Thickness of lithospheric mantle (Afonso et al., 2019; Szwilius et al., 2019), (d) Shear wave speed at 125km (SMEAN2 (2016) based on Becker et al., 2002), (e) Pressure wave speed at 150 km (Becker et al., 2002), (f) Curie temperature depth (Li et al., 2017), (g) Magnetic anomalies (Maus et al., 2009; Meyer et al., 2016), (h) Elevation (ETOPO1 Amante et al., 2009), (i) Lithosphere average density (Afonso et al., 2019), (j) Crustal average density (Afonso et al., 2019), (i) Free air gravity anomalies (Förste et al., 2013; Sinem Ince et al., 2019), (j) Geoid height (Förste et al., 2013; Sinem Ince et al., 2019), (k) Bouguer anomaly (Förste et al., 2013; Sinem Ince et al., 2019), (l) Shape index of satellite gravity gradients (Ebbing et al., 2018), (m) Tectonic regionalization classes (Schaeffer et al., 2015), (n) Lithological data classes (Hartmann et al., 2012), (o) Heat production (Gard et al., 2019), (p) Distance to nearest volcano (Global Volcanism Program, 2013). Examples of datasets are presented in more details in Supplementary Material Figure S5, and discussed in text.

Table 5.1: Heat flow records in NGHF. Number of records after cleaning of data.

N	Filtering	Min ^a mW/m ²	Max mW/m ²	Average mW/m ²	Median mW/m ²
69729	All records	-401.0	72000.0	120.5	62.0
69377	Excluded incomplete records	-401.0	72000.0	120.5	62.0
46270	Excluded deeper than 1000 m bsl	-401.0	15600.0	99.6	62.0
46113	Excluded high latitudes	-401.0	15600.0	99.6	62.0
35647	Rating A ^c , B ^d , C ^e	-3.0	15600.0	101.1	61.0
12707	Rating A ^c , B ^d	-3.0	5146.0	66.1	59.0
5792	Rating A ^c	0.8	787.5	65.8	59.0

a Negative value would here indicate heat flow into the Earth.

b Best rating, e.g. defined as 10% variation in measurement.

c Good rating, e.g. up to 20% variation in measurement.

d Average rating, e.g. up to 30% variation in measurement.

records from deep oceans, but keep those on continental shelves and measurements at depths representing the low hypsometry of West Antarctica (e.g., Artemieva et al., 2020; Morlighem et al., 2019), we exclude measurements deeper than 1000 m below sea level (Tab. 5.1 and Supplementary material Fig. S1b). The quality of heat flow measurements are rated in NGHF. The rating category for each measurement is based on e.g. the variation of heat flow in the borehole where the measurement is performed. Old and questionable measurements are generally assigned a lower rating. When removing lower rated heat flow measurements, the mean value decreases (Tab. 5.1). This is a consequence of removal of a small number of high values from locations with geothermal activity. The median of the heat flow data remains within 3 mW/m². The distribution of heat flow values, before and after removal of records as above, is provided in Figure S1a. We include only records rated *A*. For reference, we also provide a version where also *B*-rated records are used (Fig. S2). Including lower rated records generates a similar overall structure and significantly increases the uncertainty range of the model.

5.2.2 Observables

We refer to associated data, models and distances as observables, i.e. this term is used in a broad sense. Reference observables (o_R) are linked to each listing in the heat flow catalog (NGHF, Lucazeau, 2019), and target observables (o_T) are linked to each 2D grid cell for our Antarctic model. When provided, we include uncertainty estimates to guide the similarity analysis. For most of Antarctica, we are limited to datasets derived from satellite potential field measurements and large scale seismology. For outcrops along the coast and Transantarctic Mountains, we access petrological data from previous studies and compilations (Gard et al., 2019), and take advantage of geological experience, and extrapolation (Hartmann et al., 2012; Tingey et al., 1991). Additional information has been derived from existing datasets, for example, subglacial topographic shapes (e.g., Wyk de Vries et al., 2018) and curvature in the gravitational field (e.g., Ebbing et al., 2018).

18 pairs of observables are included to match heat flow measurements with Antarctic con-

tinental properties (Tab. 5.2, Fig. S3). Each observable is contributing to a decrease of cross validated root mean squared error (RMSe) and mean absolute error (MAe) for heat flow measurements in NGHF (Fig. S4). Reference observables are also plotted against measured heat flow in Figure 5.2 and maps of a selection of observables are given (Fig. S5). The four types of observables are processed differently; continuous data, sparse data, classes and distance functions.

5.2.2.1 Continuous Data

Continuous data cover most of the Antarctic continent and consist of satellite and airborne geophysical measurements, seismic tomography and elevation data. Global models often lack resolution and accuracy in Antarctica (e.g. Fig. S6). Where available, we use Antarctic studies as target observables. Global Moho depth is provided from Szwillus et al. (2019). The model is similar to CRUST1 (Laske et al., 2013), but has refined, transparent interpolation, and well defined uncertainty bounds. In Antarctica, we use AN_CRUST (An et al., 2015a) as the matching target observable. Both observables refer to Moho depth, but AN_CRUST has higher resolution and is generated from surface wave tomography and constrained by available regional receiver function studies (Fig. S5a). Similarly, we use the global Lithosphere-Asthenosphere boundary (LAB) from Afonso et al. (2019), and the model AN_LAB from An et al. (2015a) in Antarctica (Fig. S5b). Thickness of lithospheric mantle is calculated as the difference between LAB depth, and Moho depth (Afonso et al., 2019). Depth to Curie temperature is derived from magnetic data. Reference observables are from GCDM (Li et al., 2017) using data from EMAG2 (Maus et al., 2009). In Antarctica, GCDM has limited cover, and we use CTD from Martos et al. (2017) with provided uncertainty bounds (Fig. S5c). We use the EMAG2v3 magnetic anomaly map from Maus et al. (2009) and Meyer et al. (2016) as a separate reference observable and ADMAP2 (Golynsky et al., 2018) as a target observable, noting that EMAG2v3 and ADMAP2 only rely on observed data. As magnetic anomalies vary over several orders of magnitude, we apply a logarithmic function that preserves the sign: $M_{\log} = \text{sgn}(M) \times \ln(1 + M/400)$, clipped to range $[-1, 1]$, where M is the linear data and M_{\log} the re-scaled observable. Our reference digital elevation model is ETOPO1 (Amante et al., 2009), and in Antarctica we use the subglacial topography from MEaSURES BedMachine (Morlighem et al., 2019), with uncertainty bounds. A simplistic glacial isostatic adjustment (GIA) correction is performed for total ice loading relaxation (Stål et al., 2020c), using an ice density of 917 kgm^{-3} (Griggs et al., 2011) and crustal, and lithospheric mantle densities from Afonso et al. (2019). Crustal and lithospheric thickness to estimate GIA are obtained from An et al. (2015a,b). We apply a simplified flexural model as a Gaussian kernel of $\sigma=60$ km. For this context, we chose not to correct for global sea level adjustment, as it would also impact coastal reference observables (Fig. S7). By using the interpolated mean elevation for each cell, we remove most topographic effects on heat that depend on the roughness (Lees et al., 1910) as those are beyond the resolution of the target observable for most of Antarctica (Graham et al., 2017). Four aspects of the gravity field are included as observables, all derived from EIGEN-6C4 model (Förste et al., 2013). Computations of geoid, free air gravity and Bouger gravity are performed by ICGEM (Drewes et al., 2016; Sinem Ince et al., 2019) and provide a global, reliable frame covering the whole Antarctic continent. The Bouger gravity reference

Table 5.2: Observables used in this study. The content is discussed in the text.

	Observable(s) (label o_R in Fig. 5.2)	Weighting function, w
	Reference observable, o_R	Similarity range, σ_R
	Target observable, o_T	Similarity range, σ_T
Continuous	Moho depth (a)	
	o_R : Szwillus et al. (2019)	σ_R as provided.
	o_T : An et al. (2015a)	$\sigma_T = 1.0$ km
	LAB depth (b)	
	o_R : Afonso et al. (2019)	$\sigma_R = 18$ km
	o_T : An et al. (2015b)	$\sigma_T = 18$ km
	Lithospheric mantle thickness (c)	
	o_R : LAB depth - Moho depth ^a	$\sigma_R = 20$ km
	o_T : Ibid.	$\sigma_T = 20$ km
	Shear wave speed, V_s 125km	
	o_R : Becker et al. (2002)	$\sigma_T = 1.50\%$
	o_T : Ibid.	$\sigma_T = 1.50\%$
	Pressure wave speed, V_p 150 km (e)	
	o_R : Becker et al. (2002)	$\sigma_R = 0.25\%$
	o_T : Ibid.	$\sigma_T = 0.25\%$
	Curie Temperature Depth (f)	
	o_R : Li et al. (2017)	$\sigma_T = 4$ km
	o_T : Martos et al. (2017)	σ_T as provided.
	Earth Magnetic Anomaly (g) ^a	
o_R : Meyer et al. (2016)	$\sigma_R = 0.06^a$	
o_T : Golynsky et al. (2018)	$\sigma_T = 0.06^a$	
Elevation (h)		
o_R : Amante et al. (2009)	$\sigma_R = 275$ m	
o_T : Morlighem et al. (2019) ^a	σ_T as provided.	
Lithosphere average density (i)		
o_R : Afonso et al. (2019)	$\sigma_R = 12$ kg/m ³	
o_T : Ibid.	$\sigma_T = 12$ kg/m ³	
Crustal average density (j)		
o_R : Afonso et al. (2019)	$\sigma_R = 36$ kg/m ³	
o_T : Ibid.	$\sigma_T = 36$ kg/m ³	
Free Air Gravity (k)		
o_R : Förste et al. (2013)	$\sigma_T = 0.0075$ mGal	
o_T : Ibid.	$\sigma_T = 0.0075$ mGal	
Geoid height (l)		
o_R : Förste et al. (2013)	$\sigma_R = 8$ m	
o_T : Ibid.	$\sigma_T = 8$ m	
Bouguer gravity anomaly (m)		
o_R : Sinem Ince et al. (2019)	$\sigma_R = 0.03$ mGal	
o_T : Scheinert et al. (2016)	$\sigma_T = 0.03$ mGal	
Shape index of curvature (n)		
o_R : Ebbing et al. (2018)	$\sigma_R = 1/8$	
o_T : Ibid.	$\sigma_T = 1/8$	
Tectonic regionalization (o)		
o_R : Schaeffer et al. (2015)	Identical only.	
o_T : Ibid.	Identical only.	
Global lithological map (p)		
o_R : Hartmann et al. (2012)	Identical only.	
o_T : Ibid.	Identical only.	
Heat production (q)		
o_R : Gard et al. (2019) ^{a,b}	$w = 1 - \text{obs}/250$ km	
o_T : Ibid.	$\sigma_R = 0.5 \mu\text{Wm}^{-3}$	
	$\sigma_T = 0.5 \mu\text{Wm}^{-3}$	
Distance to nearest volcano (r)		
o_R : Global Volcanism Program (2013)	$w = 1 - \text{obs}/100$ km	
o_T : Ibid. Wyk de Vries et al. (2018)	$\sigma_R = 25$ km	
	$\sigma_T = 25$ km	

^aDetails provided in text.^bAnd references therein.

observable includes ETOPO1 (Amante et al., 2009). Global compilations of Bouguer corrected gravity field are not valid in ice covered areas. For Antarctica, we therefore use the Bouguer gravity model from Scheinert et al. (2016). This model covers 73% of the continent with gravity data from airborne surveys and topography model from BEDMAP2 (Fretwell et al., 2012). We also include the shape index of curvature of gravity field (Ebbing et al., 2018) from GOCE data (Pail et al., 2010) (Fig. S5d).

5.2.2.2 Discrete Class Data

We use the tectonic segmentation of Schaeffer et al. (2015). This is a robust global segmentation, but it is produced in low resolution. We note that in some locations, particularly along the circumference of Antarctica, this segmentation does not agree with geological and regional geophysical studies. Projection artifacts are mitigated using a median filter, with a $111 \text{ km} \times 111 \text{ km}$ circular kernel. We also include geological classification, including reasonable extrapolation of geological observations in Antarctica from the GLiM compilation (Hartmann et al., 2012; Tingey et al., 1991). We exclude the classes for Water Bodies (wb), Ice and Glaciers (ig) and No Data (nd). With those classes removed, only 11% of the Antarctic continent is classified, mainly in West Antarctica, along the coast, and Transantarctic Mountains.

5.2.2.3 Sparse Data

Estimates of heat production from geochemistry are taken from the compilation by Gard et al. (2019). The median heat production value and uncertainty for each grid cell are interpolated to nearest observation over unrealistic long distances, but are assigned a weighting function that decreases linearly over 250 km, as described below. We reduce errors in the sparse target observable by excluding reported observations not consistent with exposed outcrops (Burton-Johnson et al., 2016).

5.2.2.4 Distance Functions

Distance to phenomena that have an impact on heat flow are also included. Distances to nearest Holocene and Pleistocene volcano are calculated from global compilation by Global Volcanism Program (2013). In addition, as an Antarctic observable, we also include subglacial volcanoes suggested by Wyk de Vries et al. (2018) with total quality rating over 2.5. All volcanoes in the list are suggested to be shield volcanoes, as defined by the morphology (Grosse et al., 2014). It could have been beneficial for our purposes to separate Holocene and Pleistocene volcanism, but as we don't have this information for the subglacial volcanoes, we treat those reference observables equally. Distances are calculated along the great circle using *pyproj*, a PROJ4 package for Python (Snow et al., 2020).

5.2.3 Data Preparation

Using *agrid* (Stål et al., 2020a), we setup a global multivariate grid to import reference observables, in WGS 1984 (epsg:4326), with a resolution of 0.2×0.2 degrees. We exclude the few values south of 60°S and north of 80°N to avoid distortion as previously noted. For continuous data, a bi-linear interpolation of the cell center is obtained. For classes we use the nearest value

to each cell center. Heat production values are included as median of all records in each cell. Distance (in km) to the nearest Holocene and Pleistocene volcano (Global Volcanism Program, 2013) is assigned to each heat flow record.

To extract continuous data for the locations of heat flow measurements, we identify the nearest grid cells and generate an index matrix using KD-tree (Bentley, 1975). The index matrix is used to extract interpolated values from reference observables at the location of the heat flow measurement. The average distance between heat flow measurements and nearest grid center is 7.6 km, the maximum distance is 15.6 km (Fig. S8). We also extract provided uncertainty bounds for continuous data, where available.

An Antarctic grid is generated (similar to Stål et al., 2020c). The grid is in 20×20 km resolution, with an extent of 5600×5600 km in WGS 84 / Antarctic Polar Stereographic (epsg:3031). We also set up a grid in 50×50 km resolution (Fig. S9). We limit the model to the coastline and grounding line (Mouginot et al., 2017). Target observables are listed in Table 5.2. We also construct a grid to generate a test heat flow map for Australia, as a comparison of the potential, and limitations, of the methodology and observables used (Fig. S18).

5.3 Methods

Data handling and other stages of the workflow are coded in Python, using packages including *agrid* (Stål et al., 2020a), *numpy* (Harris et al., 2020), *pandas* (McKinney, 2015) and *scipy* (Jones et al., 2015). Throughout this contribution, visualization is carried out using *agrid* and *seaborn* (Waskom et al., 2020), both with underlying *matplotlib* (Hunter, 2007). We use perceptually linear color representations by Crameri et al. (SCM6 2019), as discussed by Crameri et al. (e.g. 2020) and Morse et al. (2019).

5.3.1 Degree of Similarity

Previous studies, using the methodology that we develop in this contribution, used step functions within a given range to define similarity between observables (Goutorbe et al., 2011; Lucazeau, 2019). To take full advantage of our more limited selection of data, we refine this approach by using a smoothly decreasing function derived from the Gaussian distribution. By using this relation, the precise similarity range is more robust. The main drawback is the substantially increased computational cost. Degree of similarity between each reference observable and target observable is detected as:

$$S = \exp\left(-\frac{(o_R - o_T)^2}{2 \times (\sigma_R + \sigma_T)^2 / \Psi}\right), \quad (5.1)$$

where S is a degree of similarity in the range $[0, 1]$. o_R is the value of the reference observable, o_T is the value of the target observable, σ_R is the uncertainty (as two standard errors, 95.4%, range) for the reference observable, σ_T is the uncertainty for the target observable. Values used for σ are listed in Table 5.2. We introduce Ψ , a scalar representing similarity pickiness (Fig. S10). A low value for Ψ relaxes the similarity function. We use the parameter to test and optimize the similarity detection (Fig. 5.3 and S11). When an uncertainty range has been published with the datasets used as observables, we use this range. Shape index (Ebbing

et al., 2018) is assigned a range of $1/8$, as suggested by Koenderink et al. (1992) to represent the categories of curvature shape. Classes are only accepted as similar when identical. This is achieved by using a very low value for σ . For most observables, the uncertainties are not defined. We optimize the similarity detection by performing a Monte Carlo simulation ($N=2001$) with random Ψ for each observable, and calculate cross-correlated misfit as MAe and RMSe, using the method described below. We find that the model is robust for defined ranges (Fig. 5.3a–b, Fig. S11 and Fig. S12). However, the acceptance range also functions as a spatial smoothing, as continuous data often change gradually. All acceptance ranges used are geologically and geophysical meaningful, and generally agree with our expected uncertainty in observables. Figure S12 provides the same test as Figures 5.3a–b, but also applying the step function similarity detection, to illustrate the less predictable response to parameter variations, for the limited range of observables used.

5.3.2 Weighting

A weight is introduced for sparse data and distance functions. A weighting of 1, sets the observable as fully relevant, but when the value decreases to 0, it is effectively muted from the similarity detection, and does not contribute to the heat flow estimate. The weights for heat production data are set to decrease linearly over 250 km from nearest observation (Fig. S13). The impact of distance to volcanoes is set to decrease linearly over 100 km (Fig. S14g). Beyond the maximum distance, the weighting is set to 0. Heat flow anomalies associated with advection and diffusion from shield volcanoes has a limited extent of less than 10 km (Hurwitz, 2003; Wright et al., 2008). However, the existence of volcanoes also helps us to map the tectonic settings of volcanic provinces. The weighting functions are listed in Tables 5.2. To assign dynamic weight, additional grids are constructed containing weighting factors. An example of the model with the distance-to-volcanoes observable excluded is provided by assigning a weight of zero (Figs. S14a–b). We also generate a version without Moho and LAB observables (Figs. S14c–d).

To investigate if an observable improves the result, or adds noise, we perform a Monte Carlo simulation with random weights assigned to the observables. We apply $N = 2001$ random combinations, including the case with all observables weighted to 1. Keeping all observables fully weighted is demonstrated to provide good predictions (Fig. S4).

5.3.3 Similarity Process and Optimization

For each Antarctic grid cell, observables are compared with reference observables' vectors for heat flow measurements to generate a similarity matrix. The similarities (S) are multiplied with the weighting matrix and stacked for each reference and target:

$$N_{sim} = \sum_{i=1}^{n_{obs}} S_{obs} \times w_{obs}, \quad (5.2)$$

where N_{sim} is the weighted similarity for each heat flow record, n_{obs} is the number of observables used (18), w_{obs} is the weighting for each observable for given heat flow record.

The stacked value N_{sim} is used as a power to a base K , to increase the value of multiple similar observables:

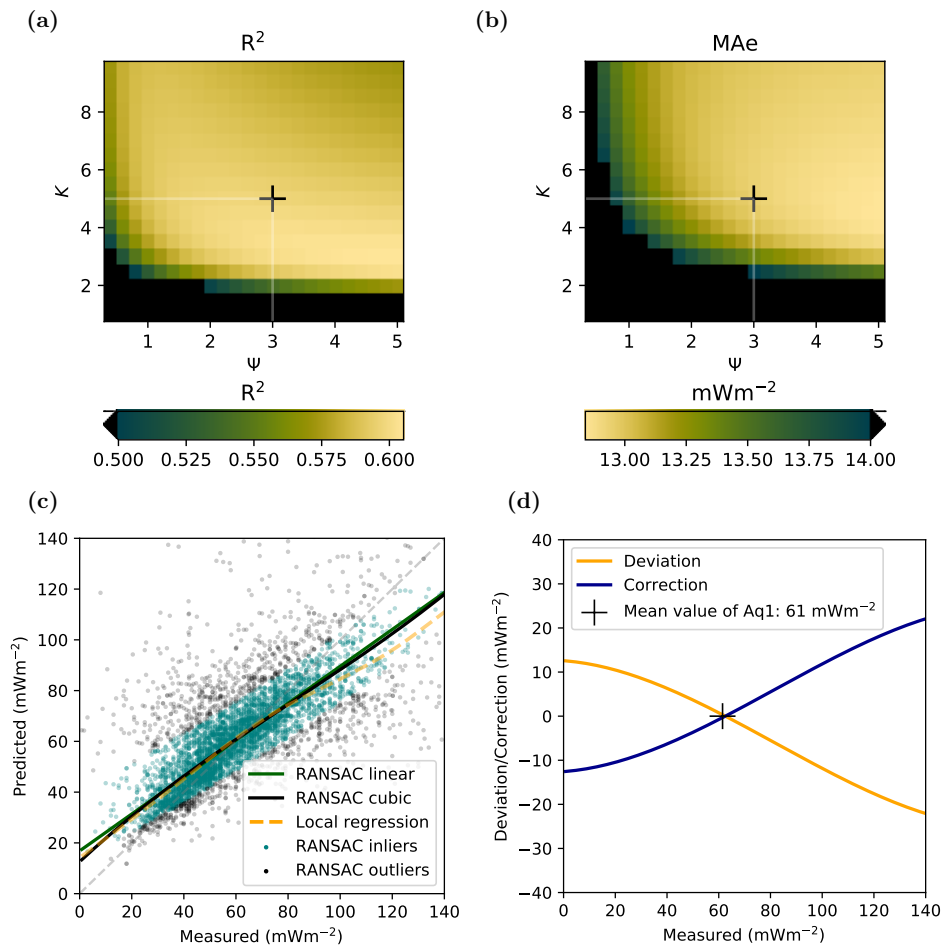


Figure 5.3: Method optimization and correction applied, using leave-one-out cross validation (LOOCV) of heat flow values in NGHF, included in this study. The R^2 value and MAe misfit cannot be optimized for the same parameter values. The choice of K and Ψ is therefore a trade-off between considerations, as discussed in text. (a) Parameter map for R^2 . (b) Parameter map for Mean absolute error (MAe) misfit. K values at y-axis, and Ψ values at x-axis. Bright colors indicates more favorable combinations, the color range is optimized and values outside this range are masked black. (c) Heat flow measurements along the x-axis, and predicted values along y-axis. The RANSAC cubic regression (black line) gives a robust value, as outliers (gray dots) are ignored and the regression is estimated from inlier data points only (green dots) (Fischler et al., 1981). A local regression (LOWESS) is shown with orange dashed line. A linear RANSAC regression line is also shown for reference (green line). (d) Applied correction to compensate variance reduction of heat flow records. Orange line shows the impact, and blue line shows the applied compensation. The black marker show the average heat flow in Aq1.

$$w_i = K^{N_{sim}} \quad (5.3)$$

To optimize and test the K parameter, together with the similarity pickiness (Ψ), we perform leave-one-out cross validation (LOOCV). We calculate misfit as root mean squared error (RMSe), mean absolute error (MAe), and coefficient of determination (R^2). The results are shown as a parameter maps in Figures 5.3a–b and Figure S12. MAe is reduced with higher K (Fig. 5.3b), but the R^2 values (Fig. 5.3a), and related RMSe (Fig. S12a), suggests a lower value of K . With increasing Ψ , the spatial resolution increases (Figs. S15d-f). K controls stability and accuracy. A high value of K would put more weight on fewer measurements, which reduces stability given the limited selection of observables available in Antarctica. In the lower range, $K < 3$, the resolution decreases and the output appears smoothed. High K and Ψ gives the best linear correlation, at the expense of increased RMSe and reduced R^2 . We hence optimize for good RMSe within acceptable range of MAe, and then correct for the effects on correlation, selecting $K=5$, and $\Psi=3$. Maps resulting from different values of K and Ψ are provided in Figure S15. When comparing the parameter maps, we note that the continuous detection (Eq. 5.1) provides a smoother, more robust and predictable response to variations in K and Ψ , for the selected parameter ranges (Fig. S11).

5.3.4 Corrections of Heat Flow Values

A scatter plot of LOOCV predicted heat flow values and measurements shows that the overall trend captures the variations (Fig. 5.3c). The residuals are heteroskedastic; high predicted values are underestimated. This is a result of extremely high values that cannot be detected due to rare combination of observables. We analyze the heteroskedasticity by fitting a local regression, a linear RANSAC regression, and a polynomial RANSAC regression (Fischler et al., 1981). The local regression and the linear regressions are almost identical up to 80 mWm². Above 80 mWm², the local regression suggests an increasing underestimation of predicted values. Generally, predicted values are likely to gravitate towards the mean of the measurements as each predicted value is a weighted average of a large number of measurements and the selected similar distribution (σ_i) relates to the distribution of the total population as $\sigma_M = \sigma_i / \sqrt{w_i}$. When the K value is higher, fewer records get more of the weight, and smaller correction is needed. However, we show that the RMS error and coefficient of determination are better for moderate values of K , as the observables used in this study generate noise (Fig. 5.3a). We accept the slightly skewed correlation, and apply a correction to account for the reduced range. We apply the RANSAC polynomial regressor to calculate a polynomial function for correction (Fig. 5.3d):

$$Q_{pc} = 2 \times Q_p - (a \times Q_p^3 + b \times Q_p^2 + c \times Q_p + d) \quad (5.4)$$

where Q_{pc} are the predicted and corrected heat flow values, Q_p are the predicted values. $a - d$ are the coefficients calculated for a cubic RANSAC regression using the Python package SKlearn (Pedregosa et al., 2011): $a = 13.72$, $b = -3.38$, $c = 0.9566$, $d = 0.01258$. The impact of the correction is shown in Figure S16, as maps and KDE plots of cross-correlation.

5.3.5 Generating maps of heat flow and model metrics

Using the optimized parameters, we calculate heat flow value and uncertainty metrics for each (x, y) target grid cell in Antarctica. Heat flow is calculated using:

$$\bar{Q} = \frac{\sum_i w_i q_i}{\sum_i w_i}, \quad (5.5)$$

where \bar{Q} is the weighted mean of all heat flow measurements for the area represented by grid cell (x, y) , q are the heat flow measurements from NGHF, and w_i is the weight from $w_i = K^{N_{sim}}$, where $K=5$. Correction for reduced range is applied, as described in previous section.

The standard deviation of the heat flow values is used to calculate uncertainty:

$$\sigma_Q = \sqrt{\frac{\sum w_i (Q_i - \bar{Q})^2}{\sum w_i}}, \quad (5.6)$$

where σ_Q is the uncertainty assigned to the grid cell (Fig. S17b). The uncertainties of the included heat flow records are not considered for this metric.

We also compute N_{total} , the amount of similarity from all observables and reference records, and present it as a logarithmic value. This is a combined measure of data availability, and how many similar reference observables are considered:

$$N_{total} = \ln \sum N_{sim}. \quad (5.7)$$

For each location, all weighted reference heat flow values are binned to a histogram, B_n , with bin size 1 mWm^{-2} in the range from 0 to 150 mWm^{-2} . The histogram is a discrete probability distribution and is normalized as:

$$p_A = \frac{B_n}{\sum B_n}. \quad (5.8)$$

Information entropy is calculated (Shannon, 1948):

$$H = - \sum_{i=1}^n p_A \ln p_A, \quad (5.9)$$

where $n = 150$, the number of bins, p_A is the normalized sum of similarity distribution (Eq. 5.8). The base is e , and hence H is given in nats. The bins are also stored to an array, and histogram can be extracted for any location. The theoretical upper range of entropy for the used histogram is $\ln 150 = 5.01$.

Figure 5.4c shows entropy detected in each distribution of reference heat flow values. To facilitate interpretation of entropy in this context, Figure 5.4d shows six normalized histograms of similar geological settings and binned heat flow values. The background colors are identical with the colormap used in Figure 5.4c. The six distributions shown are chosen to divide the total range in five equal sized bins, exact locations are only provided for reference.

We generate grids for Antarctica in resolutions $20 \times 20 \text{ km}$ and $50 \times 50 \text{ km}$ (Fig. S9). As a test case to appraise the approach and also to understand its limitations, we generate a heat flow grid of Australia in $20 \times 20 \text{ km}$ grid, GDA94 / Australian Albers (epsg:3577) (Aq1.au,

Fig. S18). For the Australian test, we exclude heat production values to provide an estimate similar to the Antarctic conditions. For this map, we also exclude all Australian measurements from NGHf.

We calculate the differences between Aq1 and six previous heat flow maps, including Burton-Johnson et al. (2017) regional map of the Antarctic Peninsula. Grids are exported in interoperable formats as geoTIFF, netCDF and ascii tables using *agrid* functionality (Stål et al., 2020a). We finally also generate a smoothed contour map by convolution with a Gaussian kernel with $\sigma = 40$ km (Fig. 5.6).

5.4 Results

We present a new heat flow map for Antarctica, Aq1 (Fig. 5.1 and Fig. 5.6, the latter labeled with geographic locations), together with maps of uncertainty metrics: standard deviation from the distribution of similar heat flow measurements in NGHf (Fig. 5.4a), total number of similarities (Fig. 5.4b), and the information entropy in the weighted heat flow histogram for each location (Fig. 5.4c). Those maps inform the robustness of the assigned heat flow value.

For most of East Antarctica, we calculate a heat flow between 40 and 70 mW/m², which is a similar range to that found in previous studies (Fig. 5.5). The lowest heat flow values are shown south of Dome Circle in interior Wilkes Land, Coats Land, and Wilkes Subglacial Basin. Elevated heat flow is shown in Victoria Land and parts of Queen Mary Land. High values of over 120 mW/m² are shown in the Thwaites Glacier region, West Antarctica, and in Marie Byrd Land and Palmer Land. The map shows areas of moderate heat flow in parts of Siple Coast, Ellsworth Land, and central Antarctic Peninsula, down to 60 mW/m².

Compared with previous studies, Aq1 is similar to Shen et al. (2020), but shows higher heat flow in some West Antarctic volcanic provinces (Lough et al., 2013; Wyk de Vries et al., 2018), and coastal East Antarctica (Fig. 5.5e). Aq1 is generally lower in large parts of West Antarctica. In most regions, the differences between Aq1 and Shen et al. (2020) are within the uncertainty ranges. Compared to earlier Antarctic heat flow models, Aq1 is most similar to An et al. (2015b), however with generally higher values in West Antarctica, and produced at higher resolution (Fig. 5.5b). Aq1 also generally agrees with Martos et al. (2017) in East Antarctica, but assigns lower values in West Antarctic interior and the Antarctic Peninsula (Fig. 5.5d). Aq1 is generally higher in East Antarctica than Fox Maule et al. (2005) (Fig. 5.5a), but lower in Ellesworth Land, Oates Land and Mac. Robertson Land. We suggest high levels of heat flow in Palmer Land in the southern Antarctic Peninsula. This is in general agreement with earlier studies, particularly the regional study by Burton-Johnson et al. (2017) (Fig. 5.5c). The pattern and range of the heat flow distribution in West Antarctica also agrees with O'Donnell et al. (2019), however, the multivariate approach provides higher spatial resolution. Finally, when Aq1 is compared with AqSS (Stål et al., 2020c), the difference potentially points to areas with a neotectonic and volcanic contribution in West Antarctica: mainly Thwaites Glacier, Marie Byrd Land, and also coastal Victoria Land, and Queen Mary Land in East Antarctica (Fig. 5.5f).

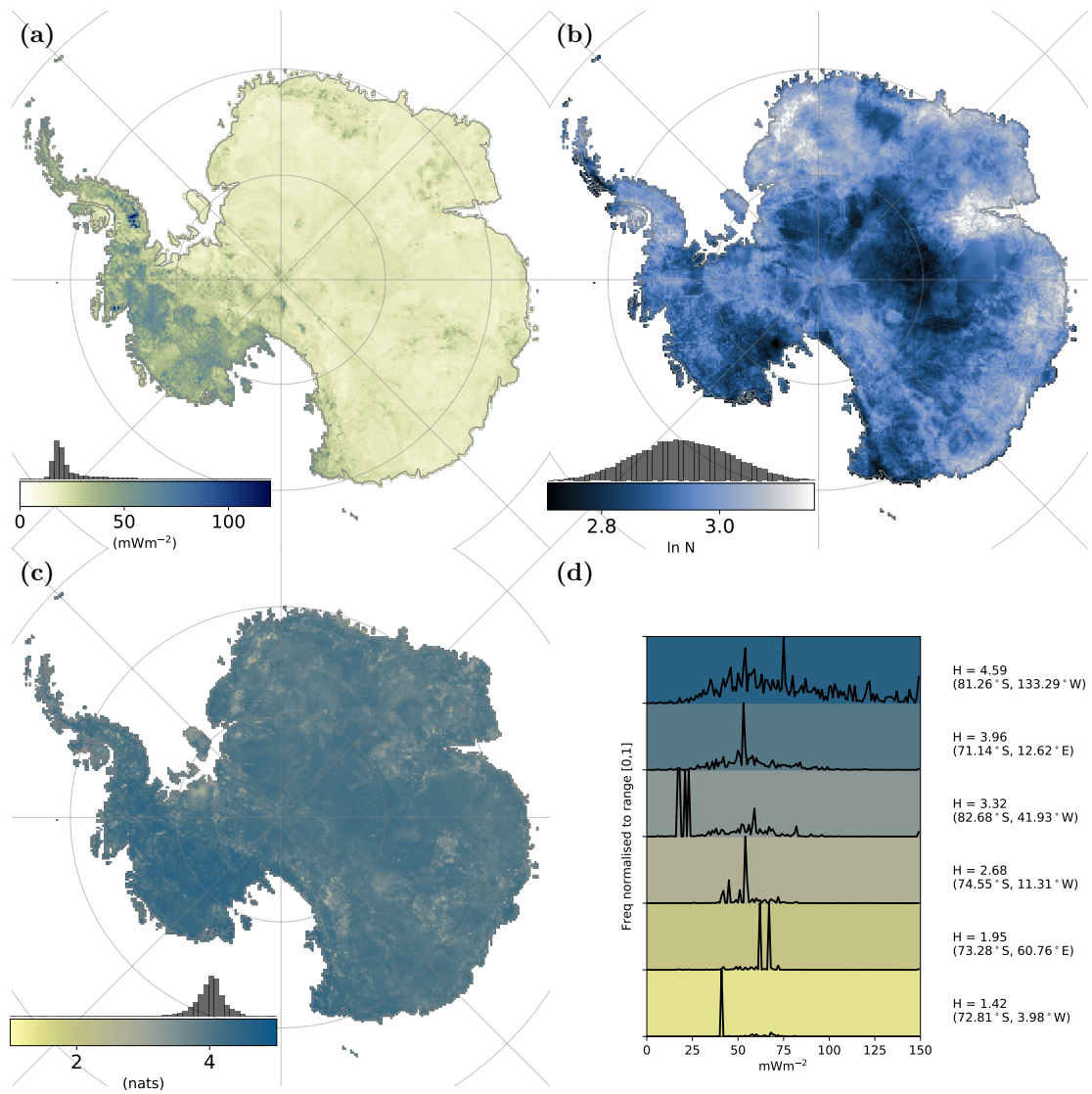


Figure 5.4: Uncertainty metrics for the Aq1 heat flow model. (a) Standard deviation of similar reference measurements. (b) Total number of similarities, in logarithmic scale. (c) Information entropy by natural logarithms, as described in methods section. (d) To assist the interpretation of information entropy, histograms from six examples are provided. The examples are the highest and lowest entropy, and four equal steps in between. The background color represent the same color as in (c). For clarity, the histograms of heat flow measurements are normalized to the range from 0 to 1. The color scales are chosen so that a darker tone indicates higher uncertainty, hence the scale for (b) is reversed.

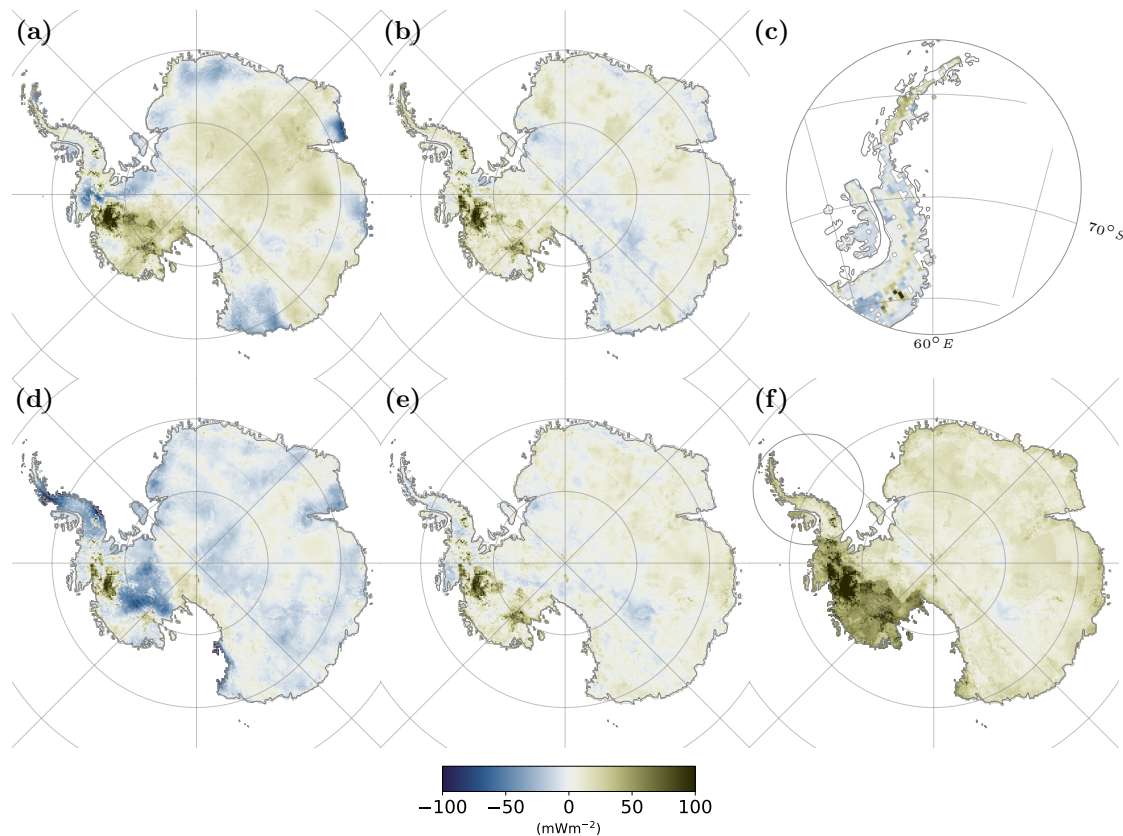


Figure 5.5: Comparison of Aq1 with previous published models. (a) Aq1 - Fox Maule et al. (2005). (b) Aq1 - An et al. (2015b). (c) Aq1 - Burton-Johnson et al. (2017). (d) Aq1 - Martos et al. (2017). (e) Aq1 - Shen et al. (2020). (f) Aq1 - AqSS (Stål et al., 2020c). Outline of the Antarctic peninsula study (c) is shown in (f). Brown-green indicates that Aq1 shows higher heat flow values, the case for most of East Antarctica. Blue indicates that the model being compared shows higher heat flow. Average continental heat flow is near 65 mW/m^2 (Pollack et al., 1993), Aq1 has a calculated average of 61.2 mW/m^2 . The average for Fox Maule et al. (2005) is 63.1 mW/m^2 , An et al. (2015b) 59.0 mW/m^2 , Martos et al. (2017) 70.4 mW/m^2 , and Shen et al. (2020) 57.1 mW/m^2 (Fig. S19), for the same extent as Aq1.

5.5 Discussion

In this section, we firstly note the limitations associated with the methodology. We then discuss how the alternative uncertainty metrics inform our appraisal and provide an interpretation of the Aq1 map.

5.5.1 Limitations of the Similarity Approach

The similarity approach relies on the compatibility between reference and target observables, and we note that some matches are not ideal. As the best available choice of target observable, we use Antarctic datasets for Curie temperature depth (Martos et al., 2017), seismic Moho depth (An et al., 2015a), LAB (An et al., 2015b), and also a unique source for distance to nearest volcano (Wyk de Vries et al., 2018). The matches between the reference and target observables across Antarctica (Fig. S6) show significant differences. While the impact of those differences is difficult to quantify, we provide robust maps of uncertainty metrics for the resulting model. The incompatibility between reference and target observables is a potential explanation for large uncertainties and information entropy (Fig. 5.4), where global and regional datasets associate different tectonic settings. The impact of uncertainties and shortcomings of the datasets used is moderated by using multiple sets of observables.

The leave-one-out cross validation Monte Carlo tests (Fig. S4) show that each used observable improves the prediction, even as some of the datasets are usually not associated with thermal properties. Instead, they support tectonic association. The MAe misfit is around 12 mWm^{-2} , which is encouraging (Fig. 5.3b). We note, however, that heat flow datasets are affected by sample bias, particularly in Antarctica's Gondwanan neighbors. Heat flow measurements are often targeted on regions with particular economic interest, and might not well represent the average Antarctic continent. Records from mountainous areas are likely to be mostly from valleys rather than ridges, and hence higher heat flow due to topographic focusing (e.g., Beardsmore et al., 2001; Lees et al., 1910). Heat production and heat flow can vary over a large range in a short distance (Fig. S13). We therefore keep all individual records instead of cell or kernel averages. This might further skew the reference heat flow distribution.

5.5.2 Methodology Appraisal

We test the methodology using the example of the Australian continent, and achieve a generally good prediction (Fig. S18). However, a few locations show values where the calculated value is far too low. The most striking misfits are generally associated with areas known for high crustal heat production (Fig. S18b) (e.g., Holgate et al., 2010; McLaren et al., 2003), and those measurements are indeed targeted on geothermal energy or mineral exploration with an interest in enriched radioactive elements. The Australian example suggest that our method captures important properties of the crust, but observables used might fail to assign an extreme value associated with shallow high heat production. The resulting ambiguity with observables used, manifests as increasing noise, uncertainty and information entropy. The cross-correlation suggests agreement with the parameter choices made in previous studies (Goutorbe et al., 2011; Lucazeau, 2019), but high value of K and Ψ create an over-fitted prediction with the observables used. We aim to avoid over-fitting by choosing parameters in a range with low sensitivity for

parameter values (Fig. 5.3a–b).

Heat flow measurements in NGHF, we assume, do not represent all tectonic settings equally. By using the exponential function controlled by the K parameter, however, only a few measurements will define the heat flow distribution from similar locations. The results depend on the accuracy resulting from the combination of observables used, and the quality and selection of heat flow records. Using different subsets of heat flow values can modify the resulting map, e.g. without the distance to volcano observable (Fig. S14a–b), without the Moho depth and LAB depth observables (Fig. S14c–d), and excluding all measurements deeper than 250 m, which yields lower calculated values in the Thwaites region (Fig. S14e–f).

5.5.3 Discussion of Uncertainties

We aim to communicate the uncertainties inherent in Aq1 in a way that is informative of the different mechanisms through which uncertainty arises. For example, mapped uncertainty measures often fail to contain the progression of uncertainty from assumptions (e.g., Pérez-Díaz et al., 2020). Our first uncertainty metric is the standard deviation of reference heat flow records weighted with similarity (Fig. 5.4a). This distribution does not account for the total range of choices made when including observables, acceptance ranges for similarity and weighting, or absent observables as heat production and sediment cover. Therefore, we also provide maps of total number of similarities, and information entropy (Shannon, 1948). The number of similarities map (Fig. 5.4b), indicates how well the tectonic setting is represented in the heat flow catalog, and how much data are available in Antarctica. In this map, e.g. the Gamburtsev Subglacial Mountains stand out as a region with few similarities elsewhere. Figure 5.4c shows how much information is captured by the similarity process. A few areas, such as the northern Antarctic Peninsula, Ellsworth Land and west of Miller Range are shown to be very robust in our model. We believe that the inclusion of information entropy as a proxy for uncertainty is a useful tool in geophysical and geological studies, particularly in multivariate and multidimensional models (e.g., Wellmann et al., 2012). In our map, the information entropy metric also captures multi modal distributions, and a low entropy value enables the reduction of apparently large uncertainty to a few discrete possibilities.

5.5.4 Interpretation

Aq1 improves the information available to the geological community by supplying a heat flow map that is of higher resolution than previous studies. The exact resolution is difficult to quantify, as each observable contributes different levels of detail. The resolution of the datasets used in previous studies (An et al., 2015b; Martos et al., 2017) is improved upon somewhat, in Aq1, through the addition of constraints from the higher resolution elevation model and airborne Bouguer anomalies. It also provides a quantified means of incorporating information through the match between reference and target observables that inform the contribution to heat flow from the probable subglacial geology. Aq1 agrees with previous studies in suggesting generally higher heat flow in West Antarctica, and lower in East Antarctica. This is also in accordance with our understanding of the tectonic development of the continent (e.g., Artemieva et al., 2020; Boger, 2011; Harley et al., 2013; Jordan et al., 2020), and large scale geophysics (e.g., Haeger et al., 2019). Our map adds detail to this relationship by suggesting a few pronounced

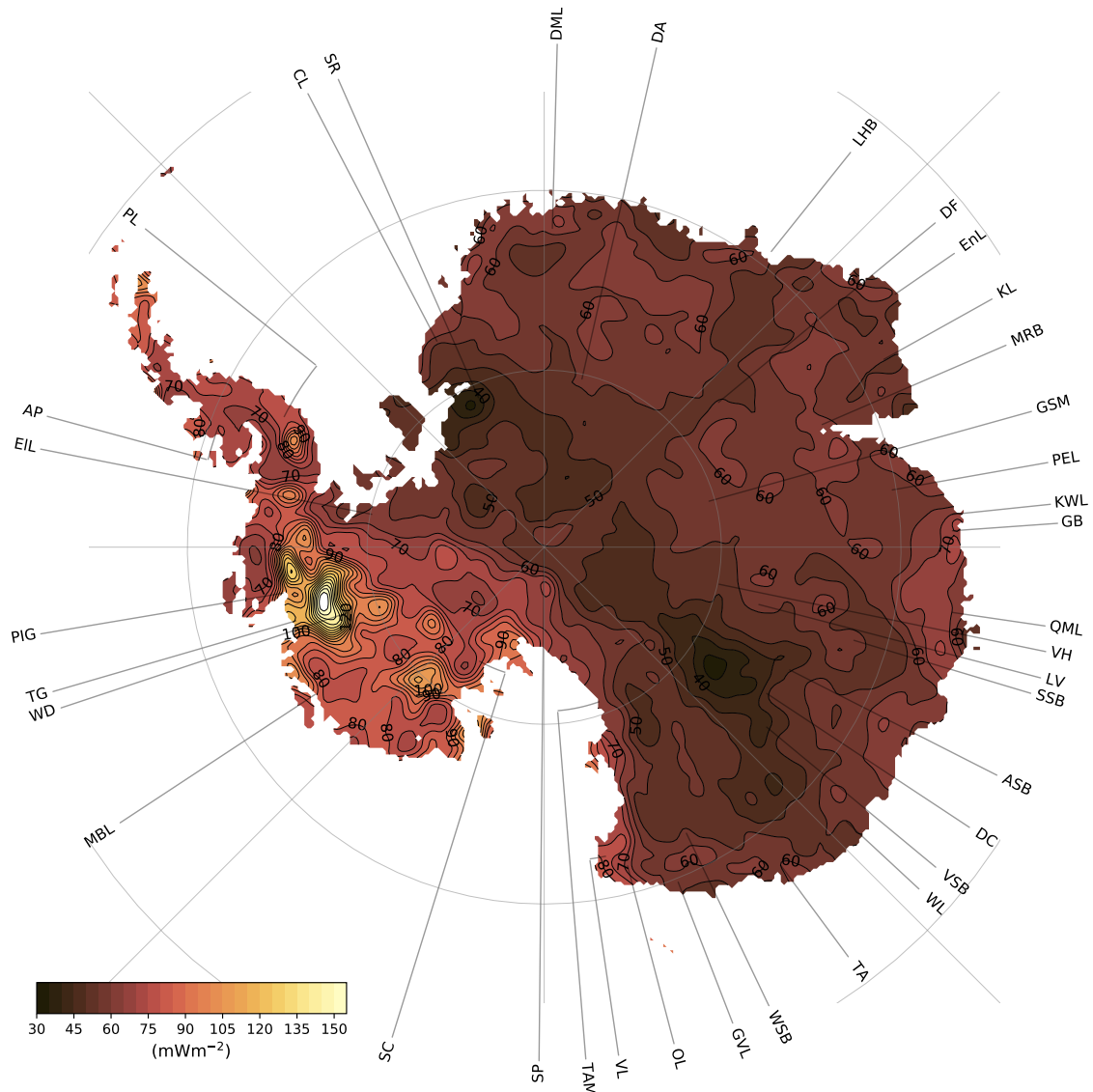


Figure 5.6: Locations mentioned in text, and an alternative visualization of Aq1. Heat flow is shown as smoothed contours to enable reading of numerical values, although some detail is lost. Smoothing is carried out using a Gaussian kernel with $\sigma = 40$ km. Geographic locations mentioned in text: AP = Antarctic Peninsula, ASB = Aurora Subglacial Basin, CL = Coats Land, DA = Dome Argus, DC = Dome Circle, DF = Dome Fuji, DML = Dronning Maud Land, EIL = Ellsworth Land, EnL = Enderby Land, GB = Gaussberg, GSM = Gamburtsev Subglacial Mountains, GVL = George V Land, KL = Kemp Land, KWL = Kaiser Wilhelm II Land, LHB = Lützow-Holm Bay, LV = Lake Vostok, MBL = Marie Byrd Land, MRB = Mac. Robertson Land, OL = Oates Land, PEL = Princess Elizabeth Land, PIG = Pine Island Glacier, PL = Palmer Land, QML = Queen Mary Land, SC = Siple Coast, SP = South Pole, SSB = Schmidt Subglacial Basin, SR = Shackleton Range, TA = Terre Adélie, TAM = Transantarctic Mountains, TG = Thwaites Glacier, VH = Vostok Highlands, VL = Victoria Land, VSB = Vincennes Subglacial Basin, WD = West Antarctic Ice Sheet (WAIS) divide, WL = Wilkes Land, WSB = Wilkes Subglacial Basin.

hot spots in East Antarctica, and also areas with moderate heat flow in parts of West Antarctica (Fig. 5.6). The highest values are computed for the interior of Thwaites Glacier and Pine Island Glacier. The region is categorized by thin crust (e.g., Damiani et al., 2014), steep geothermal gradient (e.g., O'Donnell et al., 2019), and a complex tectonic setting that is under current discussion (Artemieva et al., 2020; Ferraccioli et al., 2007; Jordan et al., 2020). Our values are locally higher than previous continental scale heat flow studies (Fig. 5.5), and in accordance with observations from radar sounding of the ice-bedrock interface (Schroeder et al., 2014) and field measurements (e.g., Clow et al., 2014), however, the uncertainties remain large. Aside from Thwaites Glacier region, the Aq1 model does not show any extended regions of heat flow over 100 mWm^{-2} (Fig. S20d).

We note that Aq1 is most similar to Shen et al. (2020), and we take this similarity as a strong evidence to support the validity of both Aq1 and Shen et al. (2020), as they are effectively independent studies. Shen et al. (2020) is not derived from the datasets used for Aq1, and a different approach is used. In particular, there is a convincing similarity between the two models in the overall pattern in West Antarctica (Fig. 5.5e), however Aq1 assigns higher values in the Thwaites region and northern Siple Coast (Fig. 5.5e).

Elevated heat, over 70 mWm^{-2} , is detected in East Antarctica, e.g. in interior Queen Mary Land, near the Gaussberg Volcano (Fig. 5.6). Due to the lack of geophysical data, the Gaussberg volcano is still poorly understood, but its recent volcanism has potential clues to the heat flow of an extended region. However, we note that even if distance to volcanoes observable is excluded (Figs. S14a–b), the model still renders an elevated heat flow in the Gaussberg region. The low heat flow values from the Wilkes Subglacial Basin and inland from Wilkes Land, and to some extent Aurora Subglacial Basin and Vincennes Subglacial Basin might be a result of sediments with low thermal conductivity (Jessop et al., 1994), or low heat production in underlying cratonic crystalline basement (Stål et al., 2020c).

Aq1 suggests a relatively moderate heat flow in central Siple Coast. Values based on direct measurements in the region gives a large range of heat flow values. This variance is likely caused by a number of local subglacial processes such as hydrothermal circulation and potentially volcanism with a very large impact the measured heat (Begeman et al., 2017; Engelhardt, 2004; Siegert et al., 2016; Tulaczyk et al., 2001). Such high values are not captured at this scale given the resolution of the available observables, and we don't expect to see extremely high values when averaged over a 400 km^2 grid cell. Sedimentary basins might also hamper the heat flow due to the lower thermal conductivity and groundwater circulation (Jessop et al., 1994).

Due to the low number of heat flow measurements in Antarctica, the high variability of heat flow, and the assumptions involved (Discussed by e.g. Burton-Johnson et al., 2020; Mony et al., 2020), we suggest that a direct comparison is not meaningful for a continental scale map. However, Aq1 still agrees well with the existing measurements compiled by Burton-Johnson et al. (2020) (Fig. S21).

5.5.5 Future Directions

The Aq1 model, released as the central product in this contribution, is a suitable input to ice sheet models and other interdisciplinary studies of interacting Earth systems in Antarctica.

However, some parts of the model show large uncertainties that should be reduced in future work. Additional datasets and data products for possible inclusion in updates include those from recent seismic studies (Lloyd et al., 2020; Shen et al., 2018a). With additional magnetic data, further derivatives could be included to assist in higher resolution tectonic association, as has been achieved in regional studies (e.g., Ferraccioli et al., 2001; Goodge et al., 2010; Ruppel et al., 2018).

Comparison with heat flow models based on solid Earth data potentially provide further constraints on the nature of the subglacial environment. Additional constraints from observed geology, and thickness and nature of subglacial sediments are further datasets of potential utility that could be included in a probabilistic framework, in the absence of well-distributed direct observations. For the next generation of Antarctic heat flow models, it may be appropriate to include data from the ice sheet community in a truly interdisciplinary initiative. The existence of subglacial melt, hydrological information, and insights from the dynamics of the ice sheet are candidate datasets for inclusion.

For some regions, the model could be refined with a topographic correction (e.g., Beardsmore et al., 2001; Lees et al., 1910), which would require additional consideration for interpolation of the roughness of subglacial topography data (Graham et al., 2017). Related to considerations of topography, the exhumation and erosion history of Antarctica has a considerable impact on subglacial heat flow and merits inclusion in future work. Our understanding of such processes has developed over the past decade (e.g., Paxman et al., 2019b; Tooze et al., 2020; Wilson et al., 2012). A recent marine seismic interpretation (Sauermilch et al., 2019) shows large volumes of offshore sediments. Considering those results may enable better constrained models of regional erosion and exhumation, with further impact on heat flow.

We hope that Aq1 will be used to provide clues on subglacial tectonic settings, and also used by the interdisciplinary community working on interactions and feedbacks of the cryosphere and solid-Earth systems. We anticipate that ice sheet evolution models will continue to be refined in response to updated heat flow maps. Adopting updatable models, such as Aq1, will readily enable the improvement of results that make use of heat flow as a model input.

5.6 Conclusion

The new geothermal heat flow model, Aq1, is based on a new approach to the estimation of subglacial heat flow for Antarctica. We use a multivariate analysis, modified to take account of the strengths and limitations of currently available geophysical and geological datasets for Antarctica. This analysis complements the univariate techniques that underpin alternative heat flow maps for the continent. The resulting maps depend on a robust number of observables and enable constraints to be included from comparative records of heat flow and tectonic setting, elsewhere in the world. The Aq1 model is supplied together with an open computational framework to facilitate future refinements as new datasets become available. In agreement with models constrained by univariate approaches, Aq1 shows elevated heat flow in West Antarctica, low heat flow values in East Antarctica, and refined heat flow estimates throughout. Highest values are shown in Thwaites Glacier. Moderate heat flow is suggested for Siple Coast and Ellsworth Land, West Antarctica. Elevated heat values are modeled for some areas of East Antarctica, for example the region near Gaussberg in Kaiser Wilhelm II Land, Queen Mary

Land, and northern Victoria Land. Aq1 provides higher resolution compared with previous models, and robust uncertainty metrics.

5.7 Acknowledgments

The Aq1 model is available in interoperable formats (geoTIFF, netCDF and comma-separated values (CSV) text file) in 20 km and 50 km resolution grids from PANGAEA data library (<https://doi.org/10.1594/PANGAEA.924857>) (Stål et al., 2020e). Python code used to generate the maps in this study is available from online repositories (latest version at <https://github.com/TobbeTripitaka/Aq1>, archived at <https://zenodo.org/record/4014430>). Details regarding data and code download are provided with the Supporting Information. The software and data framework is described in detail by Stål et al. (2020a,c).

This research is a contribution to the SCAR SERCE program. We are grateful to Rebecca Carey, Felicity McCormack, Steven Phipps, and Ross Turner for valuable discussions and feedback. We also wish to thank the two anonymous reviewers, that substantially contributed to this study. This research was supported under Australian Research Council's Special Research Initiative for Antarctic Gateway Partnership (Project ID SR140300001). The authors declare that they have no conflict of interest.

Chapter 6

Synthesis

In this thesis, I have proposed a way forward using multivariate and probabilistic methods to gain refined understanding of the lithosphere of Antarctica. In this chapter, the outcomes of the research are reviewed and contextualised. Ongoing directions of research are also noted to provide a broad picture of the tectonic and interdisciplinary lines of inquiry that have been enabled through the computing environment and novel applications of the introduced multivariate probabilistic methodology.

6.1 Gaining Value from Integrated Approaches

The motivation is strong to understand the tectonic evolution of Antarctica, given 1) the position of East Antarctica at the hub of the break-up of Gondwana and its poorly understood role in older supercontinents, and 2) interdisciplinary studies of solid Earth and cryosphere interactions and feedbacks that impact understanding of the response of ice sheets to global climate change (Ch. 1). Investigations to date have mostly comprised interpretations of univariate data; however, this thesis advocates that bringing multiple data types together is a well-posed approach, especially where they provide an independent constraint on the question being addressed.

Particularly, the tension between geological and geophysical observations have been discussed, explicitly or implicitly, throughout this thesis. The aim is to facilitate an understanding where the geological history and measurements of the resulting properties can be linked and jointly analysed. To do so, uncertainties must be included. Not only as probability distributions, however also as an appreciation and acceptance of human errors, sampling bias, and prejudices.

6.1.1 Enabling Computational Environment

Integrating datasets in different formats into one multidimensional framework is a challenging proposition. This is especially true for the mixed categorical and continuous data that are characteristic of geological and geophysical data, respectively. My solution was to develop an improved computational framework. The new Python package *agrid* provides efficient high-level scripting, and object-oriented organisation of the data and methods included (Fig. 6.1).

The open source code presented in Chapter 3a was subsequently used, and further developed throughout the work in this thesis. An updated version of *agrid* has been used to produce the boundary model in Chapter 4, and Aq1 in Chapter 5. New added features include integration with construction tool SCons (Knight, 2005), and streamlined data import and storage using the netCDF file format (Rew et al., 1990). Additional functionality, not explored in this thesis, is the possibility of adding further dimensions for geological time, including vectors of continental drift. Updated versions of *agrid* are made available from the Github repository (<https://github.com/TobbeTripitaka/agrid>) and are regularly archived on Zenodo (Stål, 2019a).

In Chapter 3b, a crustal segmentation from geophysics was merged with statistical outputs from geochronological databases, and extrapolations from a schematic geology map. The functionality of the model is demonstrated by providing a number of outputs of utility for research discussion. Of particular use is the steady-state heat flow model, AqSS, that provides a baseline map (i.e., with no neotectonic component) and is the first Antarctic continental-scale heat flow model that includes a segmented crust, beyond an applied East-West Antarctic divide (as by, e.g., Martos et al., 2017).

An important aspect of the computational framework is to enable reproducibility, so that results can be tested, and improved upon in future work. The efforts to facilitate reproducibility in geophysics follows a long tradition (e.g., Claerbout et al., 1992; Fomel, 2015). When reducing the 3D dynamic structure of the Earth to a regular grid, decisions made e.g. the resolution of the grid, and the interpolation scheme used, can impact the model output. Using a suitable projection, ensure that interpolation and assignment across the pole is treated correctly, however global data points, including interpolation across the dateline, can at this point only be solved by padding of the grid, repeating the data from the other hemisphere. A strength of the presented computational framework is that such impacts can be tested and results can be refined or corrected.

6.1.2 Reconciling Results from Univariate Approaches

The challenges that arise from interpretations of the geological history and properties of the Antarctic interior (Ch. 2), have been addressed by using a probabilistic approach that takes the spatial uncertainty and likelihood as parameters. In Chapter 4, we presented a new type of map, showing the likelihood of the location of tectonic boundaries. The boundary model is one of the first tectonic segmentation maps for Antarctica, and introduces a novel methodology that provides a new form of insight into deep lithospheric structures. Such maps offer an alternative to crisp lines and, moreover, provide additional and informative metrics of uncertainty and probability, as noted in following sections. The new models can either form a standalone probabilistic appraisal or enable the differences in the results from univariate approaches to be interpreted in terms of the insight that they bring. This comparison enables apparently conflicting results to be compared, and either reconciled or cautions offered.

Fuzzy logic approaches were implicitly used in the algorithm for Chapter 4, and provided a sensible starting point for subsequently adapting the similarity workflow in Chapter 5, and in future work introduced below. Figure 6.2 gives an illustrative example of how fuzzy boundary models relate to well founded crisp lines (Supplement to Ch. 4). In this example, Australia has

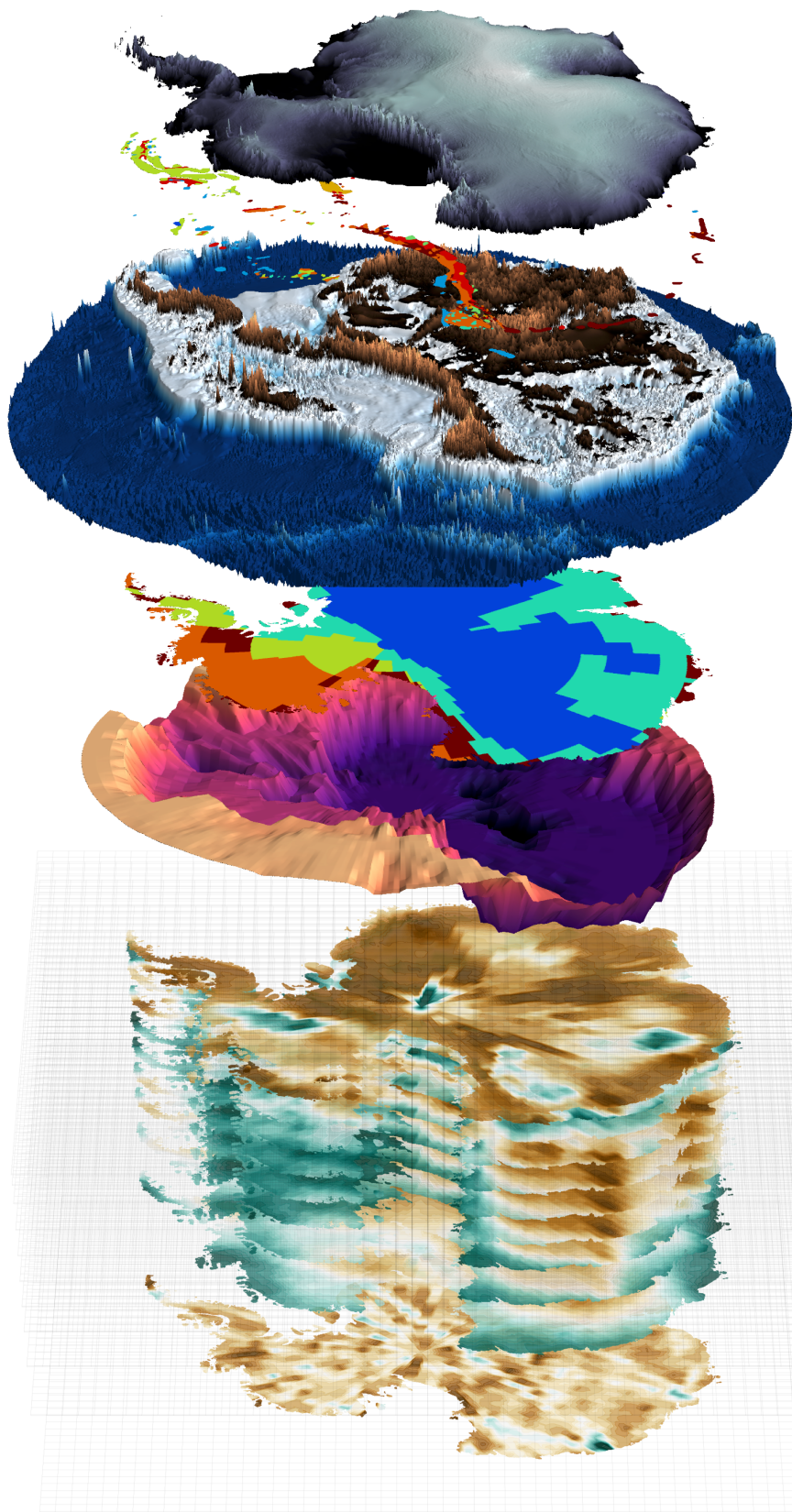


Figure 6.1: The newly developed software, *agrid*, is designed to contain multiple datasets, produced in various resolution, dimensionality, and extent. Here, illustrated, from top to bottom, with surface elevation (Fretwell et al., 2012), schematic geology (Tingey et al., 1991), subglacial elevation (Fretwell et al., 2012), crustal segmentation (Schaeffer et al., 2015), Moho depth and seismic wave speed (An et al., 2015a). Figure modified from (Stål et al., 2019b).

been interpreted in the same way as Antarctica, using similar datasets. The intersect model is shown with an overlay of boundaries from a study that is based on geological observations and airborne geophysics (Shaw et al., 1996). The underlying likelihood map provides a context for the firm interpretations implied by the drawn lines. Some tectonic boundaries in Australia are well known from geological observations and shallow geophysics, however, not captured with the methodology introduced in Chapter 4. In this situation, the more noisy versions, including any observation that might suggest deep boundaries, is useful as they suggest the smallest probable tectonic regions. In future work with a crustal focus, other datasets could be used to look for similarities to join such fuzzy polygons.

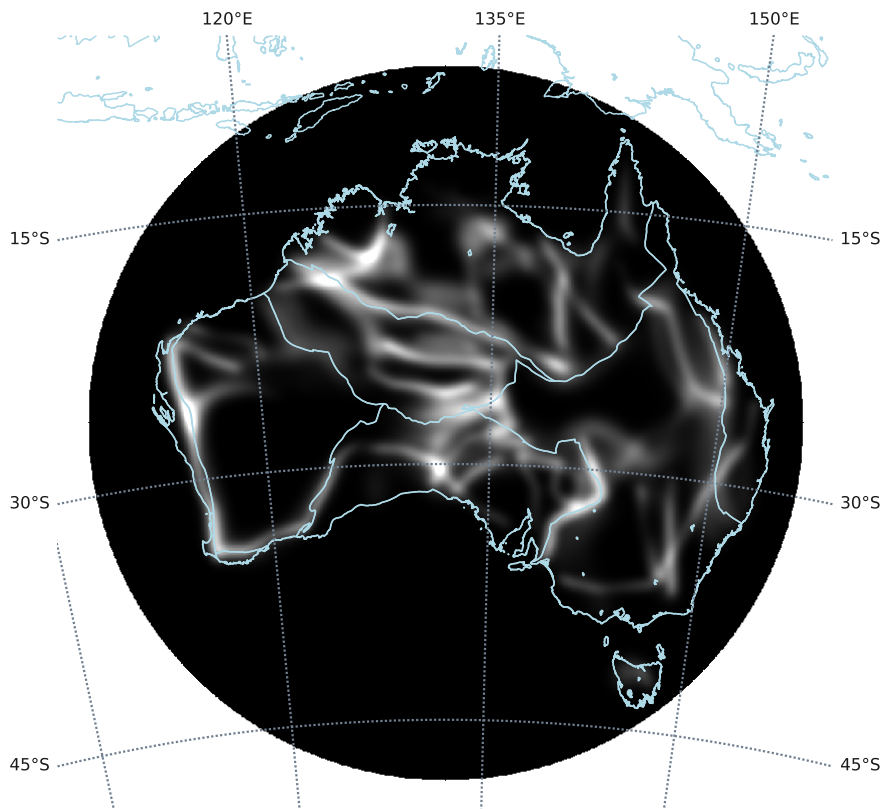


Figure 6.2: Boundary model (Ch. 4) applied to Australia, using similar datasets as for Antarctica. Cyan lines are crustal boundaries from Shaw et al. (1996) (Intersect model, as included in the supplementary material for Stål et al., 2019c).

6.1.3 Using Uncertainty to Advantage

Conventional geological interpretations and models involve an implicit selection from a range of possible interpretations. When working in Antarctica, or any region with low data density, the main benefit from such models have been that they provided a source of reference for constructive debate. In bringing the distribution of possibilities to the fore all options are preserved, and with additional data, the range of relevant choices can be narrowed (Bayes, 1763). Uncertainty becomes an advantage, as it allows interpretation of the data on its own merit. The uncertainty has variation in space, and from this distribution, we are in a better position to extract knowledge for sensible interpretation from the results. By mapping uncertainty, we

can better target future research, for example by informing logistic planning for research with optimal impact.

If the datasets used in Chapter 4 had been interpreted to extract sharp boundaries, the three inputs would rarely, if ever, agree. The resolution limits how accurately a transition can be picked. Uncertainty may be regarded as a measure of accuracy and precision of the final product. In some aspects, information entropy is a strong metric (e.g., Kuhn et al., 2016), particularly when combined with the distribution's fundamental measures, standard deviation, and potentially population or sample size (Ch. 5). The discussion derived from the entropy estimate of A_{q1} is a good example. From the binned distribution of similar locations for heat flow measurements, a few distinct and discrete possible interpretations can be extracted. The entropy map provides a good starting point for targeting new research activity or data collection to most effectively reduce the uncertainty. Compound metrics of a model, as relative robustness shown in Figure 6.5b, also provide insight for model appraisal. The interdisciplinary community, particularly ice sheet modellers, are now better positioned to take advantage of uncertainty metrics to test the range of heat flow values and to locate regions where the provided estimates of geothermal heat flow are robust. The statistical approach, calls for further investigation of what we can learn from global geothermal heat data, and for example investigate sample bias and other skew of reference distribution.

In the supplementary material for Chapters 4 and 5, I show an Australian application of used methods. Those tests provide a first order appraisal of the methodology, and particularly highlights the shortcomings. The results are encouraging, however, there is a risk of over-fitting to Australian results, and hence extrapolation of Australian lithospheric properties to Antarctica. Hence, parameters and methods have not been selected based on particularly Australian results, but instead from global compilations.

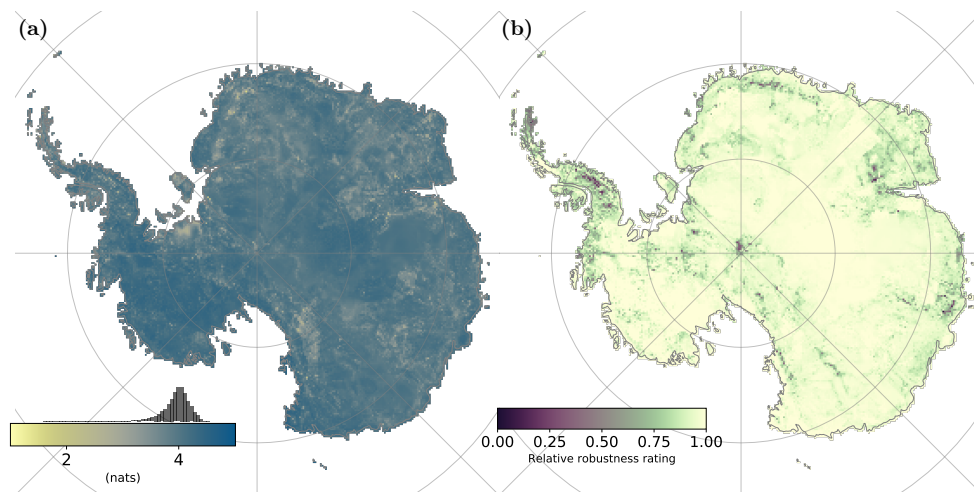


Figure 6.3: (a) Information entropy in the natural unit of information (nat), and (b) a unitless measure of robustness from Ch. 5 and supplementary material.

6.1.4 Robust Results from Well-Posed Constraints

Fitzsimons (2003) and Harley et al. (2013) highlighted the numerous possible interpretations of the crustal structure of the Antarctic interior. With the multivariate and probabilistic contribution presented in Chapter 4, we provided a robust way forward. We infer from the combined observations of independent datasets, that the subglacial interior of Antarctica is heterogeneous and complex. The concept of a large continuous East Antarctic shield has been progressed to reveal, with mapped likelihood, a lithosphere divided into distinct domains. These domains have variable characteristics, with some showing likely subdivisions and others appearing to be homogeneous blocks. There is now the opportunity to link these domains into new plate models, developing previous work that links the tectonic elements of East Antarctica (Merdith et al., 2017). This research has advanced the SCAR Horizon Scan priority science questions noted in Chapter 1 by addressing the question about the supercontinent assembly (Question No. 35), and also indirectly Questions No. 37 and 40, regarding glacial isostatic adjustment.

Disparities between previously published heat flow models derived from univariate data were addressed in Chapters 3b and 5, and in recent publications (e.g., Burton-Johnson et al., 2020; Lösing et al., 2020). Aq1 exemplifies a new paradigm of multivariate heatflow models for Antarctica (Ch. 5). Notably, the very same datasets that have been used in previous studies are also included to generate Aq1; however, the data are here used to guide interpretation of tectonic and geological setting, rather than a forward model. We compared heat flow values and observables in other continents, and found, for example, no correlation with Curie temperature depth. At the very core, we raised concerns about whether the assumption regarding the depth to Curie temperature isotherm even holds as a concept for continental crust. However, Curie temperature depth has a validity for tectonic affiliation, and in oceanic crust there is some degree of observed correlation (Li et al., 2017). Notably, Aq1 reproduces the heat flow evidences from radar observations of the Thwaites Glacier (Schroeder et al., 2014). Other studies have also suggested high heat flow levels in West Antarctica, however, not with the spatial resolution of Aq1. This research has also progressed priority science questions No. 27 and 38 in the SCAR Horizon Scan (Chapter 1), regarding ice and solid Earth interaction.

6.1.5 Probabilistic Approaches for Antarctica

In this thesis, I have provided examples of results that have not previously been represented with probability or likelihood distribution in Antarctica, such as the existence and location of tectonic boundaries, or the similarity of the tectonic setting for an estimate of geothermal heat flow. The here presented integrated approaches are aimed to incorporate multiple types of available data (Chapter 3b). In Chapter 4, we noted the good match between the probabilistic intersect model and the independently observed geology. Such results could not have been possible without a degree of freedom to allow the interpretation to vary, and a well-defined uncertainty range. The concept of treating the uncertainty as a manifestation of data is also presented in Chapter 5. We allowed the similarity to decay gradually with decreasing agreement between a target and reference observable.

The experiences from Chapter 4, and particularly the Australian test case (Fig. 6.2, and Appendix B) suggest that with the used observables, some expected deep boundaries are not

detected, particularly crossing Proterozoic orogens. Also, Phanerozoic domains appears to be difficult to detect, however, this is partly explained by the datasets used. With datasets more sensitive to shallower and crustal variations, a better representation of younger domains should be expected.

In this work, every dataset is not expected to capture all aspects of the lithosphere. Metamorphic belts of very different age might manifest similar elastic properties in seismic tomography, and distinctly different geochronology. Two geologic observations might suggest the same origin, but geophysical data may reveal structural discontinuities. Combining datasets allows us to triangulate interpretations to reduce the degrees of freedom, and hence the information entropy in our model (Shannon, 1948). This was illustrated in the uncertainty metrics for Chapter 5 that provide a means of directing new data collection and updated compilations in the future.

6.2 Progress in Parallel

Recent related multivariate work in Antarctic Earth Sciences, carried out in parallel with the research described in this thesis, similarly acknowledges the complexity of the lithosphere, and the need for interdisciplinary understanding. Pappa et al. (2019a) discuss the differences in Antarctic Moho depth and combine regional receiver function studies with gravity field modelling and isostasy. Disagreements between earlier models (An et al., 2015a; Baranov et al., 2018) might be partly explained by a low density contrast at the Moho in East Antarctica. The study by Pappa et al. (2019a) points out that tectonic understanding is required to solve the debate. As in the results arising from seismic and magnetic constraints compared in Chapter 3b (supplementary material), the difference between the results are just as informative as the individual outputs. Haeger et al. (2019) combines geophysical data with mineral physics constraints to refine temperature estimates from seismic studies. They analyse the tomographic models from An et al. (2015a) and Schaeffer et al. (2013) and find that with compositional variations incorporated, the modelled temperature in depleted areas increase up to 150 C°. Pappa et al. (2019b) analysed gravity data, and constructed a 3D model of density, temperature, and viscosity. The results suggest that most of Antarctica is in isostatic equilibrium, however, some areas might differ. A recent global lithosphere model by Afonso et al. (2019) is also derived from seismic and gravity data, and refined Moho depths from interpolated seismic measurements with uncertainty ranges are presented by Szwillus et al. (2019).

Seismic studies focused on large regions of Antarctica have made significant progress in understanding the lithospheric structure (e.g., O'Donnell et al., 2019; Ramirez et al., 2017; Shen et al., 2018b). Insights from those studies provide us a new opportunity to reconsider the assumptions of the tectonic architecture of Antarctica. Lloyd et al. (2020) generated a continental-scale full waveform tomography model of the upper mantle, using data from over 300 seismic stations. The method used is more sensitive to slow anomalies than earlier models. Localised perturbations are imaged in Lambert Graben, Marie Byrd Land, and Amundsen Sea Coast. Regional anomalies are associated with Cenozoic extension and volcanism from Balleny Islands to the Ross Embayment. However, seismometers are still sparse in large areas of East Antarctica, particularly Wilkes Land. Lloyd et al. (2020) also refines our understanding of the Transantarctic Mountains and confirms an interrupted structure beneath, as I suggested in

Chapter 4. Results from this study can refine segmentation maps of East Antarctica, taking advantage of the methodology suggested in Chapter 4. The recent heatflow map (Shen et al., 2020), that is generated from Lloyd et al. (2020) and Shen et al. (2018a) generally agrees with the here presented Aq1. The converging values constrain our understanding, compared to previous studies.

Additional types of data also have the potential to refine the understating of the 3D structure of the Antarctic lithosphere. Important insights to detect faults or the presence of fluids and melt, can be inferred from, for example, magnetotellurics (e.g., Peacock et al., 2016). Wannamaker et al. (2017) measured a transect of the southern Transantarctic Mountains to suggest a flexural, rather than thermal mechanism of regional uplift. Further, potential applications include improved estimates of mantle viscosity, the presence of volcanism, and detailed studies of the solid Earth and cryosphere interface (Hill, 2020; Selway et al., 2020). Findings could be incorporated with seismic and potential field results, building from the probabilistic methods presented in this thesis.

6.3 Ongoing Work

Ongoing work, building on the work presented in this thesis in the immediate future, will continue to progress the understanding of tectonic structure in a probabilistic frame, and will also provide regional geological and geothermal heat flow maps.

6.3.1 A Probabilistic Approach to Basement Geology

Building from the methodology introduced in Chapter 4, a crustal approach, including additional and updated datasets of crustal properties, including airborne magnetic data, regional seismic studies, plate reconstruction, and geological observations, will be generated. Chapter 4 also points towards a subsequent application where the properties of areas, or rather stochastic volumes, enclosed by the boundary distributions are analysed. This suggestion requires some additional theoretical method development. A theoretical framework to treat such enclosures are the fuzzy sets (Zadeh, 1965), applied as spatial objects. This methodology has been applied in Figures 6.4 and 6.5. Associating the fuzzy sets to a property requires further statistical analysis, and can be achieved by linking the sets to geological classes from global maps. Using a similarity approach, as refined in Chapter 5, the mode class for each fuzzy set is identified, the order of similarity to other classes is also meaningful, and the information entropy of the discrete distribution, weighted by the membership function, provides a potential function for appraisal and optimisation. Parameters to optimise includes the weight of each dataset used for the boundary model, scaling of resolution, and certainty. This workflow is related to that used in Chapter 5.

6.3.2 Regional Studies

The multivariate methods are also applicable on a regional scale, and are particularly useful in areas where few constraints are available. In the spirit of the methods used in Chapter 4 to assess likely boundaries relating to lithospheric segmentation, magnetic data could be included

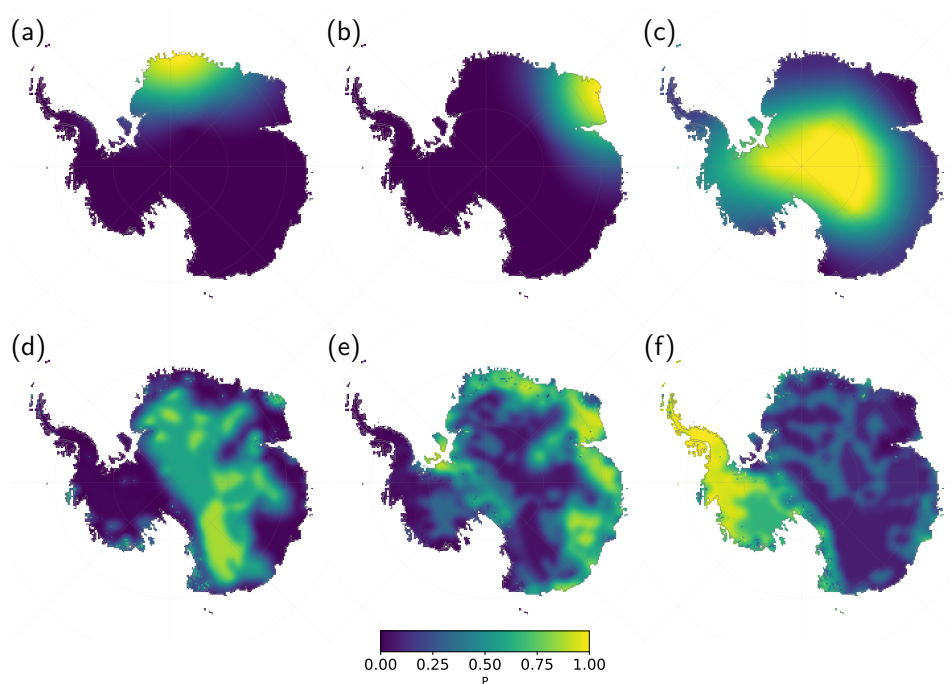


Figure 6.4: Spatial fuzzy sets on a continental scale. Upper row: (a) Likelihood of African affinity. (b) Likelihood of Indian affinity. (c) Likelihood of an unknown affinity. Lower row: (d) Likelihood for Archean crust, (e) Likelihood of Proterozoic crust, (f) Likelihood of Phanerozoic crust. Research introduced by Stål et al. (2019a).

in studies of crustal segmentation, including the analyst appraisal of accuracy and precision of constraints from all input datasets.

One further target of immediate interest is the Aurora Subglacial Basin. This region is of particular interest for ice sheet modellers due to its low topography and the potential impact of the ice contained within the basin on global sea-level rise. Its geology is unknown, and tectonic affiliations are debated. Ongoing work brings together the toolbox presented in Chapter 3, the fuzzy sets discussed here, linked to a boundary model as presented in Chapter 4, and an extended similarity detection, as constructed in Chapter 5. Multivariate, probabilistic approaches allow us to include the few existing geological observations, and observations from glacial erratics and marine cores to constrain the geology of the interior. Figure 6.5 shows a spatial probability distribution for unconsolidated sediments for the Aurora Subglacial Basin.

As with the continental-scale studies, all regional-scale ongoing work is being carried out using software and workflows that allow for rapid updating as new datasets become available, and output of uncertainty metrics to accompany the published research products provided to the interdisciplinary research community.

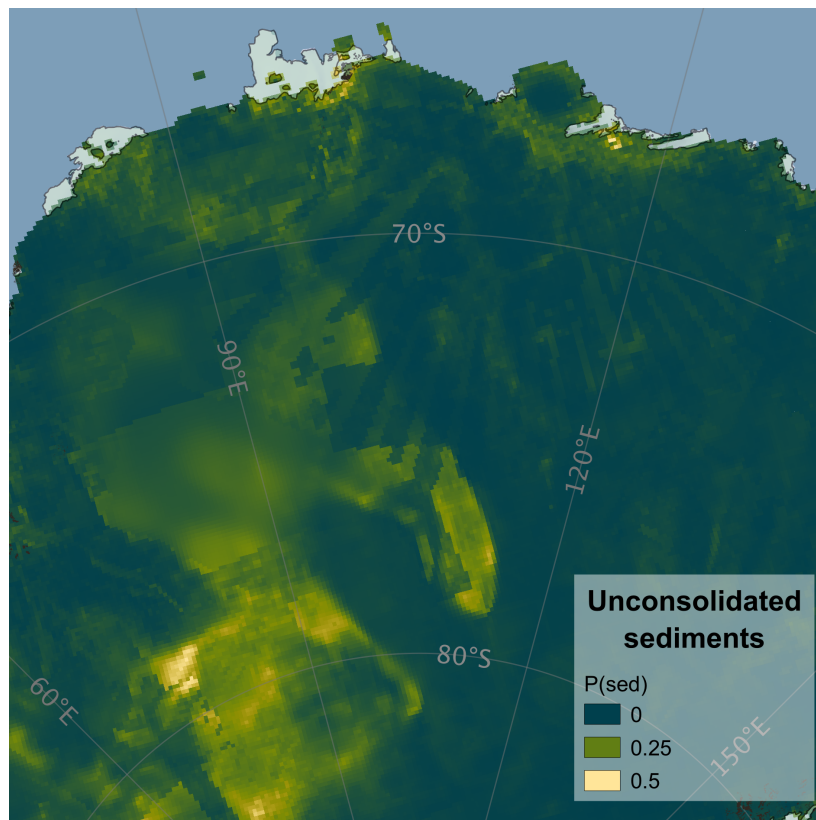


Figure 6.5: Aurora Subglacial Basin, preliminary result from ongoing work. Map showing probability of unconsolidated sediments using a naive Bayesian similarity detection. Producing the probabilistic model is facilitated by software presented in Chapter 3a. The multivariate compilation provided in Chapter 3b is used as input to a probabilistic domain model, derived from Chapter 4. Assigning likely parameters for each fuzzy polygon is done through the developed similarity detection approach, as introduced in Chapter 5. Figure from (Stål et al., 2020b, in prep.).

Chapter 7

Conclusion

In this thesis, it has been shown how multivariate methods, including those which combine geophysical and geological data, enabled by modern computational tools can advance our understanding of the Antarctic continent. The thesis has also presented data products for the interdisciplinary community to facilitate the integration of results from solid Earth research, such as inputs to ice sheet models.

I reviewed existing studies and found that recent compilations of geophysical data, plate reconstructions, geochronological data, and geological compilations and maps, represent significant progress, yet large uncertainties remain regarding the lithospheric structure in the Antarctic interior. This situation existed in parallel with calls from the interdisciplinary Antarctic research community for better constraints for the physical properties of the Antarctic interior: such as, lithospheric segmentation and heat flow. I proposed a multivariate approach, with the possible use of probabilistic methods, for large-scale geological mapping, including a better understanding of crustal properties.

To facilitate the new research, a new computational framework was developed and used to generate a model of the Antarctic crust and upper mantle, using a broad range of published datasets. By combining multiple sources, I produced a complex continental-scale 3D model of Antarctica. This framework was also used to generate a steady-state heat flow map, AqSS, and an isostasy model from seismic boundaries. I also advanced the discussion about the cause of discrepancies between existing heat flow models.

I generated probabilistic likelihood maps of domain boundaries within the lithospheric mantle, using a novel method. The method included accuracy and precision as properties of boundaries detected in input datasets. The range of combined distributions are a potentially useful tool for further refined crustal studies. The most conservative (product) likelihood map suggested nodes where we can be fairly certain about deep boundaries, and the likelihood map suggesting the most boundaries (sum) provides the minimal extent of lithospheric domains. The intersect likelihood map represents a middle way that gives a plausible, though blurry, map of major transitions in the deep Antarctic lithosphere. According to the correlation with observed geology, it also captures some important boundaries in the crust in East Antarctica. I found that parts of East Antarctica, such as Dronning Maud Land, contain a number of smaller domains, and that Wilkes Land contains larger lithospheric blocks. I also postulated the extent of the Mawson Craton and showed that the interior of East Antarctica is likely to

be similarly complex as other continents, and that some existing models of the East Antarctic lithosphere are likely to be oversimplified.

Using the computational framework, I also generated a new heat flow map of Antarctica, Aq1. The model is built from multiple observables using a similarity method, and also provides a well-defined uncertainty range. The existing methodology was expanded with a probabilistic similarity detection. I found that high heat flow is likely in Thwaites Glacier region and the Antarctic Peninsula. Elevated heat is also likely in Queen Mary Land, Victoria Land, and near the South Pole in East Antarctica. Low heat flow values are inferred in the Wilkes Subglacial Basin and Coats Land

In Chapter 4, stochastic boundaries replaced deterministic sharp borders. In Chapter 5 modelled values, and uncertainties were presented alongside the information entropy metric that is near to random noise in some locations. In chapter 6.3.2, I argued that fuzzy sets better represent our understanding of the Antarctic interior than crisp polygons. Spatial information entropy calculations are also suggested to capture and quantify our understanding of the the hidden crust and upper mantle. Such probabilistic methods provide a robust representation of our understanding of the Antarctic lithosphere. Forthcoming studies that build on the findings in this thesis include probabilistic mapping of subglacial geology and improved thermal modelling.

Antarctica remains the least known continent. I have shown, however, that the unknown interior of Antarctica is not homogeneous and featureless. I have also shown that, by drawing on more mature datasets from other continents, some information can be inferred for key properties in most locations. My thesis aimed to progress methodology and provide useful outputs for the interdisciplinary community. The aims are thus successfully addressed, and the research community may now picture this vast hidden landscape with some insight into its geological complexity. The new data outputs and tools enable us to understand the knowledge that we have, guided by a better understanding of uncertainties.



Photo: Tobias Stål.

Figure 7.1: Icebergs on Prydz Bay.

Bibliography

- Afonso, J. C., Salajegheh, F., Szwillus, W., Ebbing, J., Gaina, C. (2019). “A global reference model of the lithosphere and upper mantle from joint inversion and analysis of multiple data sets”. *Geophysical Journal International* 217.3, pp. 1602–1628. ISSN: 1365246X. DOI: 10.1093/gji/ggz094.
- Aitken, A. R., Betts, P. G., Young, D. A., Blankenship, D. D., Roberts, J. L., Siegert, M. J. (2016). “The Australo-Antarctic Columbia to Gondwana transition”. *Gondwana Research* 29.1, pp. 136–152. ISSN: 1342937X. DOI: 10.1016/j.gr.2014.10.019.
- Aitken, A. R., Young, D. A., Ferraccioli, F., Betts, P. G., Greenbaum, J. S., Richter, T. G., Roberts, J. L., Blankenship, D. D., Siegert, M. J. (2014). “The subglacial geology of Wilkes Land, East Antarctica”. *Geophysical Research Letters* 41.7, pp. 2390–2400. ISSN: 19448007. DOI: 10.1002/2014GL059405.
- Aki, K., Richards, P. G. (2002). *Quantitative Seismology, 2nd Ed.* University Science Books, 704pp. ISBN: 0-935702-96-2.
- Amalvict, M., Willis, P., Wöppelmann, G., Ivins, E. R., Bouin, M.-N. N., Testut, L., Hinderer, J. (2009). “Isostatic stability of the East Antarctic station Dumont d’Urville from long-term geodetic observations and geophysical models”. *Polar Research* 28.2, pp. 193–202. ISSN: 1751-8369. DOI: 10.1111/j.1751-8369.2008.00091.x.
- Amante, C., Eakins, B. (2009). “ETOPO1 1 Arc-Minute Global Relief Model”. *NOAA Technical Memorandum NESDIS NGDC* 24, p. 19. DOI: 10.7289/V5C8276M.
- Ammon, C. J., Randall, G. E., Zandt, G. (1990). “On the nonuniqueness of receiver function inversions”. *Journal of Geophysical Research* 95.B10, pp. 303–315. ISSN: 01480227. DOI: 10.1029/jb095ib10p15303.
- An, M. J., Shi, Y. L. (2007). “Three-dimensional thermal structure of the Chinese continental crust and upper mantle”. *Science in China, Series D: Earth Sciences* 50.10, pp. 1441–1451. ISSN: 10069313. DOI: 10.1007/s11430-007-0071-3.
- An, M. (2012). “A simple method for determining the spatial resolution of a general inverse problem”. *Geophysical Journal International* 191.2, pp. 849–864. ISSN: 0956540X. DOI: 10.1111/j.1365-246X.2012.05661.x.

- An, M., Wiens, D. A., Yue, Z. (2016). "A frozen collision belt beneath ice: an overview of seismic studies around the Gamburtsev Subglacial Mountains, East Antarctica". *Advances in Polar Science* 27.2, pp. 14–25. ISSN: 1674-9928. DOI: 10.13679/J.ADVPS.2016.2.00014.
- An, M., Wiens, D. A., Zhao, Y., Feng, M., Nyblade, A. A., Kanao, M., Li, Y., Maggi, A., L ev eque, J.-J. J. (2015a). "S-velocity model and inferred Moho topography beneath the Antarctic Plate from Rayleigh waves". *Journal of Geophysical Research: Solid Earth* 120.1, pp. 359–383. ISSN: 21699356. DOI: 10.1002/2014JB011332.
- An, M., Wiens, D. A., Zhao, Y., Feng, M., Nyblade, A., Kanao, M., Li, Y., Maggi, A., L ev eque, J. J. (2015b). "Temperature, lithosphere-asthenosphere boundary, and heat flux beneath the Antarctic Plate inferred from seismic velocities". *Journal of Geophysical Research: Solid Earth* 120.12, pp. 8720–8742. ISSN: 21699356. DOI: 10.1002/2015JB011917.
- Andersen, O. B., Knudsen, P., Berry, P. A. (2010). "The DNSC08GRA global marine gravity field from double retracked satellite altimetry". *Journal of Geodesy* 84.3, pp. 191–199. ISSN: 09497714. DOI: 10.1007/s00190-009-0355-9.
- Anderson, D. L. (1995). "Lithosphere, asthenosphere, and perisphere". *Reviews of Geophysics* 33.1, pp. 125–149. ISSN: 19449208. DOI: 10.1029/94RG02785.
- Artemieva, I. (2011). *The Lithosphere: An interdisciplinary approach*. Press, Cambridge University.
- Artemieva, I. M. (2006). "Global 1° x 1° thermal model TC1 for the continental lithosphere: Implications for lithosphere secular evolution". *Tectonophysics* 416.1-2, pp. 245–277. ISSN: 00401951. DOI: 10.1016/j.tecto.2005.11.022.
- Artemieva, I. M. (2009). "The continental lithosphere: Reconciling thermal, seismic, and petrologic data". *Lithos* 109.1-2, pp. 23–46. ISSN: 00244937. DOI: 10.1016/j.lithos.2008.09.015.
- Artemieva, I. M., Mooney, W. D. (2001). "Thermal thickness and evolution of Precambrian lithosphere: A global study". *Journal of Geophysical Research: Solid Earth* 106.B8, pp. 16387–16414. ISSN: 21699356. DOI: 10.1029/2000jb900439.
- Artemieva, I. M., Thybo, H. (2020). "Continent size revisited: Geophysical evidence for West Antarctica as a back-arc system". *Earth-Science Reviews* 202, p. 103106. ISSN: 00128252. DOI: 10.1016/j.earscirev.2020.103106.
- Ashby, F., Ennis, D. (2007). "Similarity measures". *Scholarpedia* 2.12, p. 4116. ISSN: 1941-6016. DOI: 10.4249/scholarpedia.4116.
- Australia, G. (2010). "Australian Crustal Elements". *AGSO Res. Newslett* 23, p. 162.

- Australia, G. (2017). “Digital Elevation Model DEM Shuttle radar Topography Mission SRTM 1 Second over Australian Bathymetry Topography WCS”. *Geoscience Australia*.
- Bacchin, M., Milligan, P., Tracey, R., Wynne, P. (2008). “Gravity Anomaly Map of Australia (Third Ed.), 1:5 000 000 scale”. *Geoscience Australia, Canberra*.
- Baranov, A., Morelli, A. (2013). “The Moho depth map of the Antarctica region”. *Tectonophysics* 609, pp. 299–313. ISSN: 00401951. DOI: 10.1016/j.tecto.2012.12.023.
- Baranov, A., Tenzer, R., Bagherbandi, M. (2018). “Combined Gravimetric–Seismic Crustal Model for Antarctica”. *Surveys in Geophysics* 39.1, pp. 23–56. ISSN: 15730956. DOI: 10.1007/s10712-017-9423-5.
- Barrell, J. (1914). “The Strength of the Earth’s Crust”. *The Journal of Geology* 22.4, pp. 289–314. ISSN: 0022-1376. DOI: 10.1086/622155.
- Bauer, W., Jacobs, J., Fanning, C. M., Schmidt, R. (2003). “Late mesoproterozoic arc and back-arc volcanism in the heimefrontfjella (East Antarctica) and implications for the palaeogeography at the Southeastern margin of the Kaapvaal-Grunehogna Craton”. *Gondwana Research* 6.3, pp. 449–465. ISSN: 1342937X. DOI: 10.1016/S1342-937X(05)70998-9.
- Bayes, T. (1763). *An essay towards solving a problem in the doctrine of chances*.
- Beardsmore, G. R., Cull, J. P. (2001). *Crustal Heat Flow*. Press, Cambridge University. ISBN: 0 521 79703 9. DOI: 10.1017/cbo9780511606021.
- Becker, T. W., Boschi, L. (2002). “A comparison of tomographic and geodynamic mantle models”. *Geochemistry, Geophysics, Geosystems* 3.1, n/a–n/a. ISSN: 15252027. DOI: 10.1029/2001GC000168.
- Begeman, C. B., Tulaczyk, S. M., Fisher, A. T. (2017). “Spatially Variable Geothermal Heat Flux in West Antarctica: Evidence and Implications”. *Geophysical Research Letters* 44.19, pp. 9823–9832. ISSN: 19448007. DOI: 10.1002/2017GL075579.
- Begg, G. C., Griffin, W. L., Natapov, L. M., O’Reilly, S. Y., Grand, S. P., O’Neill, C. J., Hronsky, J. M., Djomani, Y. P., Swain, C. J., Deen, T., Bowden, P. (2009). “The lithospheric architecture of Africa: Seismic tomography, mantle petrology, and tectonic evolution”. *Geosphere* 5.1, pp. 23–50. ISSN: 1553-040. DOI: 10.1130/GES00179.1.
- Bell, R. E., Small, C., Arko, R. A. (1999). “Development of a new generation gravity map of Antarctica: ADGRAV Antarctic Digital Gravity Synthesis”. *Annali di Geofisica* 42.2, pp. 261–264. ISSN: 03652556. DOI: 10.4401/ag-3720.
- Bentley, J. L. (1975). “Multidimensional Binary Search Trees Used for Associative Searching”. *Communications of the ACM* 18.9, pp. 509–517. ISSN: 15577317. DOI: 10.1145/361002.361007.

- Bergstra, J., Breuleux, O., Bastien, F., Lamblin, P., Pascanu, R., Desjardins, G., Turian, J., Warde-Farley, D., Bengio, Y. (2010). "Theano: a CPU and GPU Math Expression Compiler". *Proceedings of the Python for Scientific Computing Conference ({SciPy})*. Vol. 1. Scipy, pp. 1–7.
- Berndt, B. C., Brualdi, R. A. (1980). *Introductory Combinatorics*. Ed. by Pearson Education. Vol. 87. 6, p. 498. ISBN: 9780136020400. DOI: 10.2307/2320280.
- Betts, P. G., Armit, R. J., Stewart, J., Aitken, A. R., Ailleres, L., Donchak, P., Hutton, L., Withnall, I., Giles, D. (2016). "Australia and Nuna". *Geological Society Special Publication* 424.1, pp. 47–81. ISSN: 03058719. DOI: 10.1144/SP424.2.
- Betts, P. G., Giles, D., Lister, G. S., Frick, L. R. (2002). "Evolution of the Australian lithosphere". *Australian Journal of Earth Sciences* 49.4, pp. 661–695. ISSN: 08120099. DOI: 10.1046/j.1440-0952.2002.00948.x.
- Beyreuther, M., Barsch, R., Krischer, L., Megies, T., Behr, Y., Wassermann, J. (2010). "ObsPy: A python toolbox for seismology". *Seismological Research Letters* 81.3, pp. 530–533. ISSN: 08950695. DOI: 10.1785/gssr1.81.3.530.
- Block, A. E., Bell, R. E., Studinger, M. (2009). "Antarctic crustal thickness from satellite gravity: Implications for the Transantarctic and Gamburtsev Subglacial Mountains". *Earth and Planetary Science Letters* 288.1-2, pp. 194–203. ISSN: 0012821X. DOI: 10.1016/j.epsl.2009.09.022.
- Board, W. S., Frimmel, H. E., Armstrong, R. A. (2005). "Pan-African tectonism in the Western Maud Belt: P-T-t path for high-grade gneisses in the H.U. Sverdrupfjella, East Antarctica". *Journal of Petrology* 46.4, pp. 671–699. ISSN: 00223530. DOI: 10.1093/petrology/egh093.
- Boger, S. D., Miller, J. M. L. (2004). "Terminal suturing of Gondwana and the onset of the Ross-Delamerian Orogeny: The cause and effect of an Early Cambrian reconfiguration of plate motions". *Earth and Planetary Science Letters* 219.1-2, pp. 35–48. ISSN: 0012821X. DOI: 10.1016/S0012-821X(03)00692-7.
- Boger, S. D., Wilson, C. J., Fanning, C. M. (2001). "Early Paleozoic tectonism within the East Antarctic craton: The final suture between east and west Gondwana?" *Geology* 29.5, pp. 463–466. ISSN: 00917613. DOI: 10.1130/0091-7613(2001)029<0463:EPTWTE>2.0.CO;2.
- Boger, S. D. (2011). "Antarctica - Before and after Gondwana". *Gondwana Research* 19.2, pp. 335–371. ISSN: 1342937X. DOI: 10.1016/j.gr.2010.09.003.
- Bond, C. E. (2015). "Uncertainty in structural interpretation: Lessons to be learnt". *Journal of Structural Geology* 74, pp. 185–200. ISSN: 01918141. DOI: 10.1016/j.jsg.2015.03.003.

- Bouman, J., Ebbing, J., Fuchs, M., Sebera, J., Lieb, V., Szwillus, W., Haagmans, R., Novak, P. (2016). "Satellite gravity gradient grids for geophysics". *Scientific Reports* 6, February, pp. 1–11. ISSN: 20452322. DOI: 10.1038/srep21050.
- Boyden, J. A., Müller, R. D., Gurnis, M., Torsvik, T. H., Clark, J. A., Turner, M., Ivey-Law, H., Watson, R. J., Cannon, J. S. (2011). "Next-generation plate-tectonic reconstructions using GPlates". *Geoinformatics: Cyberinfrastructure for the Solid Earth Sciences* 9780521897, pp. 95–114. DOI: 10.1017/CB09780511976308.008.
- Bozdağ, E., Peter, D., Lefebvre, M., Komatitsch, D., Tromp, J., Hill, J., Podhorszki, N., Pugmire, D. (2016). "Global adjoint tomography: First-generation model". *Geophysical Journal International* 207.3, pp. 1739–1766. ISSN: 1365246X. DOI: 10.1093/gji/ggw356.
- Brenn, G. R., Hansen, S. E., Park, Y. (2017). "Variable thermal loading and flexural uplift along the Transantarctic Mountains, Antarctica". *Geology* 45.5, pp. 463–466. ISSN: 19432682. DOI: 10.1130/G38784.1.
- Brink, U. S. ten, Hackney, R. I., Bannister, S., Stern, T. A., Makovsky, Y. (1997). "Uplift of the Transantarctic Mountains and the bedrock beneath the East Antarctic ice sheet". *Journal of Geophysical Research: Solid Earth* 102.B12, pp. 27603–27621. ISSN: 2169-9356. DOI: 10.1029/97jb02483.
- Brown, B., Gaina, C., Müller, R. D. (2006). "Circum-Antarctic palaeobathymetry: Illustrated examples from Cenozoic to recent times". *Palaeogeography, Palaeoclimatology, Palaeoecology*. Vol. 231. 1-2, pp. 158–168. ISBN: 00310182. DOI: 10.1016/j.palaeo.2005.07.033.
- Buckley, J. J., Eslami, E. (1997). "Fuzzy plane geometry II: Circles and polygons". *Fuzzy Sets and Systems* 87.1, pp. 79–85. ISSN: 01650114. DOI: 10.1016/S0165-0114(96)00295-3.
- Burton-Johnson, A., Halpin, J. A., Whittaker, J. M., Graham, F. S., Watson, S. J. (2017). "A new heat flux model for the Antarctic Peninsula incorporating spatially variable upper crustal radiogenic heat production". *Geophysical Research Letters* 44.11, pp. 5436–5446. ISSN: 19448007. DOI: 10.1002/2017GL073596.
- Burton-Johnson, A., Riley, T. R. (2015). "Autochthonous v. Accreted Terrane development of continental margins: A revised in situ tectonic history of the Antarctic Peninsula". *Journal of the Geological Society* 172.6, pp. 822–835. ISSN: 00167649. DOI: 10.1144/jgs2014-110.
- Burton-Johnson, A., Black, M., Peter, T. F., Kaluza-Gilbert, J. (2016). "An automated methodology for differentiating rock from snow, clouds and sea in Antarctica from Landsat 8 imagery: A new rock outcrop map and area estimation for the entire Antarctic continent". *Cryosphere* 10.4, pp. 1665–1677. ISSN: 19940424. DOI: 10.5194/tc-10-1665-2016.
- Burton-Johnson, A., Dziadek, R., Martin, C. (2020). "Review article: Geothermal heat flow in Antarctica: current and future directions". *The Cryosphere* 14.11, pp. 3843–3873. ISSN: 1994-0424. DOI: 10.5194/tc-14-3843-2020.

- Cammarano, F., Goes, S., Vacher, P., Giardini, D. (2003). “Inferring upper-mantle temperatures from seismic velocities”. *Physics of the Earth and Planetary Interiors* 138.3-4, pp. 197–222. ISSN: 00319201. DOI: 10.1016/S0031-9201(03)00156-0.
- Cande, S. C., Stock, J. M. (2004). “Pacific-Antarctic-Australia motion and the formation of the Macquarie Plate”. *Geophysical Journal International* 157.1, pp. 399–414. ISSN: 0956540X. DOI: 10.1111/j.1365-246X.2004.02224.x.
- Cande, S. C., Stock, J. M., Müller, R. D., Ishihara, T. (2000). “Cenozoic motion between East and West Antarctica”. *Nature* 404.6774, pp. 145–150. ISSN: 00280836. DOI: 10.1038/35004501.
- Carson, C. J., Pittard, M. (2012). *A reconnaissance crustal heat production assessment of the Australian Antarctic Territory (AAT)*. Australia, Geoscience. ISBN: 9781922103871.
- Carson, C. J., McLaren, S., Roberts, J. L., Boger, S. D., Blankenship, D. D. (2014). “Hot rocks in a cold place: High sub-glacial heat flow in East Antarctica”. *Journal of the Geological Society* 171.1, pp. 9–12. ISSN: 00167649. DOI: 10.1144/jgs2013-030.
- Cawood, P. A., Korsch, R. J. (2008). “Assembling Australia: Proterozoic building of a continent”. *Precambrian Research* 166.1-4, pp. 1–35. ISSN: 03019268. DOI: 10.1016/j.precamres.2008.08.006.
- Cawood, P. A., Pisarevsky, S. A., Leitch, E. C. (2011). “Unraveling the New England orocline, east Gondwana accretionary margin”. *Tectonics* 30.5. ISSN: 02787407. DOI: 10.1029/2011TC002864.
- Chaput, J., Aster, R. C., Huerta, A., Sun, X., Lloyd, A., Wiens, D., Nyblade, A., Anandkrishnan, S., Winberry, J. P., Wilson, T. (2014). “The crustal thickness of West Antarctica”. *Journal of Geophysical Research: Solid Earth* 119.1, pp. 378–395. ISSN: 21699356. DOI: 10.1002/2013JB010642.
- Chen, B., Haeger, C., Kaban, M. K., Petrunin, A. G. (2018a). “Variations of the effective elastic thickness reveal tectonic fragmentation of the Antarctic lithosphere”. *Tectonophysics* 746, pp. 412–424. ISSN: 00401951. DOI: 10.1016/j.tecto.2017.06.012.
- Chen, J. (2019). “Satellite gravimetry and mass transport in the earth system”. *Geodesy and Geodynamics* 10.5, pp. 402–415. ISSN: 16749847. DOI: 10.1016/j.geog.2018.07.001.
- Chen, Y. S., Weatherill, G., Pagani, M., Cotton, F. (2018b). “A transparent and data-driven global tectonic regionalization model for seismic hazard assessment”. *Geophysical Journal International* 213.2, pp. 1263–1280. ISSN: 1365246X. DOI: 10.1093/GJI/GGY005.
- Christensen, N. I. (1988). *The Continental Crust: A Geophysical Approach*. Vol. 69. 19. Academic Press, p. 580. DOI: 10.1029/88eo00170.

- Claerbout, J. F., Karrenbach, M. (1992). "Electronic documents give reproducible research a new meaning". *1992 SEG Annual Meeting*. Society of Exploration Geophysicists, pp. 601–604. DOI: 10.1190/1.1822162.
- Clarkson, P. D., Tessensohn, F., Thomson, J. W. (1995). "Geological map of the Shackleton Range, Antarctica". *BAS GEOMAP*. Cambridge, British Antarctic Survey.
- Cleveland, W. S. (1979). "Robust locally weighted regression and smoothing scatterplots". *Journal of the American Statistical Association* 74.368, pp. 829–836. ISSN: 1537274X. DOI: 10.1080/01621459.1979.10481038.
- Clow, G. D., Cuffey, K., Waddington, E. (2014). "High Heat-Flow Beneath the Central Portion of the West Antarctic Ice Sheet". *American Geophysical Union*. Vol. 1, C31A–0577.
- Coleman, R. (2017). "A gateway to the Antarctic". *Impact* 2017.3, pp. 23–25.
- Collins, A. S., Pisarevsky, S. A. (2005). "Amalgamating eastern Gondwana: The evolution of the Circum-Indian Orogens". *Earth-Science Reviews* 71.3-4, pp. 229–270. ISSN: 00128252. DOI: 10.1016/j.earscirev.2005.02.004.
- Conrad, C. P., Lithgow-Bertelloni, C. (2006). "Influence of continental roots and asthenosphere on plate-mantle coupling". *Geophysical Research Letters* 33.5, pp. 2–5. ISSN: 00948276. DOI: 10.1029/2005GL025621.
- Cook, C. P., Hemming, S. R., Flierdt, T. van de, Pierce Davis, E. L., Williams, T., Galindo, A. L., Jiménez-Espejo, F. J., Escutia, C. (2017). "Glacial erosion of East Antarctica in the Pliocene: A comparative study of multiple marine sediment provenance tracers". *Chemical Geology* 466. June, pp. 199–218. ISSN: 00092541. DOI: 10.1016/j.chemgeo.2017.06.011.
- Corvino, A. F., Boger, S. D., Henjes-Kunst, F., Wilson, C. J., Fitzsimons, I. C. (2008). "Superimposed tectonic events at 2450 Ma, 2100 Ma, 900 Ma and 500 Ma in the North Mawson Escarpment, Antarctic Prince Charles Mountains". *Precambrian Research* 167.3-4, pp. 281–302. ISSN: 03019268. DOI: 10.1016/j.precamres.2008.09.001.
- Cowton, T., Nienow, P., Bartholomew, I., Sole, A., Mair, D. (2012). "Rapid erosion beneath the Greenland ice sheet". *Geology* 40.4, pp. 343–346. ISSN: 00917613. DOI: 10.1130/G32687.1.
- Cox, S. C., Smith-Lytle, B., Siddoway, C., Capponi, G., Elvevold, S., Burton-Johnson, A., Halpin, J., Morin, P., Elliot, D., et al. (2018). "The GeoMAP dataset of Antarctic rock exposures". *Polar2018*, p. 2428.
- Coxall, H. K., Wilson, P. A., Pälike, H., Lear, C. H., Backman, J. (2005). "Rapid stepwise onset of Antarctic glaciation and deeper calcite compensation in the Pacific Ocean". *Nature* 433.7021, pp. 53–57. ISSN: 0028-0836. DOI: 10.1038/nature03135.

- Cracknell, M. J. (2014). “Machine Learning for Geological Mapping: Algorithms and Applications”. PhD thesis. University of Tasmania, pp. 1–275.
- Cracknell, M. J., Reading, A. M. (2014). “Geological mapping using remote sensing data: A comparison of five machine learning algorithms, their response to variations in the spatial distribution of training data and the use of explicit spatial information”. *Computers and Geosciences* 63, pp. 22–33. ISSN: 00983004. DOI: 10.1016/j.cageo.2013.10.008.
- Craddock, C. (1970). “Antarctic Geology and Gondwanaland”. *Bulletin of the Atomic Scientists* 26.10, pp. 33–39. ISSN: 0096-3402. DOI: 10.1080/00963402.1970.11457870.
- Craddock, C. (1972). “Antarctic tectonics”. *Antarctic geology and geophysics. Universitetsforlaget, Oslo*, pp. 449–455.
- Cramer, F., Shephard, G. E. (2019). *Scientific Colour Maps*. DOI: 10.5281/zenodo.3596401.
- Cramer, F., Shephard, G. E., Heron, P. J. (2020). “The misuse of colour in science communication”. *Nature Communications* 11, pp. 1–10. ISSN: 2041-1723. DOI: 10.1038/s41467-020-19160-7.
- Cull, J. P. (1982). “An appraisal of Australian heat-flow data.” *BMR Journal of Australian Geology and Geophysics* 7.1, pp. 11–21. ISSN: 03129608.
- Daczko, N. R., Halpin, J. A., Fitzsimons, I. C., Whittaker, J. M. (2018). “A cryptic Gondwana-forming orogen located in Antarctica”. *Scientific Reports* 8.1, pp. 1–9. ISSN: 20452322. DOI: 10.1038/s41598-018-26530-1.
- Damiani, T. M., Jordan, T. A., Ferraccioli, F., Young, D. A., Blankenship, D. D. (2014). “Variable crustal thickness beneath Thwaites Glacier revealed from airborne gravimetry, possible implications for geothermal heat flux in West Antarctica”. *Earth and Planetary Science Letters* 407, pp. 109–122. ISSN: 0012821X. DOI: 10.1016/j.epsl.2014.09.023.
- Davies, J. H., Davies, D. R. (2010). “Earth’s surface heat flux”. *Solid Earth* 1.1, pp. 5–24. ISSN: 18699529. DOI: 10.5194/se-1-5-2010.
- De La Varga, M., Schaaf, A., Wellmann, F. (2019). “GemPy 1.0: Open-source stochastic geological modeling and inversion”. *Geoscientific Model Development* 12.1, pp. 1–32. ISSN: 19919603. DOI: 10.5194/gmd-12-1-2019.
- DeConto, R. M., Pollard, D. (2016). “Contribution of Antarctica to past and future sea-level rise”. *Nature* 531.7596, pp. 591–597. ISSN: 14764687. DOI: 10.1038/nature17145.
- Denison, D. G. T., Holmes, C. C., Mallick, B. K., Smith, A. F. M. (2002). *Bayesian Methods for Nonlinear Classification and Regression*. Ed. by Wiley, p. 296. ISBN: 978-0-471-49036-4.

- Dentith, M. C., Bruner, I., Long, A., Middleton, M. F., Scott, J. (1993). "Structure of the eastern margin of the Perth Basin, Western Australia". *Exploration Geophysics* 24.4, pp. 455–462. ISSN: 18347533. DOI: 10.1071/EG993455.
- Di Vincenzo, G., Talarico, F., Kleinschmidt, G. (2007). "An ^{40}Ar - ^{39}Ar investigation of the Mertz Glacier area (George V Land, Antarctica): Implications for the Ross Orogen-East Antarctic Craton relationship and Gondwana reconstructions". *Precambrian Research* 152.3-4, pp. 93–118. ISSN: 03019268. DOI: 10.1016/j.precamres.2006.10.002.
- Dinniman, M. S., Asay-Davis, X. S., Galton-Fenzi, B. K., Holland, P. R., Jenkins, A., Timmermann, R. (2016). "Modeling ice shelf/ocean interaction in Antarctica: A review". *Oceanography* 29.4, pp. 144–153. ISSN: 10428275. DOI: 10.5670/oceanog.2016.106.
- Drewes, H., Kuglitsch, F., Adám, J., Rózsa, S. (2016). "The geodesist's handbook 2016". *Journal of Geodesy* 90.10, pp. 907–1205. ISSN: 14321394. DOI: 10.1007/s00190-016-0948-z.
- Drewry, D. J., Jordan, S. R., Jankowski, E. (1982). "Measured properties of the Antarctic ice sheet: surface configuration, ice thickness, volume and bedrock characteristics." *Proc. 3rd international symposium on Antarctic glaciology, Columbus, Ohio, September 1981, (Annals of Glaciology, 3)* 3, pp. 83–91. ISSN: 0260-3055. DOI: 10.3189/s0260305500002573.
- Drinkwater, M. R., Floberghagen, R., Haagmans, R., Muzi, D., Popescu, A. (2003). "GOCE: ESA's First Earth Explorer Core Mission". *Sciences-New York* 18, pp. 419–432. DOI: 10.1007/978-94-017-1333-7{_}36.
- Du Toit, A. L. (1937). *Our Wandering Continents: An Hypothesis of Continental Drifting: "Africa Forms the Key"*. London, UK: Oliver and Boyd.
- Dziadek, R., Gohl, K., Diehl, A., Kaul, N. (2017). "Geothermal heat flux in the Amundsen Sea sector of West Antarctica: New insights from temperature measurements, depth to the bottom of the magnetic source estimation, and thermal modeling". *Geochemistry, Geophysics, Geosystems* 18.7, pp. 2657–2672. ISSN: 15252027. DOI: 10.1002/2016GC006755.
- Ebbing, J., Haas, P., Ferraccioli, F., Pappa, F., Szwillus, W., Bouman, J. (2018). "Earth tectonics as seen by GOCE - Enhanced satellite gravity gradient imaging". *Scientific Reports* 8.1, pp. 1–9. ISSN: 20452322. DOI: 10.1038/s41598-018-34733-9.
- Elliot, D. (1975). "Tectonics of Antarctica: a review". *American Journal of Science* 275, pp. 45–106. ISSN: 0002-9599.
- Elliot, D. H. (1992). "Jurassic magmatism and tectonism associated with Gondwanaland break-up: An Antarctic perspective". *Geological Society Special Publication* 68.1, pp. 165–184. ISSN: 03058719. DOI: 10.1144/GSL.SP.1992.068.01.11.
- Engelhardt, H. (2004). "Thermal regime and dynamics of the West Antarctic ice sheet". *Annals of Glaciology* 39, pp. 85–92. ISSN: 0260-3055. DOI: 10.3189/172756404781814203.

- England, P. C., Richardson, S. W. (1980). "Erosion and the age dependence of continental heat flow". *Geophysical Journal of the Royal Astronomical Society* 62.2, pp. 421–438. ISSN: 1365246X. DOI: 10.1111/j.1365-246X.1980.tb04865.x.
- Farra, V., Vinnik, L. (2000). "Upper mantle stratification by P and S receiver functions". *Geophysical Journal International* 141.3, pp. 699–712. ISSN: 0956540X. DOI: 10.1046/j.1365-246X.2000.00118.x.
- Fearnhead, P., Liu, Z. (2006). "Efficient online inference for multiple changepoint problems". *NSSPW - Nonlinear Statistical Signal Processing Workshop 2006*, pp. 589–605. DOI: 10.1109/NSSPW.2006.4378807.
- Federico, L., Crispini, L., Capponi, G., Bradshaw, J. D. (2009). "The Cambrian Ross Orogeny in northern Victoria Land (Antarctica) and New Zealand: A synthesis". *Gondwana Research* 15.2, pp. 188–196. ISSN: 1342937X. DOI: 10.1016/j.gr.2008.10.004.
- Ferraccioli, F., Jordan, T. A., Vaughan, D. G., Holt, J., James, M., Corr, H., Blankenship, D. D., Diehl, T. M. (2007). "New aerogeophysical survey targets the extent of the West Antarctic Rift System over Ellsworth Land, in Antarctica: A Keystone in a Changing World – Online Proceedings of the 10th ISAES X". *USGS OF-2007-1047*. Ed. by A. K. Cooper, C. R. Raymond, et al. 1996. U.S. Geological Survey and The National Academies, pp. 2004–2007.
- Ferraccioli, F., Finn, C. A., Jordan, T. A., Bell, R. E., Anderson, L. M., Damaske, D. (2011). "East Antarctic rifting triggers uplift of the Gamburtsev Mountains". *Nature* 479.7373, pp. 388–392. ISSN: 00280836. DOI: 10.1038/nature10566.
- Ferraccioli, F., Coren, F., Bozzo, E., Zanolla, C., Gandolfi, S., Tabacco, I., Frezzotti, M. (2001). "Rifted(?) crust at the East Antarctic Craton margin: Gravity and magnetic interpretation along a traverse across the Wilkes Subglacial Basin region". *Earth and Planetary Science Letters* 192.3, pp. 407–421. ISSN: 0012821X. DOI: 10.1016/S0012-821X(01)00459-9.
- Fischler, M. A., Bolles, R. C. (1981). "Random sample consensus: a paradigm for model fitting with applications to image analysis and automated cartography". *Communications of the ACM* 24.6, pp. 381–395. ISSN: 00010782. DOI: 10.1145/358669.358692.
- Fisher, A. T., Mankoff, K. D., Tulaczyk, S. M., Tyler, S. W., Foley, N. (2015). "High geothermal heat flux measured below the West Antarctic Ice Sheet". *Science Advances* 1.6, pp. 1–9. ISSN: 23752548. DOI: 10.1126/sciadv.1500093.
- Fitzsimons, I. C. (2000a). "A review of tectonic events in the east antarctic shield and their implications for gondwana and earlier supercontinents". *Journal of African Earth Sciences* 31.1, pp. 3–23. ISSN: 08995362. DOI: 10.1016/S0899-5362(00)00069-5.
- Fitzsimons, I. C. (2000b). "Grenville-age basement provinces in East Antarctica: Evidence for three separate collisional orogens". *Geology* 28.10, pp. 879–882. ISSN: 00917613. DOI: 10.1130/0091-7613(2000)28<879:GBPIEA>2.0.CO;2.

- Fitzsimons, I. C. (2003). “Proterozoic basement provinces of southern and southwestern Australia, and their correlation with Antarctica”. *Geological Society Special Publication* 206.1, pp. 93–130. ISSN: 03058719. DOI: 10.1144/GSL.SP.2003.206.01.07.
- Fitzsimons, I. C. (2016). “Pan-African granulites of Madagascar and southern India: Gondwana assembly and parallels with modern Tibet”. *Journal of Mineralogical and Petrological Sciences* 111.2, pp. 73–88. ISSN: 13493825. DOI: 10.2465/jmps.151117.
- Flowerdew, M. J., Tyrrell, S., Boger, S. D., Fitzsimons, I. C., Harley, S. L., Mikhalsky, E. V., Vaughan, A. P. (2013). “Pb isotopic domains from the Indian Ocean sector of Antarctica: Implications for past Antarctica-India connections”. *Geological Society Special Publication* 383.1, pp. 59–72. ISSN: 03058719. DOI: 10.1144/SP383.3.
- Foley, S. F., Jenner, G. A. (2004). “Trace element partitioning in lamproitic magmas—the Gaussberg olivine leucite”. *Lithos* 75.1-2, pp. 19–38. ISSN: 00244937. DOI: 10.1016/j.lithos.2003.12.020.
- Fomel, S., Hennenfent, G. (2007). “Reproducible computational experiments using SCons”. *ICASSP, IEEE International Conference on Acoustics, Speech and Signal Processing - Proceedings* 4, pp. 1257–1260. ISSN: 15206149. DOI: 10.1109/ICASSP.2007.367305.
- Fomel, S. (2013). “tour with Madagascar, Revisiting S. E. P. and SCons”. *Journal of open research software*.
- Fomel, S. (2015). “Reproducible research as a community effort: Lessons from the Madagascar project”. *Computing in Science and Engineering* 17.1, pp. 20–26. ISSN: 15219615. DOI: 10.1109/MCSE.2014.94.
- Forsberg, R., Olesen, A. V., Ferraccioli, F., Jordan, T., Corrand, H., Matsuoka, K. (2017). *PolarGap 2015/16 Filling the GOCE polar gap in Antarctica and ASIRAS flight around South Pole*. Tech. rep. DTU-space, BAS, NPI.
- Förste, C., Bruinsma, S., Flechtner, F., Marty, J.-C., Dahle, C., Abrykosov, O., Lemoine, J.-M., Neumayer, H., Barthelmes, F., Biancale, R., et al. (2013). “EIGEN-6C2-A new combined global gravity field model including GOCE data up to degree and order 1949 of GFZ Potsdam and GRGS Toulouse”. *EGU General Assembly Conference Abstracts*. Vol. 15. Vienna: EGU, p. 4077.
- Foulger, G. R. (2005). “Mantle plumes: Why the current skepticism?” *Chinese Science Bulletin* 50.15, pp. 1555–1560. ISSN: 10016538. DOI: 10.1360/982005-919.
- Foulger, G. R., Panza, G. F., Artemieva, I. M., Bastow, I. D., Cammarano, F., Evans, J. R., Hamilton, W. B., Julian, B. R., Lustrino, M., Thybo, H., Yanovskaya, T. B. (2013). “Caveats on tomographic images”. *Terra Nova* 25.4, pp. 259–281. ISSN: 09544879. DOI: 10.1111/ter.12041.

- Fowler, C. M. (1990). *The solid earth: an introduction to global geophysics*. Cambridge University Press. ISBN: 0521370256. DOI: 10.1029/90eo00309.
- Fox Maule, C., Purucker, M. E., Olsen, N., Mosegaard, K. (2005). “Geophysics: Heat flux anomalies in Antarctica revealed by satellite magnetic data”. *Science* 309.5733, pp. 464–467. ISSN: 00368075. DOI: 10.1126/science.1106888.
- Frese, R. R. B. von, Golynsky, A. V., Kim, H. R., Gaya-Piqué, L., Thébault, E., Chiappini, M., Ghidella, M., Grunow, A. (2007). “The next generation Antarctic digital magnetic anomaly map”. *Open-File Report* 10, pp. 1–4. DOI: 10.3133/ofr20071047SRP093.
- Fretwell, P., Pritchard, H. D., Vaughan, D. G., Bamber, J. L., Barrand, N. E., Bell, R., Bianchi, C., Bingham, R. G., Blankenship, D. D., Casassa, G., Catania, G., Callens, D., Conway, H., Cook, A. J., Corr, H. F. J., Damaske, D., Damm, V., Ferraccioli, F., Forsberg, R., Fujita, S., Gogineni, P., Griggs, J. A., Hindmarsh, R. C. A., Holmlund, P., Holt, J. W., Jacobel, R. W., Jenkins, A., Jokat, W., Jordan, T., King, E. C., Kohler, J., Krabill, W., Riger-Kusk, M., Langley, K. A., Leitchenkov, G., Leuschen, C., Luyendyk, B. P., Matsuoka, K., Nogi, Y., Nost, O. A., Popov, S. V., Rignot, E., Rippin, D. M., Riviera, A., Roberts, J., Ross, N., Siegert, M. J., Smith, A. M., Steinhage, D., Studinger, M., Sun, B., Tinto, B. K., Welch, B. C., Young, D. A., Xiangbin, C., Zirizzotti, A., Gim, Y., Gogineni, P., Griggs, J. A., Hindmarsh, R. C. A., Holmlund, P., Holt, J. W., Jacobel, R. W., Jenkins, A., Jokat, W., Jordan, T., King, E. C., Kohler, J., Krabill, W., Riger-Kusk, M., Langley, K. A., Leitchenkov, G., Leuschen, C., Luyendyk, B. P., Matsuoka, K., Mougnot, J., Nitsche, F. O., Nogi, Y., Nost, O. A., Popov, S. V., Rignot, E., Rippin, D. M., Rivera, A., Roberts, J., Ross, N., Siegert, M. J., Smith, A. M., Steinhage, D., Studinger, M., Sun, B., Tinto, B. K., Welch, B. C., Wilson, D., Young, D. A., Xiangbin, C., Zirizzotti, A. (2012). “Bedmap2: improved ice bed, surface and thickness datasets for Antarctica”. *The Cryosphere Discussions* 6.5, pp. 4305–4361. ISSN: 19940416. DOI: 10.5194/tcd-6-4305-2012.
- Frey, F. A., Coffin, M. F., Wallace, P. J., Weis, D., Zhao, X., Wise, S. W., Wähnert, V., Teagle, D. A., Saccocia, P. J., Reusch, D. N., Pringle, M. S., Nicolaysen, K. E., Neal, C. R., Müller, R. D., Moore, C. L., Mahoney, J. J., Keszthelyi, L., Inokuchi, H., Duncan, R. A., Delius, H., Damuth, J. E., Damasceno, D., Coxall, H. K., Borre, M. K., Boehm, F., Barling, J., Arndt, N. T., Antretter, M. (2000). “Origin and evolution of a submarine large igneous province: The Kerguelen Plateau and Broken Ridge, southern Indian Ocean”. *Earth and Planetary Science Letters* 176.1, pp. 73–89. ISSN: 0012821X. DOI: 10.1016/S0012-821X(99)00315-5.
- Frieler, K., Clark, P. U., He, F., Buizert, C., Reese, R., Ligtenberg, S. R., Van Den Broeke, M. R., Winkelmann, R., Levermann, A. (2015). “Consistent evidence of increasing Antarctic accumulation with warming”. *Nature Climate Change* 5.4, pp. 348–352. ISSN: 17586798. DOI: 10.1038/nclimate2574.
- Fudge, T. J., Steig, E. J., Markle, B. R., Schoenemann, S. W., Ding, Q., Taylor, K. C., McConnell, J. R., Brook, E. J., Sowers, T., White, J. W., Alley, R. B., Cheng, H., Clow, G. D., Cole-Dai, J., Conway, H., Cuffey, K. M., Edwards, J. S., Lawrence Edwards, R., Edwards,

- R., Fegyveresi, J. M., Ferris, D., Fitzpatrick, J. J., Johnson, J., Hargreaves, G., Lee, J. E., Maselli, O. J., Mason, W., McGwire, K. C., Mitchell, L. E., Mortensen, N., Neff, P., Orsi, A. J., Popp, T. J., Schauer, A. J., Severinghaus, J. P., Sigl, M., Spencer, M. K., Vaughn, B. H., Voigt, D. E., Waddington, E. D., Wang, X., Wong, G. J. (2013). “Onset of deglacial warming in West Antarctica driven by local orbital forcing”. *Nature* 500.7463, pp. 440–444. ISSN: 00280836. DOI: 10.1038/nature12376.
- Gard, M., Hasterok, D., Halpin, J. A. (2019). “Global whole-rock geochemical database compilation”. *Earth System Science Data* 11.4, pp. 1553–1566. ISSN: 18663516. DOI: 10.5194/essd-11-1553-2019.
- Gardner, R. L., Daczko, N. R., Halpin, J. A., Whittaker, J. M. (2015). “Discovery of a microcontinent (Gulden Draak Knoll) offshore Western Australia: Implications for East Gondwana reconstructions”. *Gondwana Research* 28.3, pp. 1019–1031. ISSN: 1342937X. DOI: 10.1016/j.gr.2014.08.013.
- Gillies, S. (2014). *The Fiona user manual*.
- Gillies, S. (2013a). *The Shapely user manual*.
- Gillies, S. (2013b). *Rasterio: geospatial raster I/O for Python programmers*.
- Global Volcanism Program (2013). *Volcanoes of the World, v. 4.9.0. Venzke, E (ed.)*. DOI: 10.5479/si.GVP.VOTW4-2013.
- Goes, S., Govers, R., Vacher, P. (2000). “Shallow mantle temperatures under Europe from P and S wave tomography”. *Journal of Geophysical Research: Solid Earth* 105.B5, pp. 11153–11169. ISSN: 2169-9356. DOI: 10.1029/1999jb900300.
- Goff, J. A., Powell, E. M., Young, D. A., Blankenship, D. D. (2014). “Instruments and methods: Conditional simulation of Thwaites Glacier (Antarctica) bed topography for flow models: Incorporating inhomogeneous statistics and channelized morphology”. *Journal of Glaciology* 60.222, pp. 635–646. ISSN: 00221430. DOI: 10.3189/2014JoG13J200.
- Golledge, N. R., Kowalewski, D. E., Naish, T. R., Levy, R. H., Fogwill, C. J., Gasson, E. G. W. (2015). “The multi-millennial Antarctic commitment to future sea-level rise”. *Nature* 526.7573, pp. 421–425. ISSN: 14764687. DOI: 10.1038/nature15706.
- Golledge, N. R., Keller, E. D., Gomez, N., Naughten, K. A., Bernales, J., Trusel, L. D., Edwards, T. L. (2019). “Global environmental consequences of twenty-first-century ice-sheet melt”. *Nature* 566.7742, pp. 65–72. ISSN: 0028-0836. DOI: 10.1038/s41586-019-0889-9.
- Golynsky, A. V., Ferraccioli, F., Hong, J. K., Golynsky, D. A., Frese, R. R. von, Young, D. A., Blankenship, D. D., Holt, J. W., Ivanov, S. V., Kiselev, A. V., Masolov, V. N., Eagles, G., Gohl, K., Jokat, W., Damaske, D., Finn, C., Aitken, A., Bell, R. E., Armadillo, E., Jordan, T. A., Greenbaum, J. S., Bozzo, E., Caneva, G., Forsberg, R., Ghidella, M., Galindo-

- Zaldivar, J., Bohoyo, F., Martos, Y. M., Nogi, Y., Quartini, E., Kim, H. R., Roberts, J. L. (2018). “New Magnetic Anomaly Map of the Antarctic”. *Geophysical Research Letters* 45.13, pp. 6437–6449. ISSN: 19448007. DOI: 10.1029/2018GL078153.
- Golynsky, A. V., Ivanov, S. V., Kazankov, A. J., Jokat, W., Masolov, V. N., Von Frese, R. R. (2013a). “New continental margin magnetic anomalies of East Antarctica”. *Tectonophysics* 585, pp. 172–184. ISSN: 00401951. DOI: 10.1016/j.tecto.2012.06.043.
- Golynsky, A., Bell, R., Blankenship, D., Damaske, D., Ferraccioli, F., Finn, C., Golynsky, D., Ivanov, S., Jokat, W., Masolov, V., Riedel, S., Von Frese, R., Young, D. (2013b). “Air and shipborne magnetic surveys of the Antarctic into the 21st century”. *Tectonophysics* 585, pp. 3–12. ISSN: 00401951. DOI: 10.1016/j.tecto.2012.02.017.
- Goodfellow, I., Bengio, Y., Courville, A. (2016). *Adaptive Computation and Machine learning*, p. 775. ISBN: 978-0-262-03561-3.
- Goodge, J. W., Vervoort, J. D., Fanning, C. M., Brecke, D. M., Farmer, G. L., Williams, I. S., Myrow, P. M., DePaolo, D. J. (2008). “A Positive Test of East Antarctica-Laurentia Juxtaposition Within the Rodinia Supercontinent”. *Science* 321.5886, pp. 235–240. ISSN: 0036-8075. DOI: 10.1126/science.1159189.
- Goodge, J. W. (2018). “Crustal heat production and estimate of terrestrial heat flow in central East Antarctica, with implications for thermal input to the East Antarctic ice sheet”. *Cryosphere* 12.2, pp. 491–504. ISSN: 19940424. DOI: 10.5194/tc-12-491-2018.
- Goodge, J. W., Fanning, C. M., Bennett, V. C. (2001). “U-Pb evidence of ~1.7 Ga crustal tectonism during the Nimrod Orogeny in the Transantarctic Mountains, Antarctica: Implications for Proterozoic plate reconstructions”. *Precambrian Research* 112.3-4, pp. 261–288. ISSN: 03019268. DOI: 10.1016/S0301-9268(01)00193-0.
- Goodge, J. W., Finn, C. A. (2010). “Glimpses of East Antarctica: Aeromagnetic and satellite magnetic view from the central transantarctic mountains of East Antarctica”. *Journal of Geophysical Research: Solid Earth* 115.9, pp. 1–22. ISSN: 21699356. DOI: 10.1029/2009JB006890.
- Goodge, J. W., Hansen, V. L., Peacock, S. M. (1992). “Multiple petrotectonic events in high grade metamorphic rocks of Nimrod group Central ATransantarctic Mountains”. *Recent Progress in Antarctic Earth Science*. Ed. by Y. Yoshida. Tokyo, pp. 203–209.
- Goutorbe, B., Poort, J., Lucazeau, F., Raillard, S. (2011). “Global heat flow trends resolved from multiple geological and geophysical proxies”. *Geophysical Journal International* 187.3, pp. 1405–1419. ISSN: 0956540X. DOI: 10.1111/j.1365-246X.2011.05228.x.
- Graham, F. S., Roberts, J. L., Galton-Fenzi, B. K., Young, D., Blankenship, D., Siegert, M. J. (2017). “A high-resolution synthetic bed elevation grid of the Antarctic continent”. *Earth System Science Data* 9.1, pp. 267–279. ISSN: 18663516. DOI: 10.5194/essd-9-267-2017.

- Grantham, G., Macey, P., Horie, K., Kawakami, T., Ishikawa, M., Satish-Kumar, M., Tsuchiya, N., Graser, P., Azevedo, S. (2013). “Comparison of the metamorphic history of the Monapo Complex, northern Mozambique and Balchenfjella and Austhameren areas, Sør Rondane, Antarctica: Implications for the Kuunga Orogeny and the amalgamation of N and S. Gondwana”. *Precambrian Research* 234, pp. 85–135. ISSN: 03019268. DOI: 10.1016/j.precamres.2012.11.012.
- Graw, J. H., Hansen, S. E., Langston, C. A., Young, B. A., Mostafanejad, A., Park, Y. (2017). “An assessment of crustal and upper-mantle velocity structure by removing the effect of an ice layer on the P-wave response: An application to antarctic seismic studies”. *Bulletin of the Seismological Society of America* 107.2, pp. 639–651. ISSN: 19433573. DOI: 10.1785/0120160262.
- Greenbaum, J. S., Blankenship, D. D., Young, D. A., Richter, T. G., Roberts, J. L., Aitken, A. R., Legresy, B., Schroeder, D. M., Warner, R. C., Van Ommen, T. D., Siegert, M. J. (2015). “Ocean access to a cavity beneath Totten Glacier in East Antarctica”. *Nature Geoscience* 8.4, pp. 294–298. ISSN: 17520908. DOI: 10.1038/ngeo2388.
- Griffiths, J. C. (1983). “Geological similarity by Q analysis”. *Journal of the International Association for Mathematical Geology* 15.1, pp. 85–108. ISSN: 0020-5958. DOI: 10.1007/BF01030077.
- Griggs, J. A., Bamber, J. L. (2011). “Antarctic ice-shelf thickness from satellite radar altimetry”. *Journal of Glaciology* 57.203, pp. 485–498. DOI: 10.3189/002214311796905659.
- Grikurov, G. E. G., Leitchenkov, G., Leychenkov, G. (2012). *Tectonic Map of Antarctica*. CCGM-CGMW.
- Groenewald, P. B., Moyes, A. B., Grantham, G. H., Krynauw, J. R. (1995). “East Antarctic crustal evolution: geological constraints and modelling in western Dronning Maud Land”. *Precambrian Research* 75.3-4, pp. 231–250. ISSN: 03019268. DOI: 10.1016/0301-9268(95)80008-6.
- Grosse, P., Euillades, P. A., Euillades, L. D., Wyk de Vries, B. van (2014). “A global database of composite volcano morphometry”. *Bulletin of Volcanology* 76.1, p. 784. ISSN: 0258-8900. DOI: 10.1007/s00445-013-0784-4.
- Guillou, L., Mareschal, J. C., Jaupart, C., Gariépy, C., Bienfait, G., Lapointe, R. (1994). “Heat flow, gravity and structure of the Abitibi belt, Superior Province, Canada: Implications for mantle heat flow”. *Earth and Planetary Science Letters* 122.1-2, pp. 103–123. ISSN: 0012821X. DOI: 10.1016/0012-821X(94)90054-X.
- Gulick, S. P., Shevenell, A. E., Montelli, A., Fernandez, R., Smith, C., Warny, S., Bohaty, S. M., Sjunneskog, C., Leventer, A., Frederick, B., Blankenship, D. D. (2017). “Initiation

- and long-term instability of the East Antarctic Ice Sheet”. *Nature* 552.7684, pp. 225–229. ISSN: 14764687. DOI: 10.1038/nature25026.
- Gunter, B. C., Didova, O., Riva, R. E., Ligtenberg, S. R., Lenaerts, J. T., King, M. A., Van Den Broeke, M. R., Urban, T. (2014). “Empirical estimation of present-day Antarctic glacial isostatic adjustment and ice mass change”. *Cryosphere* 8.2, pp. 743–760. ISSN: 19940424. DOI: 10.5194/tc-8-743-2014.
- Haeger, C., Kaban, M. K., Tesauro, M., Petrunin, A. G., Mooney, W. D. (2019). “3-D Density, Thermal, and Compositional Model of the Antarctic Lithosphere and Implications for Its Evolution”. *Geochemistry, Geophysics, Geosystems* 20.2, pp. 688–707. ISSN: 15252027. DOI: 10.1029/2018GC008033.
- Halpin, J. A., Daczko, N. R., Direen, N. G., Mulder, J. A., Murphy, R. C., Ishihara, T. (2020). “Provenance of rifted continental crust at the nexus of East Gondwana breakup”. *Lithos* 354-355, p. 105363. ISSN: 18726143. DOI: 10.1016/j.lithos.2019.105363.
- Halpin, J. A., Daczko, N. R., Milan, L. A., Clarke, G. L. (2012). “Decoding near-concordant U-Pb zircon ages spanning several hundred million years: Recrystallisation, metamictisation or diffusion?” *Contributions to Mineralogy and Petrology* 163.1, pp. 67–85. ISSN: 00107999. DOI: 10.1007/s00410-011-0659-7.
- Halpin, J. A., Gerakiteys, C. L., Clarke, G. L., Belousova, E. A., Griffin, W. L. (2005). “In-situ U-Pb geochronology and Hf isotope analyses of the Rayner Complex, east Antarctica”. *Contributions to Mineralogy and Petrology* 148.6, pp. 689–706. ISSN: 00107999. DOI: 10.1007/s00410-004-0627-6.
- Halpin, J. A., Crawford, A. J., Direen, N. G., Coffin, M. F., Forbes, C. J., Borissova, I. (2008). “Naturaliste Plateau, offshore western Australia: A submarine window into Gondwana assembly and breakup”. *Geology* 36.10, pp. 807–810. ISSN: 00917613. DOI: 10.1130/G25059A.1.
- Halpin, J. A., Daczko, N. R., Kobler, M. E., Whittaker, J. M. (2017). “Strike-slip tectonics during the Neoproterozoic–Cambrian assembly of East Gondwana: Evidence from a newly discovered microcontinent in the Indian Ocean (Batavia Knoll)”. *Gondwana Research* 51, pp. 137–148. ISSN: 1342937X. DOI: 10.1016/j.gr.2017.08.002.
- Halpin, J. A., Clarke, G. L., White, R. W., Kelsey, D. E. (2007a). “Contrasting P-T-t paths for Neoproterozoic metamorphism in MacRobertson and Kemp Lands, east Antarctica”. *Journal of Metamorphic Geology* 25.6, pp. 683–701. ISSN: 02634929. DOI: 10.1111/j.1525-1314.2007.00723.x.
- Halpin, J. A., White, R. W., Clarke, G. L., Kelsey, D. E. (2007b). “The Proterozoic P-T-t evolution of the Kemp Land Coast, East Antarctica; constraints from Si-saturated and

- Si-undersaturated metapelites". *Journal of Petrology* 48.7, pp. 1321–1349. ISSN: 00223530. DOI: 10.1093/petrology/egm020.
- Hanna, E., Navarro, F. J., Pattyn, F., Domingues, C. M., Fettweis, X., Ivins, E. R., Nicholls, R. J., Ritz, C., Smith, B., Tulaczyk, S., Whitehouse, P. L., Jay Zwally, H. (2013). "Ice-sheet mass balance and climate change". *Nature* 498.7452, pp. 51–59. ISSN: 00280836. DOI: 10.1038/nature12238.
- Hansen, S. E., Graw, J. H., Kenyon, L. M., Nyblade, A. A., Wiens, D. A., Aster, R. C., Huerta, A. D., Anandkrishnan, S., Wilson, T. (2014). "Imaging the Antarctic mantle using adaptively parameterized P-wave tomography: Evidence for heterogeneous structure beneath West Antarctica". *Earth and Planetary Science Letters* 408, pp. 66–78. ISSN: 0012821X. DOI: 10.1016/j.epsl.2014.09.043.
- Hansen, S. E., Julià, J., Nyblade, A. A., Pyle, M. L., Wiens, D. A., Anandkrishnan, S. (2009). "Using S wave receiver functions to estimate crustal structure beneath ice sheets: An application to the Transantarctic Mountains and East Antarctic craton". *Geochemistry, Geophysics, Geosystems* 10.8. ISSN: 15252027. DOI: 10.1029/2009GC002576.
- Hansen, S. E., Kenyon, L. M., Graw, J. H., Park, Y., Nyblade, A. A. (2016). "Crustal structure beneath the Northern Transantarctic Mountains and Wilkes Subglacial Basin: Implications for tectonic origins". *Journal of Geophysical Research: Solid Earth* 121.2, pp. 812–825. ISSN: 21699356. DOI: 10.1002/2015JB012325.
- Hansen, S. E., Nyblade, A. A., Heeszel, D. S., Wiens, D. A., Shore, P., Kanao, M. (2010). "Crustal structure of the Gamburtsev Mountains, East Antarctica, from S-wave receiver functions and Rayleigh wave phase velocities". *Earth and Planetary Science Letters* 300.3–4, pp. 395–401. ISSN: 0012821X. DOI: 10.1016/j.epsl.2010.10.022.
- Harley, S. L., Fitzsimons, I. C., Zhao, Y. (2013). "Antarctica and supercontinent evolution: Historical perspectives, recent advances and unresolved issues". *Geological Society Special Publication* 383.1, pp. 1–34. ISSN: 03058719. DOI: 10.1144/SP383.9.
- Harris, C. R., Millman, K. J., Walt, S. J. van der, Gommers, R., Virtanen, P., Cournapeau, D., Wieser, E., Taylor, J., Berg, S., Smith, N. J., Kern, R., Picus, M., Hoyer, S., Kerkwijk, M. H. van, Brett, M., Haldane, A., Río, J. F. del, Wiebe, M., Peterson, P., Gérard-Marchant, P., Sheppard, K., Reddy, T., Weckesser, W., Abbasi, H., Gohlke, C., Oliphant, T. E. (2020). "Array programming with NumPy". *Nature* 585.7825, pp. 357–362. ISSN: 14764687. DOI: 10.1038/s41586-020-2649-2.
- Hartmann, J., Moosdorf, N. (2012). "The new global lithological map database GLiM: A representation of rock properties at the Earth surface". *Geochemistry, Geophysics, Geosystems* 13.12, pp. 1–37. ISSN: 15252027. DOI: 10.1029/2012GC004370.
- Hasterok, D. (2019). *Thermoglobe*. www.heatflow.org.

- Hasterok, D., Chapman, D. S. (2008). *Global heat flow: a new database and a new approach*.
- Hasterok, D., Chapman, D. S. (2011). "Heat production and geotherms for the continental lithosphere". *Earth and Planetary Science Letters* 307.1-2, pp. 59–70. ISSN: 0012821X. DOI: 10.1016/j.epsl.2011.04.034.
- Hasterok, D., Gard, M., Webb, J. (2018a). "On the radiogenic heat production of metamorphic, igneous, and sedimentary rocks". *Geoscience Frontiers* 9.6, pp. 1777–1794. ISSN: 16749871. DOI: 10.1016/j.gsf.2017.10.012.
- Hasterok, D., Webb, J. (2017). "On the radiogenic heat production of igneous rocks". *Geoscience Frontiers* 8.5, pp. 919–940. ISSN: 16749871. DOI: 10.1016/j.gsf.2017.03.006.
- Hasterok, D., Gard, M., Jennings, S. (2018b). "Thermal isostatic contributions to elevation: implications for the thermal state of Antarctica". *TACTical Workshop*. Hobart: SCAR.
- Heeszel, D. S., Wiens, D. A., Anandakrishnan, S., Aster, R. C., Dalziel, I. W. D., Huerta, A. D., Nyblade, A. A., Wilson, T. J., Winberry, J. P. (2016). "Upper mantle structure of central and West Antarctica from array analysis of Rayleigh wave phase velocities". *Journal of Geophysical Research: Solid Earth* 121.3, pp. 1758–1775. ISSN: 21699356. DOI: 10.1002/2015JB012616.
- Heirtzler, J. R., Dickson, G. O., Herron, E. M., Pitman, W. C., Le Pichon, X. (1968). "Marine magnetic anomalies, geomagnetic field reversals, and motions of the ocean floor and continents". *Journal of Geophysical Research* 73.6, pp. 2119–2136. DOI: 10.1029/jb073i006p02119.
- Hill, G. J. (2020). *On the Use of Electromagnetics for Earth Imaging of the Polar Regions*. Vol. 41. 1. Springer Netherlands, pp. 5–45. ISBN: 0123456789. DOI: 10.1007/s10712-019-09570-8.
- Hinsen, K. (2011). "A data and code model for reproducible research and executable papers". *Procedia Computer Science* 4, pp. 579–588. ISSN: 18770509. DOI: 10.1016/j.procs.2011.04.061.
- Hirt, C., Rexer, M., Scheinert, M., Pail, R., Claessens, S., Holmes, S. (2016). "A new degree-2190 (10 km resolution) gravity field model for Antarctica developed from GRACE, GOCE and Bedmap2 data". *Journal of Geodesy* 90.2, pp. 105–127. ISSN: 14321394. DOI: 10.1007/s00190-015-0857-6.
- Hirth, G., Kohlstedt, D. L. (1996). "Water in the oceanic upper mantle: Implications for rheology, melt extraction and the evolution of the lithosphere". *Earth and Planetary Science Letters* 144.1-2, pp. 93–108. ISSN: 0012821X. DOI: 10.1016/0012-821x(96)00154-9.
- Holgate, F. L., Goh, H. K. H., Wheller, G., Lewis, R. G. J. (2010). "The Central Tasmanian Geothermal Anomaly : A Prospective New EGS Province in Australia". *World Geothermal Congress 2010*. April. Bali, Indonesia, pp. 25–29.

- Hood, S. B., Cracknell, M. J., Gazley, M. F. (2018). “Linking protolith rocks to altered equivalents by combining unsupervised and supervised machine learning”. *Journal of Geochemical Exploration* 186. January, pp. 270–280. ISSN: 03756742. DOI: 10.1016/j.gexplo.2018.01.002.
- Hoyer, S., Fitzgerald, C., Hamman, J., et al. (2016). *Xarray: V0.8.0*. DOI: 10.5281/zenodo.59499.
- Hoyer, S., Hamman, J. J. (2017). “xarray: N-D labeled Arrays and Datasets in Python”. *Journal of Open Research Software* 5.1, pp. 1–6. ISSN: 2049-9647. DOI: 10.5334/jors.148.
- Huerta, A. D., Harry, D. L. (2007). “The transition from diffuse to focused extension: Modeled evolution of the West Antarctic Rift system”. *Earth and Planetary Science Letters* 255.1-2, pp. 133–147. ISSN: 0012821X. DOI: 10.1016/j.epsl.2006.12.011.
- Hulot, G., Eymin, C., Langlais, B., Manda, M., Olsen, N. (2002). “Small-scale structure of the geodynamo inferred from Oersted and Magsat satellite data”. *Nature* 416.6881, pp. 620–623. ISSN: 00280836. DOI: 10.1038/416620a.
- Hunter, J. D. (2007). “Matplotlib: A 2D graphics environment”. *Computing in Science and Engineering* 9.3, pp. 99–104. ISSN: 15219615. DOI: 10.1109/MCSE.2007.55.
- Hurwitz, S. (2003). “Groundwater flow, heat transport, and water table position within volcanic edifices: Implications for volcanic processes in the Cascade Range”. *Journal of Geophysical Research* 108.B12, p. 2557. ISSN: 0148-0227. DOI: 10.1029/2003jb002565.
- Jacobs, J., Bauer, W., Fanning, C. M. (2003). “Late Neoproterozoic/Early Palaeozoic events in central Dronning Maud Land and significance for the southern extension of the East African Orogen into East Antarctica”. *Precambrian Research* 126.1-2, pp. 27–53. ISSN: 03019268. DOI: 10.1016/S0301-9268(03)00125-6.
- Jacobs, J., Fanning, C. M., Henjes-Kunst, F., Olesch, M., Paech, H. J. (1998). “Continuation of the Mozambique Belt into East Antarctica: Grenville-age metamorphism and polyphase Pan-African high-grade events in central Dronning Maud Land”. *Journal of Geology* 106.4, pp. 385–406. ISSN: 00221376. DOI: 10.1086/516031.
- Jacobs, J., Elburg, M., Läufer, A., Kleinhanns, I. C., Henjes-Kunst, F., Estrada, S., Ruppel, A. S., Damaske, D., Montero, P., Bea, F. (2015). “Two distinct Late Mesoproterozoic/Early Neoproterozoic basement provinces in central/eastern Dronning Maud Land, East Antarctica: The missing link, 15–21°E”. *Precambrian Research* 265, pp. 249–272. ISSN: 03019268. DOI: 10.1016/j.precamres.2015.05.003.
- Jamieson, S. S. R., Sugden, D. E. (2008). “Landscape evolution of Antarctica”. *Antarctica: A Keystone in a Changing World Proceedings of the 10th International Symposium on Antarctic Earth Sciences, Santa Barbara, California, August 26 to September 1, 2007*. Ed.

- by A. K. Cooper, et al. June 2014. Polar Research Board, National Research Council, U.S. Geological, pp. 39–54. ISBN: 0-309-11855-7. DOI: 10.3133/of2007-1047.kp05.
- Jamieson, S. S., Sugden, D. E., Hulton, N. R. (2010). “The evolution of the subglacial landscape of Antarctica”. *Earth and Planetary Science Letters* 293.1-2, pp. 1–27. ISSN: 0012821X. DOI: 10.1016/j.epsl.2010.02.012.
- Janse, A. J. A. (1984). “Kimberlites-where and when”. *Kimberlite occurrence and origin: A basis for conceptual models in exploration*. Issue 8 of. Westerly Center, University of Western Australia Press, pp. 19–61.
- Jaupart, C., Mareschal, J. C. (2013). “Constraints on Crustal Heat Production from Heat Flow Data”. *Treatise on Geochemistry: Second Edition*. 2nd ed. Vol. 4. Elsevier, pp. 53–73. ISBN: 9780080983004. DOI: 10.1016/B978-0-08-095975-7.00302-8.
- Jaupart, C., Mareschal, J. C., Watts, A. B. (2007). “Heat flow and thermal structure of the lithosphere”. *Treatise on geophysics* 6, pp. 217–252.
- Jaupart, C., Mareschal, J. C., Iarotsky, L. (2016). “Radiogenic heat production in the continental crust”. *Lithos* 262, pp. 398–427. ISSN: 18726143. DOI: 10.1016/j.lithos.2016.07.017.
- Jessop, A. M., Majorowicz, J. A. (1994). “Fluid flow and heat transfer in sedimentary basins”. *Geological Society Special Publication* 78.78, pp. 43–54. ISSN: 03058719. DOI: 10.1144/GSL.SP.1994.078.01.05.
- Jnr, J. M. (1995). “The age of the Ritscherflya Supergroup and Borgmassivet Intrusions, Dronning Maud Land, Antarctica”. *Antarctic Science* 7.1, pp. 87–97. ISSN: 13652079. DOI: 10.1017/S0954102095000125.
- Jones, D., Bates, M., Li, Z., Corner, B., Hodgkinson, G. (2003). “Palaeomagnetic results from the ca. 1130 Ma Borgmassivet intrusions in the Ahlmannryggen region of Dronning Maud Land, Antarctica, and tectonic implications”. *Tectonophysics* 375.1-4, pp. 247–260. ISSN: 00401951. DOI: 10.1016/S0040-1951(03)00341-X.
- Jones, E., Oliphant, T., Peterson, P., et al. (2015). *SciPy: Open Source Scientific Tools for Python, 2001* (<http://www.scipy.org/>).
- Jordahl, K. (2014). “GeoPandas: Python tools for geographic data”. URL: <https://github.com/geopandas/geopandas>.
- Jordan, T. A., Martin, C., Ferraccioli, F., Matsuoka, K., Corr, H., Forsberg, R., Olesen, A., Siebert, M. (2018). “Anomalously high geothermal flux near the South Pole”. *Scientific Reports* 8.1. ISSN: 20452322. DOI: 10.1038/s41598-018-35182-0.
- Jordan, T. H. (1981). “Global tectonic regionalization for seismological data analysis”. *Bulletin of the Seismological Society of America* 71.4, pp. 1131–1141.

- Jordan, T. A., Riley, T. R., Siddoway, C. S. (2020). “The geological history and evolution of West Antarctica”. *Nature Reviews Earth & Environment* 1.2, pp. 117–133. DOI: 10.1038/s43017-019-0013-6.
- Kaltwasser, P., Boschetti, F., Hornby, P. (2005). “Measure of similarity between geological sections accounting for subjective criteria”. *Computers & Geosciences* 31.1, pp. 29–34. ISSN: 00983004. DOI: 10.1016/j.cageo.2004.09.004.
- Kanao, M., Raymond, C. e., Tanaka, S., Tsuboi, S., Wiens, D. (2007). “Broadband seismic deployments in East Antarctica; international collaboration and IPY contribution to understanding the Earth’s deep interior”. *Open-File Report - U. S. Geological Survey*, Extended Abstract 144.
- Kanao, M. (2014). “Seismicity in the Antarctic Continent and Surrounding Ocean”. *Open Journal of Earthquake Research* 03.01, pp. 5–14. ISSN: 2169-9623. DOI: 10.4236/ojer.2014.31002.
- Kanao, M., Wiens, D. A., Tanaka, S., Nyblade, A. A., Toyokuni, G., Shore, P. J., Tsuboi, S., Heeszel, D. S., Usui, Y., Parker, T. (2014). “Broadband seismic deployments in east Antarctica: IPY contribution to monitoring the earth’s interiors”. *Annals of Geophysics* 57.3. ISSN: 15935213. DOI: 10.4401/ag-6379.
- Kaufmann, G., Wolf, D. (1999). “Effects of lateral viscosity variations on postglacial rebound: An analytical approach”. *Geophysical Journal International* 137.2, pp. 489–500. ISSN: 0956540X. DOI: 10.1046/j.1365-246X.1999.00804.x.
- Kaufmann, G., Wu, P., Ivins, E. R. (2005). “Lateral viscosity variations beneath Antarctica and their implications on regional rebound motions and seismotectonics”. *Journal of Geodynamics* 39.2, pp. 165–181. ISSN: 02643707. DOI: 10.1016/j.jog.2004.08.009.
- Kearey, P., Brooks, M. (1991). *An introduction to geophysical exploration. 2nd edition.* Sons, John Wiley &. ISBN: 0632029218.
- Kelbert, M., Stuhl, I., Suhov, Y. (2017). “Weighted entropy: basic inequalities”. *Modern Stochastics: Theory and Applications* 4.3, pp. 233–252. ISSN: 2351-6046. DOI: 10.15559/17-vmsta85.
- Kelly, N. M., Clarke, G. L., Fanning, C. M. (2002). “A two-stage evolution of the Neoproterozoic Rayner Structural Episode: New U-Pb sensitive high resolution ion microprobe constraints from the Oygarden Group, Kemp Land, East Antarctica”. *Precambrian Research* 116.3-4, pp. 307–330. ISSN: 03019268. DOI: 10.1016/S0301-9268(02)00028-1.
- Kelly, N. M., Harley, S. L. (2005). “An integrated microtextural and chemical approach to zircon geochronology: Refining the Archaean history of the Napier Complex, east Antarctica”. *Contributions to Mineralogy and Petrology* 149.1, pp. 57–84. ISSN: 00107999. DOI: 10.1007/s00410-004-0635-6.

- Kelsey, D. E., Wade, B. P., Collins, A. S., Hand, M., Sealing, C. R., Netting, A. (2008). “Discovery of a Neoproterozoic basin in the Prydz belt in East Antarctica and its implications for Gondwana assembly and ultrahigh temperature metamorphism”. *Precambrian Research* 161.3-4, pp. 355–388. ISSN: 03019268. DOI: 10.1016/j.precamres.2007.09.003.
- Kennett, B. L. N. (2005). “Seismological Tables: AK135”. *Research School of Earth Sciences, Australian National University Canberra, Australia*, pp. 1–289.
- Kennett, B. L., Fichtner, A., Fishwick, S., Yoshizawa, K. (2013). “Australian seismological referencemodel (AuSREM): Mantle component”. *Geophysical Journal International* 192.2, pp. 871–887. ISSN: 0956540X. DOI: 10.1093/gji/ggs065.
- Kennett, B., Chopping, R., Blewett, R. (2018). *The Australian Continent: A Geophysical Synthesis*. Press, A. N. U. and of Australia (Geoscience Australia), Commonwealth. ISBN: 9781760462475. DOI: 10.22459/ac.08.2018.
- Kennicutt, M. C., Chown, S. L., Cassano, J. J., Liggett, D., Massom, R., Peck, L. S., Rintoul, S. R., Storey, J. W., Vaughan, D. G., Wilson, T. J., Sutherland, W. J. (2014). “Polar research: Six priorities for Antarctic science”. *Nature* 512.1, pp. 23–25. ISSN: 14764687. DOI: 10.1038/512023a.
- Kharal, A., Ahmad, B. (2009). “Mappings on fuzzy soft classes”. *Advances in Fuzzy Systems* 2009, pp. 1–6. ISSN: 16877101. DOI: 10.1155/2009/407890.
- Killick, R., Fearnhead, P., Eckley, I. A. (2012). “Optimal detection of changepoints with a linear computational cost”. *Journal of the American Statistical Association* 107.500, pp. 1590–1598. ISSN: 01621459. DOI: 10.1080/01621459.2012.737745.
- King, M. A., Bingham, R. J., Moore, P., Whitehouse, P. L., Bentley, M. J., Milne, G. A., M.A., K., R.J., B., P., M., P.L., W., M.J., B., G.A., M. (2012). “Lower satellite-gravimetry estimates of Antarctic sea-level contribution”. *Nature* 491.7425, pp. 586–589. ISSN: 00280836. DOI: 10.1038/nature11621.
- King, M. A., Santamariá-Gómez, A. (2016). “Ongoing deformation of Antarctica following recent Great Earthquakes”. *Geophysical Research Letters* 43.5, pp. 1918–1927. ISSN: 19448007. DOI: 10.1002/2016GL067773.
- Kleinschmidt, G., Boger, S. D. (2009). “The Bertrab, Littlewood and Moltke Nunataks of Prinz-Regent-Luitpold-Land (Coats Land) - Enigma of East Antarctic Geology”. *Polarforschung* 78.3, pp. 95–104. ISSN: 00322490.
- Knight, S. (2005). “Building software with SCons”. *Computing in Science and Engineering* 7.1, pp. 79–88. ISSN: 15219615. DOI: 10.1109/MCSE.2005.11.
- Knight, S. (2010). “Scons user guide”. *Foundation, Python Software*.

- Koenderink, J. J., Doorn, A. J. van (1992). "Surface shape and curvature scales". *Image and Vision Computing* 10.8, pp. 557–564. ISSN: 02628856. DOI: 10.1016/0262-8856(92)90076-F.
- Koppes, M. N., Montgomery, D. R. (2009). "The relative efficacy of fluvial and glacial erosion over modern to orogenic timescales". *Nature Geoscience* 2.9, pp. 644–647. ISSN: 17520894. DOI: 10.1038/ngeo616.
- Korsch, R. J., Doublier, M. P. (2016). "Major crustal boundaries of Australia, and their significance in mineral systems targeting". *Ore Geology Reviews* 76, pp. 211–228. ISSN: 01691368. DOI: 10.1016/j.oregeorev.2015.05.010.
- Kreemer, C., Holt, W. E., Holt, E., Kreemer, C., Holt, W. E. (2000). "What caused the March 25, 1998 Antarctic plate earthquake?: Inferences from regional stress and strain rate fields". *Geophysical Research Letters* 27.15, pp. 2297–2300. ISSN: 00948276. DOI: 10.1029/1999GL011188.
- Kuhn, S., Cracknell, M. J., Reading, A. M. (2016). "Lithological mapping via Random Forests: Information Entropy as a proxy for inaccuracy". *ASEG Extended Abstracts* 2016.1, pp. 1–4. ISSN: 2202-0586. DOI: 10.1071/aseg2016ab196.
- Kuhn, S., Cracknell, M. J., Reading, A. M. (2018). "Lithologic mapping using Random Forests applied to geophysical and remote-sensing data: A demonstration study from the Eastern Goldfields of Australia". *Geophysics* 83.4, B183–B193. ISSN: 19422156. DOI: 10.1190/geo2017-0590.1.
- Kulp, S. A., Strauss, B. H. (2019). "New elevation data triple estimates of global vulnerability to sea-level rise and coastal flooding". *Nature Communications* 10.1, p. 4844. ISSN: 2041-1723. DOI: 10.1038/s41467-019-12808-z.
- Kumar, P., Kind, R., Hanka, W., Wylegalla, K., Reigber, C., Yuan, X., Woelbern, I., Schwintzer, P., Fleming, K., Dahl-Jensen, T., Larsen, T. B., Schweitzer, J., Priestley, K., Gudmundsson, O., Wolf, D. (2005). "The lithosphere-asthenosphere boundary in the North-West Atlantic region". *Earth and Planetary Science Letters* 236.1-2, pp. 249–257. ISSN: 0012821X. DOI: 10.1016/j.epsl.2005.05.029.
- Kusznir, N. (2008). "South Australia – Antarctica Conjugate Rifted Margins : Mapping Crustal Thickness & Lithosphere Thinning Using Satellite Gravity Inversion Summary". *GA Rep* 13722.m, pp. 1–65.
- Lamarque, G., Barruol, G., Fontaine, F. R., Bascou, J., Ménot, R. P. (2015). "Crustal and mantle structure beneath the Terre Adélie Craton, East Antarctica: Insights from receiver function and seismic anisotropy measurements". *Geophysical Journal International* 200.2, pp. 809–823. ISSN: 1365246X. DOI: 10.1093/gji/ggu430.

- Lamarque, G., Bascou, J., Maurice, C., Cottin, J. Y., Riel, N., Ménot, R. P. (2016). “Microstructures, deformation mechanisms and seismic properties of a Palaeoproterozoic shear zone: The Mertz shear zone, East-Antarctica”. *Tectonophysics* 680, pp. 174–191. ISSN: 00401951. DOI: 10.1016/j.tecto.2016.05.011.
- Larour, E., Morlighem, M., Seroussi, H., Schiermeier, J., Rignot, E. (2012). “Ice flow sensitivity to geothermal heat flux of Pine Island Glacier, Antarctica”. *Journal of Geophysical Research F: Earth Surface* 117.4, n/a–n/a. ISSN: 01480227. DOI: 10.1029/2012JF002371.
- Larter, R. D., Barker, P. F. (1991). “Effects of ridge crest-trench interaction on Antarctic-Phoenix Spreading: Forces on a young subducting plate”. *Journal of Geophysical Research: Solid Earth* 96.B12, pp. 19583–19607. ISSN: 01480227. DOI: 10.1029/91JB02053.
- Laske, G., Masters, G., Ma, Z., Pasyanos, M. (2013). “Update on CRUST1.0—A 1-degree global model of Earth’s crust”. *EGU General Assembly 2013*. Vol. 15. EGU General Assembly Vienna, Austria, p. 2658.
- Laske, G., Masters, G., Reif, C. (2001). *A new global crustal model at 2x2 degrees*.
- Lees, C. H. C. H., Districts, R.-a., Lees, C. H. C. H. (1910). “On the shapes of the isotherms under mountain ranges in radio-active districts”. *Proceedings of the Royal Society of London. Series A, Containing Papers of a Mathematical and Physical Character* 83.563, pp. 339–346. ISSN: 0950-1207. DOI: 10.1098/rspa.1910.0022.
- Leitchenkov, G. L., Antonov, A. V., Luneov, P. I., Lipenkov, V. Y. (2016). “Geology and environments of subglacial Lake Vostok”. *Philosophical Transactions of the Royal Society A: Mathematical, Physical and Engineering Sciences* 374.2059, p. 20140302. ISSN: 1364503X. DOI: 10.1098/rsta.2014.0302.
- Lekić, V., Panning, M., Romanowicz, B. (2010). “A simple method for improving crustal corrections in waveform tomography”. *Geophysical Journal International* 182.1, pp. 265–278. ISSN: 0956540X. DOI: 10.1111/j.1365-246X.2010.04602.x.
- LeMasurier, W. E. (2006). “What Supports the Marie Byrd Land Dome? An Evaluation of Potential Uplift Mechanisms in a Continental Rift System”. *Antarctica*. Berlin/Heidelberg: Springer-Verlag, pp. 299–302. ISBN: 978-3-540-32934-3. DOI: 10.1007/3-540-32934-X}_{37}.
- Lenaerts, J. T., Vizcaino, M., Fyke, J., Kampenhout, L. van, Broeke, M. R. van den (2016). “Present-day and future Antarctic ice sheet climate and surface mass balance in the Community Earth System Model”. *Climate Dynamics* 47.5-6, pp. 1367–1381. ISSN: 14320894. DOI: 10.1007/s00382-015-2907-4.
- Lenton, T. M., Rockström, J., Gaffney, O., Rahmstorf, S., Richardson, K., Steffen, W., Schellnhuber, H. J. (2019). “Climate tipping points — too risky to bet against”. *Nature* 575.7784, pp. 592–595. ISSN: 14764687. DOI: 10.1038/d41586-019-03595-0.

- Levy, F., Jaupart, C., Mareschal, J. C., Bienfait, G., Limare, A. (2010). “Low heat flux and large variations of lithospheric thickness in the Canadian Shield”. *Journal of Geophysical Research: Solid Earth* 115.6. ISSN: 21699356. DOI: 10.1029/2009JB006470.
- Lewis, A., Lymburner, L., Purss, M. B., Brooke, B., Evans, B., Ip, A., Dekker, A. G., Irons, J. R., Minchin, S., Mueller, N., Oliver, S., Roberts, D., Ryan, B., Thankappan, M., Woodcock, R., Wyborn, L. (2016). “Rapid, high-resolution detection of environmental change over continental scales from satellite data – the Earth Observation Data Cube”. *International Journal of Digital Earth* 9.1, pp. 106–111. ISSN: 17538955. DOI: 10.1080/17538947.2015.1111952.
- Lewis, A., Oliver, S., Lymburner, L., Evans, B., Wyborn, L., Mueller, N., Raevksi, G., Hooke, J., Woodcock, R., Sixsmith, J., Wu, W., Tan, P., Li, F., Killough, B., Minchin, S., Roberts, D., Ayers, D., Bala, B., Dwyer, J., Dekker, A., Dhu, T., Hicks, A., Ip, A., Purss, M., Richards, C., Sagar, S., Trenham, C., Wang, P., Wang, L. W. (2017). “The Australian Geoscience Data Cube — Foundations and lessons learned”. *Remote Sensing of Environment* 202, pp. 276–292. ISSN: 00344257. DOI: 10.1016/j.rse.2017.03.015.
- Li, C. F., Lu, Y., Wang, J. (2017). “A global reference model of Curie-point depths based on EMAG2”. *Scientific Reports* 7.March, p. 45129. ISSN: 20452322. DOI: 10.1038/srep45129.
- Lindow, J., Kamp, P. J., Mukasa, S. B., Kleber, M., Lisker, F., Gohl, K., Kuhn, G., Spiegel, C. (2016). “Exhumation history along the eastern Amundsen Sea coast, West Antarctica, revealed by low-temperature thermochronology”. *Tectonics* 35.10, pp. 2239–2257. ISSN: 19449194. DOI: 10.1002/2016TC004236.
- Liu, Y., Li, Z.-X. X., Pisarevsky, S. A., Kirscher, U., Mitchell, R. N., Stark, J. C., Clark, C., Hand, M. (2018). “First Precambrian palaeomagnetic data from the Mawson Craton (East Antarctica) and tectonic implications”. *Scientific Reports* 8.1, p. 16403. ISSN: 2045-2322. DOI: 10.1038/s41598-018-34748-2.
- Lloyd, A. J., Wiens, D. A., Zhu, H., Tromp, J., Nyblade, A. A., Aster, R. C., Hansen, S. E., Dalziel, I. W., Wilson, T. J., Ivins, E. R., O’Donnell, J. P. (2020). “Seismic Structure of the Antarctic Upper Mantle Imaged with Adjoint Tomography”. *Journal of Geophysical Research: Solid Earth* 125.3, 2019JB017823. ISSN: 21699356. DOI: 10.1029/2019JB017823.
- Lösing, M., Ebbing, J., Szwillus, W. (2020). “Geothermal Heat Flux in Antarctica: Assessing Models and Observations by Bayesian Inversion”. *Frontiers in Earth Science* 8. ISSN: 22966463. DOI: 10.3389/feart.2020.00105.
- Lough, A. C., Wiens, D. A., Grace Barcheck, C., Anandkrishnan, S., Aster, R. C., Blankenship, D. D., Huerta, A. D., Nyblade, A., Young, D. A., Wilson, T. J. (2013). “Seismic detection of an active subglacial magmatic complex in Marie Byrd Land, Antarctica”. *Nature Geoscience* 6.12, pp. 1031–1035. ISSN: 17520894. DOI: 10.1038/ngeo1992.

- Lough, A. C., Wiens, D. A., Nyblade, A. (2018). “Reactivation of ancient Antarctic rift zones by intraplate seismicity”. *Nature Geoscience* 11.7, pp. 515–519. ISSN: 1752-0894. DOI: 10.1038/s41561-018-0140-6.
- Lucazeau, F. (2019). “Analysis and Mapping of an Updated Terrestrial Heat Flow Data Set”. *Geochemistry, Geophysics, Geosystems* 20.8, pp. 4001–4024. ISSN: 15252027. DOI: 10.1029/2019GC008389.
- Luedecke, S., Barr, C. (2010). *The History of the International Polar Years (IPYs)*. Ed. by S. Barr, C. Luedecke. From Pole to Pole. Berlin, Heidelberg: Springer Berlin Heidelberg. ISBN: 978-3-642-12401-3. DOI: 10.1007/978-3-642-12402-0.
- Luttinen, A. V., Furnes, H. (2000). “Flood basalts of Vestfjella: Jurassic magmatism across an Archaean-Proterozoic lithospheric boundary in Dronning Maud Land, Antarctica”. *Journal of Petrology* 41.8, pp. 1271–1305. ISSN: 00223530. DOI: 10.1093/petrology/41.8.1271.
- Lythe, M. B., Vaughan, D. G. (2001). “BEDMAP: A new ice thickness and subglacial topographic model of Antarctica”. *Journal of Geophysical Research: Solid Earth* 106.B6, pp. 11335–11351. ISSN: 2169-9356. DOI: 10.1029/2000jb900449.
- MacGregor, J. A., Fahnestock, M. A., Catania, G. A., Aschwanden, A., Clow, G. D., Colgan, W. T., Gogineni, S. P., Morlighem, M., Nowicki, S. M. J., Paden, J. D., Price, S. F., Seroussi, H. (2016). “A synthesis of the basal thermal state of the Greenland Ice Sheet”. *Journal of Geophysical Research: Earth Surface* 121.7, pp. 1328–1350. ISSN: 21699003. DOI: 10.1002/2015JF003803.
- Mackintosh, A. N., Verleyen, E., O’Brien, P. E., White, D. A., Jones, R. S., McKay, R., Dunbar, R., Gore, D. B., Fink, D., Post, A. L., Miura, H., Leventer, A., Goodwin, I., Hodgson, D. A., Lilly, K., Crosta, X., Golledge, N. R., Wagner, B., Berg, S., Ommen, T. van, Zwartz, D., Roberts, S. J., Vyverman, W., Masse, G. (2014). “Retreat history of the East Antarctic Ice Sheet since the Last Glacial Maximum”. *Quaternary Science Reviews* 100, pp. 10–30. ISSN: 02773791. DOI: 10.1016/j.quascirev.2013.07.024.
- MacKintosh, A., Golledge, N., Domack, E., Dunbar, R., Leventer, A., White, D., Pollard, D., Deconto, R., Fink, D., Zwartz, D., Gore, D., Lavoie, C. (2011). “Retreat of the East Antarctic ice sheet during the last glacial termination”. *Nature Geoscience* 4.3, pp. 195–202. ISSN: 17520894. DOI: 10.1038/ngeo1061.
- Mareschal, J. C., Jaupart, C. (2004). “Variations of surface heat flow and lithospheric thermal structure beneath the North American craton”. *Earth and Planetary Science Letters* 223.1-2, pp. 65–77. ISSN: 0012821X. DOI: 10.1016/j.epsl.2004.04.002.
- Maritati, A., Halpin, J. A., Whittaker, J. M., Daczko, N. R. (2019). “Fingerprinting Proterozoic Bedrock in Interior Wilkes Land, East Antarctica”. *Scientific Reports* 9.1, p. 10192. ISSN: 20452322. DOI: 10.1038/s41598-019-46612-y.

- Marschall, H. R., Hawkesworth, C. J., Storey, C. D., Dhuime, B., Leat, P. T., Meyer, H. P., Tamm-Buckle, S. (2010). “The Annandagstoppane Granite, East Antarctica: Evidence for Archaean Intracrustal recycling in the Kaapvaal-Grunehogna Craton from zircon O and Hf isotopes”. *Journal of Petrology* 51.11, pp. 2277–2301. ISSN: 00223530. DOI: 10.1093/petrology/egq057.
- Marsland, S. (2014). *Machine learning: An algorithmic perspective*, pp. 1–452. ISBN: 9781466583337. DOI: 10.1201/b17476.
- Martín-Español, A., Zammit-Mangion, A., Clarke, P. J., Flament, T., Helm, V., King, M. A., Lutheke, S. B., Petrie, E., Rémy, F., Schön, N., Wouters, B., Bamber, J. L. (2016). “Spatial and temporal Antarctic Ice Sheet mass trends, glacio-isostatic adjustment, and surface processes from a joint inversion of satellite altimeter, gravity, and GPS data”. *Journal of Geophysical Research: Earth Surface* 121.2, pp. 182–200. ISSN: 21699011. DOI: 10.1002/2015JF003550.
- Martín-Español, A., King, M. A., Zammit-Mangion, A., Andrews, S. B., Moore, P., Bamber, J. L. (2016). “An assessment of forward and inverse GIA solutions for Antarctica”. *Journal of Geophysical Research: Solid Earth* 121.9, pp. 6947–6965. ISSN: 2169-9313. DOI: 10.1002/2016JB013154.
- Martos, Y. M., Catalán, M., Jordan, T. A., Golynsky, A., Golynsky, D., Eagles, G., Vaughan, D. G. (2017). “Heat Flux Distribution of Antarctica Unveiled”. *Geophysical Research Letters* 44.22, pp. 417–11. ISSN: 19448007. DOI: 10.1002/2017GL075609.
- Matsuoka, K., MacGregor, J. A., Pattyn, F. (2012). “Predicting radar attenuation within the Antarctic ice sheet”. *Earth and Planetary Science Letters* 359-360, pp. 173–183. ISSN: 0012821X. DOI: 10.1016/j.epsl.2012.10.018.
- Matthews, K. J., Maloney, K. T., Zahirovic, S., Williams, S. E., Seton, M., Müller, R. D. (2016). “Global plate boundary evolution and kinematics since the late Paleozoic”. *Global and Planetary Change* 146, pp. 226–250. ISSN: 09218181. DOI: 10.1016/j.gloplacha.2016.10.002.
- Maus, S., Barckhausen, U., Berkenbosch, H., Bournas, N., Brozena, J., Childers, V., Dostaler, F., Fairhead, J. D., Finn, C., Von Frese, R. R., Gaina, C., Golynsky, S., Kucks, R., Lühr, H., Milligan, P., Mogren, S., Müller, R. D., Olesen, O., Pilkington, M., Saltus, R., Schreck- enberger, B., Thébaud, E., Tontini, F. C. (2009). “EMAG2: A 2-arc min resolution Earth Magnetic Anomaly Grid compiled from satellite, airborne, and marine magnetic measurements”. *Geochemistry, Geophysics, Geosystems* 10.8, n/a–n/a. ISSN: 15252027. DOI: 10.1029/2009GC002471.
- Maus, S., Rother, M., Holme, R., Lühr, H., Olsen, N., Haak, V. (2002). “First scalar magnetic anomaly map from CHAMP satellite data indicates weak lithospheric field”. *Geophysical Research Letters* 29.14, pp. 45–1. ISSN: 0094-8276. DOI: 10.1029/2001gl013685.

- Maus, S., Sazonova, T., Hemant, K., Fairhead, J. D., Ravat, D. (2007). "National geophysical data center candidate for the world digital magnetic anomaly map". *Geochemistry, Geophysics, Geosystems* 8.6, pp. 1–10. ISSN: 15252027. DOI: 10.1029/2007GC001643.
- McGrayne, S. B. (2011). *The theory that would not die: How bayes' rule cracked the enigma code, hunted down russian submarines, and emerged triumphant from two centuries of controversy*. Yale University Press, pp. 1–320. ISBN: 9780300169690. DOI: 10.1080/10848770.2013.817786.
- McKenzie, D., Jackson, J., Priestley, K. (2005). "Thermal structure of oceanic and continental lithosphere". *Earth and Planetary Science Letters* 233.3-4, pp. 337–349. ISSN: 0012821X. DOI: 10.1016/j.epsl.2005.02.005.
- McKinney, W. (2015). *Pandas data analysis library*.
- McLaren, S., Sandiford, M., Hand, M., Neumann, N., Wyborn, L., Bastrakova, I. (2003). "The hot southern continent: Heat flow and heat production in Australian Proterozoic terranes". *Special Paper of the Geological Society of America* 372.July 2014, pp. 157–167. ISSN: 00721077. DOI: 10.1130/0-8137-2372-8.157.
- Meert, J. G. (2003). *A synopsis of events related to the assembly of the eastern Gondwana*. Vol. 362. 1-4. Elsevier {BV}, pp. 1–40. ISBN: 1352846241. DOI: 10.1016/S0040-1951(02)00629-7.
- Megies, T., Beyreuther, M., Barsch, R., Krischer, L., Wassermann, J. (2011). "ObsPy - what can it do for data centers and observatories?" *Annals of Geophysics* 54.1, pp. 47–58. ISSN: 15935213. DOI: 10.4401/ag-4838.
- Ménot, R. P., Duclaux, G., Peucat, J. J., Rolland, Y., Guillot, S., Fanning, M., Bascou, J., Gapais, D., Pêcher, A. (2007). "Geology of the Terre Adélie Craton". *Antarctica: A Keystone in a changing World - Online Proceedings for the Tenth International Symposium on Antarctica Earth Sciences*, p. 5. DOI: 10.3133/of2007-1047.srp048.
- Ménot, R. P., Pêcher, A., Rolland, Y., Peucat, J. J., Pelletier, A., Duclaux, G., Guillot, S. (2005). "Structural setting of the Neoproterozoic terrains in the Commonwealth Bay Area (143-145°E), Terre Adélie Craton, East Antarctica". *Gondwana Research* 8.1, pp. 1–9. ISSN: 1342937X. DOI: 10.1016/S1342-937X(05)70258-6.
- Merdith, A. S., Collins, A. S., Williams, S. E., Pisarevsky, S., Foden, J. D., Archibald, D. B., Blades, M. L., Alessio, B. L., Armistead, S., Plavsa, D., Clark, C., Müller, R. D. (2017). "A full-plate global reconstruction of the Neoproterozoic". *Gondwana Research* 50, pp. 84–134. ISSN: 1342937X. DOI: 10.1016/j.gr.2017.04.001.
- Met Office (2016). *Cartopy: a cartographic python library with a matplotlib interface*. Exeter, Devon.

- Meyer, B., Saltus, R., Chulliat, A. (2016). “EMAG2: Earth Magnetic Anomaly Grid (2-arc-minute resolution) Version 3. National Centers for Environmental Information, NOAA. Model.” *National Centers for Environmental Information, NOAA*, p. 5194. DOI: 10.7289/V5H70CVX.
- Michaut, C., Jaupart, C., Bell, D. R. (2007). “Transient geotherms in Archean continental lithosphere: New constraints on thickness and heat production of the subcontinental lithospheric mantle”. *Journal of Geophysical Research: Solid Earth* 112.4. ISSN: 21699356. DOI: 10.1029/2006JB004464.
- Mironova, Y. N. (2018). “Use of fuzzy sets in modeling of GIS objects”. *Journal of Physics: Conference Series* 1015.3. ISSN: 17426596. DOI: 10.1088/1742-6596/1015/3/032094.
- Mony, L., Roberts, J. L., Halpin, J. A. (2020). “Inferring geothermal heat flux from an ice-borehole temperature profile at Law Dome, East Antarctica”. *Journal of Glaciology* 66.257, pp. 509–519. ISSN: 00221430. DOI: 10.1017/jog.2020.27.
- Morelli, A., Danesi, S. (2004). “Seismological imaging of the Antarctic continental lithosphere: A review”. *Global and Planetary Change* 42.1-4, pp. 155–165. ISSN: 09218181. DOI: 10.1016/j.gloplacha.2003.12.005.
- Morin, R. H., Williams, T., Henrys, S. A., Mogens, D., Niessen, F., Hansaraj, D. (2010). “Heat flow and hydrologic characteristics at the AND-1B borehole, ANDRILL McMurdo Ice Shelf project, Antarctica”. *Geosphere* 6.4, pp. 370–378. ISSN: 1553-040. DOI: 10.1130/GES00512.1.
- Morlighem, M., Rignot, E., Binder, T., Blankenship, D., Drews, R., Eagles, G., Eisen, O., Ferraccioli, F., Forsberg, R., Fretwell, P., Goel, V., Greenbaum, J. S., Gudmundsson, H., Guo, J., Helm, V., Hofstede, C., Howat, I., Humbert, A., Jokat, W., Karlsson, N. B., Lee, W. S., Matsuoka, K., Millan, R., Mouginot, J., Paden, J., Pattyn, F., Roberts, J., Rosier, S., Ruppel, A., Seroussi, H., Smith, E. C., Steinhage, D., Sun, B., Broeke, M. R. d., Ommen, T. D., Wessem, M. v., Young, D. A., Broeke, M. R. van den, Ommen, T. D. van, Wessem, M. van, Young, D. A. (2019). “Deep glacial troughs and stabilizing ridges unveiled beneath the margins of the Antarctic ice sheet”. *Nature Geoscience* 13.2, pp. 132–137. ISSN: 17520908. DOI: 10.1038/s41561-019-0510-8.
- Morrissey, L. J., Hand, M., Kelsey, D. E., Wade, B. P. (2016). “Cambrian high-temperature reworking of the Rayner-Eastern ghats terrane: Constraints from the Northern Prince Charles Mountains region, East Antarctica”. *Journal of Petrology* 57.1, pp. 53–91. ISSN: 14602415. DOI: 10.1093/petrology/egv082.
- Morrissey, L. J., Payne, J. L., Hand, M., Clark, C., Taylor, R., Kirkland, C. L., Kylander-Clark, A. (2017). “Linking the Windmill Islands, east Antarctica and the Albany–Fraser Orogen: Insights from U–Pb zircon geochronology and Hf isotopes”. *Precambrian Research* 293, pp. 131–149. ISSN: 03019268. DOI: 10.1016/j.precamres.2017.03.005.

- Morse, P. E., Reading, A. M., Stål, T. (2019). “Well-Posed Geoscientific Visualization Through Interactive Color Mapping”. *Frontiers in Earth Science* 7.October, pp. 0–17. ISSN: 22966463. DOI: 10.3389/feart.2019.00274.
- Mouginot, J., Scheuchl, B., Rignot., E. (2017). *MEaSURES Antarctic Boundaries for IPY 2007-2009 from Satellite Radar, Version 2*. DOI: <https://doi.org/10.5067/AXE4121732AD>.
- Mulder, J. A., Halpin, J. A., Daczko, N. R., Orth, K., Meffre, S., Thompson, J. M., Morrissey, L. J. (2019). “A Multiproxy provenance approach to uncovering the assembly of East Gondwana in Antarctica”. *Geology* 47.7, pp. 645–649. ISSN: 19432682. DOI: 10.1130/G45952.1.
- Mulder, J. A., Karlstrom, K. E., Halpin, J. A., Merdith, A. S., Spencer, C. J., Berry, R. F., McDonald, B. (2018). “Rodinian devil in disguise: Correlation of 1.25-1.10 Ga strata between Tasmania and Grand Canyon”. *Geology* 46.11, pp. 991–994. ISSN: 19432682. DOI: 10.1130/G45225.1.
- Myers, J. S., Shaw, R. D., Tyler, I. M. (1996). “Tectonic evolution of proterozoic australia”. *Tectonics* 15.6, pp. 1431–1446. DOI: 10.1029/96tc02356.
- Nance, D. R., Murphy, B. J. (2013). “Origins of the supercontinent cycle”. *Geoscience Frontiers* 4.4, pp. 439–448. ISSN: 16749871. DOI: 10.1016/j.gsf.2012.12.007.
- Nance, R. D., Murphy, J. B., Santosh, M. (2014). “The supercontinent cycle: A retrospective essay”. *Gondwana Research* 25.1, pp. 4–29. ISSN: 1342937X. DOI: 10.1016/j.gr.2012.12.026.
- Naumenko-Dèzes, M. O., Rolland, Y., Lamarque, G., Duclaux, G., Gallet, S., Bascou, J., Ménot, R. P. (2020). “Petrochronology of the Terre Adélie Craton (East Antarctica) evidences a long-lasting Proterozoic (1.7–1.5 Ga) tectono-metamorphic evolution — Insights for the connections with the Gawler Craton and Laurentia”. *Gondwana Research* 81, pp. 21–57. ISSN: 1342937X. DOI: 10.1016/j.gr.2019.11.010.
- Nield, G. A., Barletta, V. R., Bordoni, A., King, M. A., Whitehouse, P. L., Clarke, P. J., Domack, E., Scambos, T. A., Berthier, E. (2014). “Rapid bedrock uplift in the Antarctic Peninsula explained by viscoelastic response to recent ice unloading”. *Earth and Planetary Science Letters* 397, pp. 32–41. ISSN: 0012821X. DOI: 10.1016/j.epsl.2014.04.019.
- Nield, G. A., Whitehouse, P. L., Wal, W. v. d., Blank, B., O’Donnell, J. P., Stuart, G. W. (2018). “The impact of lateral variations in lithospheric thickness on glacial isostatic adjustment in West Antarctica”. *Geophysical Journal International* 214.2, pp. 811–824. ISSN: 1365246X. DOI: 10.1093/gji/ggy158.
- Noble, T. L., Rohling, E. J., Aitken, A. R. A., Bostock, H. C., Chase, Z., Gomez, N., Jong, L. M., King, M. A., Mackintosh, A. N., McCormack, F. S., McKay, R. M., Menviel, L., Phipps, S. J., Fogwill, C. J., Gayen, B., Golledge, N. R., Gwyther, D. E., Hogg, A. M. C., Martos, Y. M., Pena-Molino, B., Roberts, J., Flierdt, T. v. d., Weber, M. E., William,

- T., Fogwill, C. J., Gayen, B., Golledge, N. R., Gwyther, D. E., Hogg, A. M. C., Martos, Y. M., Pena-Molino, B., Roberts, J., Flierdt, T. v. d., Williams, T. (2020). *The sensitivity of the Antarctic Ice Sheet to a changing climate: Past, present and future*, pp. 0–2. ISBN: 0000000153492. DOI: 10.1029/2019RG000663.
- O'Donnell, J. P., Nyblade, A. A. (2014). “Antarctica’s hypsometry and crustal thickness: Implications for the origin of anomalous topography in East Antarctica”. *Earth and Planetary Science Letters* 388, pp. 143–155. ISSN: 0012821X. DOI: 10.1016/j.epsl.2013.11.051.
- O'Donnell, J. P., Stuart, G. W., Brisbourne, A. M., Selway, K., Yang, Y., Niell, G. A., Whitehouse, P. L., Nyblade, A. A., Wiens, D. A., Aster, R. C., Anandkrishnan, S., Huerta, A. D., Wilson, T., Winberry, J. P. (2019). “The uppermost mantle seismic velocity structure of West Antarctica from Rayleigh wave tomography: Insights into tectonic structure and geothermal heat flow”. *Earth and Planetary Science Letters* 522, pp. 219–233. ISSN: 0012821X. DOI: 10.1016/j.epsl.2019.06.024.
- Oliphant, T. E. (2006). *Guide to NumPy*.
- Oliphant, T. E. (2007). “Python for scientific computing”. *Computing in Science and Engineering* 9.3, pp. 10–20. ISSN: 15219615. DOI: 10.1109/MCSE.2007.58.
- Oppenheimer, M., Glavovic, B., Hinkel, J., Wal, R. van de, Magnan, A. K., Abd-Elgawad, A., Cai, R., Cifuentes-Jara, M., DeConto, R. M., Ghosh, T., Hay, J., Isla, F., Marzeion, B., Meyssignac, B., Sebesvari, Z. (2019). “Sea Level Rise and Implications for Low Lying Islands, Coasts and Communities.” *IPCC Special Report on the Ocean and Cryosphere in a Changing Climate*. Vol. 355. 6321. Chap. 4, pp. 126–129. ISBN: 1095-9203 (Electronic) 0036-8075 (Linking). DOI: 10.1126/science.aam6284.
- Pail, R., Goiginger, H., Schuh, W. D., Hck, E., Brockmann, J. M., Fecher, T., Güruber, T., Mayer-Gürr, T., Kusche, J., Jäggi, A., Rieser, D. (2010). “Combined satellite gravity field model GOCO01S derived from GOCE and GRACE”. *Geophysical Research Letters* 37.20, pp. 2–6. ISSN: 00948276. DOI: 10.1029/2010GL044906.
- Pail, R., Bruinsma, S., Migliaccio, F., Förste, C., Goiginger, H., Schuh, W. D., Höck, E., Reguzzoni, M., Brockmann, J. M., Abrikosov, O., Veicherts, M., Fecher, T., Mayrhofer, R., Krasbutter, I., Sansò, F., Tscherning, C. C. (2011). “First GOCE gravity field models derived by three different approaches”. *Journal of Geodesy* 85.11, pp. 819–843. ISSN: 09497714. DOI: 10.1007/s00190-011-0467-x.
- Pappa, F., Ebbing, J., Ferraccioli, F. (2019a). “Moho Depths of Antarctica: Comparison of Seismic, Gravity, and Isostatic Results”. *Geochemistry, Geophysics, Geosystems* 20.3, pp. 1629–1645. ISSN: 15252027. DOI: 10.1029/2018GC008111.
- Pappa, F., Ebbing, J., Ferraccioli, F., Wal, W. van der (2019b). “Modeling Satellite Gravity Gradient Data to Derive Density, Temperature, and Viscosity Structure of the Antarctic

- Lithosphere". *Journal of Geophysical Research: Solid Earth* 124.11, pp. 12053–12076. ISSN: 21699356. DOI: 10.1029/2019JB017997.
- Pasyanos, M. E., Masters, T. G., Laske, G., Ma, Z. (2014). "LITHO1.0: An updated crust and lithospheric model of the Earth". *Journal of Geophysical Research: Solid Earth* 119.3, pp. 2153–2173. ISSN: 21699356. DOI: 10.1002/2013JB010626.
- Pattyn, F. (2010). "Antarctic subglacial conditions inferred from a hybrid ice sheet/ice stream model". *Earth and Planetary Science Letters* 295.3-4, pp. 451–461. ISSN: 0012821X. DOI: 10.1016/j.epsl.2010.04.025.
- Pattyn, F., Carter, S. P., Thoma, M. (2016). "Advances in modeling subglacial lakes and their interaction with the Antarctic ice sheet". *Philosophical Transactions of the Royal Society A: Mathematical, Physical and Engineering Sciences* 374.2059, p. 20140296. ISSN: 1364503X. DOI: 10.1098/rsta.2014.0296.
- Paxman, G. J., Watts, A. B., Ferraccioli, F., Jordan, T. A., Bell, R. E., Jamieson, S. S., Finn, C. A. (2016). "Erosion-driven uplift in the Gamburtsev Subglacial Mountains of East Antarctica". *Earth and Planetary Science Letters* 452.August, pp. 1–14. ISSN: 0012821X. DOI: 10.1016/j.epsl.2016.07.040.
- Paxman, G. J., Jamieson, S. S., Ferraccioli, F., Bentley, M. J., Ross, N., Armadillo, E., Gasson, E. G., Leitchenkov, G., DeConto, R. M. (2018). "Bedrock Erosion Surfaces Record Former East Antarctic Ice Sheet Extent". *Geophysical Research Letters* 45.9, pp. 4114–4123. ISSN: 19448007. DOI: 10.1029/2018GL077268.
- Paxman, G. J., Jamieson, S. S., Ferraccioli, F., Jordan, T. A., Bentley, M. J., Ross, N., Forsberg, R., Matsuoka, K., Steinhage, D., Eagles, G., Casal, T. G. (2019a). "Subglacial Geology and Geomorphology of the Pensacola-Pole Basin, East Antarctica". *Geochemistry, Geophysics, Geosystems* 20.6, pp. 2786–2807. ISSN: 15252027. DOI: 10.1029/2018GC008126.
- Paxman, G. J., Jamieson, S. S., Hochmuth, K., Gohl, K., Bentley, M. J., Leitchenkov, G., Ferraccioli, F. (2019b). "Reconstructions of Antarctic topography since the Eocene–Oligocene boundary". *Palaeogeography, Palaeoclimatology, Palaeoecology* 535, p. 109346. ISSN: 00310182. DOI: 10.1016/j.palaeo.2019.109346.
- Payne, J. L., Hand, M., Barovich, K. M., Reid, A., Evans, D. A. D. (2009). "Correlations and reconstruction models for the 2500-1500 Ma evolution of the Mawson Continent". *Geological Society, London, Special Publications* 323.1, pp. 319–355. ISSN: 0305-8719. DOI: 10.1144/SP323.16.
- Peacock, J. R., Selway, K. (2016). "Magnetotelluric investigation of the Vestfold Hills and Rauer Group, East Antarctica". *Journal of Geophysical Research: Solid Earth* 121.4, pp. 2258–2273. ISSN: 21699356. DOI: 10.1002/2015JB012677.

- Pedregosa, F., Weiss, R., Brucher, M., Pedregosa, F. e. a., Pedregosa, F., Varoquaux, G., Gramfort, A., Michel, V., Thirion, B., Grisel, O., Blondel, M., Prettenhofer, P., Weiss, R., Dubourg, V., Vanderplas, J., Passos, A., Cournapeau, D., Brucher, M., Perrot, M., Duchesnay, E. (2011). “Scikit-learn: Machine Learning in Python”. *Journal of Machine Learning Research* 12.Oct, pp. 2825–2830.
- Peltier, W. R. (2004a). “Global glacial isostasy and the surface of the ice-age earth: The ICE-5G (VM2) model and GRACE”. *Annual Review of Earth and Planetary Sciences* 32.1, pp. 111–149. ISSN: 00846597. DOI: 10.1146/annurev.earth.32.082503.144359.
- Peltier, W. (2004b). “Global Glacial Isostasy and ths Surface of the Ice-age Earth: The ICE-5G (VM2) Model and GRACE”. *Annual Review of Earth and Planetary Sciences* 32.1, pp. 111–149. ISSN: 0084-6597. DOI: 10.1146/annurev.earth.32.082503.144359.
- Pérez-Díaz, L., Alcalde, J., Bond, C. E. (2020). “Introduction: Handling uncertainty in the geosciences: identification, mitigation and communication”. *Solid Earth* 11.3, pp. 889–897. ISSN: 1869-9529. DOI: 10.5194/se-11-889-2020.
- Petrinin, A. G., Rogozhina, I., Vaughan, A. P., Kukkonen, I. T., Kaban, M. K., Koulakov, I., Thomas, M. (2013). “Heat flux variations beneath central Greenland’s ice due to anomalously thin lithosphere”. *Nature Geoscience* 6.9, pp. 746–750. ISSN: 17520894. DOI: 10.1038/ngeo1898.
- Peucat, J. J., Ménot, R. P., Monnier, O., Fanning, C. M. (1999). “The Terre Adelie basement in the East-Antarctica Shield: Geological and isotopic evidence for a major 1.7 Ga thermal event; comparison with the Gawler Craton in South Australia”. *Precambrian Research* 94.3-4, pp. 205–224. ISSN: 03019268. DOI: 10.1016/S0301-9268(98)00119-3.
- Phillips, G., Wilson, C. J., Campbell, I. H., Allen, C. M. (2006). “U-Th-Pb detrital zircon geochronology from the southern Prince Charles Mountains, East Antarctica-Defining the Archaean to Neoproterozoic Ruker Province”. *Precambrian Research* 148.3-4, pp. 292–306. ISSN: 03019268. DOI: 10.1016/j.precamres.2006.05.001.
- Phillips, G., Kelsey, D. E., Corvino, A. F., Dutch, R. A. (2009). “Continental reworking during overprinting orogenic events, Southern Prince Charles Mountains, East Antarctica”. *Journal of Petrology* 50.11, pp. 2017–2041. ISSN: 00223530. DOI: 10.1093/petrology/egp065.
- Pittard, M. L., Galton-Fenzi, B. K., Roberts, J. L., Watson, C. S. (2016). “Organization of ice flow by localized regions of elevated geothermal heat flux”. *Geophysical Research Letters* 43.7, pp. 3342–3350. ISSN: 19448007. DOI: 10.1002/2016GL068436.
- Pollack, H. N. (1982). “The Heat Flow from the Continents”. *Annual Review of Earth and Planetary Sciences* 10.1, pp. 459–481. ISSN: 0084-6597. DOI: 10.1146/annurev.earth.10.050182.002331.

- Pollack, H. N., Hurter, S. J., Johnson, J. R. (1993). "Heat flow from the Earth's interior: Analysis of the global data set". *Reviews of Geophysics* 31.3, pp. 267–280. ISSN: 19449208. DOI: 10.1029/93RG01249.
- Pollard, D., DeConto, R. M., Nyblade, A. A. (2005). "Sensitivity of Cenozoic Antarctic ice sheet variations to geothermal heat flux". *Global and Planetary Change* 49.1-2, pp. 63–74. ISSN: 09218181. DOI: 10.1016/j.gloplacha.2005.05.003.
- Pollett, A., Hasterok, D., Raimondo, T., Halpin, J. A., Hand, M., Bendall, B., McLaren, S. (2019). "Heat Flow in Southern Australia and Connections With East Antarctica". *Geochemistry, Geophysics, Geosystems* 20.11, pp. 5352–5370. ISSN: 15252027. DOI: 10.1029/2019GC008418.
- Potter, K., Gerber, S., Anderson, E. W. (2013). "Visualization of uncertainty without a mean". *IEEE Computer Graphics and Applications* 33.1, pp. 75–79. ISSN: 02721716. DOI: 10.1109/MCG.2013.14.
- Price, P. B., Nagornov, O. V., Bay, R., Chirkin, D., He, Y., Miocinovic, P., Richards, A., Woschnagg, K., Koci, B., Zagorodnov, V. (2002). "Temperature profile for glacial ice at the South Pole: Implications for life in a nearby subglacial lake". *Proceedings of the National Academy of Sciences of the United States of America* 99.12, pp. 7844–7847. ISSN: 00278424. DOI: 10.1073/pnas.082238999.
- Purucker, M. (2013). *Geothermal heat flux data set based on low resolution observations collected by the CHAMP satellite between 2000 and 2010, and produced from the MF-6 model following the technique described in Fox Maule et al.(2005)*.
- Qgis (2015). *QGIS geographic information system*.
- R. J. Adie (1977). "Earth sciences: The geology of Antarctica: a review". *Philosophical Transactions of the Royal Society of London. B, Biological Sciences* 279.963, pp. 123–130. ISSN: 0080-4622. DOI: 10.1098/rstb.1977.0077.
- Ramachandran, P., Varoquaux, G. (2011). "Mayavi: 3D visualization of scientific data". *Computing in Science and Engineering* 13.2, pp. 40–51. ISSN: 15219615. DOI: 10.1109/MCSE.2011.35.
- Ramirez, C., Nyblade, A., Emry, E. L., Julià, J., Sun, X., Anandakrishnan, S., Wiens, D. A., Aster, R. C., Huerta, A. D., Winberry, P., Wilson, T. (2017). "Crustal structure of the Transantarctic Mountains, Ellsworth Mountains and Marie Byrd Land, Antarctica: Constraints on shear wave velocities, Poisson's ratios and Moho depths". *Geophysical Journal International* 211.3, pp. 1328–1340. ISSN: 1365246X. DOI: 10.1093/gji/ggx333.
- Ramirez, C., Nyblade, A., Hansen, S. E., Wiens, D. A., Anandakrishnan, S., Aster, R. C., Huerta, A. D., Shore, P., Wilson, T. (2016). "Crustal and upper-mantle structure beneath ice-covered regions in Antarctica from S-wave receiver functions and implications for heat

- flow". *Geophysical Journal International* 204.3, pp. 1636–1648. ISSN: 1365246X. DOI: 10.1093/gji/ggv542.
- Ravich, M. G., Klimov, L. V., Solovev, D. S. (1965). *Dokembriy Vostochnoy Antarktity (The Precambrian of East Antarctica)*. Vol. 658.
- Reading, A. M. (2002). "Antarctic seismicity and neotectonics". *Royal Society of New Zealand Bulletin* 35, pp. 479–484.
- Reading, A. M. (2006). "The seismic structure of Precambrian and early Palaeozoic terranes in the Lambert Glacier region, East Antarctica". *Earth and Planetary Science Letters* 244.1-2, pp. 44–57. ISSN: 0012821X. DOI: 10.1016/j.epsl.2006.01.031.
- Reading, A. M. (2007). "The seismicity of the Antarctic plate". *Special Paper of the Geological Society of America* 425.18, pp. 285–298. ISSN: 00721077. DOI: 10.1130/2007.2425(18).
- Reading, A. M., Bodin, T., Sambridge, M., Howe, S., Roach, M. (2010). "Down the borehole but outside the box: innovative approaches to wireline log data interpretation". *ASEG Extended Abstracts* 2010.1, pp. 1–4. ISSN: 2202-0586. DOI: 10.1081/22020586.2010.12041870.
- Reading, A. M., Gallagher, K. (2013). "Transdimensional change-point modeling as a tool to investigate uncertainty in applied geophysical inference: An example using borehole geophysical logs". *Geophysics* 78.3, WB89–WB99. ISSN: 19422156. DOI: 10.1190/GE02012-0384.1.
- Reading, A. M., Tkalčić, H., Kennett, B. L., Johnson, S. P., Sheppard, S. (2012). "Seismic structure of the crust and uppermost mantle of the Capricorn and Paterson Orogens and adjacent cratons, Western Australia, from passive seismic transects". *Precambrian Research* 196-197, pp. 295–308. ISSN: 03019268. DOI: 10.1016/j.precamres.2011.07.001.
- Rew, R., Davis, G. (1990). "NetCDF: An Interface for Scientific Data Access". *IEEE Computer Graphics and Applications* 10.4, pp. 76–82. ISSN: 02721716. DOI: 10.1109/38.56302.
- Rezvanbehbahani, S., Stearns, L. A., Kadivar, A., Walker, J. D., Veen, C. J. van der (2017). "Predicting the Geothermal Heat Flux in Greenland: A Machine Learning Approach". *Geophysical Research Letters* 44.24, pp. 271–12. ISSN: 19448007. DOI: 10.1002/2017GL075661.
- Rignot, E., Jacobs, S., Mouginot, J., Scheuchl, B. (2013). "Ice-Shelf Melting Around Antarctica". *Science* 341.6143, pp. 266–270. ISSN: 0036-8075. DOI: 10.1126/science.1235798.
- Rintoul, S. R., Silvano, A., Pena-Molino, B., Van Wijk, E., Rosenberg, M., Greenbaum, J. S., Blankenship, D. D. (2016). "Ocean heat drives rapid basal melt of the totten ice shelf". *Science Advances* 2.12, e1601610. ISSN: 23752548. DOI: 10.1126/sciadv.1601610.

- Ritsema, J., Heijst, H. J. van, Woodhouse, J. H. (2004). "Global transition zone tomography". *Journal of Geophysical Research: Solid Earth* 109.B2. ISSN: 2169-9356. DOI: 10.1029/2003jb002610.
- Ritz, C., Edwards, T. L., Durand, G., Payne, A. J., Peyaud, V., Hindmarsh, R. C. (2015). "Potential sea-level rise from Antarctic ice-sheet instability constrained by observations". *Nature* 528.7580, pp. 115–118. ISSN: 14764687. DOI: 10.1038/nature16147.
- Ritzwoller, M. H., Shapiro, N. M., Barmin, M. P., Levshin, A. L. (2002). "Global surface wave diffraction tomography". *Journal of Geophysical Research: Solid Earth* 107.B12, pp. 4–1. ISSN: 0148-0227. DOI: 10.1029/2002jb001777.
- Ritzwoller, M. H., Shapiro, N. M., Levshin, A. L., Leahy, G. M. (2001). "Crustal and upper mantle structure beneath Antarctica and surrounding oceans". *Journal of Geophysical Research: Solid Earth* 106.B12, pp. 30645–30670. ISSN: 2169-9356. DOI: 10.1029/2001jb000179.
- Rivers, T. (1997). "Lithotectonic elements of the Grenville Province: Review and tectonic implications". *Precambrian Research* 86.3-4, pp. 117–154. ISSN: 03019268. DOI: 10.1016/s0301-9268(97)00038-7.
- Robert, A. M., Fernandez, M., Jiménez-Munt, I., Vergés, J. (2017). "Lithospheric structure in Central Eurasia derived from elevation, geoid anomaly and thermal analysis". *Geological Society Special Publication* 427.1, pp. 271–293. ISSN: 03058719. DOI: 10.1144/SP427.10.
- Roberts, J. L., Warner, R. C., Young, D., Wright, A., Van Ommen, T. D., Blankenship, D. D., Siegert, M., Young, N. W., Tabacco, I. E., Forieri, A., Passerini, A., Zirizzotti, A., Frezzotti, M. (2011). "Refined broad-scale sub-glacial morphology of Aurora Subglacial Basin, East Antarctica derived by an ice-dynamics-based interpolation scheme". *Cryosphere* 5.3, pp. 551–560. ISSN: 19940416. DOI: 10.5194/tc-5-551-2011.
- Robitaille, T. P., Tollerud, E. J., Greenfield, P., Droettboom, M., Bray, E., Aldcroft, T., Davis, M., Ginsburg, A., Price-Whelan, A. M., Kerzendorf, W. E., Conley, A., Crighton, N., Barbary, K., Muna, D., Ferguson, H., Grollier, F., Parikh, M. M., Nair, P. H., Günther, H. M., Deil, C., Woillez, J., Conseil, S., Kramer, R., Turner, J. E., Singer, L., Fox, R., Weaver, B. A., Zabalza, V., Edwards, Z. I., Azalee Bostroem, K., Burke, D. J., Casey, A. R., Crawford, S. M., Dencheva, N., Ely, J., Jenness, T., Labrie, K., Lim, P. L., Pierfederici, F., Pontzen, A., Ptak, A., Refsdal, B., Servillat, M., Streicher, O. (2013). "Astropy: A community Python package for astronomy". *Astronomy and Astrophysics* 558, A33. ISSN: 00046361. DOI: 10.1051/0004-6361/201322068.
- Rocklin, M. (2015). "Dask: Parallel Computation with Blocked algorithms and Task Scheduling". *Proceedings of the 14th Python in Science Conference*. 130-136. Citeseer, pp. 126–132. DOI: 10.25080/majora-7b98e3ed-013.

- Rohling, E. J., Hibbert, F. D., Grant, K. M., Galaasen, E. V., Irvah, N., Kleiven, H. F., Marino, G., Ninnemann, U., Roberts, A. P., Rosenthal, Y., Schulz, H., Williams, F. H., Yu, J. (2019). "Asynchronous Antarctic and Greenland ice-volume contributions to the last interglacial sea-level highstand". *Nature Communications* 10.1. ISSN: 20411723. DOI: 10.1038/s41467-019-12874-3.
- Roth, G., Matsuoka, K., Skoglund, A., Melvær, Y., Tronstad, S. (2017). "Quantarctica: A Unique, Open, Standalone GIS Package for Antarctic Research and Education". *EGU General Assembly Conference Abstracts*. Vol. 19. Vienna, p. 1973.
- Roult, G., Rouland, D. (1994a). "Antarctica I: Deep structure investigations inferred from seismology; a review". *Physics of the Earth and Planetary Interiors* 84.1-4, pp. 15–32. ISSN: 00319201. DOI: 10.1016/0031-9201(94)90032-9.
- Roult, G., Rouland, D., Montagner, J. P. (1994b). "Antarctica II: Upper-mantle structure from velocities and anisotropy". *Physics of the Earth and Planetary Interiors* 84.1-4, pp. 33–57. ISSN: 00319201. DOI: 10.1016/0031-9201(94)90033-7.
- Roy, S., Rao, R. U. (2003). "Towards a crustal thermal model for the Archaean Dharwar craton, southern India". *Physics and Chemistry of the Earth* 28.9-11, pp. 361–373. ISSN: 14747065. DOI: 10.1016/S1474-7065(03)00058-5.
- Rudnick, R., Nyblade, A. (1999). "The thickness and heat production of Archean lithosphere: constraints from xenolith thermobarometry and surface heat flow". *Mantle petrology: Field observations and high pressure Experimentation: A Tribute to Francis R. (Joe) Boyd* 6.6, pp. 3–12.
- Rudnick, R. L., Fountain, D. M. (1995). "Nature and composition of the continental crust: A lower crustal perspective". *Reviews of Geophysics* 33.3, pp. 267–309. ISSN: 19449208. DOI: 10.1029/95RG01302.
- Ruppel, A., Jacobs, J., Eagles, G., Läufer, A., Jokat, W. (2018). "New geophysical data from a key region in East Antarctica: Estimates for the spatial extent of the Tonian Oceanic Arc Super Terrane (TOAST)". *Gondwana Research* 59, pp. 97–107. ISSN: 1342937X. DOI: 10.1016/j.gr.2018.02.019.
- Rychert, C. A., Shearer, P. M. (2009). "A global view of the lithosphere-asthenosphere boundary". *Science* 324.5926, pp. 495–498. ISSN: 00368075. DOI: 10.1126/science.1169754.
- Salmon, M., Kennett, B. L., Saygin, E. (2013a). "Australian seismological referencemodel (AuS-REM): Crustal component". *Geophysical Journal International* 192.1, pp. 190–206. ISSN: 0956540X. DOI: 10.1093/gji/ggs004.
- Salmon, M., Kennett, B. L., Stern, T., Aitken, A. R. (2013b). "The Moho in Australia and New Zealand". *Tectonophysics* 609, pp. 288–298. ISSN: 00401951. DOI: 10.1016/j.tecto.2012.07.009.

- Salvioli-Mariani, E., Toscani, L., Bersani, D. (2004). “Magmatic evolution of the Gausberg lamproite (Antarctica): volatile content and glass composition”. *Mineralogical Magazine* 68.1, pp. 83–100. ISSN: 0026-461X. DOI: 10.1180/0026461046810173.
- Sauermilch, I., Whittaker, J. M., Bijl, P. K., Totterdell, J. M., Jokat, W. (2019). “Tectonic, Oceanographic, and Climatic Controls on the Cretaceous-Cenozoic Sedimentary Record of the Australian-Antarctic Basin”. *Journal of Geophysical Research: Solid Earth* 124.8, pp. 7699–7724. ISSN: 21699356. DOI: 10.1029/2018JB016683.
- Schaeffer, A. J., Lebedev, S. (2013). “Global shear speed structure of the upper mantle and transition zone”. *Geophysical Journal International* 194.1, pp. 417–449. ISSN: 0956540X. DOI: 10.1093/gji/ggt095.
- Schaeffer, A. J., Lebedev, S. (2015). “Global heterogeneity of the lithosphere and underlying mantle: A seismological appraisal based on multimode surface-wave dispersion analysis, shear-velocity tomography, and tectonic regionalization”. *The Earth’s Heterogeneous Mantle: A Geophysical, Geodynamical, and Geochemical Perspective*. Springer International Publishing, pp. 3–46. ISBN: 9783319156279. DOI: 10.1007/978-3-319-15627-9{_}1.
- Scheinert, M., Ferraccioli, F., Schwabe, J., Bell, R., Studinger, M., Damaske, D., Jokat, W., Aleshkova, N., Jordan, T., Leitchenkov, G., Blankenship, D. D., Damiani, T. M., Young, D., Cochran, J. R., Richter, T. D. (2016). “New Antarctic gravity anomaly grid for enhanced geodetic and geophysical studies in Antarctica”. *Geophysical Research Letters* 43.2, pp. 600–610. ISSN: 19448007. DOI: 10.1002/2015GL067439.
- Schroeder, D. M., Blankenship, D. D., Young, D. A., Quartini, E. (2014). “Evidence for elevated and spatially variable geothermal flux beneath the West Antarctic Ice Sheet”. *Proceedings of the National Academy of Sciences of the United States of America* 111.25, pp. 9070–9072. ISSN: 10916490. DOI: 10.1073/pnas.1405184111.
- Schroeder, W. J., Martin, K. M. (2005). *The visualization toolkit*. Tech. rep. ISBN 978-1-930934-19-1, pp. 593–614. DOI: 10.1016/B978-012387582-2/50032-0.
- Selway, K., Smirnov, M. Y., Beka, T., O’Donnell, J. P., Minakov, A., Senger, K., Faleide, J. I., Kalscheuer, T. (2020). “Magnetotelluric constraints on the temperature, composition, partial melt content and viscosity of the upper mantle beneath Svalbard”. *Geochemistry, Geophysics, Geosystems*. ISSN: 1525-2027. DOI: 10.1029/2020GC008985.
- Shannon, C. E. (1948). “A Mathematical Theory of Communication”. *Bell System Technical Journal* 27.3, pp. 379–423. ISSN: 00058580. DOI: 10.1002/j.1538-7305.1948.tb01338.x.
- Shapiro, N. M., Ritzwoller, M. H. (2002). “Monte-Carlo inversion for a global shear-velocity model of the crust and upper mantle”. *Geophysical Journal International* 151.1, pp. 88–105. ISSN: 0956540X. DOI: 10.1046/j.1365-246X.2002.01742.x.

- Shapiro, N. M., Ritzwoller, M. H. (2004). "Inferring surface heat flux distributions guided by a global seismic model: Particular application to Antarctica". *Earth and Planetary Science Letters* 223.1-2, pp. 213–224. ISSN: 0012821X. DOI: 10.1016/j.eps1.2004.04.011.
- Shaw, R. D., Wellman, P., Gunn, P., Whitaker, A. J., Tarlowski, C., Morse, M. (1996). "Australian Crustal Elements map".
- Shen, W., Wiens, D. A., Anandkrishnan, S., Aster, R. C., Gerstoft, P., Bromirski, P. D., Hansen, S. E., Dalziel, I. W., Heeszel, D. S., Huerta, A. D., Nyblade, A. A., Stephen, R., Wilson, T. J., Winberry, J. P. (2018a). "The Crust and Upper Mantle Structure of Central and West Antarctica From Bayesian Inversion of Rayleigh Wave and Receiver Functions". *Journal of Geophysical Research: Solid Earth* 123.9, pp. 7824–7849. ISSN: 21699356. DOI: 10.1029/2017JB015346.
- Shen, W., Wiens, D. A., Lloyd, A. J., Nyblade, A. A. A. (2020). "A Geothermal Heat Flux Map of Antarctica Empirically Constrained by Seismic Structure". *Geophysical Research Letters* 47.14, pp. 0–2. ISSN: 19448007. DOI: 10.1029/2020GL086955.
- Shen, W., Wiens, D. A., Stern, T., Anandkrishnan, S., Aster, R. C., Dalziel, I., Hansen, S., Heeszel, D. S., Huerta, A., Nyblade, A., Wilson, T. J., Paul Winberry, J. (2018b). "Seismic evidence for lithospheric foundering beneath the southern Transantarctic Mountains, Antarctica". *Geology* 46.1, pp. 71–74. ISSN: 19432682. DOI: 10.1130/G39555.1.
- Shepherd, A., Ivins, E. R., Geruo, A., Barletta, V. R., Bentley, M. J., Bettadpur, S., Briggs, K. H., Bromwich, D. H., Forsberg, R., Galin, N., Horwath, M., Jacobs, S., Joughin, I., King, M. A., Lenaerts, J. T., Li, J., Ligtenberg, S. R., Luckman, A., Luthcke, S. B., McMillan, M., Meister, R., Milne, G., Mouginot, J., Muir, A., Nicolas, J. P., Paden, J., Payne, A. J., Pritchard, H., Rignot, E., Rott, H., Sørensen, L. S., Scambos, T. A., Scheuchl, B., Schrama, E. J., Smith, B., Sundal, A. V., Van Angelen, J. H., Van De Berg, W. J., Van Den Broeke, M. R., Vaughan, D. G., Velicogna, I., Wahr, J., Whitehouse, P. L., Wingham, D. J., Yi, D., Young, D., Zwally, H. J. (2012). "A reconciled estimate of ice-sheet mass balance". *Science* 338.6111, pp. 1183–1189. ISSN: 10959203. DOI: 10.1126/science.1228102.
- Sheraton, J. W., Tingey, R. J., Black, L. P., Offe, L. A., Ellis, D. J. (1987). "Geology of an unusual Precambrian high-grade metamorphic terrane-Enderby Land and western Kemp Land, Antarctica". *Australian Bureau of Mineral Resources Bulletin* 223.
- Sheraton, J. W., Cundari, A. (1980a). "Leucitites from Gaussberg, Antarctica". *Contributions to Mineralogy and Petrology* 71.4, pp. 417–427. ISSN: 00107999. DOI: 10.1007/BF00374713.
- Sheraton, J. W., Offe, L. A., Tingey, R. J., Ellis, D. J. (1980b). "Enderby Land, Antarctica-an unusual Precambrian high-grade metamorphic terrain". *Journal of the Geological Society of Australia* 27.1-2, pp. 1–18. ISSN: 00167614. DOI: 10.1080/00167618008729114.

- Siddoway, C. (2008). “Tectonics of the West Antarctic Rift System: New Light on the History and Dynamics of Distributed Intracontinental Extension”. *Antarctica: A Keystone in a Changing World* January 2008, pp. 91–114.
- Siddoway, C. S., Baldwin, S. L., Fitzgerald, P. G., Fanning, C. M., Luyendyk, B. P. (2004a). “Ross sea mylonites and the timing of intracontinental extension within the West Antarctic rift system”. *Geology* 32.1, pp. 57–60. ISSN: 00917613. DOI: 10.1130/G20005.1.
- Siddoway, C. S., Richard, S. M., Fanning, C. M., Luyendyk, B. P. (2004b). “Origin and emplacement of a middle Cretaceous gneiss dome, Fosdick Mountains, West Antarctica”. *Special Paper of the Geological Society of America* 380. January, pp. 267–294. ISSN: 00721077. DOI: 10.1130/0-8137-2380-9.267.
- Siegert, M. J., Barrett, P., Deconto, R., Dunbar, R., Ó Cofaigh, C., Passchier, S., Naish, T. (2008). “Recent advances in understanding Antarctic climate evolution”. *Antarctic Science* 20.4, pp. 313–325. ISSN: 09541020. DOI: 10.1017/S0954102008000941.
- Siegert, M. J., Dowdeswell, J. A. (1996). “Spatial variations in heat at the base of the Antarctic ice sheet from analysis of the thermal regime above subglacial lakes”. *Journal of Glaciology* 42.142, pp. 501–509. ISSN: 00221430. DOI: 10.1017/S0022143000003488.
- Siegert, M. J., Ross, N., Le Brocq, A. M. (2016). “Recent advances in understanding Antarctic subglacial lakes and hydrology”. *Philosophical Transactions of the Royal Society A: Mathematical, Physical and Engineering Sciences* 374.2059, p. 20140306. ISSN: 1364503X. DOI: 10.1098/rsta.2014.0306.
- Sinem Ince, E., Barthelmes, F., Reißland, S., Elger, K., Förste, C., Flechtner, F., Schuh, H. (2019). “ICGEM – 15 years of successful collection and distribution of global gravitational models, associated services, and future plans”. *Earth System Science Data* 11.2, pp. 647–674. ISSN: 18663516. DOI: 10.5194/essd-11-647-2019.
- Slater, T., Shepherd, A., Mcmillan, M., Muir, A., Gilbert, L., Hogg, A. E., Konrad, H., Parinello, T. (2018). “A new digital elevation model of Antarctica derived from CryoSat-2 altimetry”. *Cryosphere* 12.4, pp. 1551–1562. ISSN: 19940424. DOI: 10.5194/tc-12-1551-2018.
- Sleep, N. H. (2006). “Mantle plumes from top to bottom”. *Earth-Science Reviews* 77.4, pp. 231–271. ISSN: 00128252. DOI: 10.1016/j.earscirev.2006.03.007.
- Sneeuw, N., Gelderen, M. van (1997). “The polar gap”. *Geodetic Boundary Value Problems in View of the One Centimeter Geoid*. December. Springer Berlin Heidelberg, pp. 559–568. DOI: 10.1007/bfb0011717.
- Snow, A. D., Whitaker, J., Cochran, M., Bossche, J. V. d., Mayo, C., Kloe, J. d., Karney, C., Ouzounoudis, G., Dearing, J., Lostis, G., Heitor, Filipe, May, R., Itkin, M., Couwenberg, B., Berardinelli, G., Badger, T. G., Eubank, N., Dunphy, M., Brett, M., Costa, M. A. d.,

- Evers, K., Ranalli, J., Maeyer, J. d., Popov, E., Gohlke, C., Willoughby, C., Barker, C., Wiedemann, B. M. (2020). “pyproj4/pyproj: 2.6.0 Release”. *Zenodo*. DOI: 10.5281/ZENODO.3714221.
- Spain, E. A., Johnson, S. C., Hutton, B., Whittaker, J. M., Lucieer, V., Watson, S. J., Fox, J. M., Lupton, J., Arculus, R., Bradney, A., Coffin, M. F. (2020). “Shallow Seafloor Gas emissions Near Heard and McDonald Islands on the Kerguelen Plateau, Southern Indian Ocean”. *Earth and Space Science* 7.3, pp. 0–2. ISSN: 23335084. DOI: 10.1029/2019EA000695.
- Spiegel, C., Lindow, J., Kamp, P. J., Meisel, O., Mukasa, S., Lisker, F., Kuhn, G., Gohl, K. (2016). “Tectonomorphic evolution of Marie Byrd Land – Implications for Cenozoic rifting activity and onset of West Antarctic glaciation”. *Global and Planetary Change* 145, pp. 98–115. ISSN: 09218181. DOI: 10.1016/j.gloplacha.2016.08.013.
- Stål, T. (2019a). *agrid repository*. DOI: 10.5281/zenodo.2553965.
- Stål, T. (2019b). “Conversion of geochronological data: Stacking logical matrices to generate distributions for stochastic models.” *Code*. DOI: 10.5281/zenodo.3605327.
- Stål, T., Reading, A. M. (2020a). “A Grid for Multidimensional and Multivariate Spatial Representation and Data Processing”. *Journal of Open Research Software* 8.1, pp. 1–10. ISSN: 20499647. DOI: 10.5334/jors.287.
- Stål, T., Reading, A. M. (2020b). “The probable geology of Aurora Subglacial Basin”. *In prep.*
- Stål, T., Reading, A. M., Cracknell, M. J., Morse, P., Spain, E., Veen, M. v. (2019a). “Geological mapping under Antarctic ice: A new approach to information synthesis and uncertainty representation.” *GSA SGTSG*.
- Stål, T., Reading, A. M., Halpin, J. A., Steven J, P., Whittaker, J. M., Phipps, S. J., Whittaker, J. M. (2020c). “The Antarctic Crust and Upper Mantle: A Flexible 3D Model and Software Framework for Interdisciplinary Research”. *Frontiers in Earth Science* 8.November, pp. 1–19. DOI: 10.3389/feart.2020.577502.
- Stål, T., Reading, A. M., Halpin, J. A., Whittaker, J. M. (2019b). “A computational framework and 3D model, ‘agrid’, for interdisciplinary Antarctic research.” *ISAES*. Incheon: SCAR.
- Stål, T., Reading, A. M., Halpin, J. A., Whittaker, J. M. (2019c). “A Multivariate Approach for Mapping Lithospheric Domain Boundaries in East Antarctica”. *Geophysical Research Letters* 46.17-18, pp. 10404–10416. ISSN: 19448007. DOI: 10.1029/2019GL083453.
- Stål, T., Reading, A. M., Halpin, J. A., Whittaker, J. M. (2020d). “Antarctic geothermal heat model: Aq1.” *Geochemistry, Geophysics, Geosystems*. DOI: 10.1029/2020GC009428.
- Stål, T., Reading, A. M., Halpin, J. A., Whittaker, J. (2020e). *Antarctic geothermal heat flow model: Aq1*. DOI: 10.1594/PANGAEA.924857.

- Stein, C. A. (1995). "Heat Flow of the Earth". *Global Earth Physics*, pp. 144–158. DOI: 10.1029/rf001p0144.
- Stein, S., Wysession, M. E. (2003). *An introduction to seismology, earthquakes, and earth Structure*. Vol. 84. 22. John Wiley & Sons, p. 209.
- Steinberger, B., Becker, T. W. (2018). "A comparison of lithospheric thickness models". *Tectonophysics* 746, pp. 325–338. ISSN: 00401951. DOI: 10.1016/j.tecto.2016.08.001.
- Stüwe, K., Oliver, R. (1989). "Geological history of Adélie Land and King George V Land, Antarctica: Evidence for a polycyclic metamorphic evolution". *Precambrian Research* 43.4, pp. 317–334. ISSN: 03019268. DOI: 10.1016/0301-9268(89)90063-6.
- Szwillus, W., Afonso, J. C., Ebbing, J., Mooney, W. D. (2019). "Global Crustal Thickness and Velocity Structure From Geostatistical Analysis of Seismic Data". *Journal of Geophysical Research: Solid Earth* 124.2, pp. 1626–1652. ISSN: 21699356. DOI: 10.1029/2018JB016593.
- Tapley, B., Ries, J., Bettadpur, S., Chambers, D., Cheng, M., Condi, F., Poole, S. (2007). "The GGM03 Mean Earth Gravity Model from GRACE". *AGU Fall Meeting Abstracts*. Vol. -1. m, p. 03.
- Tauxe, L., Sugisaki, S., Jiménez-Espejo, F., Escutia, C., Cook, C. P., Fliedert, T. van de, Iwai, M. (2015). "Geology of the Wilkes land sub-basin and stability of the East Antarctic Ice Sheet: Insights from rock magnetism at IODP Site U1361". *Earth and Planetary Science Letters* 412, pp. 61–69. ISSN: 0012821X. DOI: 10.1016/j.epsl.2014.12.034.
- Taylor, G. (1914). "Physiography and Glacial Geology of East Antarctica". *The Geographical Journal* 44.4, p. 365. ISSN: 00167398. DOI: 10.2307/1778593.
- Tenzer, R., Chen, W., Baranov, A., Bagherbandi, M. (2018). "Gravity Maps of Antarctic Lithospheric Structure from Remote-Sensing and Seismic Data". *Pure and Applied Geophysics* 175.6, pp. 2181–2203. ISSN: 14209136. DOI: 10.1007/s00024-018-1795-z.
- Tessensohn, F., Kleinschmidt, G., Talarico, F., Buggisch, W., Brommer, A., Henjes-Kunst, F., Kroner, U., Millar, I. L., Zeh, A. (1999). "Ross-age amalgamation of East and West Gondwana: Evidence from the Shackleton Range, Antarctica". *Terra Antarctica* 6.3-4, pp. 317–325. ISSN: 11228628.
- Thébault, E., Purucker, M., Whaler, K. A., Langlais, B., Sabaka, T. J. (2010). "The magnetic field of the Earth's lithosphere". *Space Science Reviews* 155.1-4, pp. 95–127. ISSN: 00386308. DOI: 10.1007/s11214-010-9667-6.
- Thompson, J. F., Soni, B. K., Weatherill, N. P., Llc, C. R. C. P. (1998). *Handbook of Grid Generation*. CRC press. DOI: 10.1201/9781420050349.
- Tingey, R. J., Swoboda, R., Gallagher, J. (1991). *Schematic Geological Map of Antarctica*.

- Tingey, R. J., McDougall, I., Gleadow, A. J. (1983). "The age and mode of formation of gausberg, antarctica". *Journal of the Geological Society of Australia* 30.1-2, pp. 241–246. ISSN: 00167614. DOI: 10.1080/00167618308729251.
- Tooze, S., Halpin, J. A., Noble, T. L., Chase, Z., O'Brien, P. E., Armand, L. (2020). "Scratching the surface: a marine sediment provenance record from the continental slope of central Wilkes Land, East Antarctica". *Geochemistry, Geophysics, Geosystems*, pp. 1–23. ISSN: 1525-2027. DOI: 10.1029/2020gc009156.
- Torsvik, T. H., Gaina, C., Redfield, T. F. (2008). "Antarctica and Global Paleogeography: From Rodinia, Through Gondwanaland and Pangea, to the Birth of the Southern Ocean and the Opening of Gateways". *Antarctica: A Keystone in a Changing World - Online Proceedings for the 10th International Symposium on Antarctic Earth Sciences* 1047.KP11, pp. 125–140. DOI: 10.3133/of2007-1047.kp11.
- Torsvik, T. H., Steinberger, B., Gurnis, M., Gaina, C. (2010). "Plate tectonics and net lithosphere rotation over the past 150 My". *Earth and Planetary Science Letters* 291.1-4, pp. 106–112. ISSN: 0012821X. DOI: 10.1016/j.epsl.2009.12.055.
- Tsuboi, S., Kikuchi, M., Yamanaka, Y., Kanao, M. (2000). "The March 25,1998 Antarctic Earthquake: Great earthquake caused by postglacial rebound". *Earth, Planets and Space* 52.2, pp. 133–136. ISSN: 18805981. DOI: 10.1186/BF03351621.
- Tucker, N. M., Payne, J. L., Clark, C., Hand, M., Taylor, R. J., Kylander-Clark, A. R., Martin, L. (2017). "Proterozoic reworking of Archean (Yilgarn) basement in the Bunger Hills, East Antarctica". *Precambrian Research* 298, pp. 16–38. ISSN: 03019268. DOI: 10.1016/j.precamres.2017.05.013.
- Tulaczyk, S. M., Scherer, R. P., Clark, C. D. (2001). "A ploughing model for the origin of weak tills beneath ice streams: a qualitative treatment". *Quaternary International* 86.1, pp. 59–70. DOI: 10.1016/s1040-6182(01)00050-7.
- Turner, R. J., Reading, A. M., King, M. A. (2020). "Separation of tectonic and local components of horizontal GPS station velocities: a case study for glacial isostatic adjustment in East Antarctica". *Geophysical Journal International* 222.3, pp. 1555–1569. ISSN: 0956-540X. DOI: 10.1093/gji/ggaa265.
- Uieda, L. (2018). "Verde: Processing and gridding spatial data using Green's functions". *Journal of Open Source Software* 3.30, p. 957. ISSN: 2475-9066. DOI: 10.21105/joss.00957.
- Van Der Walt, S., Colbert, S. C., Varoquaux, G. (2011). "The NumPy array: A structure for efficient numerical computation". *Computing in Science and Engineering* 13.2, pp. 22–30. ISSN: 15219615. DOI: 10.1109/MCSE.2011.37.

- Van Liefferinge, B., Pattyn, F. (2013). "Using ice-flow models to evaluate potential sites of million year-old ice in Antarctica". *Climate of the Past* 9.5, pp. 2335–2345. ISSN: 18149324. DOI: 10.5194/cp-9-2335-2013.
- Van Liefferinge, B., Pattyn, F., Cavitte, M. G., Karlsson, N. B., Young, D. A., Sutter, J., Eisen, O. (2018). "Promising oldest ice sites in east antarctica based on thermodynamical modelling". *Cryosphere* 12.8, pp. 2773–2787. ISSN: 19940424. DOI: 10.5194/tc-12-2773-2018.
- Veevers, J. J. (2012). "Reconstructions before rifting and drifting reveal the geological connections between Antarctica and its conjugates in Gondwanaland". *Earth-Science Reviews* 111.3-4, pp. 249–318. ISSN: 00128252. DOI: 10.1016/j.earscirev.2011.11.009.
- Velicogna, I. (2009). "Increasing rates of ice mass loss from the {Greenland} and Antarctic ice sheets revealed by {GRACE}". *Geophysical Research Letters* 36.19.
- Visser, P. N. (1999). "Gravity field determination with GOCE and GRACE". *Advances in Space Research* 23.4, pp. 771–776. ISSN: 02731177. DOI: 10.1016/S0273-1177(99)00154-4.
- Von Frese, R. R., Kim, H. R., Leftwich, T. E., Kim, J. W., Golynsky, A. V. (2013). "Satellite magnetic anomalies of the Antarctic Wilkes Land impact basin inferred from regional gravity and terrain data". *Tectonophysics* 585. February, pp. 185–195. ISSN: 00401951. DOI: 10.1016/j.tecto.2012.09.009.
- Wang, C. C., Jacobs, J., Elburg, M. A., Läufer, A., Elvevold, S. (2020). "Late Neoproterozoic–Cambrian magmatism in Dronning Maud Land (East Antarctica): U–Pb zircon geochronology, isotope geochemistry and implications for Gondwana assembly". *Precambrian Research* 350. July, p. 105880. ISSN: 03019268. DOI: 10.1016/j.precamres.2020.105880.
- Wannamaker, P., Hill, G., Stodt, J., Maris, V., Ogawa, Y., Selway, K., Boren, G., Bertrand, E., Uhlmann, D., Ayling, B., Green, A. M., Feucht, D. (2017). "Uplift of the central transantarctic mountains". *Nature Communications* 8.1, p. 1588. ISSN: 20411723. DOI: 10.1038/s41467-017-01577-2.
- Wareham, C. D., Pankhurst, R. J., Thomas, R. J., Storey, B. C., Grantham, G. H., Jacobs, J., Eglinton, B. M. (1998). "Pb, Nd, and Sr Isotope Mapping of Grenville-Age Crustal Provinces in Rodinia". *The Journal of Geology* 106.6, pp. 647–660. ISSN: 0022-1376. DOI: 10.1086/516051.
- Warmerdam, F., Contributors, G. (2018). *GDAL/OGR Geospatial Data Abstraction Library*.
- Waskom, M., Botvinnik, O., Ostblom, J., Lukauskas, S., Hobson, P., MaozGelbart, Gemperline, D. C., Augspurger, T., Halchenko, Y., Cole, J. B., Warmenhoven, J., Ruiter, J. D., Pye, C., Hoyer, S., Vanderplas, J., Villalba, S., Kunter, G., Quintero, E., Bachant, P., Martin, M., Meyer, K., Corban Swain, Miles, A., Brunner, T., O’Kane, D., Yarkoni, T., Williams,

- M. L., Evans, C. (2020). *mwaskom/seaborn: v0.10.0 (January 2020)*. DOI: 10.5281/ZENODO.592845.
- Watson, C., Burgette, R., Tregoning, P., White, N., Hunter, J., Coleman, R., Handsworth, R., Broksma, H. (2010). "Twentieth century constraints on sea level change and earthquake deformation at Macquarie Island". *Geophysical Journal International* 182.2, pp. 781–796. ISSN: 0956540X. DOI: 10.1111/j.1365-246X.2010.04640.x.
- Watson, S. J., Whittaker, J. M., Halpin, J. A., Williams, S. E., Milan, L. A., Daczko, N. R., Wyman, D. A. (2016). "Tectonic drivers and the influence of the Kerguelen plume on seafloor spreading during formation of the early Indian Ocean". *Gondwana Research* 35, pp. 97–114. ISSN: 1342937X. DOI: 10.1016/j.gr.2016.03.009.
- Watson, T., Nyblade, A., Wiens, D. A., Anandakrishnan, S., Benoit, M., Shore, P. J., Voigt, D., VanDecar, J. (2006). "P and S velocity structure of the upper mantle beneath the Transantarctic Mountains, East Antarctic craton, and Ross Sea from travel time tomography". *Geochemistry, Geophysics, Geosystems* 7.7, n/a–n/a. ISSN: 15252027. DOI: 10.1029/2005GC001238.
- Wellmann, J. (2013). "Information Theory for Correlation Analysis and Estimation of Uncertainty Reduction in Maps and Models". *Entropy* 15.12, pp. 1464–1485. ISSN: 1099-4300. DOI: 10.3390/e15041464.
- Wellmann, J. F., Regenauer-Lieb, K. (2012). "Uncertainties have a meaning: Information entropy as a quality measure for 3-D geological models". *Tectonophysics* 526-529, pp. 207–216. ISSN: 00401951. DOI: 10.1016/j.tecto.2011.05.001.
- White, D. A., Fink, D., Gore, D. B. (2010). "Cosmogenic nuclide evidence for enhanced sensitivity of an East Antarctic ice stream to change during the last deglaciation". *Geology* 39.1, pp. 23–26. ISSN: 00917613. DOI: 10.1130/g31591.1.
- Whitehouse, P. L. (2018). "Glacial isostatic adjustment modelling: Historical perspectives, recent advances, and future directions". *Earth Surface Dynamics* 6.2, pp. 401–429. ISSN: 2196632X. DOI: 10.5194/esurf-6-401-2018.
- Whitehouse, P. L., Bentley, M. J., Milne, G. A., King, M. A., Thomas, I. D. (2012). "A new glacial isostatic adjustment model for Antarctica: Calibrated and tested using observations of relative sea-level change and present-day uplift rates". *Geophysical Journal International* 190.3, pp. 1464–1482. ISSN: 0956540X. DOI: 10.1111/j.1365-246X.2012.05557.x.
- Whitehouse, P. L., Gomez, N., King, M. A., Wiens, D. A. (2019). "Solid Earth change and the evolution of the Antarctic Ice Sheet". *Nature Communications* 10.1, p. 503. ISSN: 20411723. DOI: 10.1038/s41467-018-08068-y.
- Whitehouse, P., Latychev, K., Milne, G. A., Mitrovica, J. X., Kendall, R. (2006). "Impact of 3-D Earth structure on Fennoscandian glacial isostatic adjustment: Implications for space-

- geodetic estimates of present-day crustal deformations". *Geophysical Research Letters* 33.13, pp. 3–7. ISSN: 00948276. DOI: 10.1029/2006GL026568.
- Whittaker, J. M., Müller, R. D., Sdrolias, M., Heine, C. (2007). "Sunda-Java trench kinematics, slab window formation and overriding plate deformation since the Cretaceous". *Earth and Planetary Science Letters* 255.3-4, pp. 445–457. ISSN: 0012821X. DOI: 10.1016/j.epsl.2006.12.031.
- Whittaker, J. M., Goncharov, A., Williams, S. E., Müller, R. D., Leitchenkov, G. (2013a). "Global sediment thickness data set updated for the Australian-Antarctic Southern Ocean". *Geochemistry, Geophysics, Geosystems* 14.8, pp. 3297–3305. ISSN: 15252027. DOI: 10.1002/ggge.20181.
- Whittaker, J. M., Williams, S. E., Müller, R. D. (2013b). "Revised tectonic evolution of the Eastern Indian Ocean". *Geochemistry, Geophysics, Geosystems* 14.6, pp. 1891–1909. ISSN: 15252027. DOI: 10.1002/ggge.20120.
- Wiens, D. A. (2003). "Broadband Seismology in Antarctica : Recent Progress and Plans for the International Polar Year Recent Advances – the TAMSEIS project". *Proc. Inter. Symp.-Asian Collaboration in IPY 2007-2008*. Figure 1, pp. 21–24.
- Wilkinson, M. D., Dumontier, M., Aalbersberg, I. J., Appleton, G., Axton, M., Baak, A., Blomberg, N., Boiten, J.-W., Silva Santos, L. B. da, Bourne, P. E., Bouwman, J., Brookes, A. J., Clark, T., Crosas, M., Dillo, I., Dumon, O., Edmunds, S., Evelo, C. T., Finkers, R., Gonzalez-Beltran, A., Gray, A. J., Groth, P., Goble, C., Grethe, J. S., Heringa, J., 't Hoen, P. A., Hooft, R., Kuhn, T., Kok, R., Kok, J., Lusher, S. J., Martone, M. E., Mons, A., Packer, A. L., Persson, B., Rocca-Serra, P., Roos, M., Schaik, R. van, Sansone, S.-A., Schultes, E., Sengstag, T., Slater, T., Strawn, G., Swertz, M. A., Thompson, M., Lei, J. van der, Mulligen, E. van, Velterop, J., Waagmeester, A., Wittenburg, P., Wolstencroft, K., Zhao, J., Mons, B. (2016). "The FAIR Guiding Principles for scientific data management and stewardship". *Scientific Data* 3.1, p. 160018. ISSN: 2052-4463. DOI: 10.1038/sdata.2016.18.
- Will, T. M., Frimmel, H. E., Zeh, A., Le Roux, P., Schmädicke, E. (2010). "Geochemical and isotopic constraints on the tectonic and crustal evolution of the Shackleton Range, East Antarctica, and correlation with other Gondwana crustal segments". *Precambrian Research* 180.1-2, pp. 85–112. ISSN: 03019268. DOI: 10.1016/j.precamres.2010.03.005.
- Will, T. M., Zeh, A., Gerdes, A., Frimmel, H. E., Millar, I. L., Schmädicke, E. (2009). "Palaeoproterozoic to Palaeozoic magmatic and metamorphic events in the Shackleton Range, East Antarctica: Constraints from zircon and monazite dating, and implications for the amalgamation of Gondwana". *Precambrian Research* 172.1-2, pp. 25–45. ISSN: 03019268. DOI: 10.1016/j.precamres.2009.03.008.

- Williams, M. A., Kelsey, D. E., Hand, M., Raimondo, T., Morrissey, L. J., Tucker, N. M., Dutch, R. A. (2018). “Further evidence for two metamorphical events in the Mawson Continent”. *Antarctic Science* 30.1, pp. 44–65. ISSN: 13652079. DOI: 10.1017/S0954102017000451.
- Williams, S. E., Whittaker, J. M., Halpin, J. A., Müller, R. D. (2019). “Australian-Antarctic breakup and seafloor spreading: Balancing geological and geophysical constraints”. *Earth-Science Reviews* 188.June 2018, pp. 41–58. ISSN: 00128252. DOI: 10.1016/j.earscirev.2018.10.011.
- Williams, S. E., Whittaker, J. M., Müller, R. D. (2011). “Full-fit, palinspastic reconstruction of the conjugate Australian-Antarctic margins”. *Tectonics* 30.6, pp. 1–21. ISSN: 02787407. DOI: 10.1029/2011TC002912.
- Williams, S. E., Joanne Whittaker, P. D., Halpin, J. A., Müller, D. (2016). “A recipe for balancing geological and geophysical constraints to derive continental fit reconstructions”. *Manuscript for submission*.
- Wilson, D. S., Jamieson, S. S., Barrett, P. J., Leitchenkov, G., Gohl, K., Larter, R. D. (2012). “Antarctic topography at the Eocene-Oligocene boundary”. *Palaeogeography, Palaeoclimatology, Palaeoecology* 335-336, pp. 24–34. ISSN: 00310182. DOI: 10.1016/j.palaeo.2011.05.028.
- Wilson, G., Aruliah, D. A., Brown, C. T., Chue Hong, N. P., Davis, M., Guy, R. T., Haddock, S. H., Huff, K. D., Mitchell, I. M., Plumbley, M. D., Waugh, B., White, E. P., Wilson, P. (2014). “Best Practices for Scientific Computing”. *PLoS Biology* 12.1, e1001745. ISSN: 15457885. DOI: 10.1371/journal.pbio.1001745.
- Winberry, J. P., Anandakrishnan, S. (2004). “Crustal structure of the West Antarctic rift system and Marie Byrd Land hotspot”. *Geology* 32.11, pp. 977–980. ISSN: 00917613. DOI: 10.1130/G20768.1.
- Winkelmann, R., Martin, M. A., Haseloff, M., Albrecht, T., Bueler, E., Khroulev, C., Levermann, A. (2011). “The Potsdam Parallel Ice Sheet Model (PISM-PIK) - Part 1: Model description”. *Cryosphere* 5.3, pp. 715–726. ISSN: 19940416. DOI: 10.5194/tc-5-715-2011.
- Wombacher, F., Münker, C. (2000). “Pb, Nd, and Sr Isotopes and REE Systematics of Cambrian Sediments from New Zealand: Implications for the Reconstruction of the Early Paleozoic Gondwana Margin along Australia and Antarctica”. *The Journal of Geology* 108.6, pp. 663–686. ISSN: 0022-1376. DOI: 10.1086/317950.
- Wright, A. P., Young, D. A., Roberts, J. L., Schroeder, D. M., Bamber, J. L., Dowdeswell, J. A., Young, N. W., Le Brocq, A. M., Warner, R. C., Payne, A. J., Blankenship, D. D., Van Ommen, T. D., Siegert, M. J. (2012). “Evidence of a hydrological connection between the ice divide and ice sheet margin in the Aurora Subglacial Basin, East Antarctica”. *Journal*

- of Geophysical Research: Earth Surface* 117.1, pp. 1–15. ISSN: 21699011. DOI: 10.1029/2011JF002066.
- Wright, R., Pilger, E. (2008). “Radiant flux from Earth’s subaerially erupting volcanoes”. *International Journal of Remote Sensing* 29.22, pp. 6443–6466. ISSN: 0143-1161. DOI: 10.1080/01431160802168210.
- Wyk de Vries, M. van, Bingham, R. G., Hein, A. S. (2018). “A new volcanic province: An inventory of subglacial volcanoes in West Antarctica”. *Geological Society Special Publication* 461.1, pp. 231–248. ISSN: 03058719. DOI: 10.1144/SP461.7.
- Xu, Y., Shankland, T. J., Linhardt, S., Rubie, D. C., Langenhorst, F., Klasinski, K. (2004). “Thermal diffusivity and conductivity of olivine, wadsleyite and ringwoodite to 20 GPa and 1373 K”. *Physics of the Earth and Planetary Interiors* 143.1-2, pp. 321–336. ISSN: 00319201. DOI: 10.1016/j.pepi.2004.03.005.
- Yakymchuk, C., Brown, C. R., Brown, M., Siddoway, C. S., Fanning, C. M., Korhonen, F. J. (2015). “Paleozoic evolution of western Marie Byrd Land, Antarctica”. *Bulletin of the Geological Society of America* 127.9-10, pp. 1464–1484. ISSN: 19432674. DOI: 10.1130/B31136.1.
- Yoshida, M., Funaki, M., Vitanage, P. W. (1992). “Proterozoic to Mesozoic East Gondwana: The juxtaposition of India, Sri Lanka, and Antarctica”. *Tectonics* 11.2, pp. 381–391. ISSN: 19449194. DOI: 10.1029/91TC02386.
- Yoshida, M., Jacobs, J., Santosh, M., Rajesh, H. M. (2003). “Role of Pan-African events in the Circum-East Antarctic Orogen of East Gondwana: A critical overview”. *Geological Society Special Publication* 206.1, pp. 57–75. ISSN: 03058719. DOI: 10.1144/GSL.SP.2003.206.01.05.
- Young, D. A., Wright, A. P., Roberts, J. L., Warner, R. C., Young, N. W., Greenbaum, J. S., Schroeder, D. M., Holt, J. W., Sugden, D. E., Blankenship, D. D., Van Ommen, T. D., Siegert, M. J. (2011). “A dynamic early East Antarctic Ice Sheet suggested by ice-covered fjord landscapes”. *Nature* 474.7349, pp. 72–75. ISSN: 00280836. DOI: 10.1038/nature10114.
- Zadeh, L. A. (1965). “Fuzzy Sets”. *Information and control* 8.1, pp. 338–353. ISSN: 11254653.
- Zhao, G., Sun, M., Wilde, S. A., Li, S. (2004). “A Paleo-Mesoproterozoic supercontinent: assembly, growth and breakup”. *Earth-Science Reviews* 67.1-2, pp. 91–123. ISSN: 00128252. DOI: 10.1016/j.earscirev.2004.02.003.
- Zwally, J. H., Giovinetto, M. B., Beckley, M. A., Saba, J. L. (2012). “Antarctic and Greenland Drainage System”. *GSFC Cryospheric Sciences Laboratory* 1, pp. 2–7.

Appendix A

Chapter 3 Supplementary Material: The Antarctic Crust and Upper Mantle

A.1 Geological samples

The spatial distribution of geological and geochemical samples available for Antarctica is uneven (Fig. A.1).

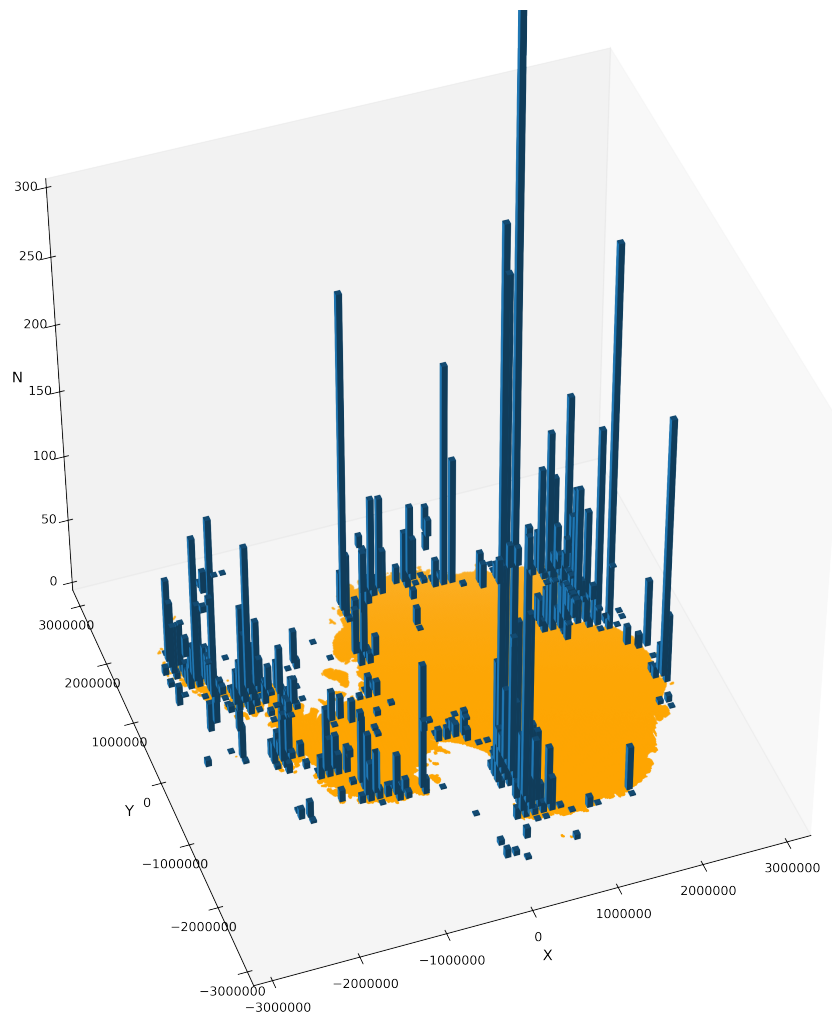


Figure A.1: Number of samples per 100×100 km bin in the compilation of Gard et al. (2019).

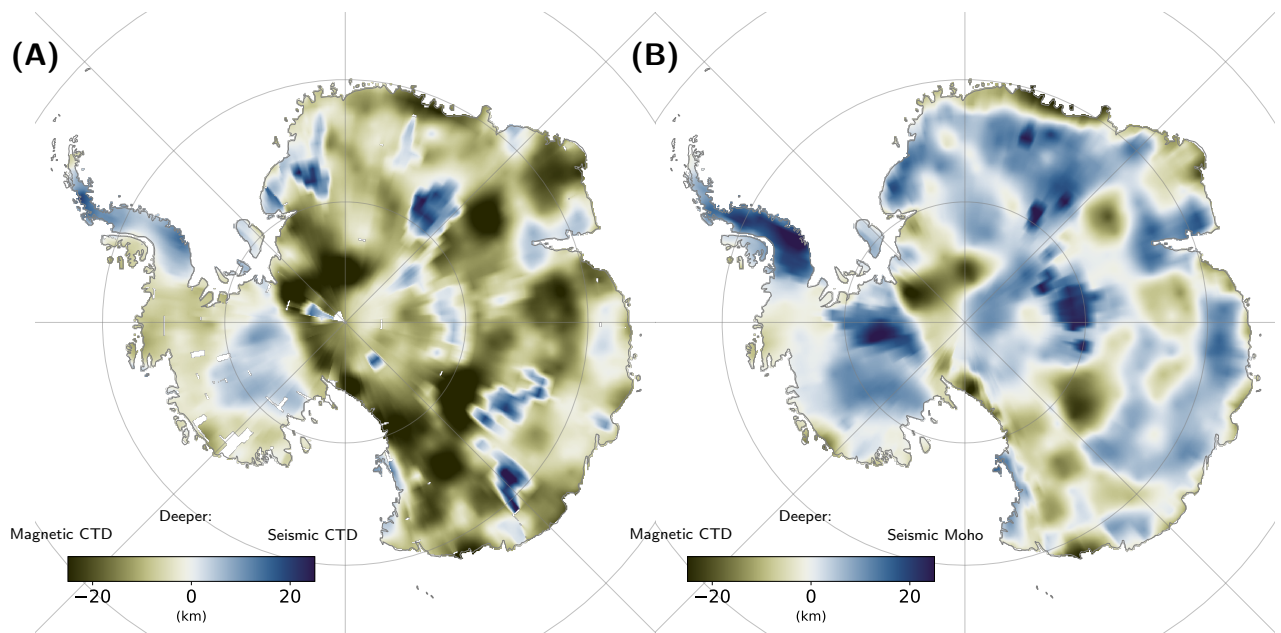


Figure A.2: Illustration of framework capability to compare and appraise different models: (A) Comparison of Curie temperature depth (CTD) from magnetic and seismic studies; CTD derived from seismic study (An et al., 2015b) minus CTD from magnetic study (Martos et al., 2017). Magnetic CTD is deeper at negative values (green), and seismic CTD is deeper at positive values (blue). (B) Comparison of CTD from magnetic study and seismic tomography derived Moho, constrained by receiver function studies; Moho depth (An et al., 2015a) minus magnetic CTD (Martos et al., 2017). Magnetic CTD is deeper at negative values (green), the Moho is deeper at positive values (blue).

A.2 Moho and Curie Temperature depth

Figure A.2A shows the difference between a Curie temperature depth (CTD) derived from seismic constraints (An et al., 2015b) and a magnetic derived estimate (Martos et al., 2017). When expressed in kilometres, we see that the larger disagreements occur in East Antarctica. In the green colored areas, such as for the Transantarctic Mountains, the magnetic model suggests a deeper isotherm. This can either indicate overestimated temperatures from the seismic model, or an overestimation of the CTD in the magnetic study. In blue areas, the seismic CTD is deeper than the magnetically derived isotherm. This is caused either by the temperature in the seismic model being underestimated, or the magnetic derived isotherm being too shallow. Figure A.2B similarly shows the difference between the seismic Moho (An et al., 2015b) and the CTD from magnetic constraints, 'the magnetic Moho' (Martos et al., 2017). Notably, we have generally a closer agreement, and the pattern is different from figure A.2A. This suggests that the magnetic method is sensitive to the seismic Moho rather than the temperature isotherm, as the Curie temperature isotherm has no direct impact on elastic properties.

A.3 Ternary maps

We demonstrate the capability to visualise multivariate data through the construction and use of ternary images from three colour renderings. Such renderings can assist in segmentation of the crust and pattern recognition, and suggest a highly heterogeneous Antarctic interior, more complex than suggested in many previous studies.

Three-colour renderings are produced using RGB channels, with each band (RGB) representing a dataset. Three examples are provided. The values are not directly meaningful, but the color representation can reveal contrasts in lithospheric properties.

Each dataset (D) is standardised:

$$D_S = \frac{D - \bar{D}}{s(D)} \quad (\text{A.1})$$

Where \bar{D} is the average value, $s(D)$ is the standard deviation for D , and D_S is the standardised data set. To enhance the visualisation, the dataset is clipped at the 5% percentile and 95% percentile of the standardised values. Missing data in one of the three datasets are removed from all three to provide a consistent color rendering.

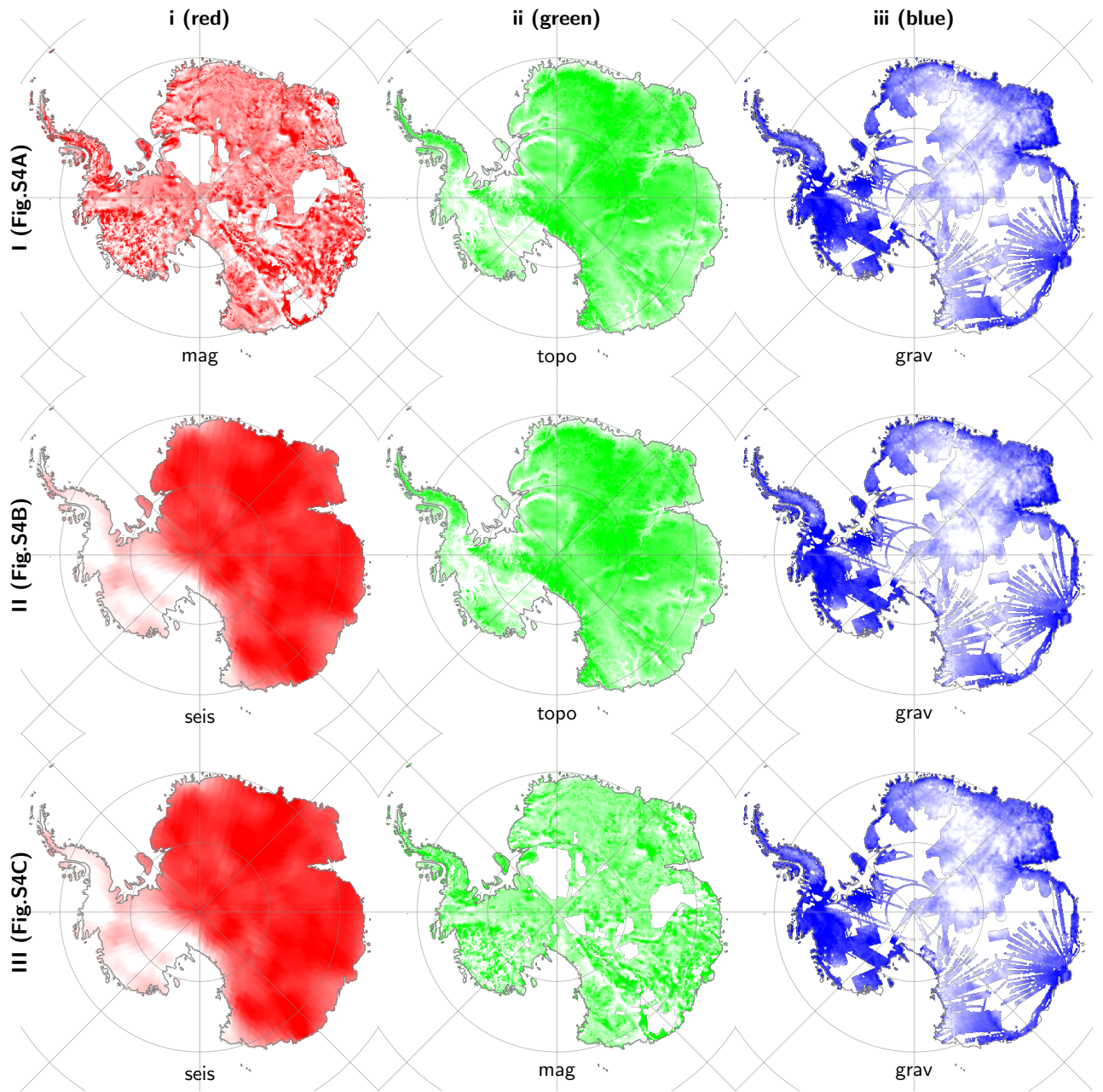


Figure A.3: (Caption next page.)

Figure A.3: Illustration of framework capability to visualise multivariate data. Three-colour rendering of input data for fig. C2. The rows represents the sub-figures (fig. S3: A, B, and C), and the columns (i, ii, iii) represent the datasets used. Shown standardized and clipped, as described in text. Upper row: input to figure S3A, Magnetic-Topography-Gravity. (i) Total magnetic intensity (Golynsky et al., 2018) in red, (ii) Subglacial topography (Fretwell et al., 2012) in green, (iii) Bouguer gravity (Scheinert et al., 2016) in blue. Middle row: input to figure S3B, Seismic-Topography-Gravity. (i) Seismic wave speed at 100km depth (An et al., 2015a) in red, (ii) Subglacial topography (Fretwell et al., 2012) in green, (iii) Bouguer gravity (Scheinert et al., 2016) in blue. Lower row: input to figure S3C, Seismic-Magnetic-Gravity. (i) Seismic wave speed at 100km depth (An et al., 2015a) in red, (ii) Total magnetic intensity (Golynsky et al., 2018) in green, (iii) Bouguer gravity (Scheinert et al., 2016) in blue.

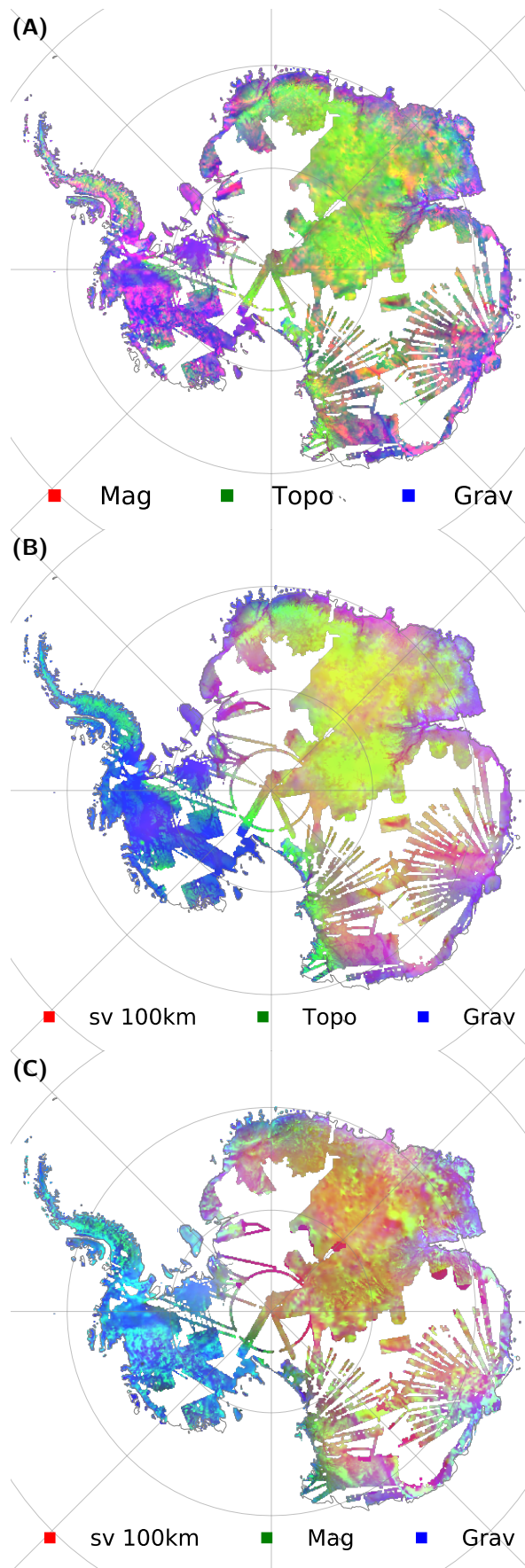


Figure A.4: (Caption next page.)

Figure A.4: Ternary plots as an illustration of framework capability to visualise multivariate data. (A) Three colour rendering of the relation between the total magnetic intensity (Golynsky et al., 2018) in red, subglacial topography (Fretwell et al., 2012) in green with isostatic correction (figure and discussion in main article), and Bouguer gravity (Scheinert et al., 2016) in blue. (B) Three colour rendering of the relation between the seismic wave speed at 100 km depth (An et al., 2015a) in red, subglacial topography (Fretwell et al., 2012) in green and Bouguer gravity (Scheinert et al., 2016) in blue. (C) Three colour rendering of the relation between the seismic wave speed at 100km depth (An et al., 2015a) in red, magnetic intensity (Golynsky et al., 2018) in green, and Bouguer gravity (Scheinert et al., 2016) in blue. All datasets are individually standardised and clipped, as described in text.

A.4 Short User Guide to agrid

In this supplementary section, we provide a short user guide for *agrid*. We provide a synthetic example to introduce the basic use of the software.

A.4.1 Installation

There are many options to access the code:

1. Download the module directly from GitHub and incorporate into your project with a relative path to the module used. Alternatively, a subset of the provided methods can be copied into a project:

```
https://github.com/TobbeTripitaka/agrid/tree/master/agrid
```

2. Clone the Git repository:

```
$ git clone https://github.com/tobbetripitaka/agrid
```

3. Install with PIP:

```
$ pip install agrid
```

4. Conda users can also use anaconda installer (presently only OSX):

```
$ conda install -c tobbetripitaka agrid
```

5. Use the Virtual Machine provided

```
https://www.dropbox.com/s/1qp4ddlvjoyfwwq/agrid_ubuntu-disk001.vmdk?dl=1
```

Now, we can test the installation by setting up a grid model of, for example, Antarctica:

```

1 # Python 3
2 from agrid.grid import Grid
3 from agrid.acc import download
4
5 km = 1000
6 ant = Grid(crs=3031, res = [25*km, 25*km],
7           left = -3100*km, up=3100*km,
8           right = 3100*km, down = -3100*km)
9 print('Number of cells in X, Y, Z directions:', ant.nnn)

```

Listing A.1: Setting up a grid model.

We have now defined a Grid object that contains variable that defines or model. For example `ant.nn` returns a tuple of the horizontal size of the grid, and `ant.nx` returns the number of cells along x-axis.

We also generated a dataset, `ant.ds`, that is used to contain arrays and metadata. It also contains coordinates and dimension data:

```

1 print(ant.ds)
2
3 <xarray.Dataset>
4 Dimensions:  (RGB: 3, X: 248, X_edge: 249, Y: 248, Y_edge: 249, Z: 5, Z_edge: 6)
5 Coordinates:
6   * X          (X) float32  -3100000.0 -3074898.8 ... 3074898.8 3100000.0
7   * Y          (Y) float32  -3100000.0 -3074898.8 ... 3074898.8 3100000.0
8   * Z          (Z) float32   0.0 8000.0 16000.0 40000.0 350000.0
9   * X_edge     (X_edge) float32 -3112500.0 -3087399.2 ... 3087399.2 3112500.0
10  * Y_edge     (Y_edge) float32 -3112500.0 -3087399.2 ... 3087399.2 3112500.0
11  * Z_edge     (Z_edge) float64 -4e+03 4e+03 1.2e+04 2.8e+04 1.95e+05 5.05e+05
12  * RGB        (RGB) <U1 'R' 'G' 'B'
13   XV         (Y, X) float32 -3100000.0 -3074898.8 ... 3074898.8 3100000.0
14   YV         (Y, X) float32 -3100000.0 -3100000.0 ... 3100000.0 3100000.0
15   lat        (Y, X) float32 -51.15066 -51.296318 ... -51.296318 -51.15066
16   lon        (Y, X) float32 -135.0 -135.23291 -135.46771 ... 44.76709 45.0
17 Data variables:
18   *empty*

```

Listing A.2: ant.ds content.

X, Y are coordinates for center points of grid cells, and `_edge` are the corners between the cells. XV, YV are 2D grids that contain coordinates for each cell in used projection. Similarly, lat and lon contains geographical coordinates for each grid cell. There are no data variables yet.

Numpy arrays can be assigned to the grid:

```

1 import numpy as np
2 checkerboard = np.kron([[1, 0] * 4, [0, 1] * 4] * 4,
3                       np.ones(np.array(ant.nn)//8))
4 ant.ds['CHESS'] = (('Y', 'X'), checkerboard)
5 ant.map_grid(checkerboard, save_name='chess.pdf')

```

Listing A.3: Make synthetic data.

Note that the grid data array is defined in order Y, X, as the coordinates refers to rows and columns of for 2D arrays.

Online data sources can be linked to the grid, and are only downloaded once, unless specified. The `meta_dict` variable adds meta data to the array. The `assign_shape` method assigns polygon vector data file to the grid, using attribute data. Here, we generate a Boolean map:

```

1 url_land_polygon = ('https://www.naturalearthdata.com/'
2                    'http://www.naturalearthdata.com/'
3                    'download/10m/physical/ne_10m_land.zip')
4 download(url_land_polygon,
5          'ne_10m_land.zip',
6          meta_dict={'Type' : 'Land Polygons'})
7 ant.ds['LAND'] = (('Y', 'X'),
8                 -1 < ant.assign_shape('ne_10m_land.shp', 'scalerank'))
9 ant.ds['LAND'] = ant.ds['LAND'].where(ant.ds['LAND']) # Assigns not a number

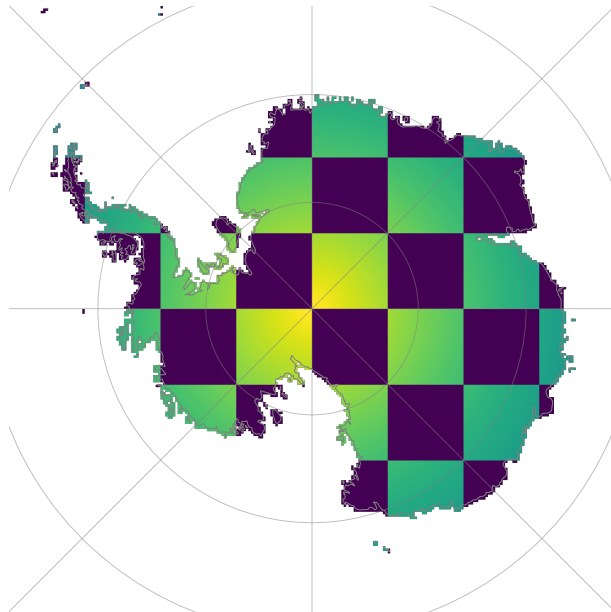
```

Listing A.4: Import data.

The framework allows computations to be defined with just a few lines of code:

```
1 example = ant.ds['LAND']*ant.ds['CHESS']*ant.ds.coords['lat']
2 ant.map_grid(example, cmap='viridis',
3               vmin = -90, vmax=-60,
4               save_name='fig/quick_guide.pdf')
```

Listing A.5: Make map.



A.4.2 Further resources

- Software paper in Journal of Open Research Software (Stål et al., 2020a).
- Tutorials at <https://github.com/TobbeTripitaka/agrid/tree/master/tutorials>
- Code to reproduce this paper and additional links at https://github.com/TobbeTripitaka/ant_lithosphere

A.4.3 Version compatibility.

This short guide refers to version 0.3.x. Complete backward compatibility might not be supported in future releases, however; v. 0.3.x will be kept, and maintained.

Appendix B

Chapter 4 Supplementary Material: "A Multivariate Approach for Mapping Lithospheric Domain Boundaries in East Antarctica"

Results for Australia In this supplement, we apply the multivariate method to the investigation of lithospheric boundaries in Australia. Compared to East Antarctica, the large-scale tectonic structure of Australia is relatively well known. Hence, this investigation provides us a reference study for the methods used.

B.1 Data

We use the following datasets: seismic wavespeed (SV at 150 km) from AuSREM (Kennett et al., 2013); free air gravity anomaly (Bacchin et al., 2008); and elevation model (Australia, 2017). A detailed survey of geophysical data coverage of Australia is provided by Kennett et al. (2018) and references therein.

B.2 Methods

All methods used to prepare and process the data are the same as for the Antarctic example, as described in the methods section. Datasets are subsampled for comparison with the Antarctic example, and the same Gaussian kernels as for Antarctica are used for each model, even though higher resolution data are available for the Australian continent. We acknowledge that bias from previous knowledge could influence the line picking, but we attempt to keep the picking process objective, as noted in the main text. GDA94 / Australian Albers projected coordinate reference system (EPSG:3577) is used for picking and processing.

B.3 Results and Discussion

The six resulting likelihood maps from the multivariate approach are shown in Figure B.1 and Figure B.2, with comments provided in Table B.1. We compare the lithospheric boundaries that we infer with Australia (2010), Betts et al. (2002), Cawood et al. (2008), Korsch et al. (2016), and Myers et al. (1996). The geological comparison interpretations themselves contain inferred and interpolated boundaries, but serve as a geologically based model for reference to assess the likelihood maps. Many boundaries are well detected in the maps, especially where old cratonic lithosphere meets younger orogenic belts. However, boundaries between orogens are less pronounced. We note that some boundaries are blurred by subsampling the Australian datasets to match the Antarctic example.

Sum (Fig. B.1 A) and union (Fig. B.1 B) are the method combinations that suggest the highest number of likely boundaries. An intermediate result is given by squared sum (Fig. B.1 C) and intersect (Fig. B.1 D). The most conservative results, suggesting fewest lithospheric boundaries, are product (Fig. B.1 E) and squared intersect (Fig. B.1 F). Conservative combinations indicate high likelihood for the existence of actual lithospheric boundaries with reduced false positive detection.

In summary, the Australian example shows the power of the multivariate method to reveal lithospheric boundaries and also provides insight into which tectonic boundaries might not be well captured by the method.

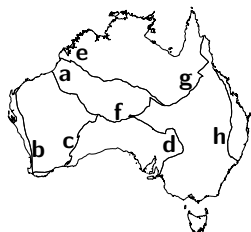
	Sum	Union	Squared Sum	Intersect	Product	Squared intersect
Pilbara Craton (a)	●	●	●	●	*	*
Darling Fault (b)	●	●	●	●	●	●
Yilgarn Craton / Albany - Fraser Orogen (c)	●	●	●	●	*	
Gawler Craton (d)	*	*	*	*	●	●
Kimberley Craton (e)	●	●	●	●	●	●
Musgrave Block (f)	·	·	●	●	·	·
Northern Tasman Line (g)	●	●	*	*		
New England Orogen (h)	*	*	*	*	*	·

Table B.1: Description of some of the main lithospheric features in Australia and the rate of success (● well captured, * captured, · poorly captured).

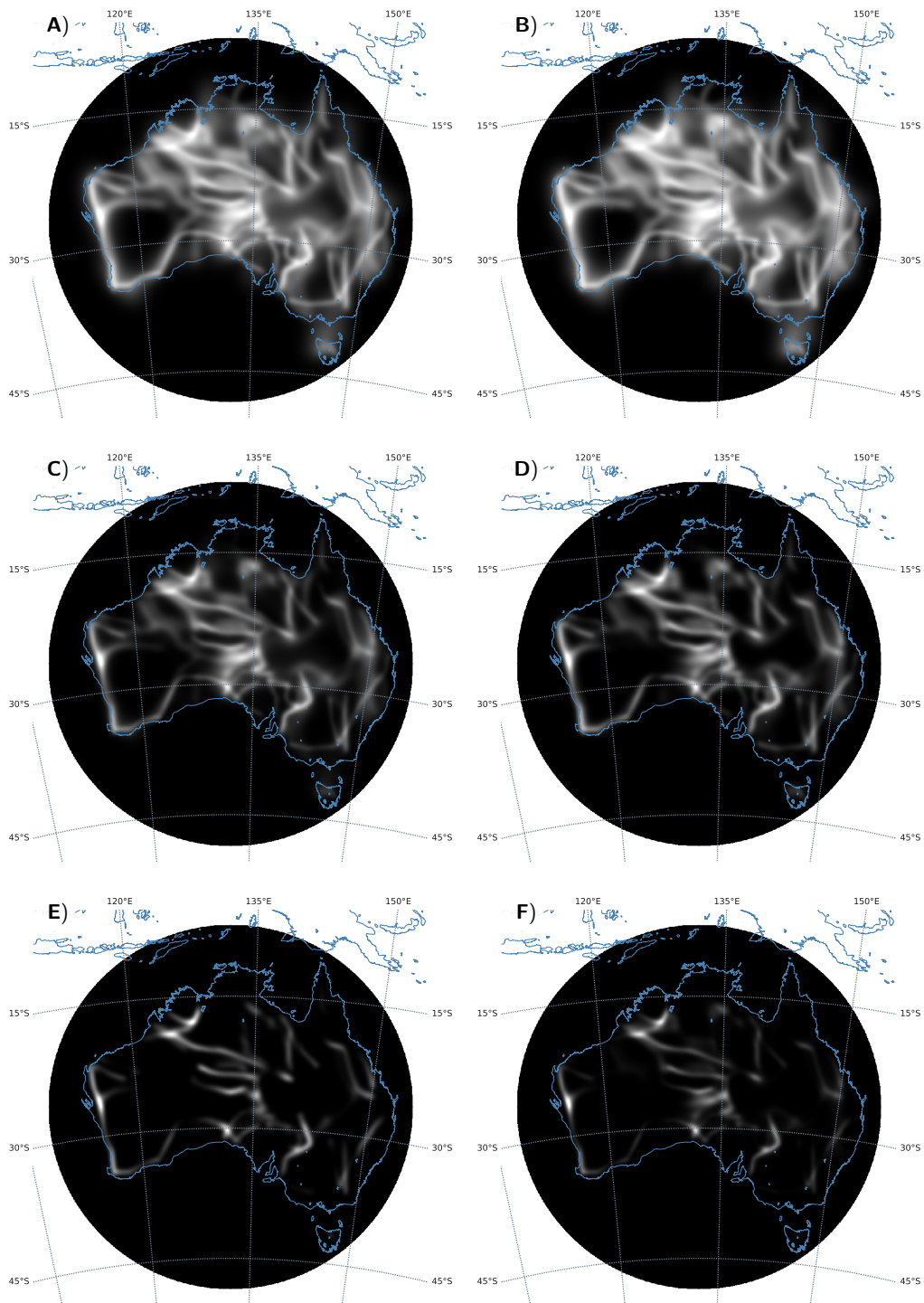


Figure B.1: Combined likelihood maps of the Australian continent, generated using six different methods. A) sum, B) union, C) squared sum, D) intersect, E) product, and F) squared intersect. Each map is normalised to the maximum value for each combination.

B.4 Additional material

Geotiff formats available at <https://doi.org/10.5281/zenodo.2649561>.

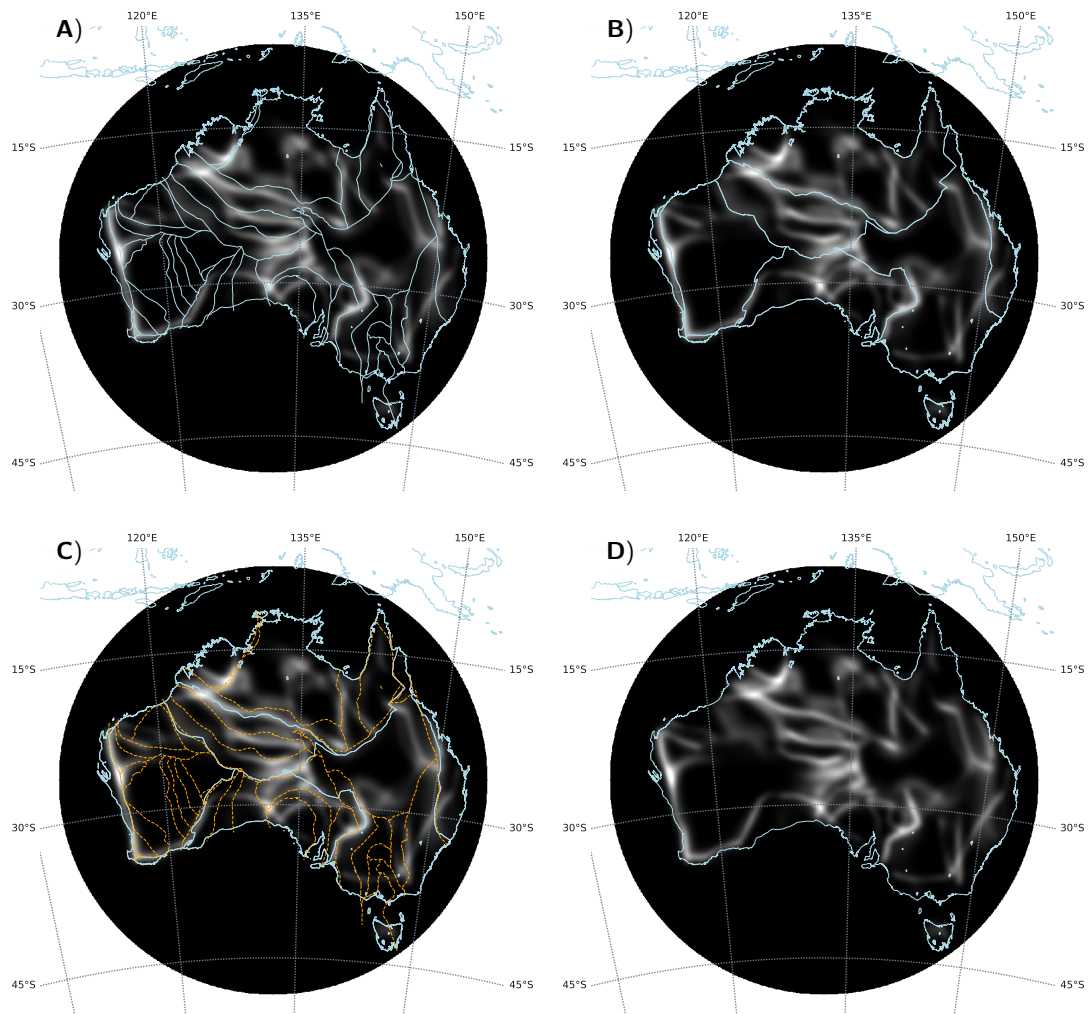


Figure B.2: Intersect of Australian likelihood distributions with overlay crustal models from (A) Korsch et al. (2016), (B) Australia (2010), (C) both with Korsch et al. (2016) in orange and Australia (2010) in cyan (D) Intersect (B.1 D) without overlay. The underlying datasets and reference models are further discussed by e.g. Cawood et al. (2008) and Kennett et al. (2018).

1. SCons script (sconstruct) to build this paper and figures. Includes all used code (url TBC).
2. Files of output Antarctic maps, GeoTIFF, and netCDF (url TBC):
 - (a) Antarctica sum
 - (b) Antarctica product
 - (c) Antarctica intersect
 - (d) Antarctica union
 - (e) Antarctica squared intersect
 - (f) Antarctica squared union
3. Raster files of output Australian maps, GeoTIFF and netCDF (url TBC):
 - (a) Australia sum
 - (b) Australia product
 - (c) Australia intersect
 - (d) Australia union
 - (e) Australia squared intersect
 - (f) Australia squared union

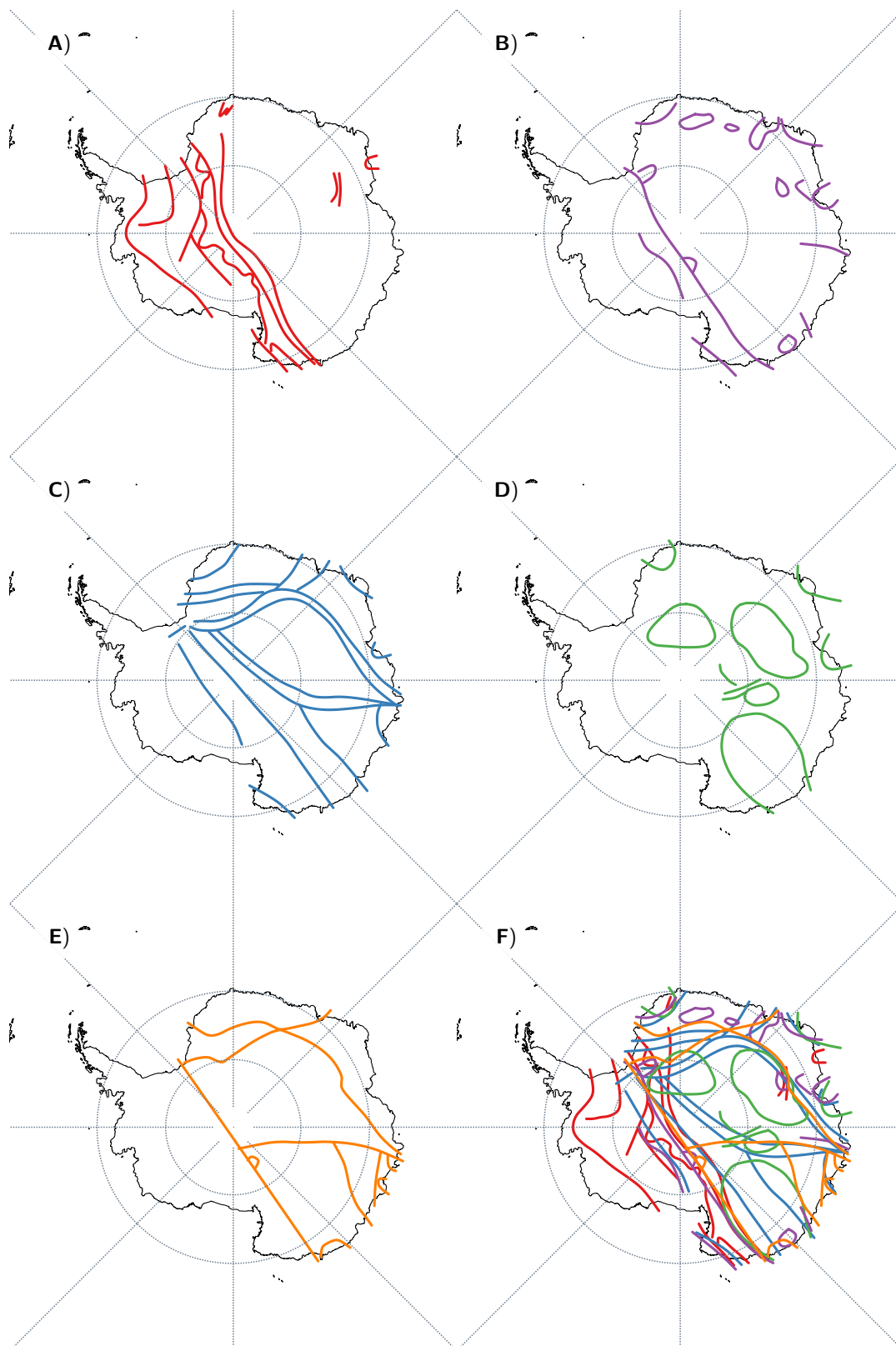


Figure B.3: A) Sketch of major boundaries suggested in previous studies and compilations. Red (Craddock, 1970), East Antarctica as one large Precambrian unit, in contrast to the better exposed dynamic, and young, West Antarctica. Blue (e.g. Boger, 2011), the continent defined as an extrapolation from the Gondwanian and Rodinian neighbours, or lack of such candidates. Green (e.g. Leitchenkov et al., 2016), Antarctica as an unknown entity with mainly inferred geophysical properties. Purple (e.g. Fitzsimons, 2000a), a tectonic narrative constrained by geological and geophysical observations. Orange (e.g. Liu et al., 2018; Morrissey et al., 2017); segmentation of the entire continent.

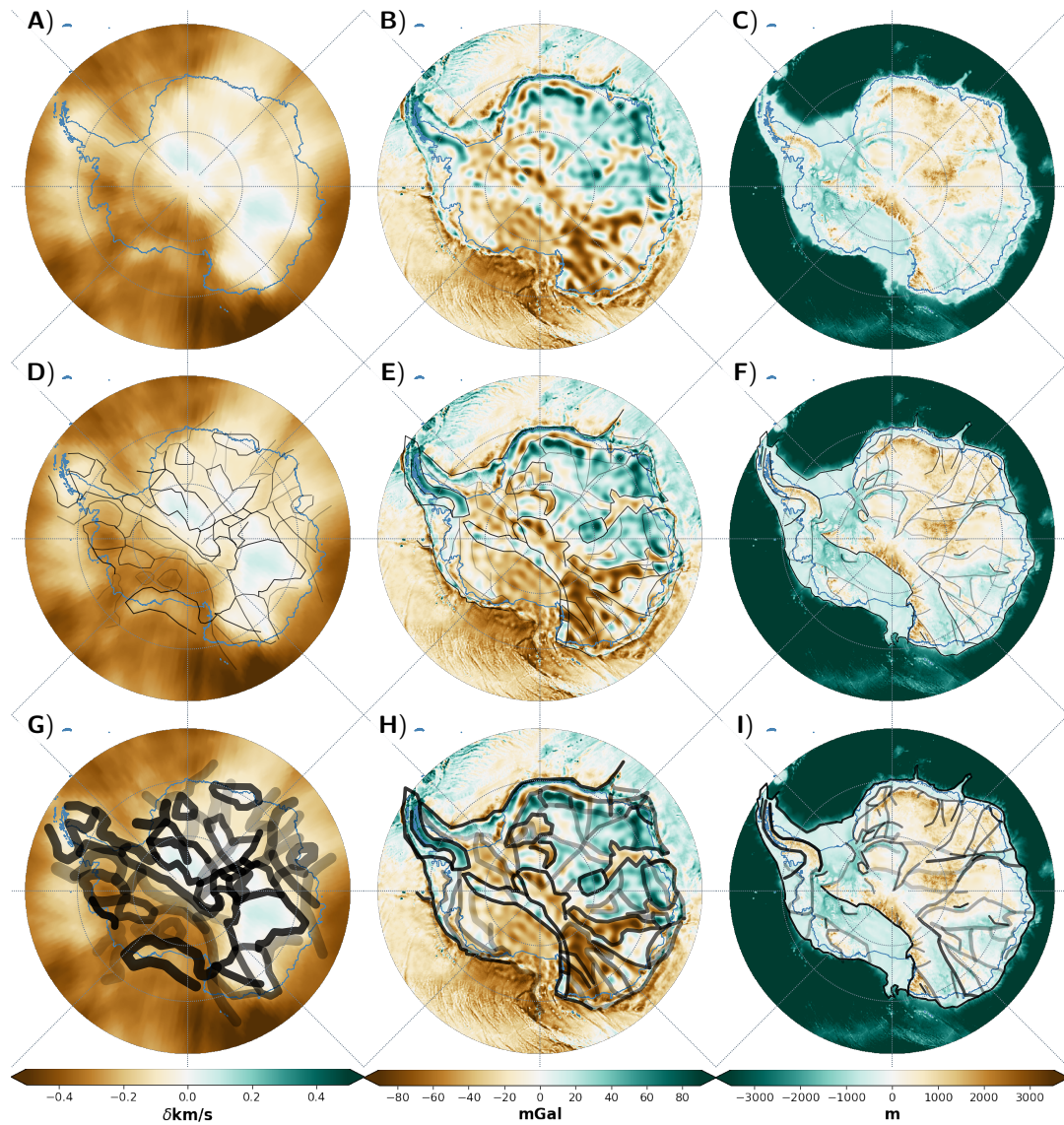


Figure B.4: Datasets used for this study and picked boundaries (black lines). Opacity illustrates the relative accuracy and line-widths indicate precision. B) Seismic shear wave speed at 150 km as perturbation from AK135 in absolute speed anomaly, modified from An et al. (2015a). C) Gravity anomaly map EIGEN-6C4, modified from Förste et al. (2013). D) Bed elevation model BEDMAP2, modified from Fretwell et al. (2012).

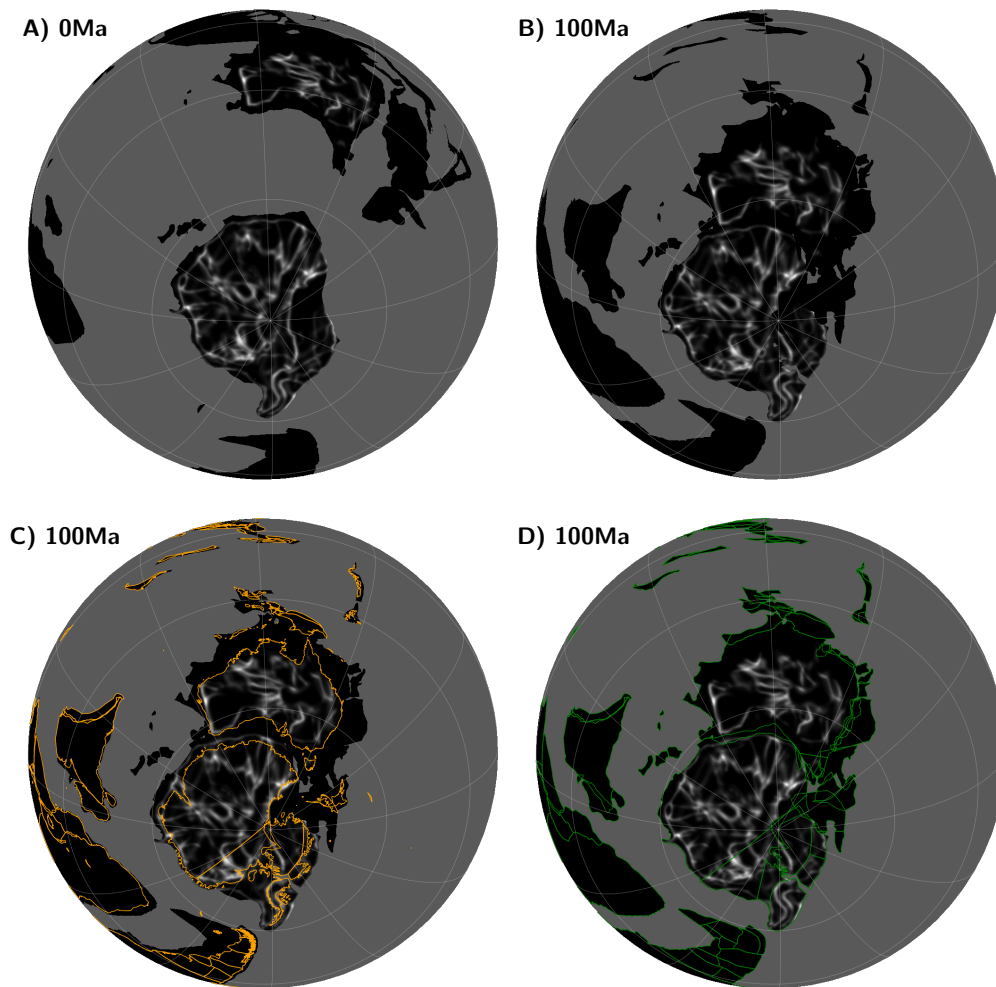


Figure B.5: Matthews et al. (2016) tectonic reconstruction in the Gplates (Boyden et al., 2011). Australia and Antarctica are represented by intersect likelihood maps from this study. A) Present positions. B) 100 Ma, intersect likelihood. C) Same as (B) but with added coastlines. D) Detailed view of Australia and East Antarctica (Matthews et al., 2016).

Appendix C

Chapter 5 Supplementary Material: Antarctic Geothermal Heat Flow Model: Aq1

Introduction

As Supporting Information, we provide figures and maps in addition to those in the main text. We also include technical details regarding some data processing steps, descriptions of data file formats, and code available for download.

The color ranges used in the maps might vary from map to map, and are stated on the color bars. However, the heat flow color representation is kept constant. Maps showing impact of for example parameter values are plotted as differences: Aq1 (preferred version) - variant. Brown indicates that the preferred version produces a higher value, and blue indicates that the variant produces a higher value.

Table of Contents

The order of sections generally follows the order of first mention in the paper.

1. NGHF database. Heat flow records used in this study.
2. Aq1.AB, generated with additional *B*-rated records in NGHF.
3. Histogram of misfit and sensitivity analysis of observables.
4. RMSe and MAe misfit with decreased weighting of observables.
5. Examples of datasets used.
6. Comparing global and Antarctic datasets.
7. Applied glacial isostatic correction.
8. Distance to grid centers.
9. Aq1 in lower resolution.
10. Similarity detection methods and Ψ values illustrated.
11. Ψ values for each observable to optimize similarity range by RMSe and MAe metrics.
12. Parameter maps of metrics for K and Ψ , comparing step function similarity detection with the Gaussian similarity detection used.
13. Heat production difference versus separation distance.
14. Aq.nv, Aq.ns, and Aq1.h250m; without selected observables and different heat flow catalog.
15. Maps of heat flow model generated with various parameter values.
16. Aq1.nc, without applied correction, and difference from Aq1.
17. Metrics of cross-validation.
18. Aq1.au test case for Australia, including metrics and brief discussion.
19. Comparison of heat flow distributions in previous studies.
20. Binary maps showing areas below or over threshold.
21. Heat flow measurements in Antarctica.
22. Robustness map.
23. Model download and file formats.
24. Code download.

C.1 NGHF Database. Heat flow Records Used in this Study

The NGHF (New Global Heat Flow) database can be downloaded from Lucazeau (2019): <https://agupubs.onlinelibrary.wiley.com/doi/abs/10.1029/2019GC008389>.

In the construction of model Aq1, we exclude input measurements of low quality (lower than *A* rating), measurements in a deep marine setting, and data from high latitudes (north of 80°N and south of 60°S) to reduce the size of the grid and to avoid spatial distortion from the interpolation in some of the observables used. Hence, the few existing Antarctic measurements are also excluded (further discussed in main text).

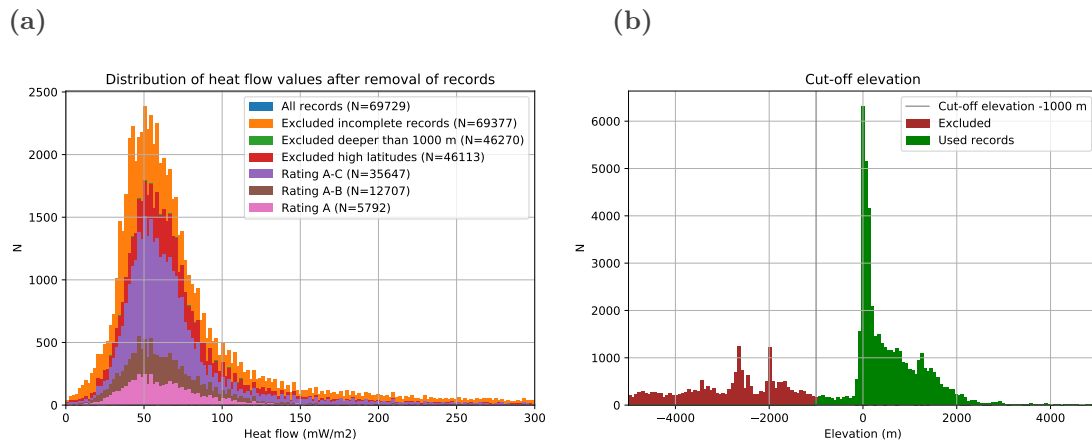
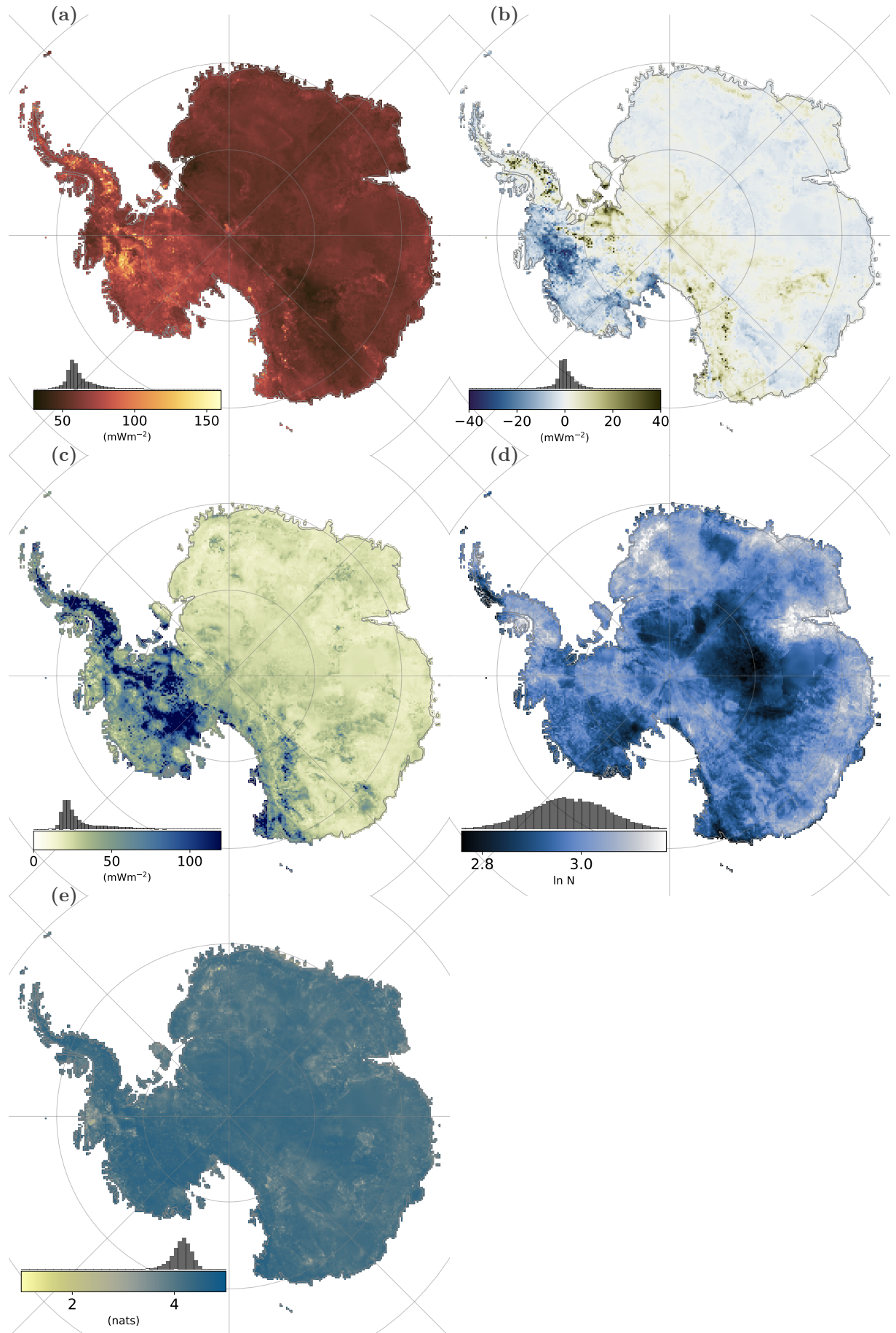


Figure C.1: Histogram of heat flow measurements in the NGHF database (Lucazeau, 2019). (a) Removal of incomplete records, deep sea records, polar region locations, and lower rated records. (b) The removed measurements below 1000 m depth (further details in main text).

C.2 Aq1.AB, Generated with Additional *B*-rated Records in NGHF

Here we show a version of the heat flow map and metrics, including records in the NGHF with rankings *A* and *B*.

Figure C.2: Aq1.AB, as generated from NGHF records with *A* and *B* ratings (instead of only *A*). *A* ratings indicates for example up to 10 mWm^{-2} variation at the measurement, while *B* ratings indicates for example up to 20 mWm^{-2} variation. (a) Aq1.AB, using same color representation as main article. (b) Difference between Aq1 and Aq1.AB-Aq1. Blue indicates higher values in Aq1, brown indicates that Aq1.AB generates higher values. (c) Uncertainty. Using this catalog, extremely high values are generated in for example Palmer Land. (d) Log of total similarity. (e) Information entropy.



C.3 Histogram of Misfit, and Sensitivity Analysis of Observables

The misfit of prediction for cross-validation using A ranked records and $A + B$ ranked records. An example of Aq1, but including B rated records is provided in Figure C.2.

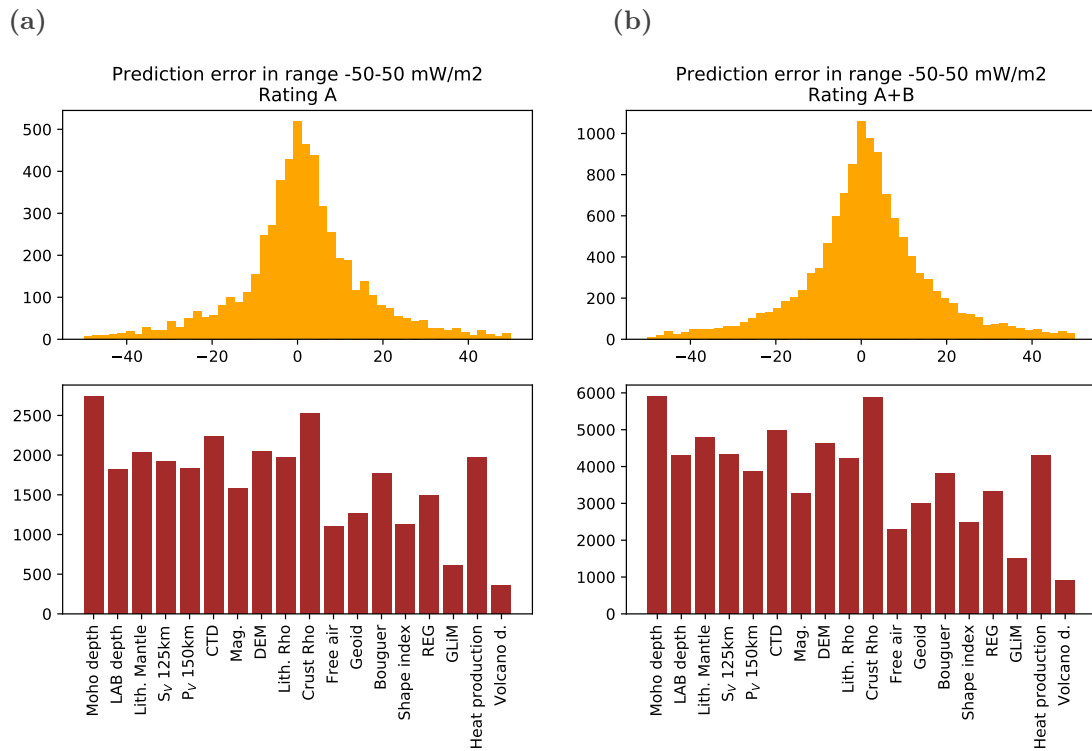


Figure C.3: Histogram of cross-correlated prediction errors for (a) A rated heat flow measurements, and (b) A+B rated heat flow measurements. Added sum of observables' similarity.

C.4 RMSe and MAe Misfit with Decreased Weighting of Observables

We show that retaining all observables at their full weight is close to the optimum result for RMSe, and the optimal weighting for MAe. The slope of the impact is also listed in Table 2 (main text). We also show that all observables improve the prediction when included, by calculating a linear regression from a Monte Carlo test of observables with weighting. The number of Monte Carlo simulation $N = 2001$.

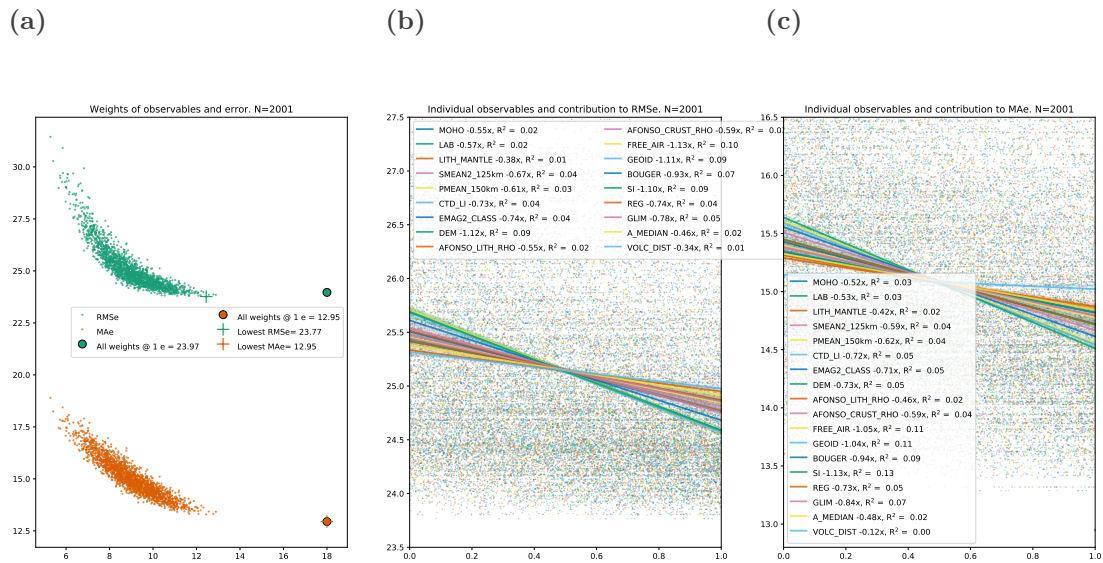


Figure C.4: Monte Carlo test of weightings and misfit. (a) Sum of all weights along x-axis and misfit on y-axis for RNMSe and MAe. (b) Weight for each observable along x-axis and resulting misfit RMSe on y-axis. (c) Weight for each observable along x-axis and resulting misfit MAe on y-axis. A linear regression is fit to the cross relation.

C.5 Examples of Datasets Used

All datasets included in this study are available from open repositories. Links given in the provided code are correct as of August 2020.

Here, we show maps of a selection of the observables used to illustrate how reference and target observable are related. Maps of datasets that are uninformative in small scale, and maps from publications without an open data policy are not shown.

In Figure C.3 (a-d) for each observable: (I) shows the reference map with heat flow measurements used in the study shown in the same color as a darker shade. (II) shows the target observables for Antarctica, and (III) show the relation with heat flow, as scatter plot and a contoured Gaussian kernel density estimate.

- a Moho depth
- b LAB depth
- c Curie temperature depth
- d Gravity curvature

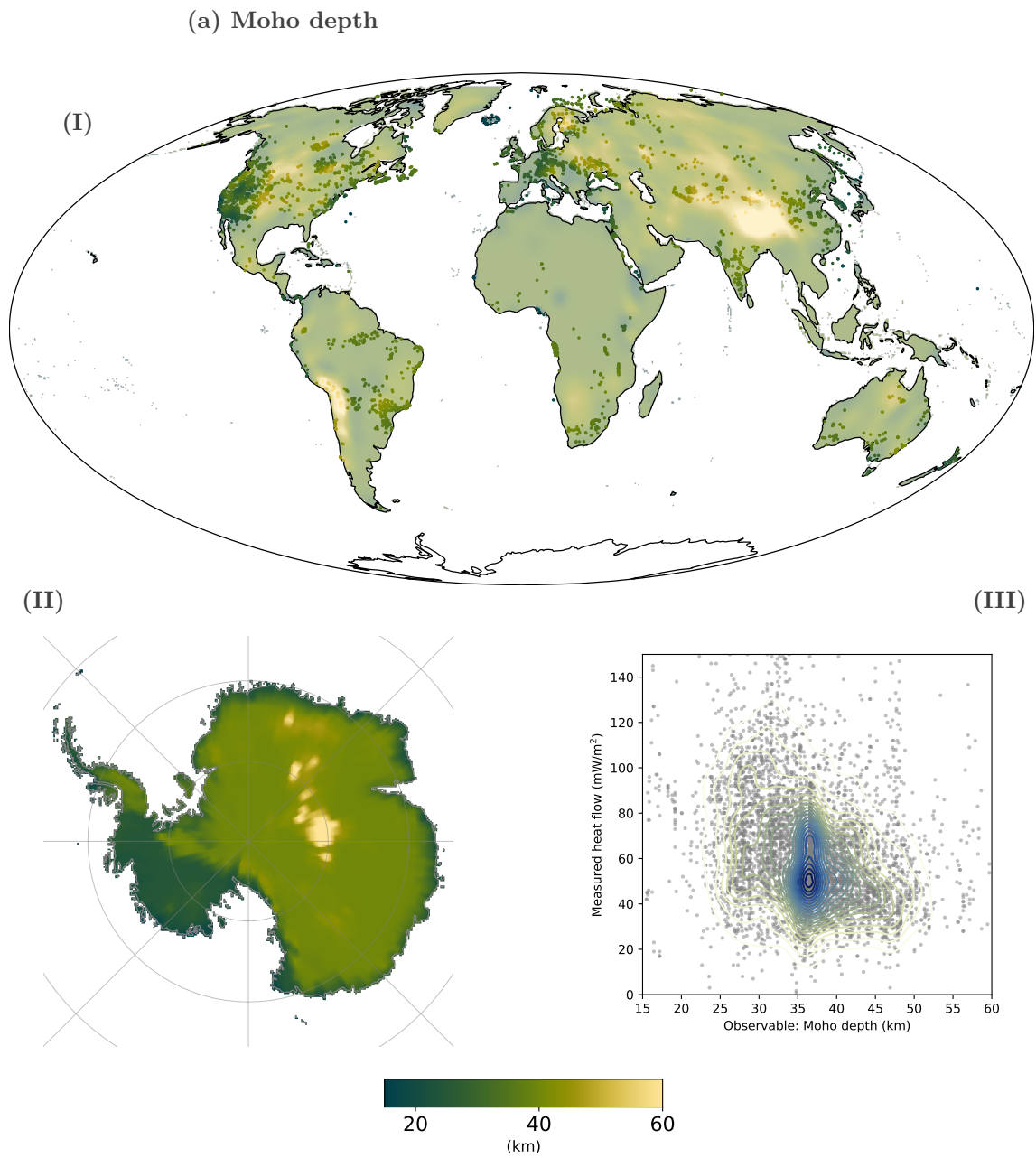


Figure C.5: (a) Moho depth, (I) Reference observable: Szwilius et al. (2019), (II) Target observable: An et al. (2015a), (III) Observable plotted with heat flow values (Lucazeau, 2019).

(b) LAB depth

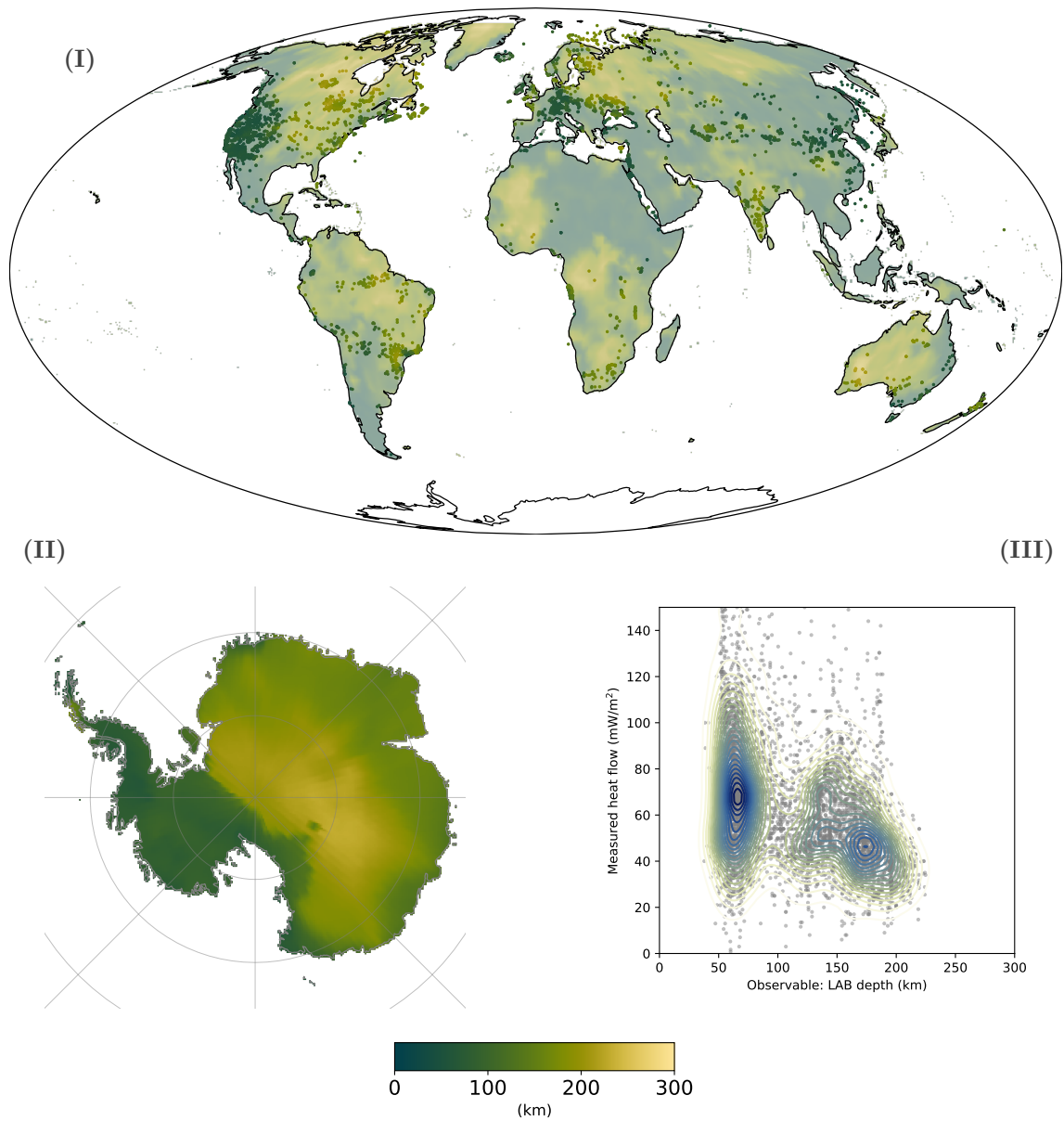


Figure C.5: (b) LAB (lithosphere-asthenosphere boundary) depth, (I) Reference observable: Afonso et al. (2019), (II) Target observable: An et al. (2015b), (III) Observable plotted with heat flow values (Lucazeau, 2019).

(c) Curie temperature depth

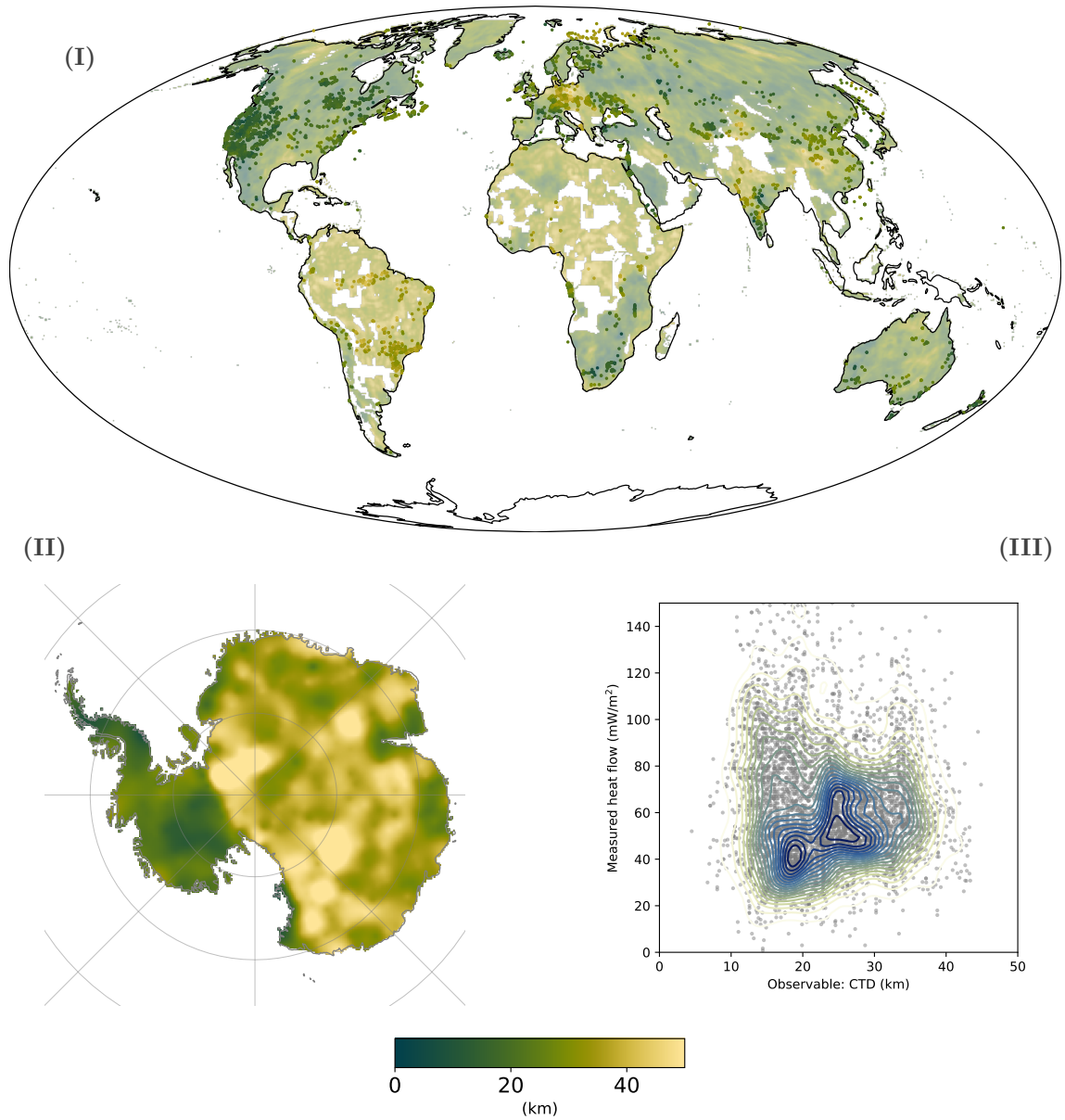


Figure C.5: (c) Curie temperature depth, (I) Reference observable: Li et al. (2017), (II) Target observable: Martos et al. (2017), (III) Observable plotted with heat flow values (Lucazeau, 2019).

(d) Curvature of gravitational field, shape index

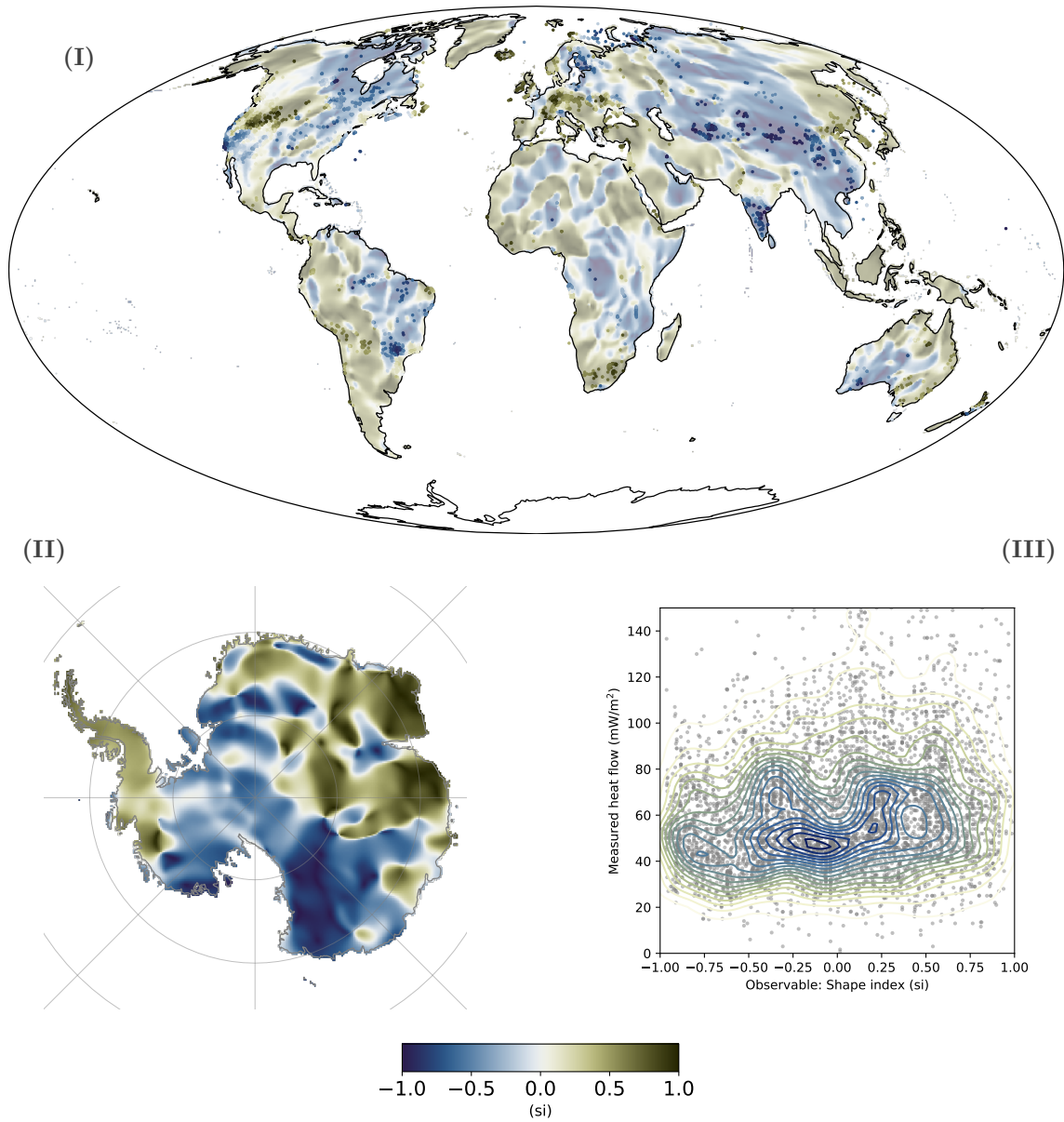


Figure C.5: (d) Curvature of gravitational field, (I) Reference observable: Ebbing et al. (2018), (II) Target observable: Ebbing et al. (2018), (III) Observable plotted with heat flow values (Lucazeau, 2019).

C.6 Comparing Global and Antarctic Datasets

The target observables for Antarctica are, in some cases, from different sources than the reference observable. The Antarctic observables are refined, include additional data and we suggest that they are more robust for the Antarctic continent than their global counterpart (where this exists). Here, we show a comparison for three observables, where the reference observable covers Antarctica, but it differs from the target observable dataset. Difference is calculated as:

$$\text{DIFF} = o_T - o_R. \quad (\text{C.1})$$

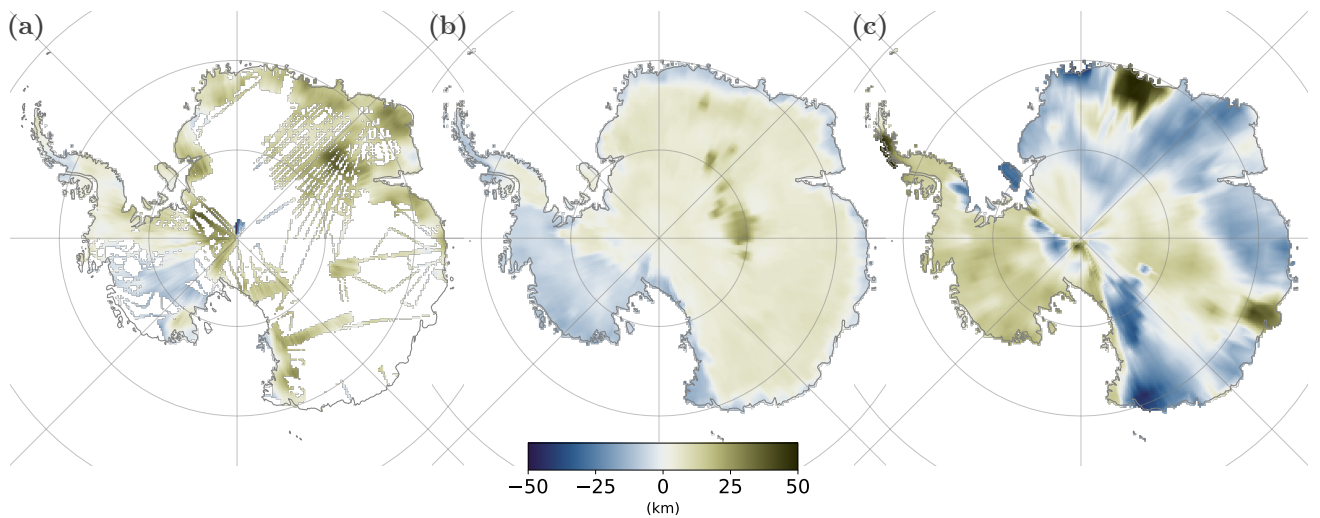


Figure C.6: Comparison of global and regional datasets in Antarctica. (a) Difference between Curie temperature depth (CTD) from Martos et al. (2017) and GCDM (Li et al., 2017). GCDM has limited cover of Antarctica. The extreme values above the South Pole in Li et al. (2017) appear to be an artifact in the provided file, but do not affect our model, as Martos et al. (2017) is used as target observable. (b) Difference between crustal thickness from An et al. (2015a) and Szwillus et al. (2019). (c) Difference between LAB (lithosphere-asthenosphere boundary) depth from An et al. (2015a) and Afonso et al. (2019). For all figures, blue colors indicate that the global dataset shows a deeper boundary, and brown colors show that the used Antarctic dataset is deeper.

C.7 Applied Glacial Isostatic Correction

The Antarctic crust is depressed in elevation due to the weight of the ice sheets. To generate an equivalent elevation dataset, we remove the impact of this load by applying the simplified approach of Stål et al. (2020c):

$$\text{DEM}_{\text{iso}} = \text{DEM}_{\text{sg}} + \frac{(\text{DEM}_{\text{s}} - \text{DEM}_{\text{sg}}) \times \rho_{\text{ice}} \times D_{\text{LAB}}}{\rho_{\text{crust}} \times D_{\text{Moho}} + \rho_{\text{mantle}} \times (D_{\text{LAB}} - D_{\text{Moho}})}, \quad (\text{C.2})$$

where DEM_{iso} is the adjusted elevation model, DEM_{sg} is the subglacial elevation, DEM_{s} is the surface elevation (Morlighem et al., 2019), ρ_{ice} is the density of ice, assumed to be constant (916.7 kg/m³), ρ_{crust} is the average density of the crust from Afonso et al. (2019), ρ_{mantle} is an average density of the lithospheric mantle (Afonso et al., 2019), D_{Moho} is the depth to Moho, and D_{LAB} is the depth to LAB (An et al., 2015a,b). We also correct for ocean loading where sea water replaces ice, using an water density of 1025 kg/m³ (a minor addition). To provide a simple approach to the lithospheric flexure, the uplift is convolved with a $\sigma = 60$ km Gaussian kernel. The uncertainty is represented by the similarity range, and is due to ongoing uplift and subsidence impacting on the target observable. Global sea-level rise is not considered, as reference observables would be similarly affected.

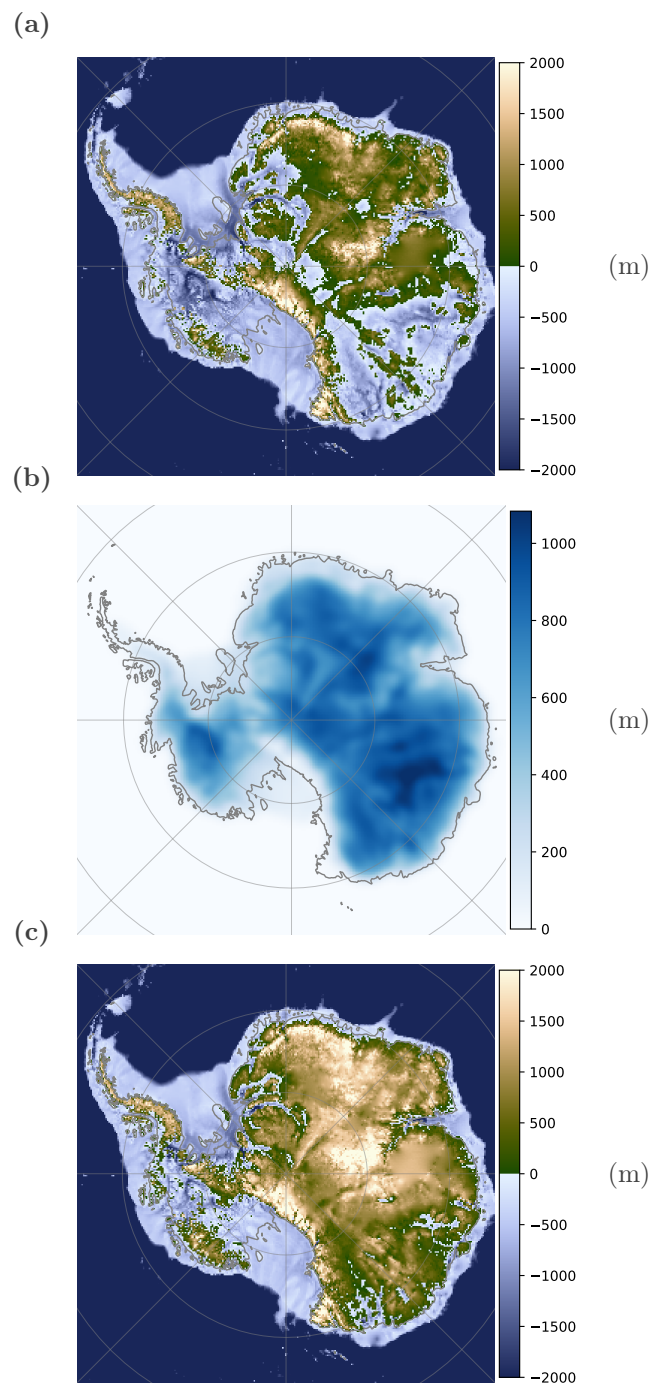


Figure C.7: Steady-state isostatic correction for ice removed using the simplified method of Stål et al. (2020c). (a) Bedmachine (Morlighem et al., 2019). (b) Calculated uplift, with removed ice and sea water filling the void to present sea level. (c) Adjusted elevation, used as target observable.

C.8 Distance to Grid Centers

Reference observables are linked to heat flow measurements via a global regular grid. This reduces the computational complexity, and we demonstrate here that the distance between an interpolated point and heat flow measurement is less than the resolution of datasets used. The exception is topography where we use a smoothed topography to match the resolution in Antarctica, as provided in BedMachine (Morlighem et al., 2019). The maximum distance from heat flow measurement to nearest grid cell is shorter than the grid resolution used in Antarctica (20 km). Here, we show heat flow measurements used, and distance in km to the nearest grid center, calculated using the Haversine formula:

$$d = 2r \arcsin \left(\sqrt{\text{hav}(\varphi_2 - \varphi_1) + \cos(\varphi_1) \cos(\varphi_2) \text{hav}(\lambda_2 - \lambda_1)} \right),$$

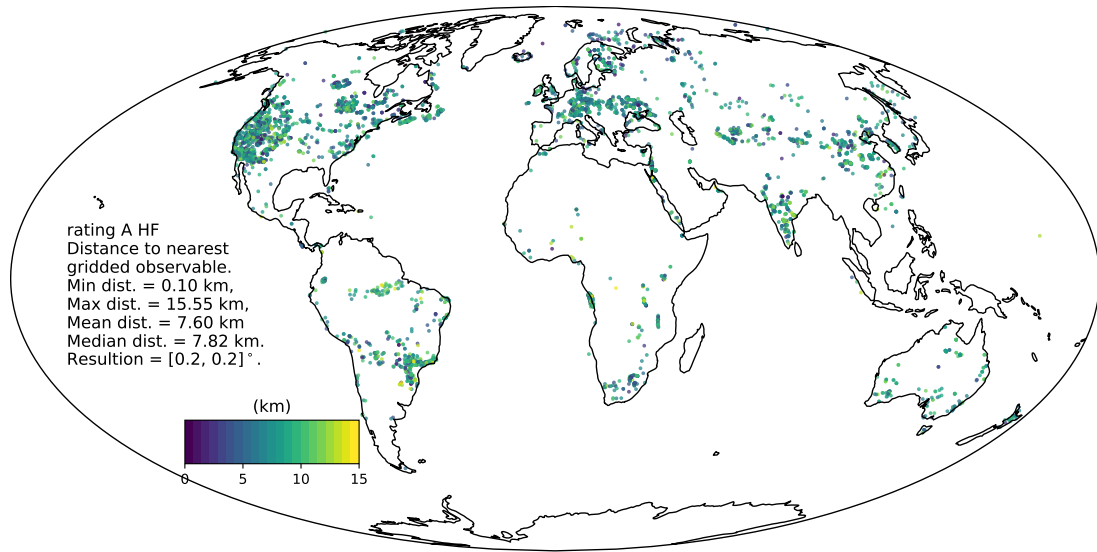
where:

$$\text{hav}(\theta) = \sin^2 \left(\frac{\theta}{2} \right).$$

The Haversine distance calculation is performed in python using the *numpy* library:

```
import numpy as np
def distance(lat1, lon1, lat2, lon2):
    p = 0.017453292519943295 # pi/180
    a = 0.5 - np.cos((lat2-lat1)*p)/2 +
        np.cos(lat1*p)*np.cos(lat2*p) *
        (1-np.cos((lon2-lon1)*p)) / 2
    return 12742.0176 * np.arcsin(np.sqrt(a)) # in km
```

(a)



(b)

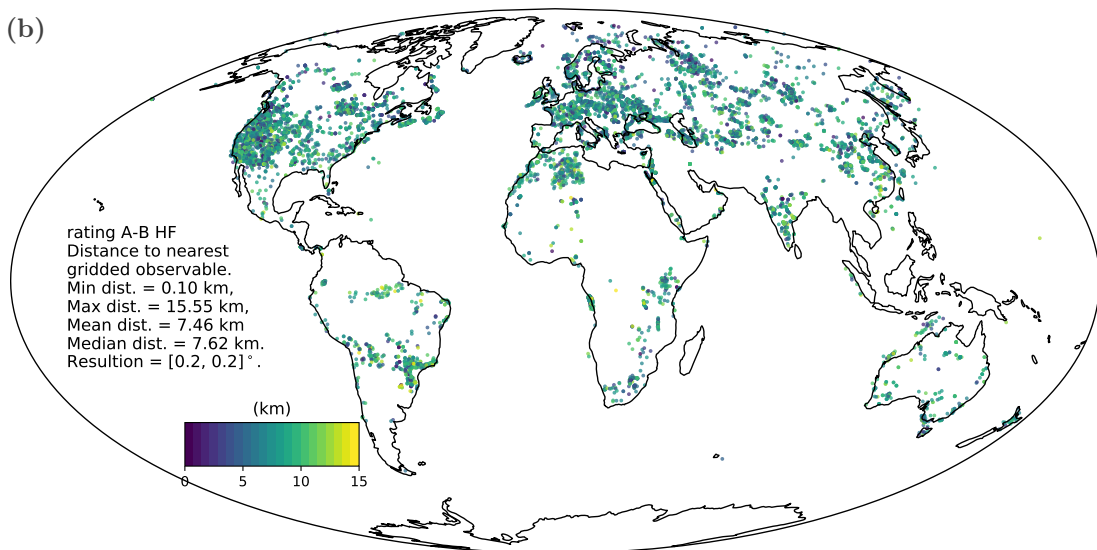


Figure C.8: Distance between heat flow measurements and grid cell centers. (a) *A* rated measurements, (b) *A* and *B* rated measurements (Lucazeau, 2019).

C.9 Aq1 in Lower Resolution

We also generate the model in lower resolution. This gives us the option to further test the robustness and resolution of the model. We find that the resolution does not impact the result significantly, but might improve the robustness. A low resolution model is in some aspects more true to the observables used, of which most are coarser than 20 km.

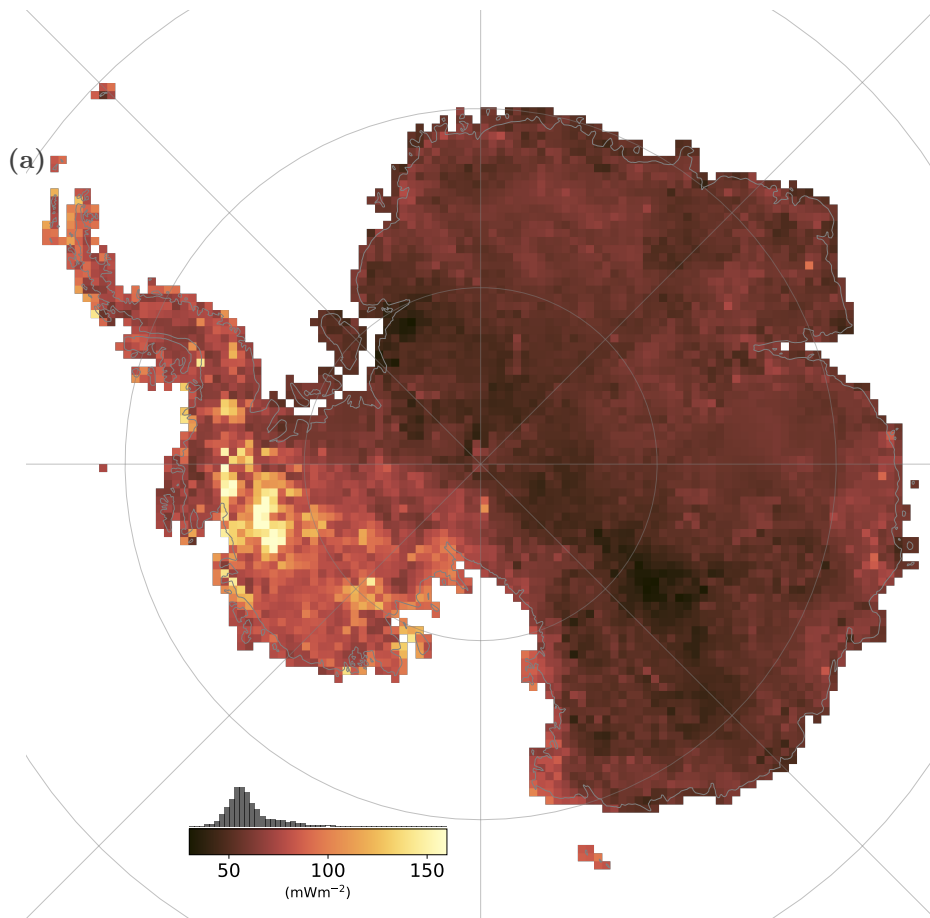


Figure C.9: A version of Aq1, generated in lower resolution, using a 50 km × 50 km grid.

C.10 Similarity detection and Ψ values illustrated

Here, we show the range of similarity for different values of Ψ , and how the step function relates to our continuous Gaussian detection function.

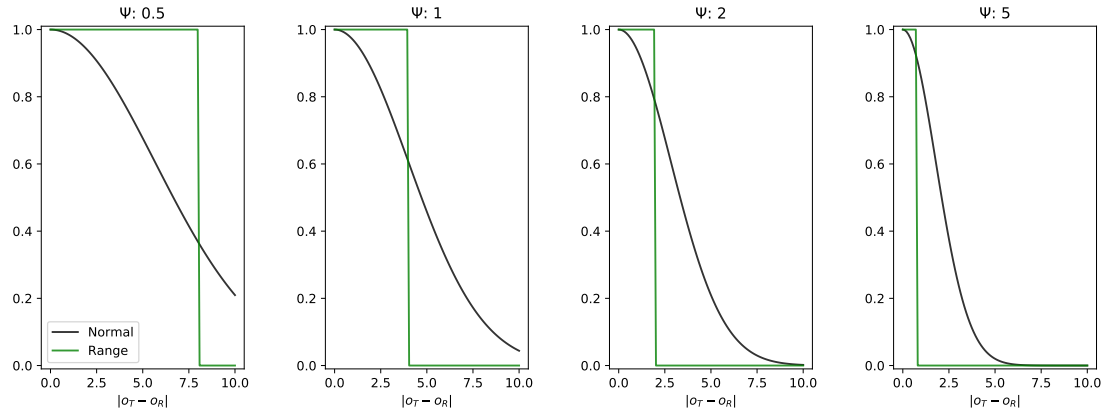


Figure C.10: Similarity for $\Psi = 0.1, 0.5, 1,$ and 1.5 . Green curve is a step function detection, and black curve is the Gaussian continuous function used for Aq1.

C.11 Monte Carlo simulation of Ψ values for each observable to optimize similarity range

To test and optimize the similarity range function, we investigate the response of each observable with varying Ψ . For many observables, there is a tradeoff between optimizing RMSe and MAe. Note that classes are excluded, as we only regard identical values as similar. The result is not overly sensitive to the exact range used.

(a)

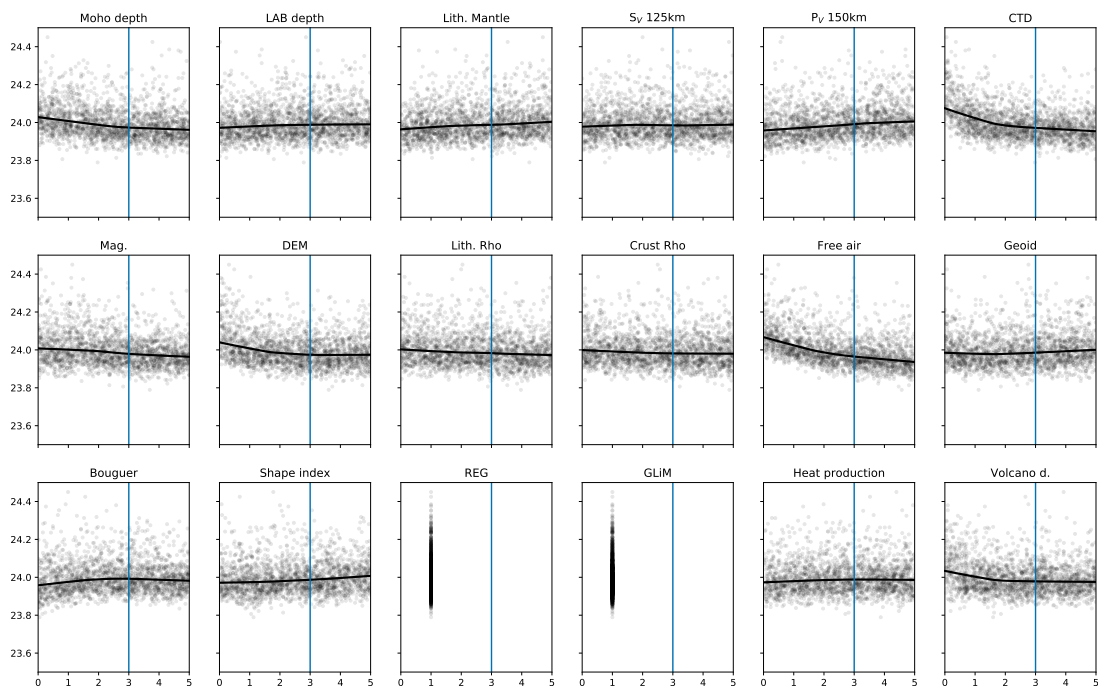


Figure C.11: a

(b)

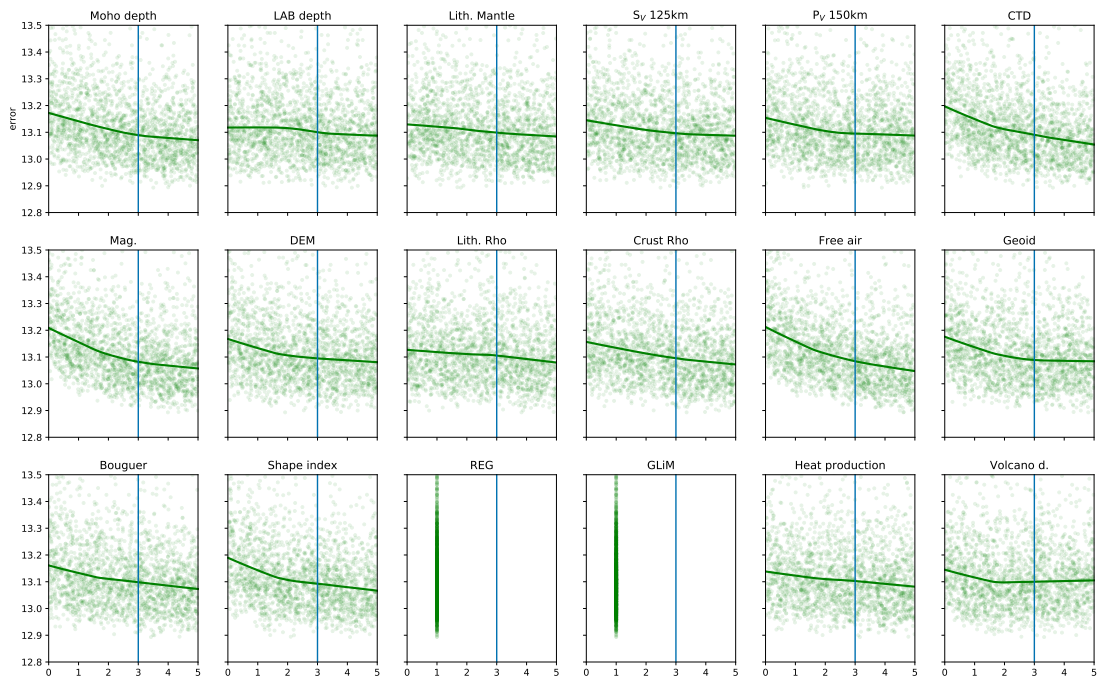
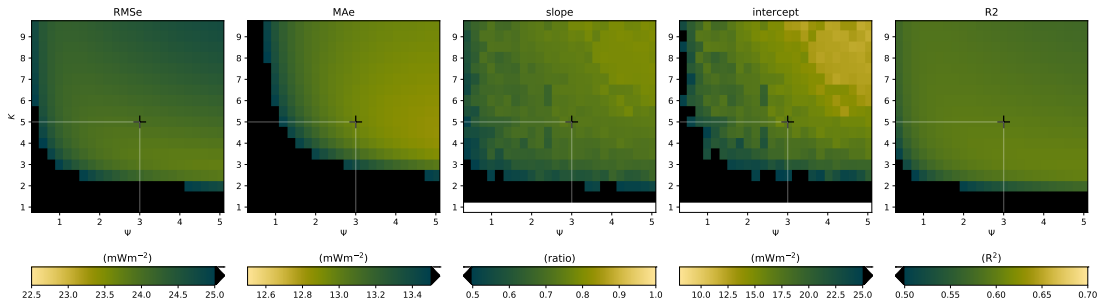


Figure C.11: Monte Carlo test of Ψ for each observable. Blue line shows selected value of Ψ .
 (a) RMSe and (b) MAe.

C.12 Parameter maps of metrics for K and Ψ , comparing step function similarity detection with the Gaussian similarity detection used.

Previous studies using similar methodology (Goutorbe et al., 2011; Lucazeau, 2019) applied a step function to define similar observables. For our limited range of observables, we find that this approach can cause unpredictable distributions, where an arbitrary choice (e.g., of acceptance range) impacts the resulting assigned heat flow unless suitable observables were used. Here, we show the response of RMSe, MAe, slope and intercept of a RANSAC linear regression, and R2 value from variations of K and Ψ (as described in main text).

(a)



(b)

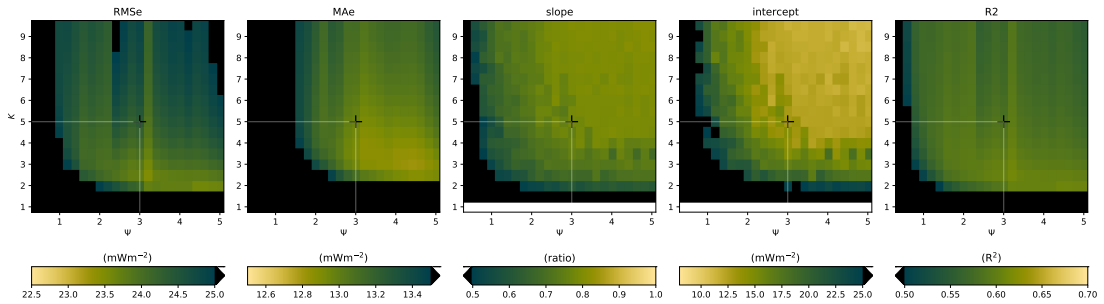


Figure C.12: Parameter maps of metrics for: (a) Gaussian function for continuous similarity detection, as described in article. (b) Step function detected similarity. To facilitate comparison, the color range for each (a-b) pair is identical.

C.13 Heat Production Diverging over Distance

We plot differences in heat production values (Gard et al., 2019) to show how the differences in values increases with distance. Beyond about 250 km, there is no apparent association. We also note the large range of values from samples collected in a near proximity.

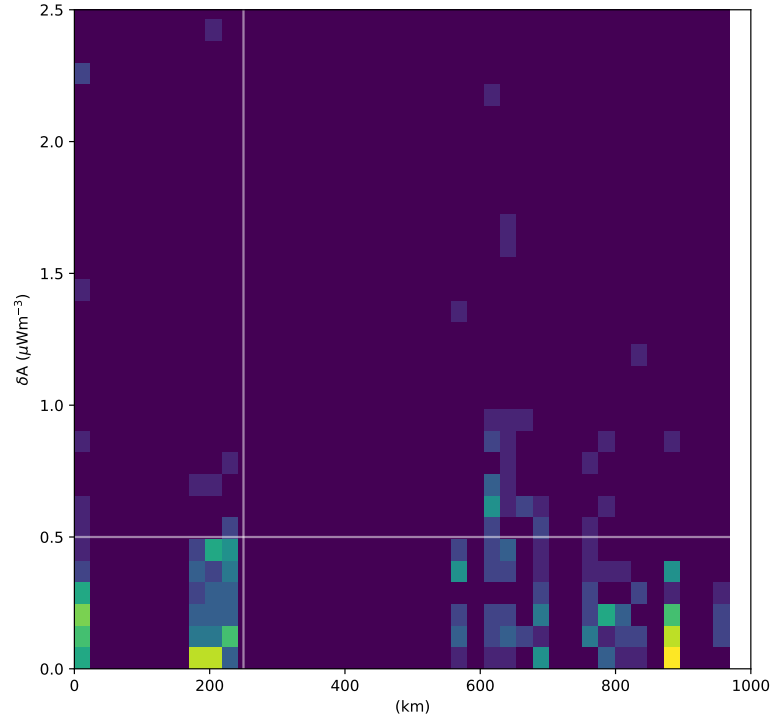
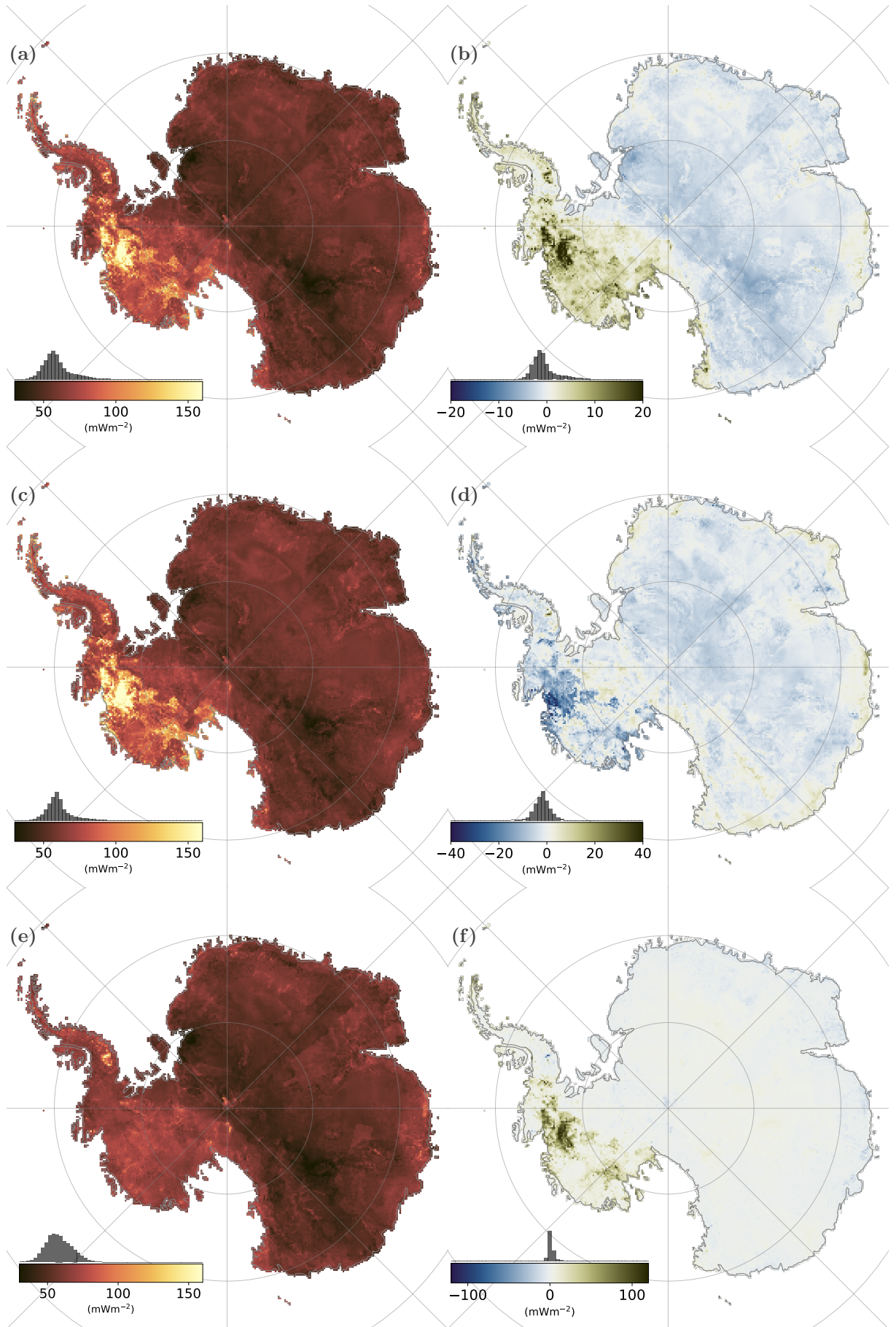


Figure C.13: Heat production difference over length. White lines show $w_0 = 250$ km and the acceptance range $S_{\delta A} = 0.5 \mu\text{W}^{-3}$.

C.14 **Aq1.nv, Without Distance-to-Volcanoes Observable, Aq1.ns, without Moho and LAB Observables with Differences from Aq1, and Aq1.h250m, with a Differently Selected Heat Flow Catalog**

Aq1.nv is a version where the volcano observable is excluded. Aq1.ns similarly excludes Moho depth and LAB depth from (An et al., 2015a,b). Aq1.h250m shows how a different criterion when selecting heat flow catalog impacts the result. Here, all heat flow records deeper than 250 m below sea level are excluded.



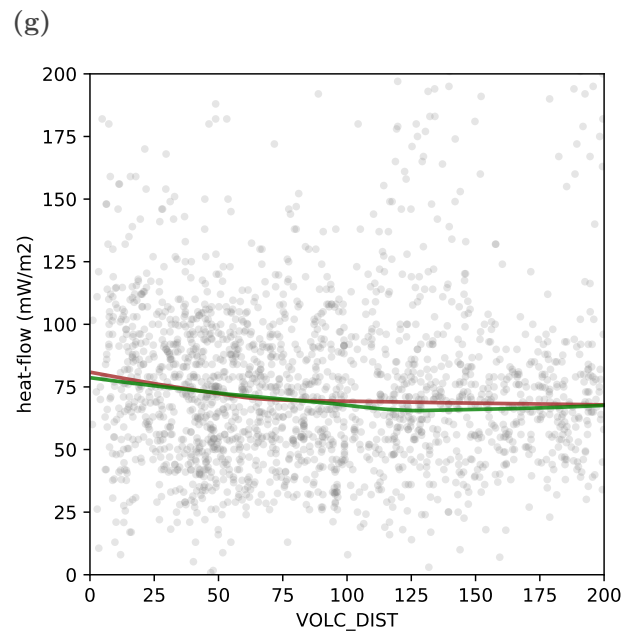


Figure C.14: Illustration of the effect of modelling choices. (a) Aq1 without distance-to-volcanoes observable. (b) Difference between models: Aq1-Aq1.nv. A brown color indicates that the predicted heat flow is lower without the volcano observable, and blue indicates that the predicted heat flow is higher, without the distance to volcano observable. Figure 14g shows how heat flow depends on distance from volcano. (c) Aq1 without Moho (An et al., 2015a) and LAB (An et al., 2015b) observables. (d) Difference between models: Aq1-Aq1.ns variant. A brown color indicates that the predicted heat flow is lower without the observables, and blue indicates that the predicted heat flow is higher without the observables. (e) Aq1.h250m shows a more limited selection of heat flow values, that produce larger uncertainty, particularly for Thwaites Glacier and Siple Coast. Depth cutoff is 250 m below sea level instead of 1000 m below sea level (f) Difference between models: Aq1-Aq1.h250m. Note that the color range for difference (subplots b,d,f) have different ranges. (g) Detailed view of heat flow up to 200 km from a volcano (Lucazeau, 2019) versus distance from volcanoes, as compiled by the Global Volcanism Program (2013). Green is $A + B$ rated records, brown shows only A rated records, with little difference. This relation exemplifies that absence of volcanoes actually increase the average heat flow at a certain distance.

C.15 Maps of Heat Flow Model Generated with Various Parameter Values

This assessment is performed to investigate the impact of different values of K and Ψ . We apply identical correlation, and use the optimized K and Ψ values unless noted. Generally, low values of K produce a smoothed map, while high values of K generate noise. Ψ has a similar impact, as fewer records are incorporated with high pickiness. With low pickiness, the class observables gain relevance as they are precisely defined and not sensitive to the range. With updated datasets, the K parameter can likely be increased, similar to value suggested by Goutorbe et al. (2011). A higher value would increase resolution and potentially predict shallow mechanisms responsible for high heat flow.

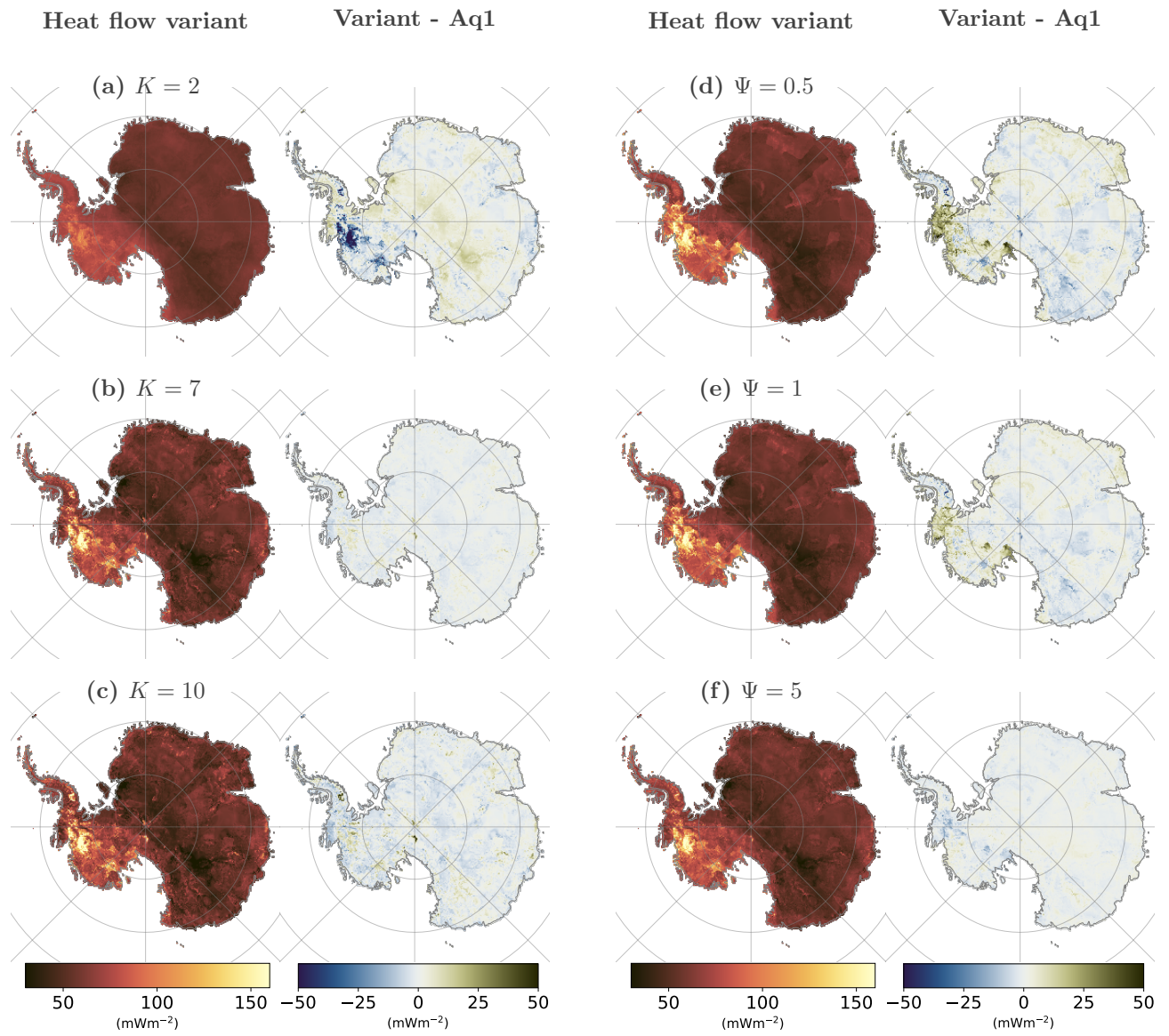


Figure C.15: (a-c) K tests and comparison with Aq1. (d-f) Ψ tests and comparison with Aq1.

C.16 Aq1.nc, without Applied Correction, and Difference from Aq1.

The misfit between cross-validated predictions and measurements are used to compute a RANSAC regression. The slope and intercept of the regression is used to correct for the expected reduced range of the prediction, as discussed in the article.

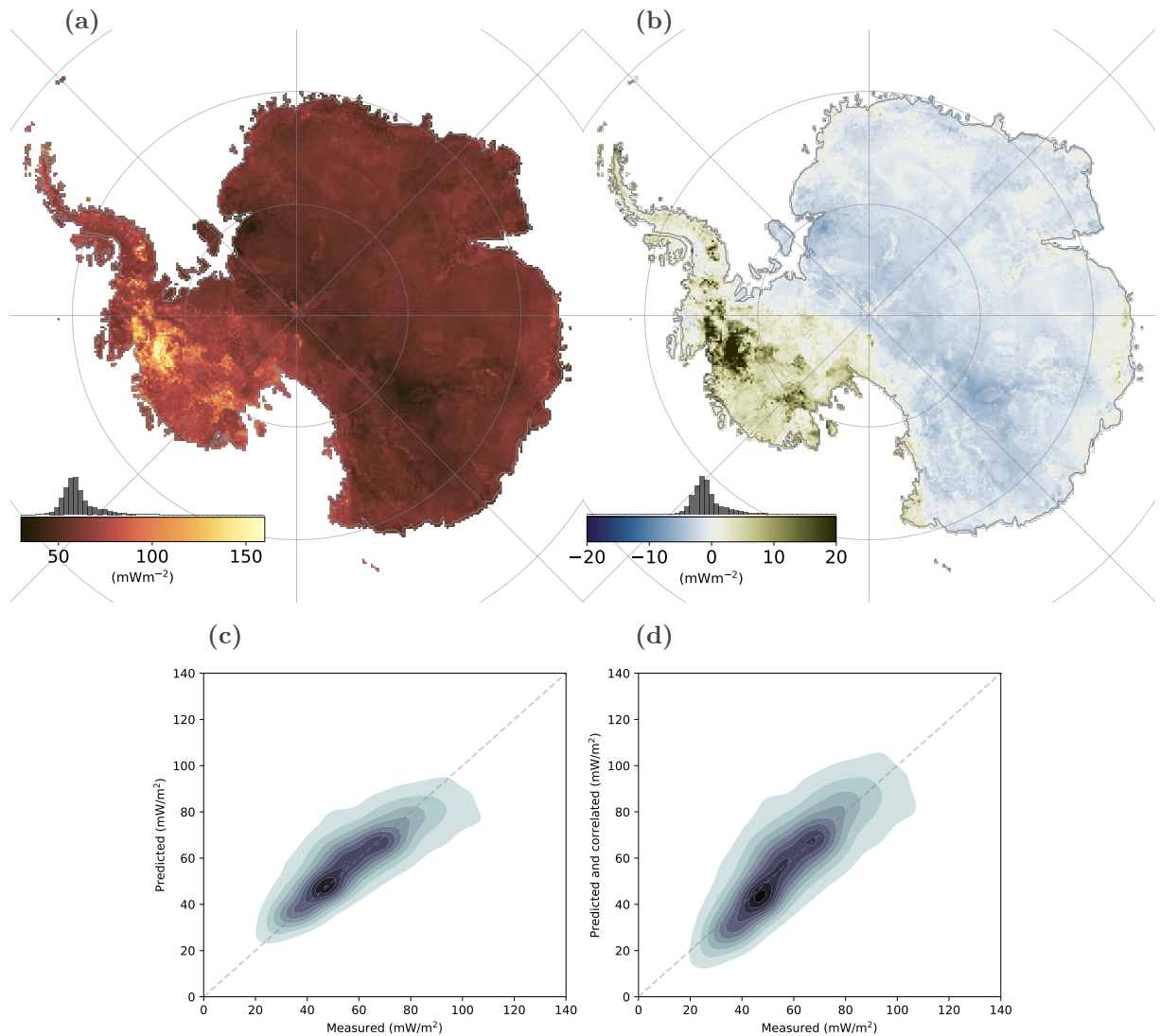


Figure C.16: Impact of compensation function, as maps and KDE. Leave-one-out cross-validation (LOOCV) of heat flow values in NGHF used in this study, and applied correction. Heat flow measurements along the x-axis, and predicted values along the y-axis. (a) Uncorrected version of Aq1 and Aq1.nc. (b) Aq1-Aq.nc variant. Brown indicates that the values are adjusted up, blue indicates that values are adjusted down. (c) Cross plot of measurements and predictions shown as a kernel density estimate (KDE). (d) From the RANSAC regression, a slope and intercept value are calculated. Those values are used to adjust the predictions. For clarity, the axes are cropped, but the complete range of values are used in the regression. Figure is generated using *SKlearn* (Pedregosa et al., 2011) for regression and *seaborn* (Waskom et al., 2020) for KDE (methods described in main text).

C.17 Metrics of Cross-Validated Heat Flow Values

There is some correlation between heat flow and uncertainty, and between uncertainty and entropy. However, each metric provides a different perspective against which to assess the results.

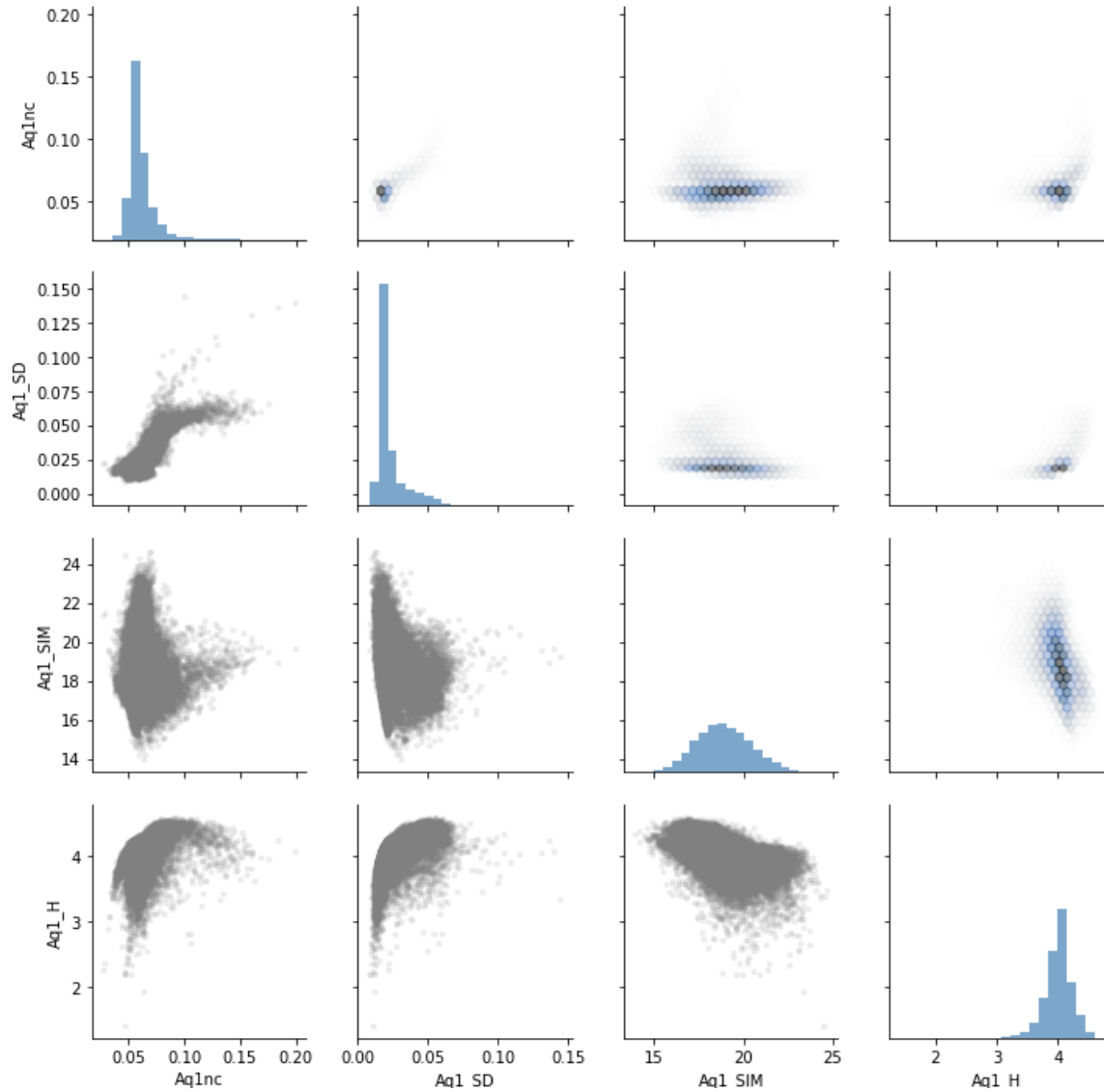


Figure C.17: (a) Cross plot of Aq1.nc and metrics. Aq1 SD is the uncertainty, as standard deviation. Aq1 SIM is the log sum of similarity. Aq1 H is the information entropy. Upper relations are plotted as hexbin density, the lower relations are plotted as scatter plot.

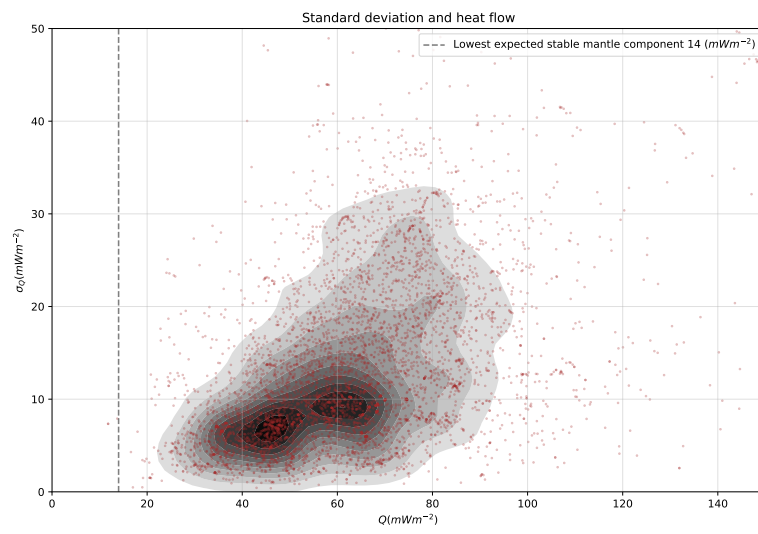
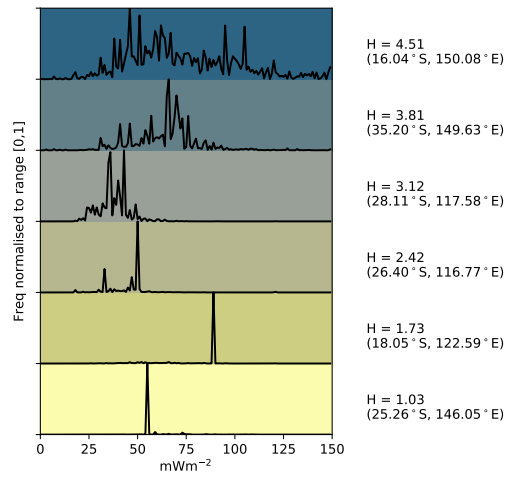
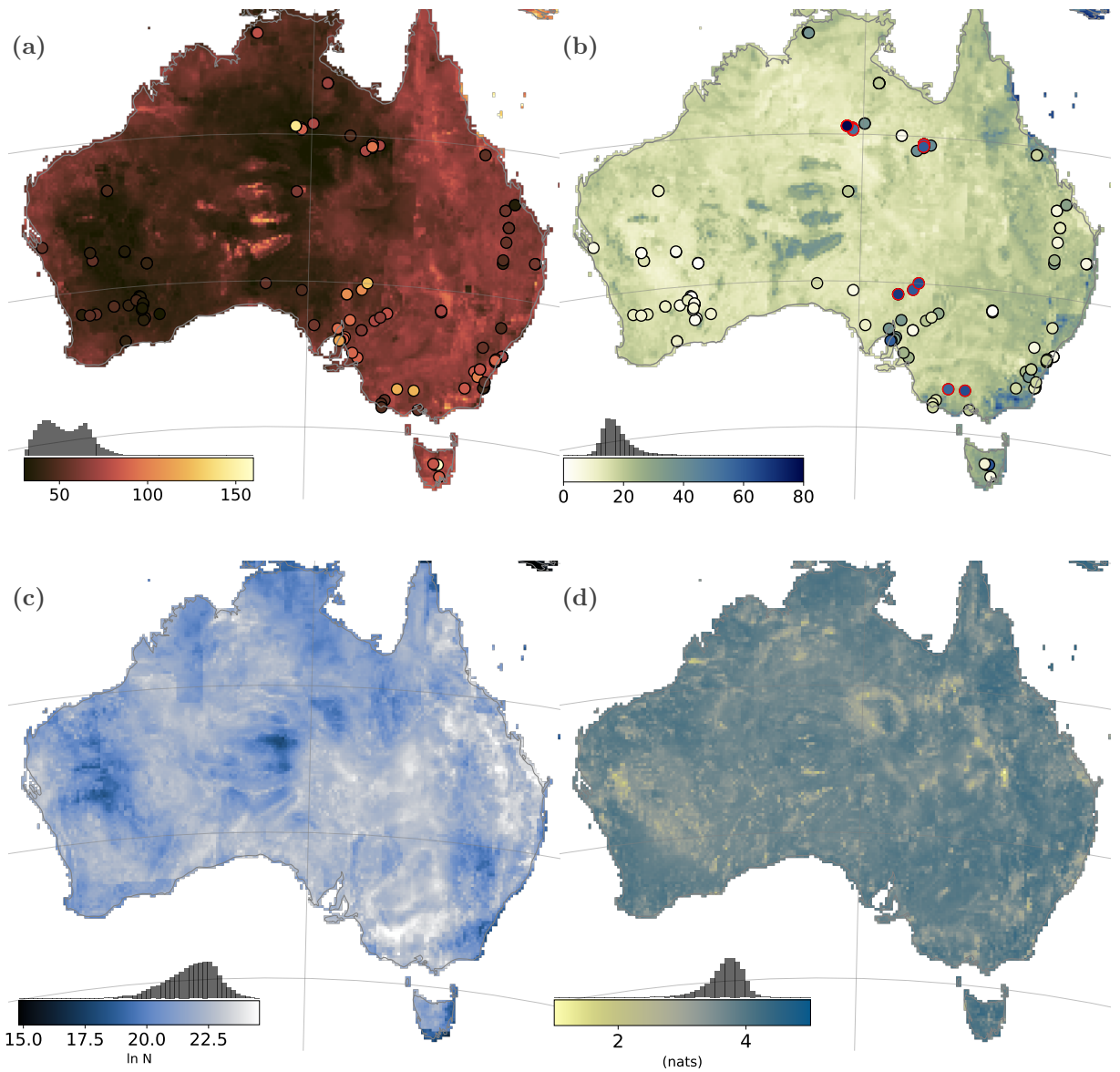


Figure C.17: (b) Detailed view of KDE plot of cross-correlated uncertainty and heat flow.

C.18 Aq1.au A Test Case for Australia, including Metrics and Brief Discussion

The methodology and datasets are applied to Australia as a comparison example. In order to replicate processing considerations as for the Antarctic example, we exclude all heat production data and refined regional datasets, except Moho depth (Salmon et al., 2013a). The data coverage for Australia is, however, generally better than for the target observables used in Antarctica, so this comparison example provides a best case scenario. In total, 143 measurements from NGHF are shown. Those records are not included when generating Aq1.au. If such measurements were to be included, every heat flow record would indeed be perfectly predicted.

Figure C.18: Maps of an equivalent Australian geothermal heat flow model, Aq1.au. (a) Modeled heat flow, using same color space as Antarctic map. Filled circles represent measurements in NGHF (Lucazeau, 2019) in quality category *A*. (b) Uncertainty of the model. Filled circles show the disagreement between model and measurements. Measurements that differ by more than 30 mWm^{-2} from the uncertainty ranges are highlighted with red rings. 86 of 143 measurements are correctly predicted within uncertainty bounds, 100/143 are within 10 mWm^{-2} , and 115/143 are within 20 mWm^{-2} from the uncertainty bounds. Where uncertainty is not provided with the heat flow measurements, the arithmetic mean of all Australian records are used as range. Most striking are the high values in Tasmania, Northern Territories, and near Northern Gawler Craton. Those locations are all likely to be related to local elevated heat production. (c) Sum of similarities. (d) Information entropy. (e) Examples of histograms and the calculated entropy, as described in main text.



C.19 Comparison of Heat Flow Distributions in Different Studies

Here we show the frequency distribution of heat flow estimates in Antarctica (a-d), and NGHF selected records (above 1000 m below sea level, and rating A). We also calculate the mean and median for each record. All models are clipped to the Antarctic coastline and grounding line (Mouginot et al., 2017).

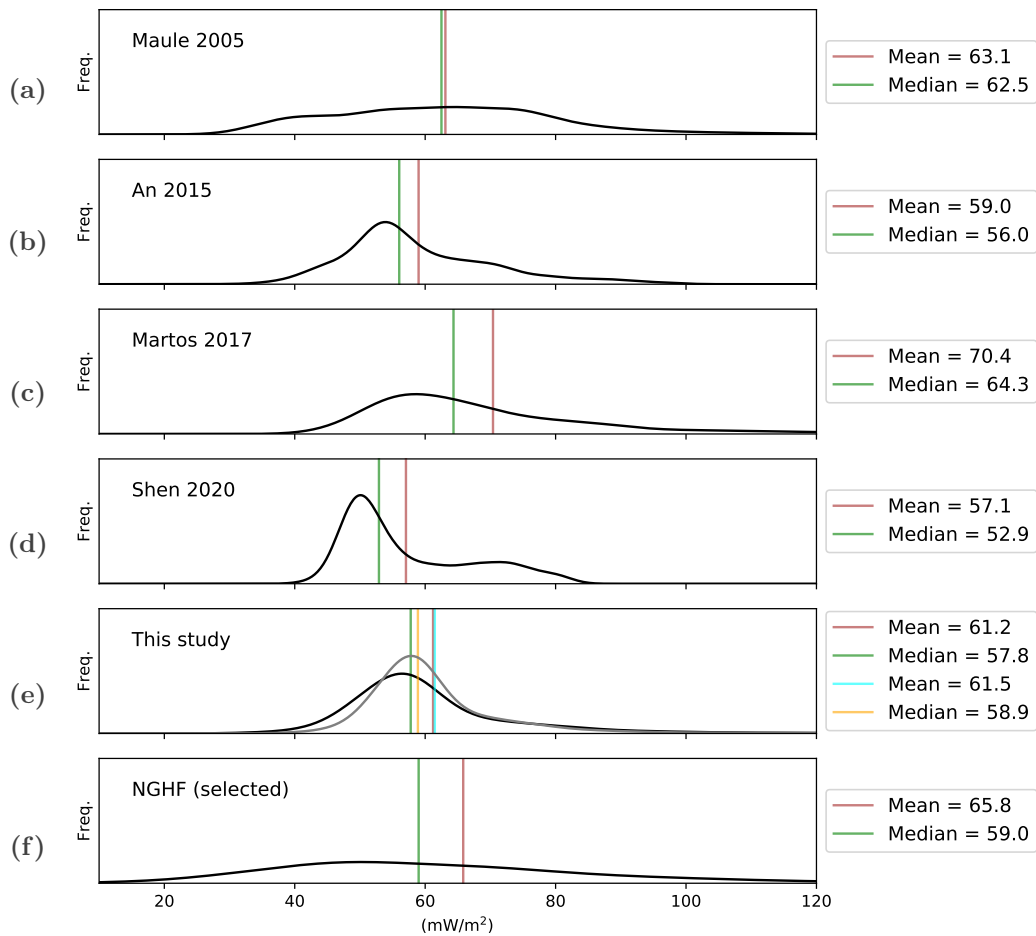


Figure C.19: Distribution of heat flow values. (a) Fox Maule et al. (2005). (b) An et al. (2015b) (c) Martos et al. (2017) (d) Shen et al. (2020) (e) This study. Gray curve is uncorrected, and black curve is corrected. Orange and cyan lines indicated median and mean for the non-corrected distribution. (f) Distribution of selected records from NGHF (Lucazeau, 2019). in previous studies, this study, and the records from NGHF used in this study.

C.20 Threshold Maps

Binary maps showing areas below or above a threshold value.

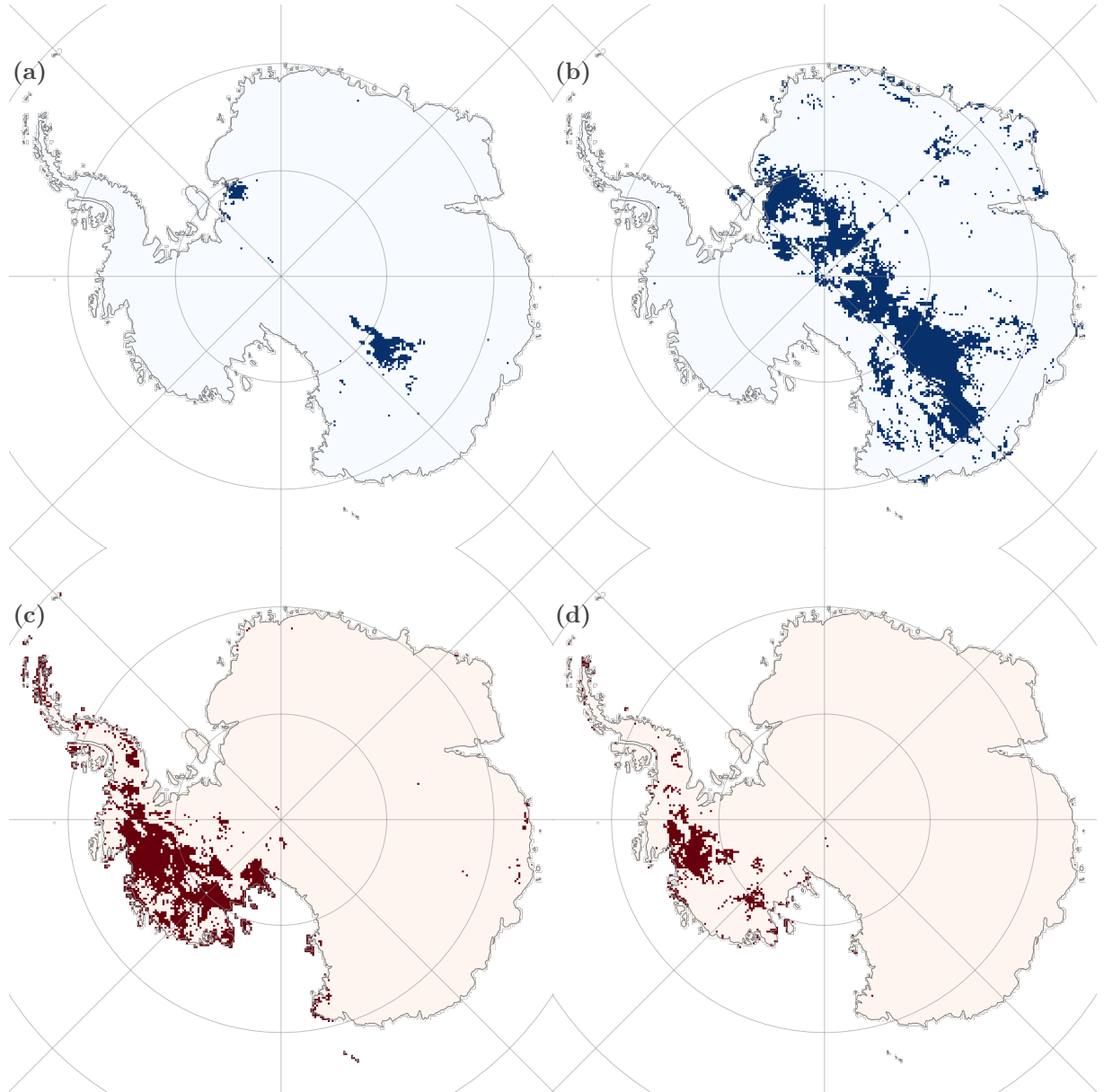


Figure C.20: Selected values in Aq1: (a) Areas under 30 mWm⁻², (b) areas under 40 mWm⁻², (c) areas above 80 mWm⁻², (d) areas above 100 mWm⁻².

C.21 Heat Flow Measurements in Antarctica

As discussed in the main text, there exist very few heat flow measurements in Antarctica and the uncertainties are very large. Moreover, local measurements might not well represent the total heat, when integrated over hundreds of square kilometers. For further discussion, we refer to (Burton-Johnson et al., 2020). The compilation is available from: <https://github.com/RicardaDziadek/Antarctic-GHF-DB>.

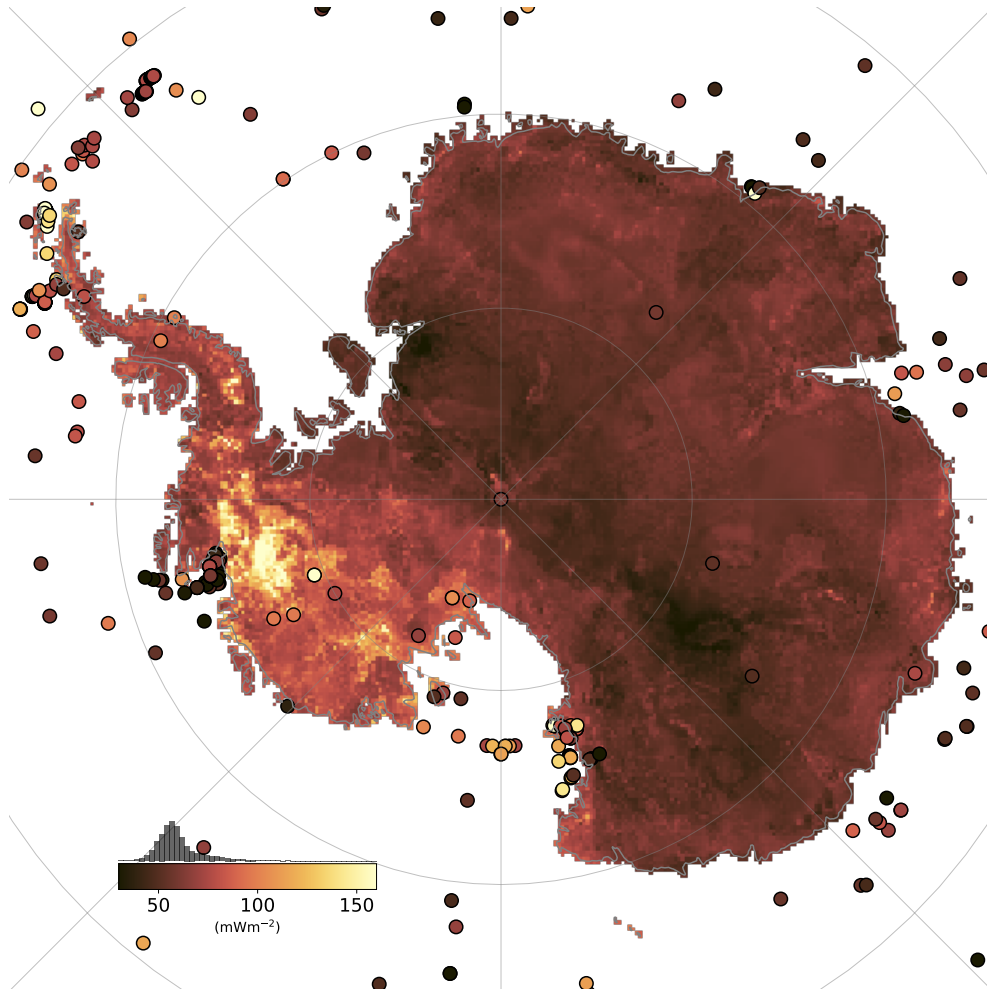


Figure C.21: Heat flow measurements in Antarctica. Compiled by Burton-Johnson et al. (2020). Aq1 in background, in same color representation.

C.22 Robustness Map

To provide a composite product for interdisciplinary use, we calculate a robustness map as an informal product with general utility. The map shows the product of total log sum of similarity, inverted entropy value, and inverted uncertainty value (normalized and clipped to 5% and 95% percentiles before multiplication). The robustness is relative, so values of 1 indicate the best predictions within the model.

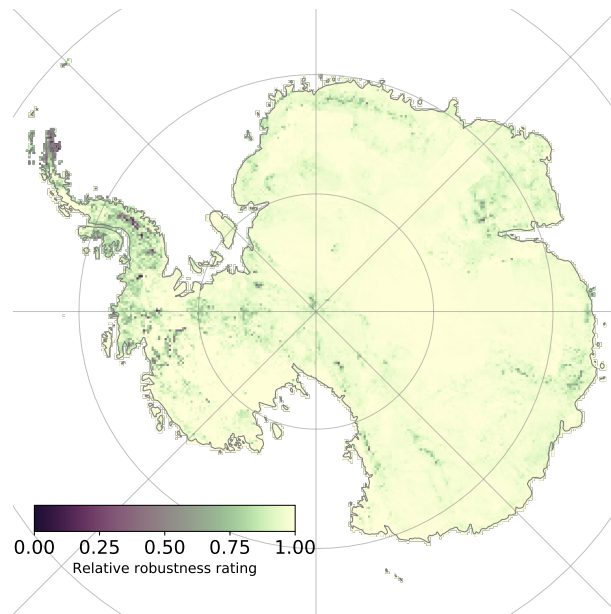


Figure C.22: Robustness of Aq1, shown as relative values.

C.23 Model Download and File Formats

Aq1 is available in netCDF format, saved with uncertainty, sum of similarity, and entropy grids. It is also available as geoTIFF raster files and delimited text formats.

Naming convention of files:

`Aq1_vv_rr`

where `vv` is revision version, set to 1.0 (10) at the time of publication, and `rr` is resolution in kilometers. `u` is the uncertainty, as described in the main article. Coordinates are included as WGS 84 Antarctic Polar Stereographic (EPSG:3031) and WGS 84 WGS84 World Geodetic System 1984 (EPSG:4326).

- `Aq1_10_20.nc`
- `Aq1_10_50.nc`
- `Aq1_10_20.tiff`
- `Aq1_10_20_u.tiff`
- `Aq1_10_50.tiff`
- `Aq1_10_50u.tiff`
- `Aq1_10_20.csv`
- `Aq1_10_50.csv`
- `Aq1_10_20.xyq`
- `Aq1_10_50.xyq`

C.24 Code Download

The complete Python code to generate all figures and files in this paper is available from <https://zenodo.org/record/4014430>. We also share a Jupyter Notebook with some additional plots and analysis at <https://github.com/TobbeTripitaka/Aq1>. The code is commented and aimed to be easy to modify and update, however; we don't guarantee compatibility with future packages, operation system, etc., and might only provide limited support.

Latest version of *agrid* is available from <https://github.com/TobbeTripitaka/agrid>.

